

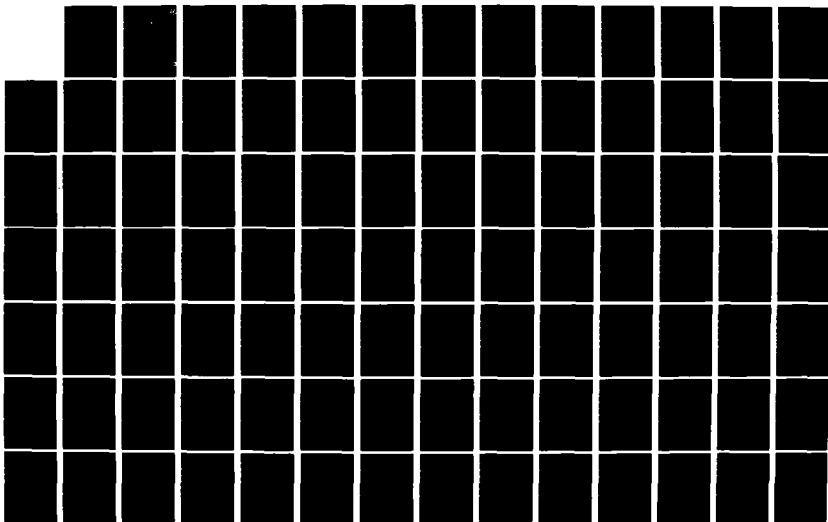
AD-A124 896

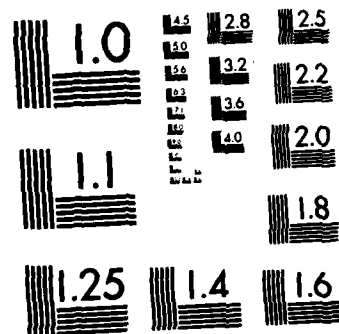
COMPUTATION OF INCOMPRESSIBLE POTENTIAL FLOW OVER AN  
AIRFOIL USING A HIGH. (U) AIR FORCE INST OF TECH  
WRIGHT-PATTERSON AFB OH SCHOOL OF ENGI.. J DEJONGH  
AUG 82 AFIT/DS/AR/82-1 F/G 12/1

1/3

UNCLASSIFIED

NL

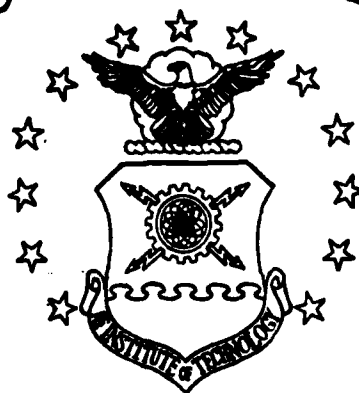




MICROCOPY RESOLUTION TEST CHART  
NATIONAL BUREAU OF STANDARDS-1963-A

AD A124896

# AIR FORCE INSTITUTE OF TECHNOLOGY



AIR UNIVEI SITY  
UNITED STATES , IR FORCE

COMPUTATION OF INCOMPRESSIBLE POTENTIAL  
FLOW OVER AN AIRFOIL USING A HIGH ORDER  
AERODYNAMIC PANEL METHOD BASED ON  
CIRCULAR ARC PANELS

DISSERTATION

AFIT/DS/AA/82-1

Jay DeJongh  
Major USAF

SCHOOL OF ENGINEERING

WRIGHT-PATTERSON AIR FORCE BASE, OHIO

DTIC  
ELECTE  
FEB 25 1983

D

DTIC FILE COPY

83 02 024 030

DISTRIBUTION STATEMENT A

AFIT/DS/AA/82-1

|                    |                                     |
|--------------------|-------------------------------------|
| Accession For      |                                     |
| NTIS GRA&I         | <input checked="" type="checkbox"/> |
| DTIC TAB           | <input type="checkbox"/>            |
| Unannounced        | <input type="checkbox"/>            |
| Justification      |                                     |
| By                 |                                     |
| Distribution/      |                                     |
| Availability Codes |                                     |
| Dist               | Avail and/or<br>Special             |
| A                  |                                     |



COMPUTATION OF INCOMPRESSIBLE POTENTIAL  
FLOW OVER AN AIRFOIL USING A HIGH ORDER  
AERODYNAMIC PANEL METHOD BASED ON  
CIRCULAR ARC PANELS

DISSERTATION

AFIT/DS/AA/82-1

Jay DeJongh  
Major USAF

Approved for public release; distribution unlimited.

UNCLASSIFIED

SECURITY CLASSIFICATION OF THIS PAGE (When Data Entered)

| REPORT DOCUMENTATION PAGE   |                                  | READ INSTRUCTIONS<br>BEFORE COMPLETING FORM   |
|---|----------------------------------|---|
| 1. REPORT NUMBER<br>AFIT/DS/AA/82-1   | 2. GOVT ACCESSION NO.<br>AD A224 | 3. RECIPIENT'S CATALOG NUMBER<br>896  |
| 4. TITLE (and Subtitle)<br>COMPUTATION OF INCOMPRESSIBLE POTENTIAL<br>FLOW OVER AN AIRFOIL USING A HIGH ORDER<br>AERODYNAMIC PANEL METHOD BASED ON<br>CIRCULAR ARC PANELS   |                                  | 5. TYPE OF REPORT & PERIOD COVERED<br>PhD Dissertation  |
| 7. AUTHOR(s)<br>Jay DeJongh<br>Major USAF   |                                  | 6. PERFORMING ORG. REPORT NUMBER  |
| 9. PERFORMING ORGANIZATION NAME AND ADDRESS<br>Air Force Institute of Technology (AFIT-EN)<br>Wright-Patterson AFB, Ohio 45433  |                                  | 8. CONTRACT OR GRANT NUMBER(s)  |
| 11. CONTROLLING OFFICE NAME AND ADDRESS   |                                  | 10. PROGRAM ELEMENT, PROJECT, TASK<br>AREA & WORK UNIT NUMBERS  |
| 14. MONITORING AGENCY NAME & ADDRESS (if different from Controlling Office)   |                                  | 12. REPORT DATE<br>August 1982  |
|   |                                  | 13. NUMBER OF PAGES<br>266  |
|   |                                  | 15. SECURITY CLASS. (of this report)<br>UNCLASSIFIED  |
|   |                                  | 15a. DECLASSIFICATION/DOWNGRADING<br>SCHEDULE   |
| 16. DISTRIBUTION STATEMENT (of this Report)<br><br>APPROVED FOR PUBLIC RELEASE; DISTRIBUTION UNLIMITED.   |                                  |   |
| 17. DISTRIBUTION STATEMENT (of the abstract entered in Block 20, if different from Report)  |                                  |   |
| 18. SUPPLEMENTARY NOTES<br>Approved for public release; IAW AFR 190-17<br><br>Frederick C. Lynch, Major, USAF, Director Public Affairs  |                                  | Approved for public release: IAW AFR 190-17.<br>LYNN E. WOLAVER<br>Dean for Research and Professional Development<br>Air Force Institute of Technology (AFIT)<br>Wright-Patterson AFB OH 45433<br>4 JAN |
| 19. KEY WORDS (Continue on reverse side if necessary and identify by block number)<br>Panel Method<br>Incompressible Flow<br>Airfoils<br>Source Distribution<br>Vortex Distribution<br>Potential Theory   |                                  |   |
| 20. ABSTRACT (Continue on reverse side if necessary and identify by block number)<br>A new two dimensional panel method has been developed. This method used a new approximating element; the circular arc, and a new singularity representation; the sine series, and all integrations are performed analytically for maximum computational efficiency. The method was applied to a circular cylinder and to several different types of airfoils, and a number of characteristics which define the method were varied to determine |                                  |   |

DD FORM 1 JAN 73 1473

EDITION OF 1 NOV 65 IS OBSOLETE

UNCLASSIFIED

SECURITY CLASSIFICATION OF THIS PAGE (When Data Entered)

their effect on the solution.

The body is represented by a series of circular arcs which are defined by sets of three points on the surface. The singularity distribution is modeled by a power series expansion in terms of the sine of an angular variable which is related to the arc length of each panel. The method was applied to the problem of flow over a circular cylinder, and characteristics which define the method were varied. Results indicated that accuracy was not significantly affected by the type of singularity, while dramatic reductions in velocity errors were achieved by increasing the number of terms in the singularity series. Further, increasing the number of panels also increased the accuracy of the solution; the effect of singularity continuity was more apparent in the smoothness of the resulting velocity distributions than in the accuracy of the solutions; the method was not critically sensitive to control point location; and the method was found to be computationally efficient as the number of terms in the series was increased.

The method was then applied to a Joukowski airfoil, a NACA 0024 airfoil, a thin symmetric airfoil, and to both a symmetric and a cambered Karman-Trefftz airfoil.

Major conclusions from this study were that the method produced very accurate solutions over the major part of the airfoil, error reduction occurred as both the number of panels and the number of terms in the series were increased, the effect of point source location was large but was local and could be controlled, the method was generally insensitive to minor variations in panelling, and the accuracy of the solution increased as panel curvature was increased from relatively flat to circular.

COMPUTATION OF INCOMPRESSIBLE POTENTIAL FLOW OVER AN AIRFOIL  
USING A HIGH ORDER AERODYNAMIC PANEL METHOD  
BASED ON CIRCULAR-ARC PANELS

by

Jay E. DeJongh, Maj, USAF

Approved:

Stephen J Koob 9 Aug 82  
Chairman Date

David A. Lee 9 August 82

Harold E. Wright 9 Aug 82

Michael Lyn Smith 9 Aug 82

Accepted:

J. Przemieniecki 10 Aug 82  
Dean, School of Engineering

COMPUTATION OF INCOMPRESSIBLE POTENTIAL  
FLOW OVER AN AIRFOIL USING A HIGH ORDER  
AERODYNAMIC PANEL METHOD BASED ON  
CIRCULAR ARC PANELS

DISSERTATION

Presented to the Faculty of the School of Engineering  
of the Air Force Institute of Technology  
Air University  
in Partial Fulfillment of the  
Requirements for the Degree of  
Doctor of Philosophy

by

Jay DeJongh B.S., M. Engin.

Major

USAF

Approved for public release; distribution unlimited



## ACKNOWLEDGMENTS

I would like to thank my advisor, Dr. Stephen Koob, for his help and advice in planning and developing this study, and for his constant encouragement during the course of its completion. In addition I would like to express gratitude to the members of my committee, Dr. Harold Wright, Dr. David Lee, and Major Michael Smith for their interest in and insights into this effort. I must also thank Dr. Thomas Weeks and Lt. Col. Lowell Keel of the Flight Dynamics Laboratory for their support during this investigation, and Mrs. Maripat Meer for her excellent typing services.

Finally, I wish to express my deepest appreciation to my wife, Candy, for her strong and unfailing support, encouragement, and motivation during the entire period of this study, and to my daughters Jenny and Julie, who were forced to sacrifice a large measure of normal family life in order that this work could be completed.

## Contents

|  |      |
|--|------|
| Acknowledgements . . . . .   | ii   |
| List of Figures . . . . .  | vi   |
| List of Tables . . . . .   | xi   |
| Notation . . . . .   | xii  |
| Abstract . . . . .   | xvii |
| I. Introduction . . . . .  | 1    |
| Linearized Potential Flow. . . . .   | 3    |
| Statement of the Problem . . . . .   | 5    |
| Literature Review. . . . .   | 12   |
| Two Dimensional Methods . . . . .  | 13   |
| Three Dimensional Methods . . . . .  | 16   |
| Objectives of Dissertation . . . . .   | 23   |
| II. Two Dimensional Potential Theory . . . . .   | 26   |
| Harmonic Functions . . . . .   | 26   |
| Green's Theorem Formulation. . . . .   | 27   |
| Velocity Potential. . . . .  | 30   |
| Stream Function . . . . .  | 32   |
| Doublet-Vorticity Sheet Equivalence . . . . .  | 33   |
| Singularity Behavior . . . . .   | 34   |
| Transfer of Boundary Conditions . . . . .  | 35   |
| Singularity behavior at Corners . . . . .  | 36   |
| Integral Equations - Existence and Uniqueness . . . . .                                      | 38   |
| Reduction of the Singularity Distribution Form-<br>ulation to an Integral Equation . . . . . | 40   |
| Surface Source Distribution . . . . .  | 40   |
| Conditions for Solvability. . . . .  | 43   |
| Surface Vorticity Distribution. . . . .  | 45   |
| III. Panel Method Approach. . . . .  | 51   |
| Surface Representation . . . . .   | 52   |
| Conic Arc Approximation . . . . .  | 53   |
| Circular Arc Approximation. . . . .  | 55   |
| Numerical Implementation. . . . .  | 57   |
| Singularity Representation . . . . .   | 61   |
| Series Expansion. . . . .  | 61   |
| Continuity Conditions . . . . .  | 64   |
| Boundary Conditions. . . . .   | 67   |
| Velocity Boundary Condition . . . . .  | 68   |
| Kutta Condition . . . . .  | 70   |

|     |   |     |
|-----|---|-----|
|     | Numerical Implementation . . . . .                | 74  |
|     | Matrix Equation Formulation . . . . .             | 74  |
|     | Method of Solution. . . . .                       | 75  |
| IV. | Application to the Circular Cylinder . . . . .    | 79  |
|     | Exact Solution . . . . .                          | 80  |
|     | Source Distribution . . . . .                     | 80  |
|     | Vorticity Distribution. . . . .                   | 83  |
|     | Combined Source/Vorticity Distribution. . . . .   | 87  |
|     | Panel Method Solution. . . . .                    | 89  |
|     | Results. . . . .                                  | 91  |
|     | Global Error. . . . .                             | 91  |
|     | Efficiency. . . . .                               | 102 |
|     | Local Error . . . . .                             | 104 |
|     | Parameter Study . . . . .                         | 116 |
|     | Combined Distribution . . . . .                   | 128 |
|     | Summary . . . . .                                 | 132 |
| V.  | Application to Airfoils. . . . .                  | 133 |
|     | Joukowski Airfoil. . . . .                        | 134 |
|     | Modeling. . . . .                                 | 135 |
|     | Results . . . . .                                 | 135 |
|     | NACA 0024 Airfoil. . . . .                        | 141 |
|     | Results . . . . .                                 | 141 |
|     | Thin Symmetrical Airfoil . . . . .                | 143 |
|     | Karman-Trefftz Airfoil . . . . .                  | 146 |
|     | Geometric Modeling. . . . .                       | 146 |
|     | Preliminary Results . . . . .                     | 150 |
|     | Detailed Parameter Studies. . . . .               | 156 |
|     | Effects of N and Q. . . . .                       | 156 |
|     | Effect of Point Source Location . . . . .         | 160 |
|     | Effect of Panel Geometry Characteristics. . . . . | 166 |
|     | Effect of Panel Curvature . . . . .               | 182 |
|     | Effect of Angle of Attack . . . . .               | 183 |
|     | Effect of Control Point Location. . . . .         | 190 |
|     | Effect of Camber. . . . .                         | 206 |
|     | Summary. . . . .                                  | 211 |
| VI. | Conclusions and Recommendations. . . . .          | 214 |
|     | Conclusions . . . . .                             | 214 |
|     | Recommendations. . . . .                          | 217 |

## List of Figures

| Figure  | Page |
|---|------|
| 1. Flow Over an Arbitrary Body . . . . .  | 6    |
| 2. Green's Theorem Formulation . . . . .  | 29   |
| 3. Doublet/Vortex Sheet Equivalence. . . . .  | 34   |
| 4. Properties of Singularity Sheets. . . . .  | 35   |
| 5. Behavior of a Source Sheet at a Corner. . . . .  | 37   |
| 6. Reduction to an Integral Equation . . . . .  | 41   |
| 7. Linear Approximating Elements . . . . .  | 54   |
| 8. Tangent - Normal Coordinate System . . . . .   | 54   |
| 9. Surface Coordinate Order of Input . . . . .  | 58   |
| 10. Circular Arc Panel Geometric Definition . . . . .   | 58   |
| 11. Curvature Effect on Panel Defining Geometry . . . . .   | 60   |
| 12. Circular Arc Panel Representation . . . . .   | 63   |
| 13. Kutta Condition Specification . . . . .   | 71   |
| 14. Control Point Spacing . . . . .   | 76   |
| 15. Flow Over a Circular Cylinder . . . . .   | 81   |
| 16. Internal Flow Patterns. . . . .   | 84   |
| 17. Circular Cylinder Paneling. . . . .   | 90   |
| 18. Maximum Absolute Normal Velocity Error on a Circle,<br>Source Distribution, Normal Velocity Boundary Con-<br>dition. . . . .    | 92   |
| 19. Maximum Absolute Tangential Velocity Error on a<br>Circle, Source Distribution, Normal Velocity,<br>Boundary Condition. . . . . | 93   |

|     |  |     |
|-----|--|-----|
| 20. | Maximum Absolute Normal Velocity Error on a Circle, Vortex Distribution, Normal Velocity Boundary Condition, $\Gamma=0$ . . . . .                  | 94  |
| 21. | Maximum Absolute Tangential Velocity Error on a Circle, Vortex Distribution, Normal Velocity Boundary Condition, $\Gamma=0$ . . . . .              | 95  |
| 22. | Maximum Absolute Normal Velocity Error on a Circle, Source and Vortex Distributions for Different QC Combinations. . . . .                         | 103 |
| 23. | Effect of Q on Normal Velocity Error for a Circle .  |     |
| a.  | QC = 10 . . . . .  | 105 |
| b.  | QC = 20 and QC = 30 . . . . .  | 106 |
| 24. | Effect of N on Normal Velocity Error for a Circle .  | 107 |
| 25. | Effect of C on Normal Velocity Error for a Circle  |     |
| a.  | QC = 20 and QC = 21 . . . . .  | 108 |
| b.  | QC = 30 and QC = 32 . . . . .  | 109 |
| 26. | Effect of Q on Tangential Velocity Error for a Circle  |     |
| a.  | QC = 10 . . . . .  | 110 |
| b.  | QC = 20 and QC = 30 . . . . .  | 111 |
| 27. | Effect of N on Tangential Velocity Error for a Circle . . . . .  | 112 |
| 28. | Effect of C on Tangential Velocity Error for a Circle  |     |
| a.  | QC = 20 and QC = 21 . . . . .  | 113 |
| b.  | QC = 30 and QC = 32 . . . . .  | 114 |
| 29. | Effect of Control Point Location on Maximum Absolute Velocity Error for Circle, Source Distribution with Different QC Combinations, and with N=16. |     |
| a.  | Normal Velocity Error . . . . .  | 118 |
| b.  | Tangential Velocity Error . . . . .  | 119 |
| 30. | Comparison of Effect of Control Point Location on Maximum Absolute Normal and Tangential Velocity Error for a Circle. . . . .                      | 121 |
| 31. | Effect of Varying Two Control Points on Absolute Velocity Error for a Circle . . . . .   | 122 |

|     |  |     |
|-----|--|-----|
| 32. | Effect of Control Point Location on Normalized Maximum Velocity Error for a Circle, Source Distribution, $N=16$      |     |
| a.  | Normal Velocity, 1 Control Point Cases. . . . .  | 123 |
| b.  | Tangential Velocity, 1 Control Point Cases. . . . .  | 124 |
| c.  | Normal Velocity, Remaining Cases. . . . .  | 125 |
| d.  | Tangential Velocity, Remaining Cases. . . . .  | 126 |
| 33. | Maximum Absolute Error in Normal Velocity for a Circle, Source/Vortex Combination with $\Gamma=0$ . . . . .          | 130 |
| 34. | Maximum Absolute Error in Tangential Velocity for a Circle, Source/Vortex Combination with $\Gamma=0$ . . . . .      | 131 |
| 35. | Comparison of Panel Model with Actual Surface for a Joukowski Airfoil  |     |
| a.  | $N=30$ Elements . . . . .  | 136 |
| b.  | $N=10$ Elements . . . . .  | 136 |
| 36. | Pressure Coefficient Sensitivity to $N$ for a Joukowski Airfoil, $QC=10$ , Source Distribution . . . . .             | 137 |
| 37. | Pressure Coefficient Sensitivity to $N$ for a Joukowski Airfoil, $QC=20$ , Source Distribution . . . . .             | 138 |
| 38. | Pressure Coefficient Sensitivity to Panel Curvature for a Joukowski Airfoil, $QC=10$ , Source Distribution . . . . . | 139 |
| 39. | Pressure Coefficient Sensitivity to Panel Curvature for a Joukowski Airfoil, $QC=20$ , Source Distribution . . . . . | 140 |
| 40. | Tangential Velocity Comparisons for the NACA 0024 Airfoil . . . . .  | 142 |
| 41. | Perturbation Velocity on a thin Symmetrical Airfoil . . . . .  | 144 |
| 42. | Karman-Trefftz Airfoil Modeled with 45 panels . . . . .  | 147 |
| 43. | Surface Points for Velocity Error Comparison. . . . .  | 149 |
| 44. | Karman-Trefftz Airfoil, Successful Cases, Source Distribution. . . . .   | 153 |
| 45. | Karman-Trefftz Airfoil, Successful Cases, Vortex Distribution. . . . .   | 153 |
| 46. | Karman-Trefftz Airfoil, Unsuccessful Cases, Source Distribution. . . . .   | 154 |

|     |   |     |
|-----|---|-----|
| 47. | Effect of N on Tangential Velocity Error, QC=21,<br>for a Karman-Trefftz Airfoil                |     |
| a.  | $\alpha = .0$   | 157 |
| b.  | $\alpha = .1$ radians, Upper Surface  | 158 |
| c.  | $\alpha = .1$ radians, Lower Surface  | 159 |
| 48. | Effect of Q on Tangential Velocity Error for a<br>Karmon-Trefftz Airfoil.                       | 161 |
| 49. | Effect of N on Source Induced Tangential Velocity<br>Error for a Karman-Trefftz Airfoil.        | 160 |
| 50. | Effect of Point Source Location on Tangential<br>Velocity Error for a Karman-Trefftz Airfoil    |     |
| a.  | QC=21   | 163 |
| b.  | QC=31   | 164 |
| 51. | Paneling Geometric Characteristics for a Karman-<br>Trefftz Airfoil                             |     |
| a.  | Panel Subtended Angle   | 168 |
| b.  | Panel Radius.   | 169 |
| c.  | Panel Arc Length.   | 170 |
| 52. | Comparison of Panel Model with Actual Surface for a<br>Karman-Trefftz Airfoil                   |     |
| a.  | Paneling = 45.101   | 171 |
| b.  | Paneling = 45.102   | 172 |
| c.  | Paneling = 45.103   | 173 |
| d.  | Paneling = 49.101   | 174 |
| 53. | Effect of Paneling Characteristics on Tangential<br>Velocity Error for a Karman-Trefftz Airfoil |     |
| a.  | QC=21, $\alpha = .0$ radians  | 175 |
| b.  | QC=31, $\alpha = .0$ radians  | 176 |
| c.  | QC=21, $\alpha = .1$ radians, Upper Surface.  | 177 |
| d.  | QC=21, $\alpha = .1$ radians, Lower Surface.  | 178 |
| e.  | QC=31, $\alpha = .1$ radians, Upper Surface.  | 179 |
| f.  | QC=31, $\alpha = .1$ radians, Lower Surface.  | 180 |
| 54. | Effect of Panel Curvature on Tangential Velocity<br>Error for a Karman-Trefftz Airfoil          |     |
| a.  | QC=21, $\alpha = .0$ radians  | 184 |
| b.  | QC=21, $\alpha = .1$ radians, Upper Surface.  | 185 |
| c.  | QC=21, $\alpha = .1$ radians, Lower Surface.  | 186 |
| d.  | QC=31, $\alpha = .0$ radians  | 187 |
| e.  | QC=31, $\alpha = .1$ radians, Upper Surface.  | 188 |
| f.  | QC=31 $\alpha = .1$ radians, Lower Surface.   | 189 |

|     |   |     |
|-----|---|-----|
| 55. | Effect of Angle of Attack on Lift Coefficient for a Karman-Treffitz Airfoil. . . . .                          | 191 |
| 56. | Effect of Angle of Attack on Lift Coefficient Error for a Karman-Treffitz Airfoil. . . . .                    | 192 |
| 57. | Effect of Control Point Location and Slope on Tangential Velocity Error for a Karman-Treffitz Airfoil, $N=9$  |     |
| a.  | QC=21, $\alpha = .0$ radians . . . . .  | 194 |
| b.  | QC=31, $\alpha = .0$ radians . . . . .  | 195 |
| c.  | QC=21, $\alpha = .1$ radians, Upper Surface. . . . .  | 196 |
| d.  | QC=21, $\alpha = .1$ radians, Lower Surface. . . . .  | 197 |
| e.  | QC=31, $\alpha = .1$ radians . . . . .  | 198 |
| 58. | Effect of Control Point Location and Slope on Tangential Velocity Error for a Karman-Treffitz Airfoil, $N=10$ |     |
| a.  | QC=21, $\alpha = .0$ radians . . . . .  | 199 |
| b.  | QC=31, $\alpha = .0$ radians . . . . .  | 200 |
| c.  | QC=21, $\alpha = .1$ radians, Upper Surface. . . . .  | 201 |
| d.  | QC=21, $\alpha = .1$ radians, Lower Surface. . . . .  | 202 |
| e.  | QC=31, $\alpha = .1$ radians . . . . .  | 203 |
| 59. | Error in Surface Slope at Computed Control Points for a Karman-Treffitz Airfoil. . . . .                      | 205 |
| 60. | Tangential Velocity Error for a Cambered Karman-Treffitz Airfoil . . . . .                                    |     |
| a.  | QC=21, $\alpha = .0$ radians . . . . .  | 207 |
| b.  | QC=21, $\alpha = .1$ radians . . . . .  | 208 |
| c.  | QC=31, $\alpha = .0$ radians . . . . .  | 209 |
| d.  | QC=31, $\alpha = .1$ radians . . . . .  | 210 |
| 61. | Panel Influence at a Point P . . . . .  | 233 |
| 62. | Limiting Behavior as $P(r, \theta)$ goes to $P(a, \theta)$ . . . . .  | 243 |
| 63. | Reverse Curvature Formulation . . . . .   | 243 |



### List of Tables

|       |   |     |
|-------|---|-----|
| I.    | Two-Dimensional Panel Methods . . . . .                         | 14  |
| II.   | Three-Dimensional Panel Methods . . . . .                       | 17  |
| III.  | Boundary Value Problem Solutions . . . . .                      | 28  |
| IV.   | Definition of Continuity Parameter C . . . . .                  | 65  |
| V.    | Fixed Control Point Location . . . . .                          | 117 |
| VI.   | Maximum Absolute Normal and Tangential Velocities               | 127 |
| VII.  | Paneling Nomenclature . . . . .                                 | 148 |
| VIII. | Preliminary Results for the Karman-Trefftz<br>Airfoil . . . . . | 150 |
| IX.   | Form of $e_i$ , $i = 1, \dots, N$ . . . . .                     | 230 |
| X.    | Form of $f_i$ , $i = 1, \dots, N$ . . . . .                     | 231 |

## NOTATION

### Symbols

|                             |  |
|-----------------------------|--|
| $a$                         | Radius of a circle, or a constant  |
| $A$                         | Constant   |
| $b$                         | Boundary curve, or a constant  |
| $B$                         | Boundary curve, or a constant  |
| $c$                         | Constant   |
| $C$                         | Continuity parameter   |
| $C_L$                       | Lift Coefficient   |
| $C_p$                       | Pressure Coefficient   |
| $[C_k^C]$                   | Continuity coefficient matrix  |
| $d$                         | Non dimensional radius   |
| $D$                         | Constant   |
| $e$                         | Constant   |
| $e_i$                       | Element of the continuity coefficient matrix   |
| $\hat{e}_r, \hat{e}_\theta$ | Unit vectors in polar coordinate system  |
| $\epsilon$                  | Constant   |
| $E_c, E_e, E_f, E_p$        | Approximating error for a circular, elliptic, flat and parabolic element, respectively |
| $E_{QC}$                    | Error for the QC case  |
| $f(s)$                      | Known function   |
| $f_i$                       | Element of continuity coefficient matrix   |
| $f_k$                       | Known function   |
| $F$                         | Constant   |

|                 |  |
|-----------------|--|
| $F_1, F_2$      | Functions from influence coefficient integration           |
| $K(x,y)$        | Kernel function of integral equation                       |
| $K_s$           | Source kernel function in two dimensions                   |
| $l$             | Integration variable                                       |
| $\ell$          | Parameter used to define panel curvature                   |
| $L$             | Number of control point per panel                          |
| LE              | Leadding edge of airfoil                                   |
| $n$             | Normal to a surface  |
| $N$             | Number of panels   |
| $p, P$          | Field points   |
| $P_M$           | Control point on a panel                                   |
| $P_S$           | Surface point associated with $P_M$                        |
| $\hat{p}$       | Coordinate used in reverse curvature formulation           |
| $q$             | Field point  |
| $q_k$           | Unknown singularity strength                               |
| $Q$             | Number of terms in singularity series                      |
| $Q_S$           | Total source strength                                      |
| $[Q_k]$         | Column vector of unknowns                                  |
| $r$             | Distance between two points                                |
| $r_c, r_e, r_p$ | Equations of a circle, ellipse, and parabola, respectively |
| $R$             | Region   |
| $[R_k]$         | Normal velocity aerodynamic influence coefficient matrix   |
| $s$             | Integration variable, or arc length                        |

|                          |  |
|--------------------------|--|
| $S$                      | Surface  |
| $t$                      | Unknown error in normal velocity                             |
| $t/c$                    | Thickenss to chord ratio                                     |
| $\{T\}$                  | Vector of unknown errors in normal velocity                  |
| $\hat{T}$                | Coordinate used in reverse curvature formulation             |
| $[T_k]$                  | Tangential velocity aerodynamic influence coefficient matrix |
| $TE$                     | Trailing edge of airfoil                                     |
| $u(x)$                   | Eigenfunction of integral equation                           |
| $v$                      | Perturbation velocity  |
| $V$                      | Total velocity   |
| $w$                      | Integration variable   |
| $w(x)$                   | Eigenfunction of integral equation                           |
| $W$                      | Denominator in equation for circle, or integration variable  |
| $x, y, z$                | Coordinates  |
| $x/c, y/c$<br>$X/c, V/c$ | Nondimensional airfoil coordinates                           |
| $X_s$                    | Point source location  |

#### Greek Symbols

|                      |  |
|----------------------|--|
| $\alpha$             | Angle of attack                                    |
| $\beta$              | Panel curvature                                    |
| $\Gamma$             | Circulation  |
| $\gamma$             | Vorticity strength                                 |
| $\gamma_u, \gamma_l$ | Vorticity on upper and lower surface, respectively |
| $\delta$             | Half angle of a panel                              |

|                                |   |
|--------------------------------|---|
| $\epsilon$                     | Positive constant, or small angle   |
| $\xi$                          | Coordinate for approximating curve  |
| $\xi_c, \xi_e, \xi_f, \xi_p$   | Equation for a circular, elliptic, flat, and parabolic segment, respectively            |
| $\theta$                       | Angular variable  |
| $\theta_1, \theta_M, \theta_2$ | Angular coordinate of initial point, mid point, and end point, respectively, on a panel |
| $\theta_S$                     | Angular position of rear stagnation point   |
| $\lambda$                      | Parameter in integral equation  |
| $\mu$                          | Doublet strength  |
| $\xi$                          | Coordinate for approximating curve  |
| $\sigma$                       | Source strength   |
| $\phi$                         | Perturbation velocity potential   |
| $\psi$                         | Perturbation stream function  |
| $\Psi$                         | Total stream function   |

#### Superscripts

|                                    |  |
|------------------------------------|--|
| $(\vec{\phantom{x}})$              | Vector quantity                          |
| $(\phantom{x})^+, (\phantom{x})^-$ | Opposite sides of a surface              |
| $(\phantom{x})^n$                  | $n^{\text{th}}$ derivative of a function |

#### Subscripts

|      |  |
|------|--|
| comp | Computed   |
| e    | Exterior side of a surface                       |
| er   | Error  |
| ex   | Exact  |
| h    | Index  |
| i    | Interior side of a surface, or refers to panel i |

|          |                                  |
|----------|----------------------------------|
| j        | Refers to panel j                |
| k        | Index                            |
| m        | Index                            |
| n        | Normal direction                 |
| p,q      | Conditions at these field points |
| r        | r direction                      |
| rel      | Relative                         |
| s        | Source                           |
| t        | Tangential direction             |
| v        | Vortex                           |
| $\theta$ | $\theta$ direction               |
| $\infty$ | Free stream conditions           |

Prefix

|                               |  |
|-------------------------------|--|
| $\frac{\partial}{\partial n}$ | Derivative in the normal direction     |
| $\frac{\partial}{\partial t}$ | Derivative in the tangential direction |

## ABSTRACT

A new two dimensional panel method has been developed. This method uses a new approximating element; the circular arc, and a new singularity representation; the sine series, and all integrations are performed analytically for maximum computational efficiency. The method was applied to a circular cylinder and to several different types of airfoils, and a number of characteristics which define the method were varied to determine their effects on the solution.

The body is represented by a series of circular arcs which are defined by sets of three points on the surface. The singularity distribution is modeled by a power series expansion in terms of the sine of an angular variable which is related to the arc length of each panel. The method was applied to the problem of flow over a circular cylinder, and characteristics which define the method were varied. Results indicated that accuracy was not significantly affected by the type of singularity, while dramatic reductions in velocity errors were achieved by increasing the number of terms in the singularity series. Further, increasing the number of panels also increased the accuracy of the solution, the effect of singularity continuity was

more apparent in the smoothness of the resulting velocity distributions than in the accuracy of the solutions, the method was not critically sensitive to control point location, and the method was found to be computationally efficient as the number of terms in the series was increased.

The method was then applied to a Joukowski airfoil, a NACA 0024 airfoil, a thin symmetric airfoil, and to both a symmetric and a cambered Karman-Trefftz airfoil.

Major conclusions from this study were that the method produced very accurate solutions over the major part of the airfoil, error reduction occurred as both the number of panels and the number of terms in the series were increased, the effect of point source location was large but was local and could be controlled, the method was generally insensitive to minor variations in panelling, and the accuracy of the solution increased as panel curvature was increased from relatively flat to circular.



COMPUTATION OF INCOMPRESSIBLE POTENTIAL  
FLOW OVER AN AIRFOIL USING A HIGH ORDER  
AERODYNAMIC PANEL METHOD BASED ON  
CIRCULAR ARC PANELS

I. Introduction

The central problem in aerodynamics is to predict the pressures, forces, and moments exerted on a body immersed in a flowing fluid. One would like to be able to solve the full Navier-Stokes equations for any configuration at one's desk, but this is not possible today. Fortunately the real needs of the engineering, research, and development community both in the Air Force and in industry allow this problem to be approached from several different levels. At one level is the engineer who requires the details of a full viscous solution, and is willing to spend the time and computer resources required, and to accept the limitations in geometric complexity which in some cases are necessary, in order to obtain solutions of this nature. At the other extreme is the engineer involved in perhaps a preliminary design application. His requirement is for very rapid solutions for general configurations which can be used to develop airfoil or aircraft performance characteristics. He

might also require the capability for rapid development of parametric studies to assess effects of small changes in geometry or flight conditions on the flow over an airfoil, a wing, or a full aircraft configuration.

While it is true that much progress has been made over the last several years in the development of both Navier-Stokes solutions and non-linear potential solutions, these areas cannot as yet satisfy the engineering requirements described above. For this reason much interest and attention has been (and continues to be) focused on the development and improvement of linear potential flow solutions in general, and in the panel method approach to obtaining such solutions in particular. The features of the panel method approach which make it particularly attractive are its computational efficiency, and its ability to accommodate accurate geometric modeling. In addition, it has been found that the linear potential flow model provides sufficient accuracy for many engineering applications, and indeed the panel method approach is used on a daily basis by industry and government workers to solve a wide variety of two and three dimensional aerodynamic problems.

Given the unquestioned value and utility of the panel method approach to solving the linear potential flow problem, the general goal of this dissertation, which will be discussed further in this chapter, is to develop and investigate a particular panel method approach in order to

add to the level of understanding of such methods. The purpose of this chapter, then, is to review the importance of this theory and discuss the assumptions which led to it; to formulate the mathematical statement of potential flow over a body; to review and note limitations of current methods for solving this problems; and to present the objective of this dissertation.

### Linearized Potential Flow

The ability of the linearized potential flow equation to accurately model flow fields about realistic flight vehicle configurations over a wide range of realistic flight conditions is well known to aerodynamicists. These results are used in two ways. First, they can predict lift, moments, and induced drag for complex vehicles, and second, they can be used as input to boundary layer calculations which will predict friction drag and separation. In fact, the accuracy of boundary layer calculations is generally dependent on the accuracy of the input potential flow solution.

The basic assumptions leading to potential flow are that the fluid is inviscid, non-heat conducting, isentropic, and irrotational. The success of the theory lies in the fact that for the flow of air over a body the effects of viscosity and heat transfer are confined to the boundary

applicable, and in fact form the basis of the solution method to be used in this study.

A crucial step in the solution of Laplace's equation is the application of boundary conditions. In small disturbance theory the boundary conditions are often applied on a plane rather than on the actual surface of the configuration. Although this linearization of the boundary conditions is justified if the body is thin and if the angle of attack is small, it produces a non-physical singularity at the airfoil leading edge. This singularity can be removed, however, by applying the boundary conditions on the actual surface of the configuration, even though the governing equation was derived using small perturbation assumptions. This ability to apply boundary conditions exactly and in a convenient way is an important feature of the panel method approach to solving the potential flow problem.

#### Statement of the Problem

The mathematical problem of potential flow about the exterior of a body may be formulated in the following manner. Consider a closed surface,  $S$ , (Figure 1) immersed in a flow with free stream velocity  $\vec{V}_\infty$ . Let

$$\vec{V} = \vec{V}_\infty + \vec{v} \quad (3)$$

where  $\vec{V}$  is the total velocity and  $\vec{v}$  is a perturbation

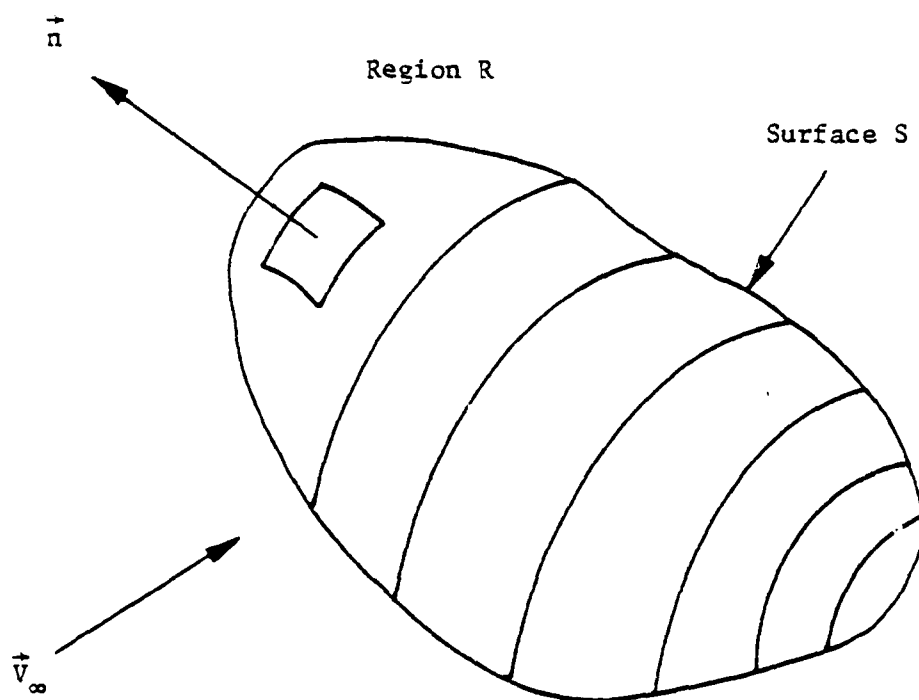


Figure 1 - Flow Over an Arbitrary Body

velocity. Now  $\vec{v}$  is irrotational; therefore

$$\vec{v} = \nabla \phi \quad (4)$$

where  $\phi$  is the perturbation potential. Assuming  $M_\infty = 0$  for convenience, the governing equation for the flow becomes

$$\nabla^2 \phi = 0 \quad (5)$$

in the region exterior to  $S$ . The boundary conditions for this problem are that the surface is impermeable, and the perturbation velocities are zero at infinity. That is,

$$|\nabla \phi| \rightarrow 0 \text{ at infinity} \quad (6a)$$

$$\nabla \phi \cdot \vec{n} + \vec{V}_\infty \cdot \vec{n} = 0 \text{ on } S \quad (6b)$$

where  $\vec{n}$  is the outward surface normal vector on  $S$ . Once a solution for  $\phi$  is determined, the pressure on  $S$  is found from Bernoulli's equation as

$$C_p = 1 - \frac{|\vec{v}|^2}{|V_\infty|^2} \quad (7)$$

Many approaches have been used to solve the problem posed in equations five and six, including conformal mapping, finite difference, finite element, and singularity methods. Conformal mapping methods (Refs 3,4) have been used to obtain accurate solutions in two dimensional cases,

but they can not be extended to three dimensions. The problem with using a conformal mapping approach is the generation of mappings for arbitrary shapes.

There are many finite difference methods (Refs 5,6,7,8) which solve the exterior potential flow problem, but they are usually applied to the linear one represented by Eq 5. These methods use transformations to map the physical space into a computational space in which boundary conditions can be applied with less difficulty. Results for general two dimensional shapes have been obtained, but the methods have only limited ability to handle complex three dimensional geometry. Disadvantages of finite difference methods as applied to either the linear or non-linear problem are that the solution must be found throughout the entire flow field and that computer time and storage requirements are large (even in two dimensions).

A newer approach is the finite element technique (Refs 9,10,11). Developed initially as a structural analysis tool, there has been considerable application of the method to fluid dynamics problems. It has had, however, relatively little application to problems involving complex geometric configurations, and shares with finite difference methods both the disadvantage of requiring a solution throughout the flow field, and the advantage of being applicable to the non-linear formulation of the problem.

Finally, singularity methods have been used for many

a plane surface (for example, the camber line of a wing or airfoil) with no thickness to model the desired configuration.

Compared to a discrete singularity method, a panel method (or actually any distributed singularity method) has advantages which are related to the order of the singularity. One cannot compute flow quantities at a point singularity because they are mathematically undefined there. One can, however, make such computations on a panel containing a distributed singularity, except at the endpoints of the panel where the flow quantities are again singular. However, this singularity is of a lower order than the point singularity. This means that for a given level of accuracy one can perform computations closer to the endpoints of the distributed singularity panel than one can to the point singularity. This is important because most configurations of interest contain regions where one part of the surface is near another part of the surface. An example would be the upper and lower surfaces at the trailing edge of a wing or airfoil.

Compared to finite difference (FD) and finite element (FE) methods, panel methods may require less computer resources for a given configuration and level of accuracy. The reason for this is that to solve a three dimensional problem, the FD or FE method must solve a partial differential equation in three independent variables.



a plane surface (for example, the camber line of a wing or airfoil) with no thickness to model the desired configuration.

Compared to a discrete singularity method, a panel method (or actually any distributed singularity method) has advantages which are related to the order of the singularity. One cannot compute flow quantities at a point singularity because they are mathematically undefined there. One can, however, make such computations on a panel containing a distributed singularity, except at the endpoints of the panel where the flow quantities are again singular. However, this singularity is of a lower order than the point singularity. This means that for a given level of accuracy one can perform computations closer to the endpoints of the distributed singularity panel than one can to the point singularity. This is important because most configurations of interest contain regions where one part of the surface is near another part of the surface. An example would be the upper and lower surfaces at the trailing edge of a wing or airfoil.

Compared to finite difference (FD) and finite element (FE) methods, panel methods may require less computer resources for a given configuration and level of accuracy. The reason for this is that to solve a three dimensional problem, the FD or FE method must solve a partial differential equation in three independent variables.

This requires generation of a mesh of grid points which fills the volume of the flow field. To solve the same problem, the panel method must solve a two dimensional integral equation. This requires generation of a mesh of grid points only on the surface of the configuration. In effect, the dimension of the problem that must be solved has been reduced by one. This reduction also occurs if the original problem is that once the panel method solution has been obtained, the flow quantities can be determined at any other point in the flow field by a simple matrix multiplication. This is in contrast to the FD or FE methods for which the solution in the flowfield is computed certainly only at the grid points used to obtain it. One could, of course, interpolate these values, but to obtain velocities, for example, from a solution for potential, one would have to use a numerical differentiation scheme of some sort which would introduce additional inaccuracy into the result.

Another advantage of the panel method compared to a FD method is that the panel method can often model complicated geometries more easily. The reason for this is that FD methods often require a coordinate system which is fitted to the configuration surface in order to simplify application of boundary conditions. Generation of this coordinate system can in itself require the numerical solution of a set

of partial differential equations. The panel method, however, requires only the surface geometry as input.

Although the advantages of panel methods as described above are important, it must be remembered that the method gives a linearized potential flow solution to a given problem. Both FD and FE methods are applicable to the non-linear problem (potential and non-potential) as well. There are many situations in which a non-linear solution about a simplified configuration is more useful than a linearized potential flow solution about a more detailed and exact geometric representation of the configuration. Conversely, it is also true that there are a great many applications for which the linearized potential flow solution is satisfactory and in these cases its characteristics of geometric complexity and computational efficiency are highly desirable.

#### Literature Review

The basic theory behind the use of a panel method to solve the potential flow problem (a review of which is given by Hess, Ref. 12) was developed from the principles of potential theory (Ref. 13,14). The practical application of the method was not feasible, however, until the digital computer became available. Since the early 1960's work in this area has increased greatly from initial efforts at computing axisymmetric and non-lifting three dimensional

flow, through higher order lifting two dimensional flow, and lifting three dimensional flow, to the present day where complex configurations are being calculated in supersonic flow. This review will cover the major two dimensional panel methods available today, followed by a discussion of representative three dimensional work, and will conclude with a summary of limitations in the methods available at the present time.

Two Dimensional Methods. A large number of two dimensional methods have been developed over the past several years. Since many of them are similar in concept, a representative sample illustrative of different approaches has been selected for discussion. Table I presents some general characteristics and unique features of these methods.

Hess's low order method (Ref 18) used constant source and vorticity distributions on flat panels. His higher order method (Ref 15,16) models the surface as a series expansion, truncated such that the representation is parabolic, while the integrand in the velocity influence integral is expanded in a series that assumes the surface is nearly flat. The method also used source and vorticity distributions in which the vorticity is assumed to vary parabolically in arc length from the trailing edge of the airfoil through the leading edge and back to the trailing edge where it is zero. The higher order method shows

TABLE 1. Two-Dimensional Panel Methods

| Method               | Refs  | Singularity                               | Paneling                             | Boundary Cond.          | Integration | Mach Range     | Comments                                      |
|----------------------|-------|---|--------------------------------------|-------------------------|-------------|----------------|---|
| Douglas<br>(Hess)    | 15-18 | Linear Source<br>Parabolic<br>Vorticity   | Parabolic<br>(series ex-<br>pansion) | Velocity                | Analytic    | Incompressible |   |
| Douglas<br>(Bristow) | 29-31 | Linear<br>Vorticity<br>Constant<br>Source | Parabolic<br>(series ex-<br>pansion) | Interior<br>Potential   | Analytic    | Incompressible | Kutta Condi-<br>tion uses Error<br>Parameter. |
| Henshaw              | 19-28 | Linear Source<br>Parabolic<br>Vorticity   | Quartic<br>(series ex-<br>pansion)   | Velocity                | Numerical   | Incompressible | Kutta Condi-<br>tion uses Error<br>Parameter  |
| Keller               | 33    | Linear Source<br>Linear<br>Vorticity      | Numerical<br>Repre-<br>sentation     | Velocity &<br>Potential | Numerical   | Incompressible | Uses Conformal<br>Mapping.                    |
| Raj                  | 32    | Linear<br>Vorticity                       | Numerical<br>Representa-<br>tion.    | Velocity                | Numerical   | Incompressible |   |

increased accuracy over the lower order method, particularly for internal flows.

Henshaw (Refs 19-28) has developed a variant of Hess's higher order method which used a quartic polynomial representation of the surface, and which expands the velocity influence integrand about a circular arc rather than about a flat panel. He reports an improved accuracy with this formulation but his results are difficult to interpret. Henshaw has also formulated an approach using vorticity only, with an error parameter which allows specification of circulation. This parameter is added to the left hand side of the boundary condition equations with a coefficient which is specified according to certain criteria.

Bristow (Refs 29-31), using Hess's basic as well as his higher order method has formulated two interesting approaches to the problem. Using the basic method, he has incorporated a singularity strength minimization procedure which reduces source strength gradients, and thus errors in tangential velocities. Using the higher order method, his formulation allows a priori determination of the source strengths, coupled with an error parameter approach to obtaining the vorticity strengths. The second method also produces singularity strengths with mild gradients and good accuracy, but at lower computing cost than the first. Both

of these methods have a design capability as well.

The methods of Raj (Ref 32) and Keller (Ref 34) provide different approaches. Raj used a piecewise linear vorticity distribution on a surface described numerically, and all the integrations are performed numerically in the physical airfoil plane. His results are accurate, but the method is time consuming. Keller's approach is to generate a transformation which maps an airfoil into a near circle. He then performs all integrations numerically in the circle plane. This is advantageous because the integrals are easier to integrate numerically on a circular or nearly circular surface than on an arbitrary surface. This method is not, however, extendable to three dimensions.

Three Dimensional Methods. A significant amount of work has been done in the area of three dimensional panel methods. Characteristics of the more important of these are shown in Table II. These methods will be discussed further in the following.

Hess's method (Refs 18,34,35) was the first surface paneling method applicable to arbitrary geometries. It is an incompressible method which uses flat panels to model a configuration. Constant sources are used on body panels while constant vorticity is used on wing panels. The wing panels are lumped into chordwise strips over which a parabolic distribution of vorticity is placed, so that only one vorticity unknown is associated with each strip. A

Table II. Three-Dimensional Panel Methods

| Method         | Refs  | Singularity                                 | Paneling                  | Bound. Cond.          | Integration | Mach Range              | Comments                                      |
|----------------|-------|---|---------------------------|-----------------------|-------------|-------------------------|---|
| Douglas (Hess) | 34-36 | Linear Source<br>Parabolic<br>Vorticity     | Flat/Para-<br>bolic       | Velocity              | Analytic    | Subsonic                | Parabolic Paneling for<br>Non Lifting Case    |
| Roberts        | 40-42 | Quadratic<br>Source<br>Quadratic<br>Doublet | Parabolic                 | Velocity              | Numerical   | Subsonic                |   |
| Woodward       | 37-39 | Linear Source<br>Linear<br>Vorticity        | Flat                      | Velocity              | Analytic    | Subsonic/<br>supersonic | Kutta Condition uses<br>Interior Point Source |
| Morino         | 43-45 | Constant<br>Source                          | Hyper-<br>boloidal        | Interior<br>Potential | Analytic    | Subsonic/<br>Supersonic | Unsteady Method                               |
| Doering        | 46-52 | Linear<br>Source<br>Quadratic<br>Doublet    | Flat<br>(Contin-<br>uous) | Interior<br>Potential | Analytic    | Subsonic/<br>Supersonic |   |



Kutta condition is applied at the trailing edge of each strip to obtain this unknown, while the source unknowns are found by applying a normal velocity boundary condition on each panel. Hess has also developed a higher order three dimensional method (Ref 36) which is basically an extension of his two dimensional work. The new method has shown an improved accuracy for a given number of panels, but is at present a non-lifting method.

Woodward's basic method (Ref 37) was the first unified (subsonic and supersonic) method for general configurations. It modeled a surface with flat panels, which were not necessarily contiguous. Linear sources and constant vorticity were distributed on the panels to account for lift effects and line sources and doublets provided body thickness effects. A normal velocity boundary condition was applied at a control point whose location was chosen so as to provide the best results. This method was successful, but was limited in the degree of geometric complexity that it could model, and was sensitive to control point placement.

In 1973 an improved version of the method (Ref 38) was presented which retained a flat panel surface representation but used linear source and linear vorticity singularities, and which had planar and non-planar boundary condition options. Linear sources were distributed on body surface

panels for both options, while on wing panels the planar option used linear source and vorticity distributions, and the non-planar option used only linear vorticity. A normal velocity boundary condition was applied at a control point located at a panel centroid. This method allowed more accurate modeling of body shapes and exhibited reduced sensitivity to control point location. There was a difficulty, however, in using the non-planar option in supersonic flow because the panels exhibited discontinuities in slope and position. This caused disturbances to propagate downstream inside the configuration being modeled (that is, in the non-physical interior flow) in such a way as to eventually destroy the solution on the exterior of the body.

Woodward has recently developed a solution to this problem (Ref 39) using a combined source and vortex called a triplet singularity. This singularity controls the interior flow by cancelling perturbation velocities there without explicitly applying boundary conditions in the interior region. This approach has shown good results when applied to bodies, but has yet to be applied to wings, or more general configurations.

Robert's method (Refs 40-42) uses surface sources and internal doublet sheets to compute subsonic flow about general configurations. The surface is mapped to a parametric plane where it is represented as a bicubic

spline, and the singularity distributions are modeled as bicubic splines on this surface. This approach is capable of yielding very accurate solutions, but all the mappings and the integrations of the influence coefficients are done numerically; thus an extremely large amount of computer time is required to obtain a solution. For this reason the method has not been widely used.

Morino's method (Refs 43-45) is a general method for unsteady subsonic or supersonic flow over arbitrary configurations. It uses constant source and doublet distributions on hyperboloidal surface panels, with an interior potential boundary condition. Preliminary results using this method seem to be good, but it has not been tested extensively to date. It should be emphasized that the method was developed to solve the general unsteady problem, and is perhaps the most advanced in this area.

Over the past ten years, researchers at the Boeing Company have developed a general subsonic and supersonic method applicable to arbitrary configurations. The method has evolved from a low order subsonic method to a higher order supersonic method known as the PANAIR (Paneling Aerodynamics) system. In 1967 Rubbert et al (Ref 46) described a subsonic method using flat panels with a surface distribution of constant sources, and an interior doublet distribution. The method produced good results, but the use

of the internal lifting system, coupled with the use of flat panels limited the degree of geometric complexity which could be easily and accurately modeled.

In 1972 Rubbert and Saaris (Ref 47) presented additional results using the same basic method, but with the addition of internal singularity sheets which were used to maintain an internal flow which (although of no physical interest) would improve the external flow characteristics. This method was sensitive to the paneling arrangement since it was a low order method.

To correct some of these problems, Johnson and Rubbert (Ref 48) developed a higher order subsonic method. Key features were the use of linear sources and quadratic doublets distributed on curved panels, with internal doublet sheets to provide lift effects. Since these panels were developed by fitting, in a least squares sense, parabolic curves through the actual surface points, the panels were discontinuous. Further, the panels were restricted to being only slightly curved through the use of a near field expansion for calculating the influence coefficients. A far field expansion was also used to increase computational efficiency. Results were obtained for a randomly paneled sphere and wing, which indicated the versatility of the method.

The method was then extended to supersonic flow by Ehlers, Johnson, and Rubbert (Ref 49) using linear sources

and quadratic doublets on slightly curved panels with a linearized mass flux boundary condition instead of the usual velocity boundary condition. In addition, an internal potential boundary condition was used to control disturbances in the interior flow which tended to amplify as they were reflected by the interior surface and which would perturb or destroy the exterior solution. This approach also allowed a-priori determination of source strengths which reduced the order of the system of linear equations which had to be solved. Results were presented for a randomly paneled spindle, an inlet with nacelle, and several wings which showed excellent agreement between experiment or theory, and the computed results. A problem developed however, because both the paneling and the doublet distribution (which was found using a least squares approach) were slightly discontinuous. This generated singularities which propagated along Mach lines with undiminished strength, and which, if downstream control points were too close, could cause the influence coefficient matrix to be singular.

The solution to this problem, given by Ehlers et al (Refs 50-52) was to replace the discontinuous curved panel concept by a continuous flat panel concept. Previous flat panel methods used four input corner points to define a single flat panel which did not necessarily pass through the

input points. This new method used four input corner points to define five planar subpanels which passed through the corner points and which were continuous with all neighboring panels. The result modeled a surface with continuous flat panels, and allowed the quadratic doublet distributions on each subpanel to be exactly continuous along all edges. This method has produced good results to date (Ref 53), and is the first higher order supersonic method capable of accurately modeling extremely complex geometric configurations.

In general, low order three dimensional panel methods are fairly complex, require large numbers of panels to achieve a reasonable accuracy, and are sensitive to panel and control point placement. The higher order methods have reduced the number of panels required to achieve the same or better accuracy, but at a cost of increased complexity and computational requirements. Some comparisons between several of these methods are given by Thomas and Miller (Ref 54), and Landrum and Miller (Ref 55).

#### Objective of Dissertation

The motivation for studying linear potential flow methods in general and panel methods in particular stems from the proven usefulness of these methods in a wide range of engineering and research activity. It has also been shown that current available methods are in general

complicated require in many cases large numbers of panels to achieve a given level of accuracy, and require a large degree of expertise on the part of the user in order to obtain satisfactory results. A partial reason for these deficiencies is that the influence of a number of the characteristics that define the panel method approach, in both two and three dimensional cases, are not adequately understood. These characteristics include panel curvature, singularity distribution continuity, type of singularity, order of the singularity approximation, the type of boundary condition, the numerical implementation of the Kutta condition, and control point location. The question of the effects of these characteristics on solution accuracy for a given method has not been fully answered.

The objective of this dissertation is to answer these questions within the framework of a two dimensional incompressible method as a first step in developing a fuller understanding of the effects of these characteristics. The results of such an investigation will provide guidance to others who wish to develop two or three dimensional panel methods for their own specific applications. To accomplish this objective, a new two dimensional method, based on the use of circular arc panels, has been formulated, and has been extensively tested in applications to the cases of flow over a circular cylinder and flow over several types of airfoils.

The results have shown that accuracy increased as additional terms in the series representing the singularity distribution are kept, as panel curvature is varied from flat to circular and as continuity of the vorticity distribution is enforced. Additionally, the effect of control point location has been found to be relatively small, and the required number of panels for a given accuracy has been found to be less than that required by the method of Raj. The present method has also been compared to Hess's higher order method as formulated by Bristow for a thin airfoil, and has been found to give a small improvement in computed perturbation velocities.

The following chapters of this dissertation will discuss these points in detail. The next chapter will briefly present some highlights of potential theory, and the general panel method approach. Then the details of a new paneling method based on circular arc panels will be presented, followed by the application of this method to the circular cylinder problem, and then to the airfoil problem. Finally the conclusions resulting from this work and ideas concerning possible extensions of the method will be presented.



## II. Two Dimensional Potential Theory

The purpose of this chapter is to present briefly some basic facts about potential theory and surface singularity distributions which will have direct application to the work that follows. It will be seen that the panel method approach to solving flow problems is dependent on the results of potential theory. Harmonic functions will first be discussed from a partial differential equation viewpoint, followed by a presentation of the Green's theorem representation of a harmonic function. Some characteristics of surface singularity distributions and some relevant properties of integral equations will then be discussed. Finally the reduction of the Green's theorem formulation to an integral equation will be considered along with some unresolved questions which arise in this formulation.

### Harmonic Functions

Solutions to Laplace's equation are called harmonic functions. Such functions have properties which allow the development of the integral equation method which is the basis of the panel method approach to solving Laplace's equation. This equation has also been studied considerably from a partial differential equation viewpoint in which one determines conditions which guarantee the existence and

uniqueness of solutions to a given equation which is subject to a particular specification of boundary conditions.

The general boundary value problem can be stated as follows: find a function  $\phi$  which satisfies  $\nabla^2 \phi = 0$  in a region  $R$  and where either  $\phi = f(s)$  or  $\frac{\partial \phi}{\partial n} = f(s)$  on the boundary of  $R$ , and where  $f(s)$  is a known function. If

is specified, this problem is called a Dirichlet problem; while if  $\frac{\partial \phi}{\partial n}$  is specified, it is called a Neumann problem. The existence and uniqueness of solutions to these problems depends on whether  $R$  is an interior or exterior region. Given that the boundary values are continuous and that the boundary is sufficiently regular, Table III (Ref 14) summarizes the conditions for which these problems have solutions.

These results from the theory of partial differential equations will be used to verify the correctness of the integral equation formulation of the problem which leads to the panel method solution to Laplace's equation. This formulation is dependent on the property of harmonic functions that is stated in Green's theorem.

#### Green's Theorem Formulation

Using Green's theorem, the value of a harmonic function at any point in a region may be expressed in terms of its value on the boundary of the region. This form may then be interpreted as a singularity distribution on the boundary.

TABLE III  
Boundary Value Problem Solutions

| Boundary Value Prob. | Region    |             |
|----------------------|-----------|-------------|
|                      | Interior  | Exterior    |
| Dirichlet            | Solution  | No Solution |
| Neumann              | Solution* | Solution    |

\* If and only if 
$$\oint_B \frac{\partial \phi}{\partial n} dl = 0$$

Green's theorem may be applied to harmonic functions which are single valued in some region. The problem may be formulated in two dimensions by considering (Figure 2) two harmonic functions,  $\phi$  and  $\phi_1$ , and two regions,  $R$  and  $R_1$  which are divided by a boundary curve  $B$ . The curve  $b$  is called a barrier and is required to make  $R$  a simply connected region which then insures that  $\phi$  will be single valued there. If  $P$  is a point in  $R$ , it can be shown (Refs 13,14,56) that

$$\phi(P) = \frac{-1}{2\pi} \oint_B (\log r \frac{\partial \phi}{\partial n} - \phi \frac{\partial}{\partial n} (\log r)) dl \quad (8)$$

$$+ \frac{1}{2\pi} \int_b (\phi^+ - \phi^-) \frac{\partial}{\partial n} (\log r) db$$

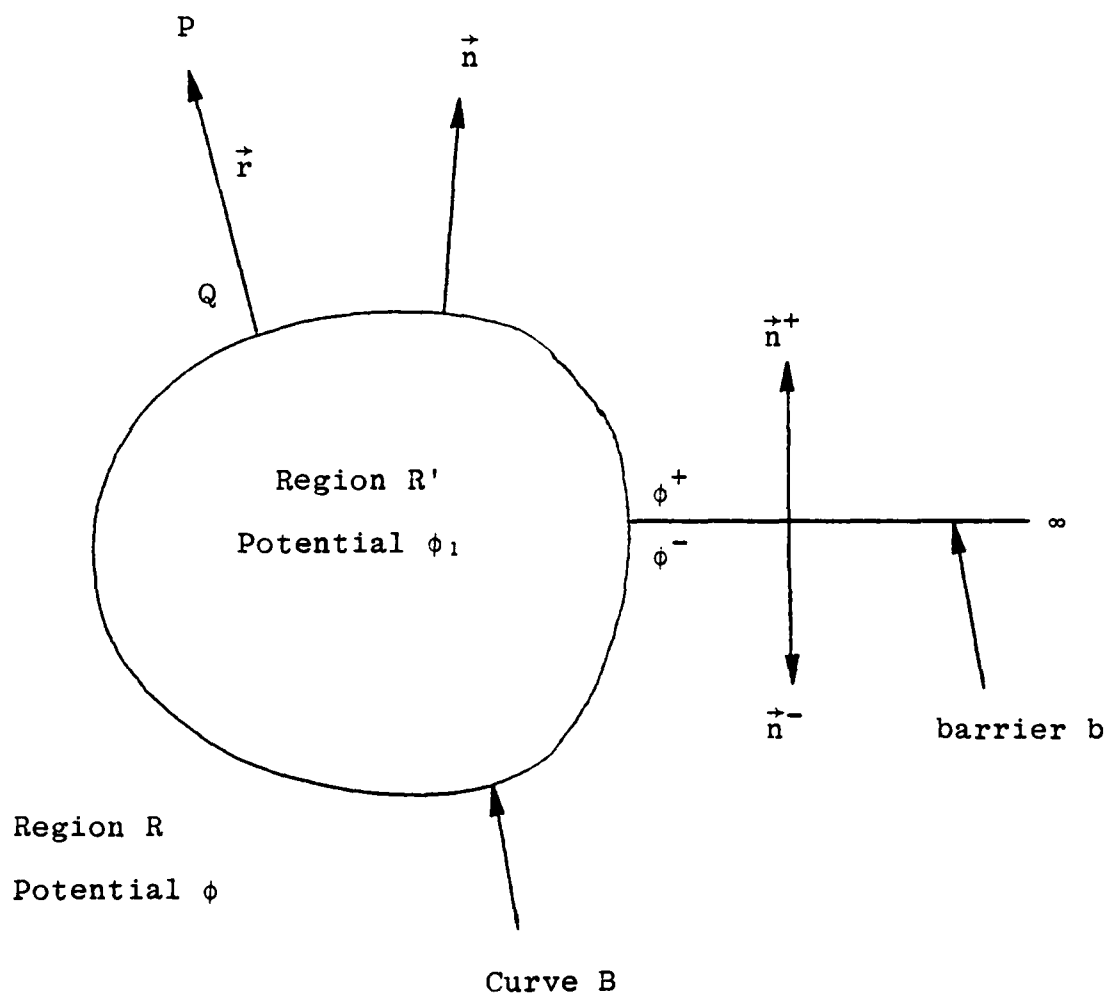


Figure 2. Green's Theorem Formulation.

and also that

$$\phi_1(P) = \frac{1}{2\pi} \oint_B (\log r \frac{\partial \phi_1}{\partial n} - \phi_1 \frac{\partial}{\partial n}(\log r)) dl = 0 \quad (9)$$

Adding Eqs 8 and 9 gives

$$\phi(P) = \frac{-1}{2\pi} \oint_B (\log r (\frac{\partial \phi}{\partial n} - \frac{\partial \phi_1}{\partial n}) - (\phi - \phi_1) \frac{\partial}{\partial n}(\log r)) dl \quad (10)$$

$$+ \frac{1}{2\pi} \int_b (\phi^+ - \phi^-) \frac{\partial}{\partial n}(\log r) db$$

Equations 8 and 10 show that  $\phi$  is not uniquely determined until both  $\phi$  and  $\phi_1$  are specified on B. This means that the solutions for R and  $R_1$  are independent in the sense that the solution could be changed in one region without changing the solution in the other region.

Velocity Potential. If  $\phi$  and  $\phi_1$  are assumed to be velocity potential functions and if  $\sigma \equiv \frac{\partial \phi}{\partial n} - \frac{\partial \phi_1}{\partial n}$  and  $\mu \equiv \phi - \phi_1$  then Eq 10 becomes

$$\phi(P) = \frac{1}{2\pi} \oint_B (\sigma \log r - \mu \frac{\partial}{\partial n}(\log r)) dl \quad (11)$$

$$+ \frac{1}{2\pi} \int_b (\phi^+ - \phi^-) \frac{\partial}{\partial n}(\log r) db$$

The first integral in this equation can be interpreted as the potential due to a source distribution of strength  $\sigma$  and a doublet distribution of strength  $\mu$  on B

while the second can be interpreted as the potential due to a doublet distribution of strength  $\mu$  on  $b$ . As noted above,  $\phi$  is not unique unless both  $\sigma$  and  $\mu$  are determined. One procedure would be to specify a-priori either  $\sigma$  or  $\mu$ , and then apply another boundary condition to determine the remaining unknown. This is equivalent to specifying the solution in  $R_1$  and then solving for the solution in  $R$ .

Suppose  $\sigma$  is specified on  $B$  to be  $\sigma = 0$ . Then Eq 10 becomes

$$\phi(P) = \frac{1}{2\pi} \oint_B \mu \frac{\partial}{\partial n} (\log r) dl + \frac{1}{2\pi} \int_b \Delta\phi \left( \frac{\partial}{\partial n} (\log r) \right) db \quad (12)$$

where

$$\Delta\phi = \phi^+ - \phi^-$$

Since  $\phi$  is a velocity potential  $\Delta\phi$  is the circulation around  $B$ , and is constant. Also, since the location of  $b$  is arbitrary, the normal and tangential derivatives of  $\phi$  are continuous across  $b$  (Ref 13). Therefore  $\Delta\phi$  is constant on  $b$ , and the second integral in Eq 12 represents a constant strength doublet sheet extending to infinity and is equivalent to a wake. If, however,  $\mu=0$  on  $B$ , then Eq 10 becomes

$$\phi(P) = \frac{-1}{2\pi} \oint_B \sigma \log r \, dl \quad (13)$$

In this case  $\mu = 0$  implies that  $\phi = \phi_1$  on B and thus that  $\phi^+ = \phi^-$  because  $\phi_1$  is single valued in  $R_1$ ; therefore the integral over b is zero. This also means that one cannot obtain circulation, or lift, using a source distribution only.

Stream Function. In the last section  $\phi$  was assumed to be a velocity potential function, although the general formulation is not dependent on this interpretation. Since  $\phi$  may be any harmonic function, assume that it represents a stream function  $\psi$ . If there are no sources inside B then  $\psi$  will be constant (single valued) on B because it is a measure of the mass flux across the curve B. Thus  $\psi^+ = \psi^-$ , and the expression equivalent to Eq 10 is

$$\psi(P) = \frac{-1}{2\pi} \oint_B (\log r \left( \frac{\partial \psi}{\partial n} - \frac{\partial \psi_1}{\partial n} \right) - (\psi - \psi_1) \frac{\partial}{\partial n} (\log r)) \, dl \quad (14)$$

If it is assumed that  $\psi = \psi_1$  on B, and that  $\gamma \equiv \frac{\partial \psi}{\partial n} - \frac{\partial \psi_1}{\partial n}$  then

$$\psi(P) = \frac{-1}{2\pi} \oint_B \gamma \log r \, dl \quad (15)$$

Thus the stream function can be represented in terms of a surface distribution of vorticity with strength  $\gamma$ . Although Eq 15 does not contain a wake term as does Eq 12, it does not necessarily represent a zero circulation case.

#### Doublet-Vorticity Sheet Equivalence

Hess (Ref 35) has shown that the velocity field due to a surface distribution of doublets (whose axes are normal to the surface) is equivalent to the combined fields of a distribution of vorticity on the surface where  $\vec{\gamma} = \vec{n} \times \nabla\mu$ , and a line vortex on the bounding curve of the surface whose strength is equal to the strength of the doublet distribution on the curve. For the two dimensional case (Figure 3) a constant doublet sheet of strength  $\mu$  from A to B is equivalent to two point vortices at A and B of strength  $\mu$ . This means that a velocity field represented by a distribution of sources and/or doublets can also be represented by a distribution of sources and/or vortices. In the case of a constant doublet distribution on a wake, the equivalent vorticity distribution consists of a pair of point vortices, one at the start of the wake, and one at infinity. On the wake  $\mu = \text{constant}$  implies  $\nabla\mu = 0$ , and thus  $\gamma = 0$  on the wake. Therefore Eqs 12 and 15 are consistent and in fact are equivalent.



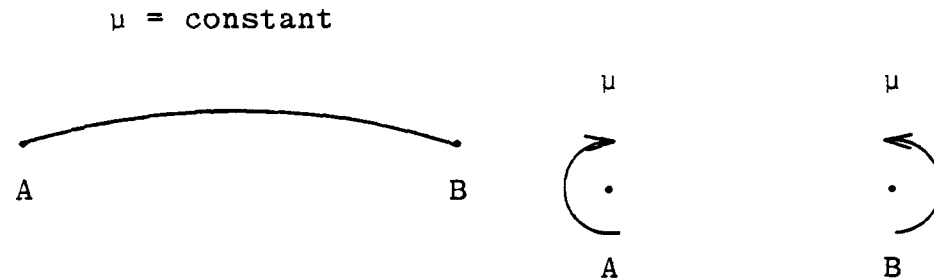


Figure 3. Doublet/Vortex Sheet Equivalence

### Singularity Behavior

Using Green's theorem it is clear that the problem of potential flow over a body can be modeled using several types of singularity distributions. These surface distributions exhibit certain properties which affect how

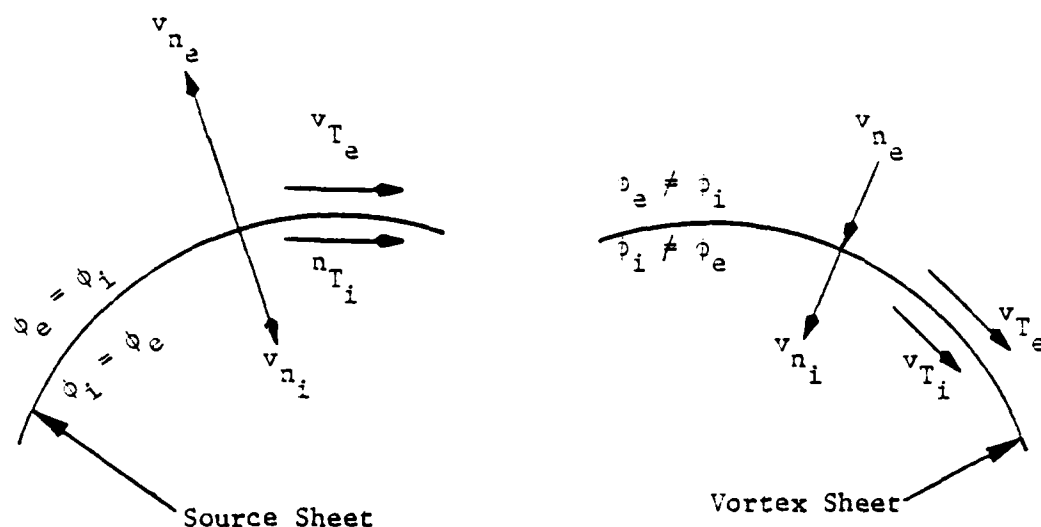


Figure 4 - Properties of Singularity Sheets

they may be used to model different types of flow.

Transfer of boundary conditions. Consider the singularity distributions shown in Figure 4 where subscripts  $e$  and  $i$  stand for surface exterior and interior, respectively. For the source sheet, the potential and the tangential velocity are continuous across the sheet, while the normal velocity is discontinuous. For the vortex sheet the opposite is true; that is, the potential and the tangential velocity are discontinuous across the sheet while the normal velocity is continuous. The importance of these properties, as emphasized by Rubbert (Ref 57) is that they cause certain characteristics to be transferred across the surface. For example, consider a source sheet on a closed

surface. If somehow a distribution is specified that gives a particular solution in the exterior region, the resultant exterior tangential velocity distribution is carried across the sheet and becomes the boundary condition specification on the interior region. In the case of a vortex distribution, the normal velocity is transferred across the sheet so that the interior problem becomes effectively a Neumann problem. But recall that the condition ensuring a solution to this problem is that the net normal velocity, or flow, be zero, which is simply a statement that an incompressible fluid cannot be pumped into a closed region. One procedure for alleviating the problem of a non zero net normal flow would be to place a sink inside the surface to remove any excess fluid.

Singularity Behavior at Corners. The above properties of singularity sheets apply to surfaces which are smooth to some order. However, many bodies of interest have slope discontinuities at one or more points, such as an airfoil with a sharp trailing edge. Craggs and Mangler (Ref 58) have studied the behavior of source distributions at corner points. They find that the source distribution behaves as a power of distance to the point with the value of the power depending on whether the flow is symmetric about the corner and whether the corner is concave or convex to the flow. For the case shown in Figure 5, which is symmetrical flow

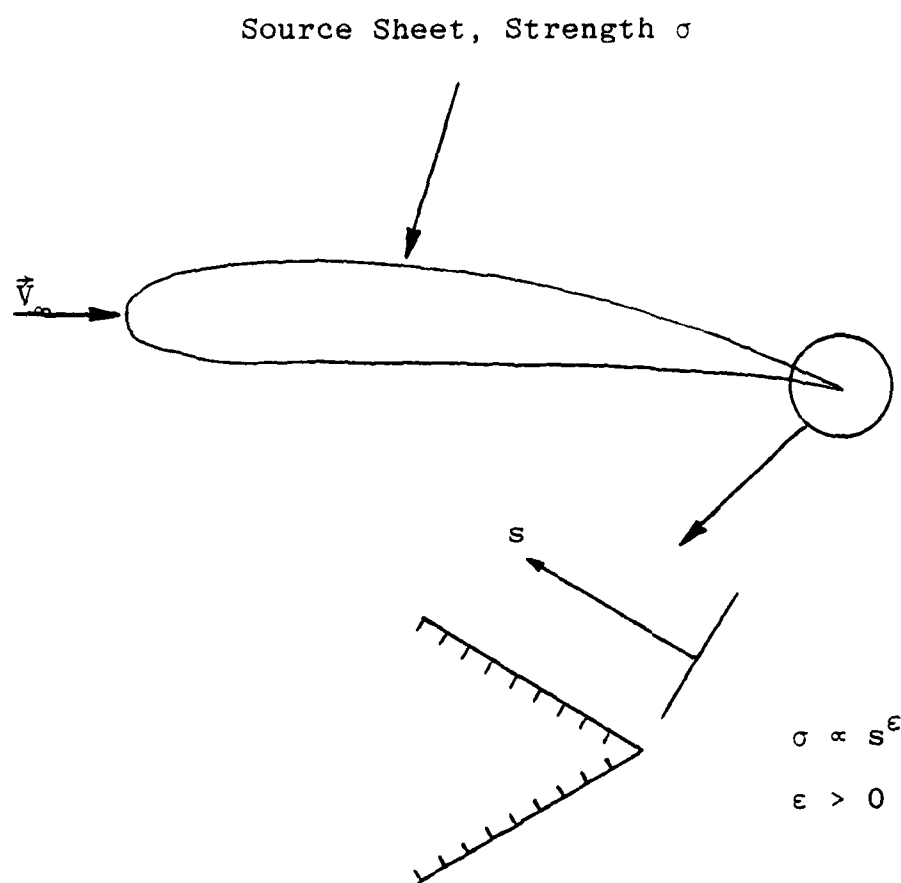


Figure 5. Behavior of a Source Sheet at a Corner.

about a convex corner, the power is positive, so that  $\sigma \rightarrow 0$  as  $s \rightarrow 0$ . Thus in modeling an airfoil with a source distribution this behavior should be considered.

### Integral Equations - Existence and Uniqueness

In this section some results from the theory of integral equations (Refs 59, 60, 61), which will be applied in the following sections, will be discussed. Equation 16 is the general form of a Fredholm integral equation of the second kind where  $K(x,y)$  is a given kernel function,

$$\phi(x) - \lambda \int_a^b K(x,y)\phi(y) dy = f(x) \quad (16)$$

$f(x)$  is a given function,  $\lambda$  is a parameter, and  $\phi(x)$  is the unknown. Several results can be stated about this equation.

1. Either Eq 16 has a nontrivial solution, or the associated homogeneous equation

$$w(x) - \lambda \int_a^b K(x,y)w(y)dy = 0 \quad (17)$$

has a nontrivial solution. The values of  $\lambda$  for which Eq 17 has nontrivial solutions are called eigenvalues, and the solutions  $w(x)$  are called eigenfunctions.

2. If  $\lambda$  is an eigenvalue of Eq 16 then this equation

is an inconsistent equation (i.e. has no solution) unless

$$\int_a^b u(x) f(x) dx = 0 \quad (18)$$

where

$$u(x) - \lambda \int_a^b K(y, x) u(y) dy = 0 \quad (19)$$

3. If Eq 18 holds, then there are an infinite number of solutions to Eq 16 of the form

$$\phi(x) = \phi_p(x) + \sum_m c_m w_m(x) \quad (20)$$

where  $\phi_p$  is a particular solution, the  $c_m$  are arbitrary constants, and the summation extends over the set of linearly independent eigenfunctions,  $w_m$ . Another important property of a Fredholm equation of the second kind is that it is equivalent to a system of linear algebraic equations.

While Fredholm integral equations of the second kind have some very nice properties, Fredholm equations of the first kind, of which Eq 21 is the general form, do not.

$$\lambda \int_a^b K(x, y) \phi(y) dy = f(x) \quad (21)$$

$f(x)$  = known function

It can be shown that equations of this type do not always

have solutions, and the solutions of solvable cases are often not unique. This question can be related to the properties of the Dirichlet and Neumann problems which required, essentially, that there be no net flux into a closed region. Equations 16 and 21 will be used, with some modification, to solve several problems in the succeeding sections.

### Reduction of the Singularity Distribution Formulation to an Integral Equation

Consider the problem of two dimensional incompressible flow about a body,  $B$ , immersed in a free stream,  $\vec{V}_\infty$ , as shown in Figure 6, where  $P$  is a field point,  $q$  is any point on  $B$ ,  $r(P,q)$  is the distance between  $P$  and  $q$ , and  $\vec{n}_q$  is the outward normal to  $B$  at  $q$ .

Surface Source Distribution. The velocity potential function may be represented as a source distribution on  $B$  by

$$\phi(P) = \frac{-1}{2\pi} \oint_B \sigma(q) K_S(P,q) dl \quad (22)$$

where  $K(P,q)$  is the source kernel function in two dimensions

$$K_S(P,q) = \log(r(P,q))$$

It can be shown (Ref 14) that if Eq 22 is differentiated and

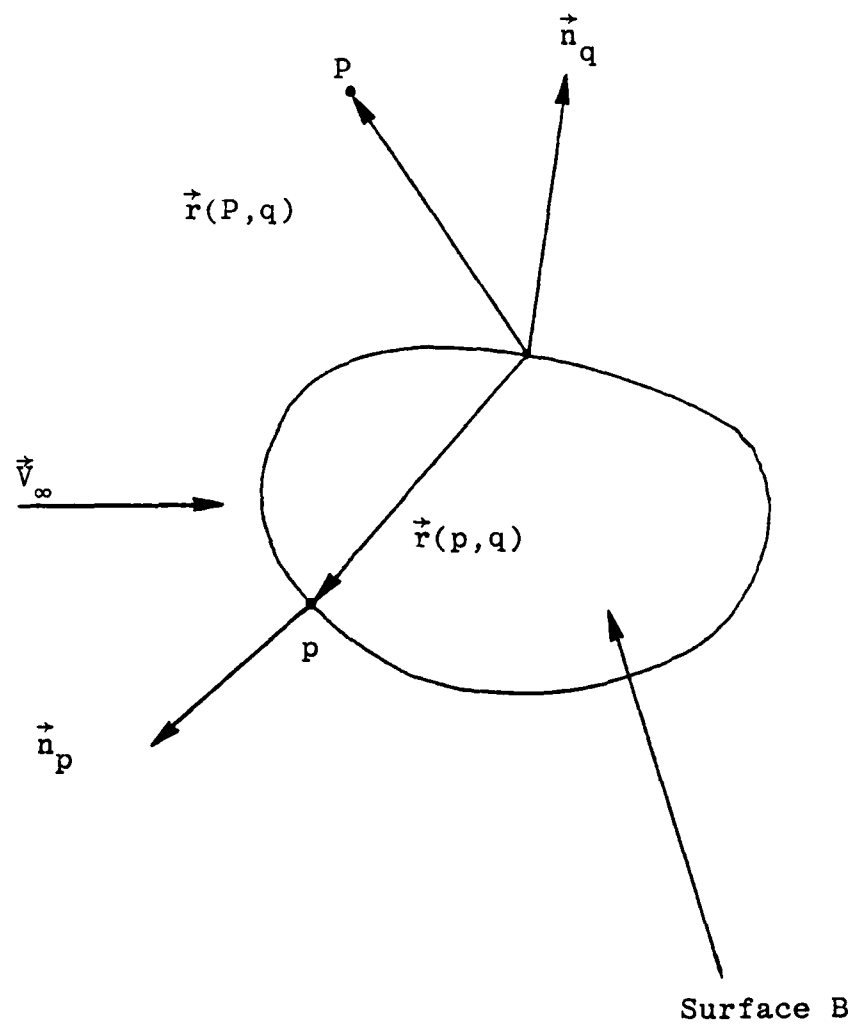


Figure 6. Reduction to an Integral Equation.



if the field point P goes to a surface point p one obtains

$$\left. \frac{\partial \phi}{\partial n_p} \right)_e = \frac{\sigma(p)}{2} - \frac{1}{2\pi} \oint_B \sigma(q) \frac{\partial}{\partial n_p} (K_S(p, q)) dl \quad (23)$$

where  $\partial/\partial n_p$  means the derivative in the normal direction to B at p, and the subscript e means that P goes to p in the region exterior to B. Similarly,

$$\left. \frac{\partial \phi}{\partial n_p} \right)_i = \frac{-\sigma(p)}{2} - \frac{1}{2\pi} \oint_B \sigma(q) \frac{\partial}{\partial n_p} (K_S(p, q)) dl \quad (24)$$

If the total velocity in the field is  $\vec{V} = \vec{V}_\infty + \vec{v}$  where  $\vec{V} = \nabla \phi$ , then the standard boundary condition of zero external normal velocity can be written

$$V_{n_e}(p) = V_{\infty n}(p) + v_{n_e}(p) = 0 \quad (25)$$

or

$$v_{n_e}(p) = -V_{\infty n}(p) \quad (26)$$

but

$$v_{n_e}(p) = \left. \frac{\partial \phi}{\partial n_p} \right)_e = \frac{\sigma(p)}{2} - \frac{1}{2\pi} \oint_B \sigma(q) \frac{\partial}{\partial n_p} (K_S(p, q)) dl \quad (27)$$

therefore

$$\sigma(p) - \frac{1}{\pi} \oint_B \sigma(q) \frac{\partial}{\partial n_p} (K_S(p,q)) dl = -2V_{\infty n}(p) \quad (28)$$

This is a Fredholm Equation of the Second Kind for the source strength  $\sigma(p)$  on  $B$ . Before the results presented earlier for this type of equation can be applied, the kernel

$$K(p,q) = \frac{\partial}{\partial n_p} (K_S(p,q))$$

must be considered. A cursory examination indicates that  $K(p,q)$  is singular at  $q=p$ , but it can be shown that in the two dimensional case the singularity is removable if the curve  $B$  is sufficiently smooth.

Conditions for Solvability. What constitutes sufficient smoothness is not completely clear, Tricomi (Ref 59) and Sternberg and Smith (Ref 62) specify that  $B$  have continuous curvature. Mikhlin (Ref 63) and Pogorzelski (Ref 64) require that the surface satisfy the following conditions (which are called Liapunov conditions):

1. The surface has a definite normal at each point.
2. There exists a number  $c > 0$  such that a sphere of radius  $c$  centered at a point on the surface cuts a portion of the surface such that every line parallel to the normal at

the point cuts the portion only once.

3. The angle between the normals to any two points on the surface satisfies the following:

$$|\theta| \geq ar^\epsilon$$

where  $\theta$  is the angle between the normals,  $r$  is the distance between the points, and  $a$  and  $\epsilon$  are positive constants. This question will arise again when these theories are applied to shapes of actual aerodynamic interest, the majority of which have at least one point of slope discontinuity. The question of applicability of the theories to such surfaces has not been satisfactorily resolved to the author's knowledge. It might be reasoned that the actual viscosity in the boundary layer will effectively round off any corners, and this may be the answer. Also, although all methods exhibit decreased accuracy in the trailing edge region, the quality of solutions over the remainder of the airfoil does not seem to be adversely affected.

If it is assumed that  $B$  has the requisite smoothness, and noting that  $\lambda = \frac{1}{\pi}$  is not an eigenvalue of Eq 28, it is known that a unique solution exists for any given free stream flow. The problem just posed is equivalent to the Neumann exterior problem seen earlier and does indeed have a unique solution. Recalling the discussion of the properties of source sheets, since the potential is continuous across

the sheet, a Dirichlet boundary value problem is effectively imposed on the interior of B.

Surface Vorticity Distribution. Now consider the same problem assuming a vortex distribution on B. The stream function for the singularity distribution is

$$\psi(P) = \frac{-1}{2\pi} \oint_B \gamma(q) \log(r(P,q)) dl \quad (29)$$

where  $\gamma(q)$  is the vortex strength. But the boundary condition will be applied in a way first suggested by Martenson (Ref 65). Consider the total stream function of the flow,

$$\Psi = \Psi_\infty + \psi \quad (30)$$

Now on a streamline, such as a body surface,  $\psi = \text{constant}$ , or

$$\frac{\partial \psi}{\partial t} = 0 \quad (31)$$

where  $t$  is the surface tangent direction. Equation 31 is actually a statement of zero external normal velocity. To see this, consider the following boundary condition:

$$\frac{\partial \Psi}{\partial n_i} = \frac{\partial \Psi_\infty}{\partial n} + \frac{\partial \psi}{\partial n_i} = 0 \quad (32)$$

which is a statement that the total internal tangential velocity on B is zero. Now Green's theorem for  $\Psi$  states that

$$\iint_S (\Psi \nabla^2 \Psi + \nabla \alpha \cdot \nabla \Psi) ds = \oint_B \Psi \frac{\partial \Psi}{\partial n_i} dl \quad (33)$$

where S is interior to B. Also,

$$\nabla^2 \Psi = 0 \quad \text{in } S$$

and

$$\nabla \Psi \cdot \nabla \Psi = V^2$$

where V is the total velocity inside B. Thus

$$\iint_S V^2 ds = \oint_B \Psi \frac{\partial \Psi}{\partial n_i} dl \quad (34)$$

Now the boundary condition is

$$\frac{\partial \Psi}{\partial n_i} = 0 \quad \text{on } B \quad (35)$$

so that

$$\iint_S V^2 ds = 0 \quad (36)$$

but this means that  $V \equiv 0$  inside B. Further, this implies that  $\Psi = \text{constant}$  inside B, and thus

$$\frac{\partial \Psi}{\partial t_i} = 0 \quad \text{on } B \quad (37)$$

Now  $\frac{\partial \Psi}{\partial t_i}$  is the interior normal velocity on B, and since the tangential derivative (normal velocity) is continuous across a vortex sheet

$$\frac{\partial \Psi}{\partial t_e} = 0 \quad \text{on } B \quad (38)$$

This is just a statement of zero exterior normal velocity, as it was desired to show. Now computing explicitly,

$$\left( \frac{\partial \Psi}{\partial n_p} \right)_e = \frac{\gamma(p)}{2} - \frac{1}{2\pi} \oint_B \gamma(q) \frac{\partial}{\partial n_p} (\log r) dl \quad (39)$$

and

$$\left( \frac{\partial \Psi}{\partial n_p} \right)_i = \frac{-\gamma(p)}{2} - \frac{1}{2\pi} \oint_B \gamma(q) \frac{\partial}{\partial n_p} (\log r) dl \quad (40)$$

so that subtracting these gives

$$\left( \frac{\partial \Psi}{\partial n_p} \right)_e - \left( \frac{\partial \Psi}{\partial n_p} \right)_i = \gamma(p) \quad (41)$$

Now consider the total external tangential velocity given by Eq 42 which is actually the quantity of interest.

$$\frac{\partial \Psi}{\partial n})_e = \frac{\partial \Psi_\infty}{\partial n} + \frac{\partial \psi}{\partial n})_e \quad (42)$$

Using Eqs 32 and 41, this can be written

$$\frac{\partial \psi}{\partial n})_e = \gamma(p) \quad (43)$$

This states the important property that the total external tangential velocity is equal to the local vorticity strength.

Now consider the integral equation results as they apply to this formulation. Applying Eqs 32 and 40 one obtains

$$\begin{aligned} \frac{\partial \psi}{\partial n})_i &= \frac{-\gamma(p)}{2} - \frac{1}{2\pi} \oint_B \gamma(q) \frac{\partial}{\partial n_p} (\log r) dl = \frac{-\partial \Psi_\infty}{\partial n} \\ \gamma(p) + \frac{1}{\pi} \oint_B \gamma(q) \frac{\partial}{\partial n_p} (\log r) dl &= 2 \frac{\partial \Psi_\infty}{\partial n} \end{aligned} \quad (44)$$

This is again a Fredholm equation of the second kind, but now the parameter  $\lambda = \frac{1}{\pi}$  is in fact an eigenvalue. From the earlier discussion of integral equations it is known that when a solution does exist, it is not unique. This non-uniqueness will be removed by the application of a Kutta condition. In later parts of this work a vortex distribution to which is applied the standard zero exterior

The problem of two dimensional incompressible potential flow over a body can be formulated, using the concepts discussed above, in terms of a singularity distribution on the surface of the body. The different singularity types have different characteristics which determine whether they will be effective in a particular application. Once the singularity has been chosen and the problem has been reduced to the appropriate integral equation, additional numerical approximations must be introduced in order to obtain solutions for arbitrary geometries. The details of these approximations form the basis of the panel method approach to solving this problem.

In the next chapter a new panel method will be presented. The method is based on the use of circular arc panels with higher order singularity distributions.



### III. Panel Method Approach

The purpose of this chapter is to formulate a new method of obtaining an approximate solution to the integral equations developed in the preceeding chapter using the panel method approach. This method is based on the concept of approximating the surface of a two dimensional body by a series of circular arcs on which higher order source and vorticity distributions are placed.

Any panel method consists of certain assumptions and approximations concerning the basic elements of the integral equation. These elements include the approximate representation of the surface over which the integral is taken, the approximate representation of the singularity distribution which is assumed on the surface, the type of boundary conditions which are applied, and the procedure by which the Kutta condition is satisfied.

The next section will discuss different ways of representing the surface, and will give the rationale for the choice of the circular arc element, as well as details of the numerical implementation. This will be followed by a discussion of the types of singularities available and the procedure by which the singularity strength is approximated on a panel. A discussion of the boundary conditions that

will be applied will follow. This will include the reduction of the velocity boundary conditions to a matrix equation, and a discussion of the form of the Kutta condition which will be used. Finally, the reduction of the method to a system of linear algebraic equations and the procedure by which the system is solved will be presented.

### Surface Representation

The integral equation to be solved contains an integral over a surface for which an analytic description will not usually be available, and even if it were available, the evaluation in closed form of the resulting integral would generally be impossible. Therefore, a suitable approximation to the surface must be found which will capture those features of the surface essential for an accurate solution, while allowing evaluation of the resulting integrals in a straightforward way. Geometric features which characterize a curve include position, slope, curvature, and higher order derivatives; but the question as to which of these features is essential for an accurate solution has not been adequately answered in the literature.

The approach which will be used has been considered by Johnson (Ref 66) in a computer graphics context. This approach is to approximate a curve in a simple way by using a set of standard, or primitive, elements and accepting the level of error which results from the choice of the element.

As noted by Johnson, this is in contrast to a spline approach in which geometric properties of a curve are matched by using as complex an element as is required to accomplish the matching.

The simplest way to approximate a plane curve of moderate curvature is to use a series of straight line segments (Figure 7). Increasing the accuracy of the approximation can be achieved by increasing the number of linear elements. The use of higher order curves may reduce the required number, although at the cost of introducing additional complexity. In an attempt to balance accuracy with complexity, several conic arc curves were considered. In the next section flat, parabolic, circular, and elliptic arcs will be evaluated as to their use as a standard approximating element.

Conic Arc Approximation. Consider an arbitrary curve  $\eta = \eta(\xi)$  described in a tangent-normal coordinate system with the origin at some point on (Figure 8) so that

$$\eta(0) = \eta'(0) = 0$$

The problem is to approximate this curve in the region  $a \leq \xi \leq b$  using the following:

1. a straight line segment given by  $\eta_f(\xi)$
2. a parabolic arc given by  $\eta_p(\xi)$
3. a circular arc given by  $\eta_c(\xi)$

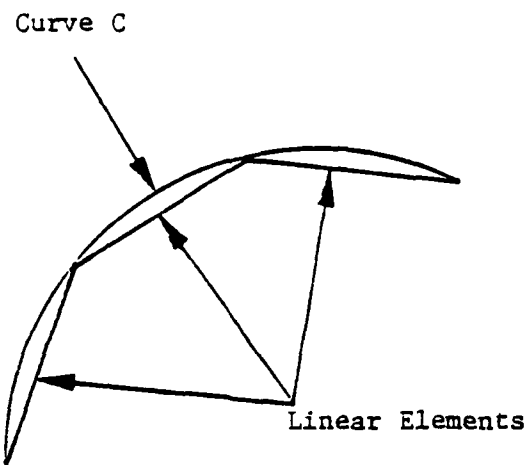


Figure 7 - Linear Approximating Elements

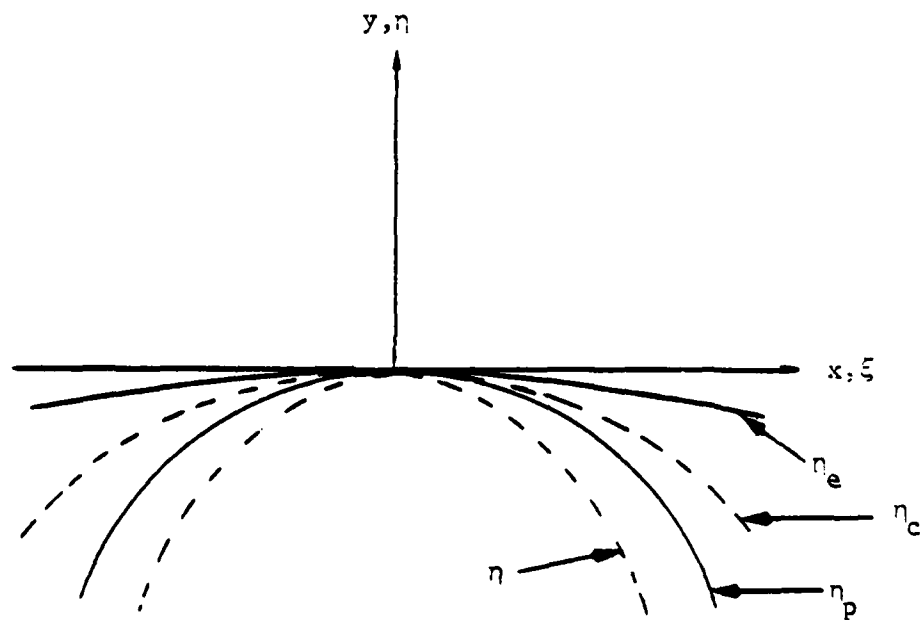


Figure 8 - Tangent-Normal Coordinate System

4. an elliptic arc given by  $\eta_e(\xi)$   
 where these curves are given in the tangent-normal  
 coordinate system such that

$$\eta_h(0) = \eta'_h(0) = 0 \quad h = f, p, c, e$$

An error function  $E_h(\xi)$  can then be defined to describe the  
 approximation in terms of the error in position, slope, or  
 higher order derivatives. That is

$$E_h^n(\xi) = \eta^n(\xi) - \eta_h^n(\xi)$$

where  $n$  is the  $n$ th derivative of the function. If these  
 curves are expanded in a power series about  $\eta = 0$ , and if  
 the approximating curves are equated term by term with the  
 actual curve, the errors of the approximation are given by

$$E_f(\xi) = O(\xi^2)$$

$$E_p(\xi) = O(\xi^3)$$

$$E_c(\xi) = O(\xi^3)$$

$$E_e(\xi) = O(\xi^5)$$

Circular Arc Approximation. The circular arc has been  
 chosen as the standard element for several reasons. From  
 the analysis above it can be seen that the accuracy of the  
 approximation increased as the nature of the element changes  
 from flat to elliptic, and that the errors resulting from

Numerical Implementation. The problem is to model a planar curve using a piecewise continuous set of circular arc elements. It is assumed that the curve can not be described analytically, and will be represented by a set of coordinate points, input in the case of an airfoil from the trailing edge in the order indicated in Fig 9. The general equation of a circle is

$$x^2+y^2+Dx+Ey+F = 0$$

where D, E, and F are constants; where the center of the circle is located at  $x_0 = \frac{-D}{2}$ , and  $y_0 = \frac{-E}{2}$ ; and where the radius of the circle is  $a = \sqrt{D^2/4 + E^2/4 - F}$ . Given three points on the surface (Fig 10) these three constants can be obtained. Let  $P_m(x_m, y_m)$  for  $m=1,2,3$  be three points on the surface such that

$$x_m D + y_m E + F = -(x_m^2 + y_m^2) \quad m = 1, 2, 3$$

This system can be solved to give

$$D = \frac{[x_3^2 + y_3^2 - (x_1^2 + y_1^2)](y_2 - y_3) - (y_1 - y_3)[x_3^2 + y_3^2 - (x_2^2 + y_2^2)]}{W}$$

$$E = \frac{(x_1 - x_3)[x_3^2 + y_3^2 - (x_2^2 + y_2^2)] - (x_2 - x_3)[x_3^2 + y_3^2 - (x_1^2 + y_1^2)]}{W}$$

$$F = -(x_2^2 + y_3^2) - x_3 D - y_3 E$$

where

$$W = (x_1 - x_3)(y_2 - y_3) - (x_2 - x_3)(y_1 - y_3)$$

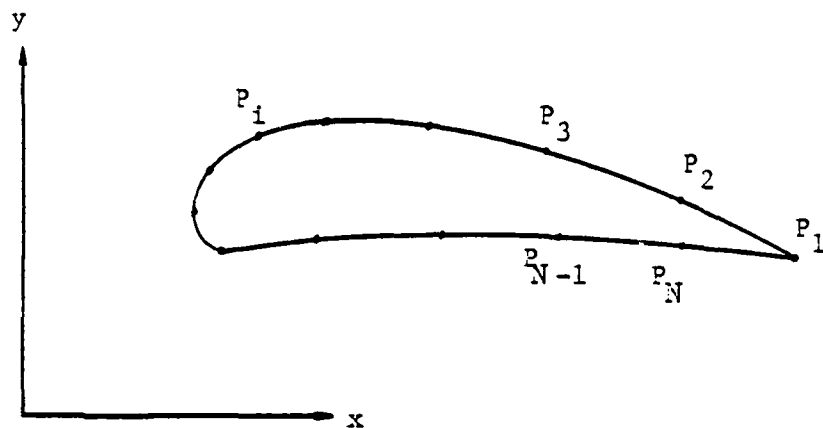


Figure 9 - Surface Coordinate Order of Input

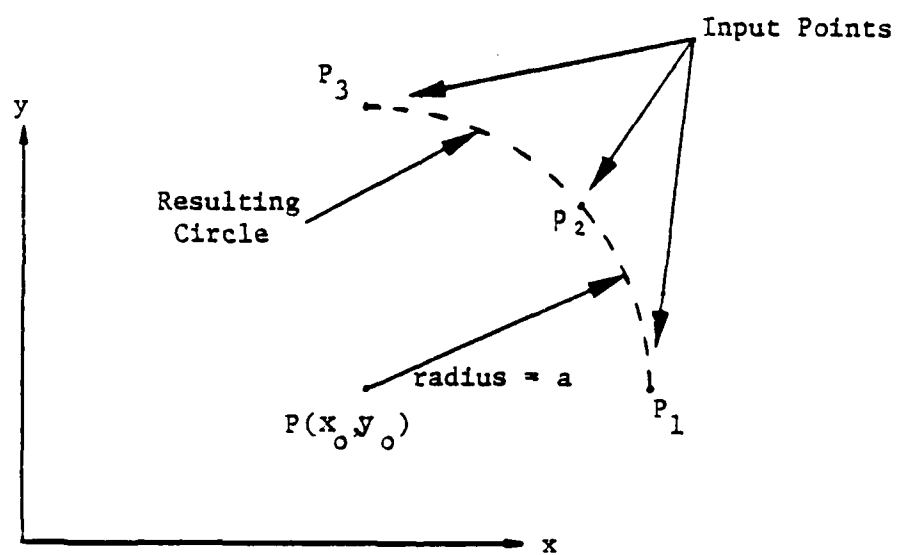


Figure 10 - Circular Arc Panel Geometric Definition

and from these the circle radius and the location of the center can be obtained.

The computer program which implements this procedure sets an arbitrary lower bound for  $|W|$  which effectively determines how close the three points can be to lying on a straight line. While a straight line can be interpreted as a circle of infinite radius, the computer code will not accept this.

The effects of element curvature can be studied by passing the approximating circular arc through three points  $P_1$ ,  $P_2$ , and  $P$  (Figure 11) rather than through  $P_1$ ,  $P_2$ , and  $P_3$  as described above. The point  $P$  is defined by a parameter  $\beta$  given by

$$0 \leq \beta = \frac{\ell_p}{\ell} \leq 1$$

where  $\ell$  and  $\ell_p$  are defined in Figure 11. As  $\beta$  varies from 0 to 1,  $P$  moves from  $P_4$  to  $P_3$ , and the curvature of the resulting circular arc changes from 0 to the curvature of the circle through the original input points  $P_1$ ,  $P_2$  and  $P_3$ . Note that the approximating arc always goes through the points  $P_1$  and  $P_2$ . The result is that the actual airfoil is modeled as a series of connected circular arcs. Having developed an approximation to the surface geometry, the next step in the formulation of a panel method is the representation of the surface singularity distribution. This will be discussed in the next section.



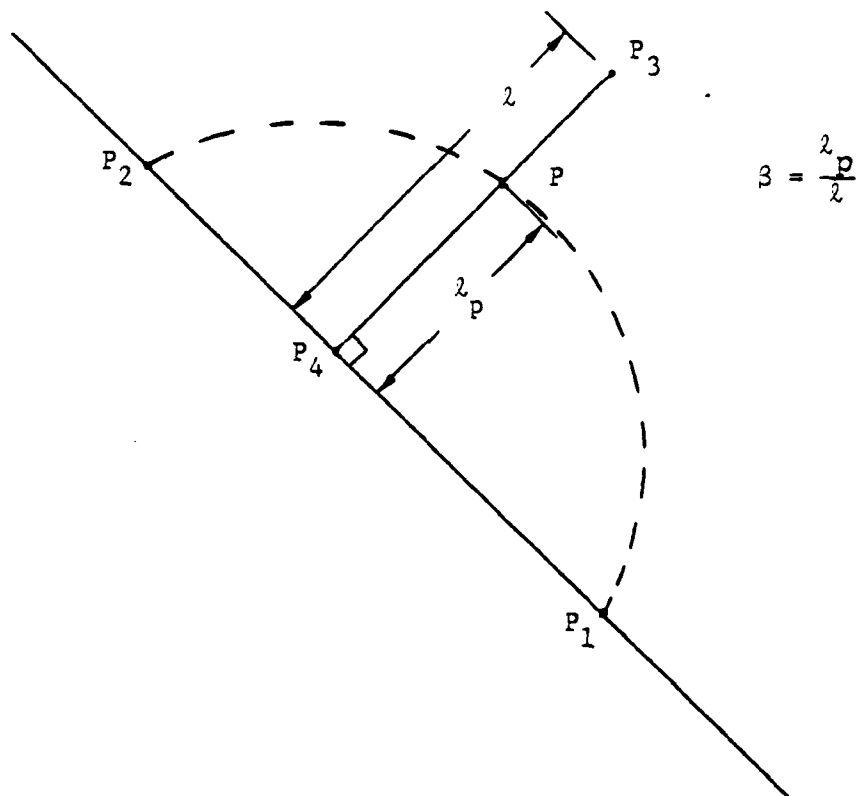


Figure 11 - Curvature Effect on Panel Defining Geometry

### Singularity Representation

It has been shown that source, doublet, or vortex singularities can be used to model potential flow problems, and that the doublet and vortex singularities are equivalent. The source singularity is incapable of generating lift on a body and its exclusive use would be unsuitable for lifting cases. Beyond this, however, there is little information available to indicate which singularity is the better one to use for particular applications. In terms of modeling the physical flow it is felt that the vortex singularity is more directly related to the actual flow since one is trying to model the viscous effects of the boundary layer by using the potential vortex sheet on the surface. The source or doublet singularity is more difficult to interpret physically, and for this reason it is believed that the vortex singularity provides more insight into what is actually happening in the flow near the surface. Since part of the purpose of this effort is to study the effect of choice of singularity on the solution the use of both the source and the vortex singularities will be investigated.

Series Expansion. The singularity strength distribution will be represented as a series expansion of the form

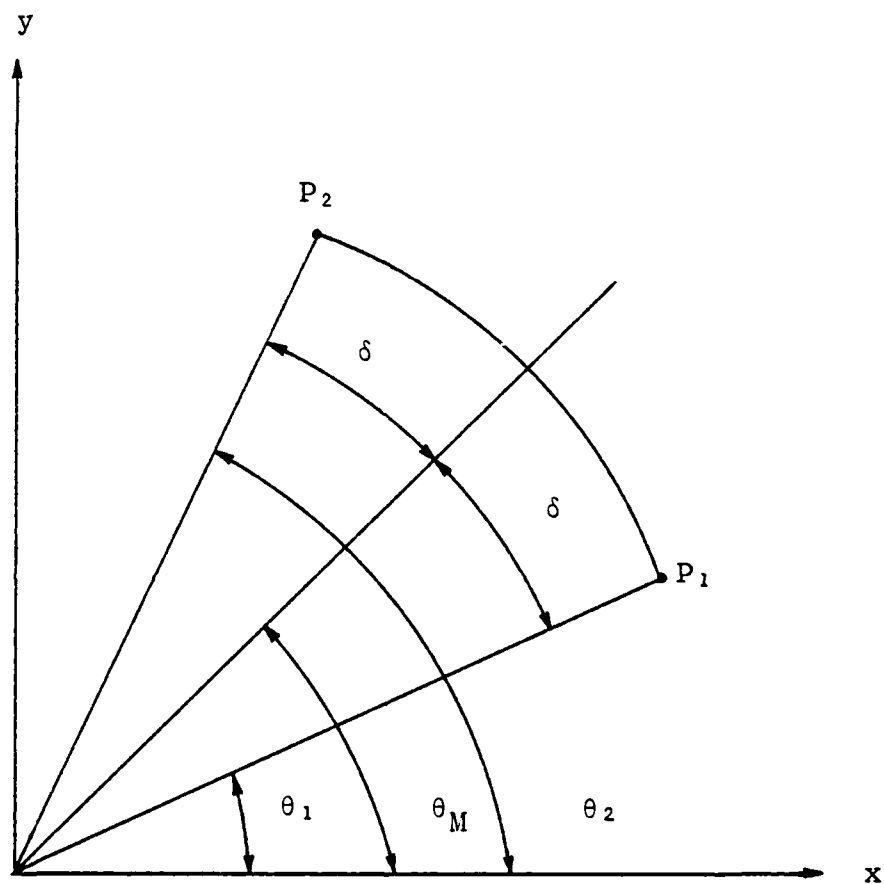


Figure 12. Circular Arc Panel Representation.

$$\sigma(\theta) = \sum_{k=0}^{Q-1} q_k \sin^k(\theta - \theta_1) \quad (47)$$

while for the airfoil cases the series used was an expansion about the panel midpoint  $\theta_M$ , so that

$$\sigma(\theta) = \sum_{k=0}^{Q-1} q_k \sin^k(\theta - \theta_M) \quad (48)$$

Here  $Q$  is the number of terms in the series. In the applications to follow  $Q$  will be varied from 1 to 4 in order to study its effect on the solution. It should be noted that  $Q$  is also the total number of unknowns on a panel so that the total number of unknowns for a problem which is modeled by  $N$  panels will be  $Q \cdot N$ . The two forms for singularity strength given above are essentially equivalent, although they exhibit certain differences in numerical characteristics which will be discussed in later sections where they are applied.

Continuity Conditions. An important part of this study will be to consider the effects of singularity strength continuity on the accuracy of the solution. This can be done by numerically requiring continuity of the singularity strength and its derivatives across panel junctures. The purpose of specifying continuity of derivatives is to obtain continuity of slope (or higher derivatives) of the function

TABLE IV

## Definition of Continuity Parameter C

| C | Singularity characteristic at panel junctures |
|---|---|
| 0 | discontinuous                                 |
| 1 | continuous                                    |
| 2 | continuous derivative                         |
| 3 | continuous 2nd derivative                     |

with respect to arc length along the airfoil. It will be convenient to characterize the singularity strength in terms of the degree of continuity which is imposed. For this purpose a continuity class parameter, C, can be defined as in Table IV.

On a circular arc of radius a the arc length S is given by  $s = a\theta$  so that

$$\frac{\partial^n \sigma}{\partial s^n} = \frac{1}{a^n} \frac{\partial^n \sigma}{\partial \theta^n}$$

Now if  $( )_j$  refers to quantities on the  $j^{\text{th}}$  panel, then the condition of continuity of the function from panel j to panel  $j + 1$  (that is a class C = 1 function) can be expressed using Eq 48 as

$$\sigma_j(\theta_{M_j} + \delta_j) = \sigma_{j+1}(\theta_{M_{j+1}} - \delta_{j+1}) \quad (49)$$

Likewise the condition for continuity of derivatives can be expressed as

$$\frac{1}{a_j^n} \frac{\partial^n \sigma_j(\theta_{M_j} + \delta_j)}{\partial \theta^n} = \frac{1}{a_j^n} \frac{\partial^n \sigma_{j+1}(\theta_{M_{j+1}} - \delta_{j+1})}{\partial \theta^n} \quad (50)$$

Equating these expressions gives equations which enforce continuity of the function across panel junctures through the derivative. The singularity strengths can be written using Eq 48 as

$$\sigma_j(\theta_{M_j} + \delta_j) = \sum_{k=0}^{Q-1} q_{k_j} \sin^k(\delta_j) \quad Q = 1, 2, 3, \text{ or } 4$$

and

$$\sigma_{j+1}(\theta_{M_{j+1}} - \delta_{j+1}) = \sum_{k=0}^{Q-1} q_{k_{j+1}} \sin^k(\delta_{j+1})$$

Substituting these into Eq 49 and 50 gives a matrix equation which prescribes continuity to class C at panel junctures of the form

$$\sum_{k=0}^{Q-1} [C_k^C] \{Q_k\} = 0 \quad (51)$$

Here the  $[C_k^C]$  denote  $N \times N$  continuity coefficient matrices and the  $\{Q_k\}$  denote  $N \times 1$  column vectors whose elements are the unknown  $q_k$ 's. The derivation of the  $[C_k^C]$  matrices

procedure for reducing the velocity boundary condition to a matrix equation will be given, followed by a discussion of the Kutta condition which will be used.

Velocity Boundary Condition. To illustrate the procedure of reducing the boundary condition to a matrix equation, consider the case of a normal velocity boundary condition applied to a surface on which is placed a source distribution. From Chapter II (Eq 27) the induced normal velocity at a point p on the surface is given by

$$v_n(p) = \lim_{p \rightarrow p} \frac{1}{2\pi} \oint_B \sigma(q) \frac{\partial K_s}{\partial n_p} dl$$

which becomes

$$v_n(p) = \frac{\sigma(p)}{2} - \frac{1}{2\pi} \oint_B \sigma(q) \frac{\partial}{\partial n_p} (K_s) dl$$

Now if the surface is modeled with N panels, and if the source distribution on panel j is

$$\sigma_j(q) = \sum_{k=0}^{Q-1} q_{k_j} f_{k_j}(q)$$

where the  $f_{k_j}$  are known functions and the  $q_{k_j}$  are unknown constants, then the normal velocity at the  $i^{th}$  control point is

$$v_n(p_i) = \sum_{j=1}^N \sum_{k=0}^{Q-1} \lim_{P \rightarrow p_i} \frac{1}{2\pi} \int_{\text{panel}_j} q_{k_j} f_{k_j} \frac{\partial}{\partial n_{p_i}} (K_{s_{ij}}) dl_j$$

The integral over the surface becomes a sum of integrals over each panel which can be computed analytically. In matrix form this can be written

$$\{v_n\} = \sum_{k=0}^{Q-1} [R_k] \{Q_k\}$$

where  $[R_k]$  are called aerodynamic influence coefficients and are given by

$$R_{k_{ij}} = \lim_{P \rightarrow p_i} \frac{1}{2\pi} \int_{\text{panel}_j} f_{k_j} \frac{\partial (K_{s_{ij}})}{\partial n_{p_i}} dl_j$$

If  $V_{\infty n}(p_i)$  is the normal velocity at the  $i^{\text{th}}$  control point due to the free stream, the statement of zero total normal velocity becomes

$$\sum_{k=0}^{Q-1} [R_k] \{Q_k\} = \{-V_{\infty n}\}$$

The detailed equations for the  $[R_k]$  are given in Appendix B. The formulation if a vortex singularity is used is the same, and influence coefficients for this case are also given in Appendix B. As noted earlier the vortex case

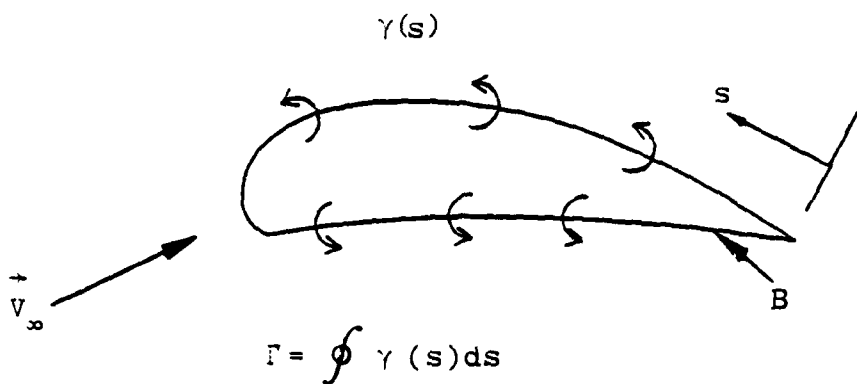


requires an additional condition to ensure uniqueness of the solution.

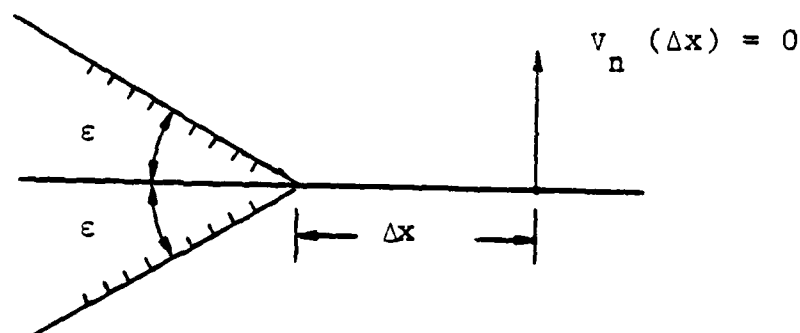
Kutta Condition. The requirement for a Kutta condition in a lifting potential flow model is well known. In Chapter II it was noted that such a condition was needed to obtain a unique solution to the problem of flow over a body using a surface vorticity distribution. The application of the Kutta condition is an important step in a potential flow model because it is essentially the link between the real viscous flow and the potential model that allows an accurate determination of the lift on a body.

Theoretically the Kutta condition requires a finite flow velocity at a sharp trailing edge. While there are many ways to achieve this requirement, three methods, depicted in Figure 13, have been used in this study; a specification of net circulation, a trailing edge bisector condition, and a specification of zero vorticity at the trailing edge. The specification of net circulation will be used to study the circular cylinder problem, but it is not useful in the study of a general airfoil since the net circulation is not known.

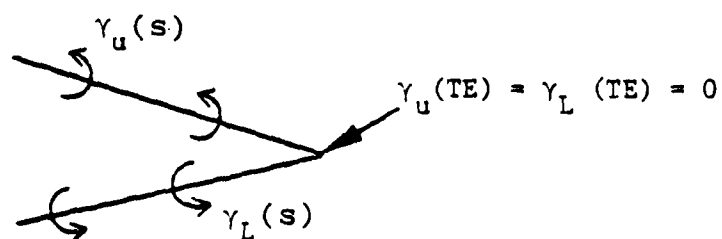
The trailing edge bisector condition (Figure 13b) involves a specification of zero velocity at a point  $\Delta x$  from the airfoil trailing edge, and in a direction normal to a line which bisects the airfoil



a. Specification of Net  $\Gamma$



b. Trailing Edge Bisector



c. Specification of  $\gamma$  at Trailing Edge

Figure 13 - Kutta Condition Specification

trailing edge angle. The distance  $\Delta x$ , which must be specified a priori, should be small, but beyond that it is arbitrary. While this procedure has given good results in solving the airfoil problem, the arbitrariness in choosing  $\Delta x$  is undesirable.

The last method, specification of zero vorticity at the trailing edge, has been used to obtain the majority of the airfoil results which will be presented later because it is felt that it is conceptually the most logical approach. It is based on the fact that, for a surface distribution of vorticity with an appropriate boundary condition such that the internal flow is stagnated, the surface vorticity equals the tangential velocity on the surface. Since the trailing edge should be a stagnation point where the tangential velocity is zero, a specification of zero vorticity at the trailing edge, both upper and lower surface, is an equivalent Kutta condition. A problem with this specification is that two equations are required, one for the upper surface and one for the lower surface, and thus the complete problem is overspecified by one equation.

One way to circumvent this is to use an error parameter approach (Refs 26, 31) in which a uniform but unknown error  $t$  in normal velocity is assumed at each control point. The equation for zero normal velocity becomes

$$t + V_{n_i} = -V_{\infty} n_i$$

where  $V_{n_i}$  is the  $i^{\text{th}}$  row of

$$\{V_n\} = \sum_{k=0}^{Q-1} [R_k] \{Q_k\}$$

More generally this can be written as

$$[M]\{T\} + \{V_n\} = \{-V_{\infty n}\}$$

where

$$\{T\} = \begin{Bmatrix} t \\ \cdot \\ \cdot \\ \cdot \\ t \end{Bmatrix}$$

and  $E$  is a diagonal matrix of weighting factors which selects the control points at which the error will be applied. Usually the nonzero elements of  $M$  would be 1. Henshaw and Bristow have had success with this approach, but it is felt that the major drawback to it is the high degree of arbitrariness it introduces into the formulation.

In a second method, used by Woodward (Ref 38), a source of unknown strength is placed inside the airfoil to provide the required additional unknown. Recalling the discussion of potential theory it was found that the problem of a vortex distribution on a closed body with an external normal velocity boundary condition produced an ill posed problem unless the net inflow through the surface was zero. Theoretically this is the problem under consideration, but in the numerical formulation, the net inflow condition

cannot be satisfied because boundary conditions are applied only at discrete points. The internal point source can be thought of as a method of removing any excess fluid that flows into the body as a result of imperfect satisfaction of the boundary condition. The procedure is to place a point source inside the body, and add a term reflecting the effect of the source to the equation for normal velocity at each control point. Since the location of the source is arbitrary, this is a parameter whose effect on solution accuracy must be studied.

#### Numerical Implementation

The basic elements of a new panel method have been developed in the preceding sections. They include the choice of surface and singularity representations, the selection of velocity and continuity boundary conditions, and if necessary the choice of a Kutta condition. In this section these elements will be combined into a system of linear algebraic equations which will be solved using standard methods.

Matrix Equation Formulation. The procedure for obtaining the solution to the airfoil problem using a source distribution is to model the airfoil with  $N$  panels. The number of terms,  $Q$ , in the singularity representation is then chosen, so that the problem has a total of  $Q \cdot N$  unknowns. The desired continuity class,  $C$ , of the

singularity strength is then chosen. This formulation means that with  $Q$  unknowns per panel and  $C$  continuity conditions per panel, a total of  $L = Q - C$  velocity boundary conditions must be applied on each panel in order to have a determinate linear algebraic system. These control points will in general be equally spaced on a panel, as shown in Figure 14.

The full system of normal velocity boundary conditions and continuity conditions can be written

$$\sum_{k=0}^{Q-1} [R_k^h] \{Q_k\} = -V_{\infty n} \quad h = 1, 2, \dots, L$$

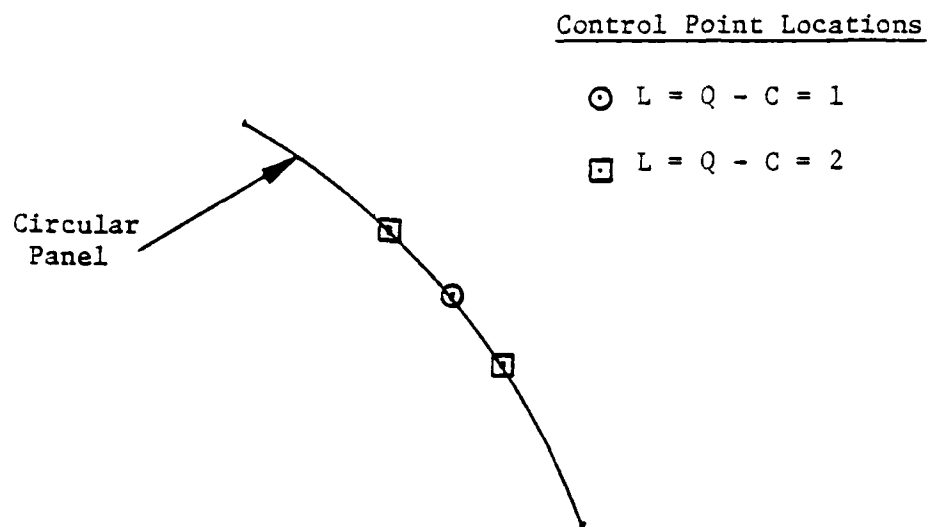
$$\sum_{k=0}^{Q-1} [C_k^m] \{Q_k\} = 0 \quad m = 0, 1, \dots, C$$

These can be combined into one  $Q \cdot N$  by  $Q \cdot N$  system

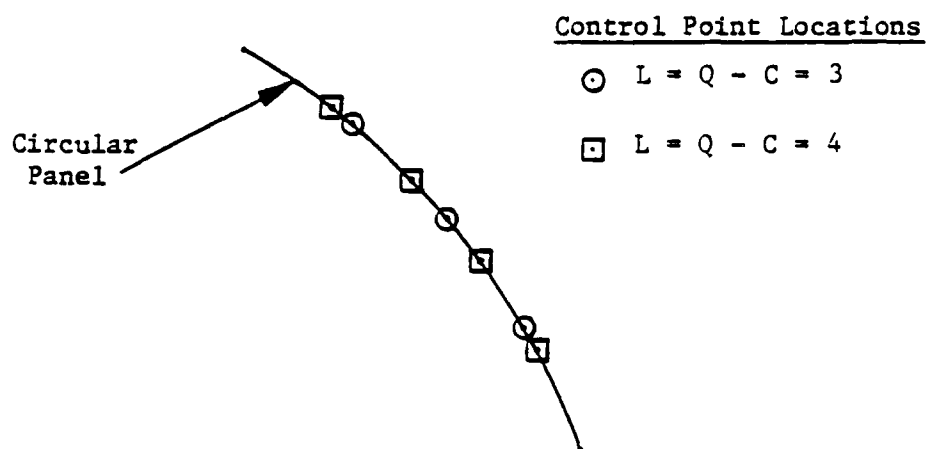
$$[A]\{X\} = \{B\}$$

For the vortex singularity case in which an internal point source is added, and the vorticity is specified as zero at the trailing edge, an additional unknown and one equation must be added so that the full system is  $(Q \cdot N + 1)$  by  $(Q \cdot N + 1)$ .

Method of Solution. Although many algorithms are



a. 1 and 2 Control Points per Panel



b. 3 and 4 Control Points per Panel

Figure 14 - Control Point Spacing

available for solving systems of linear equations, no special effort was made in this study to evaluate different methods. A standard routine from the International Mathematical and Statistical Library (IMSL)(Ref 67) was used in all cases. This routine performs matrix inversion using Gaussian elimination with equilibration and partial pivoting. It should be noted that the system developed above exhibits no special characteristics such as bandedness or symmetry which would allow the use of solvers designed for such cases.

In this chapter the general panel method approach to solving potential flow problems has been outlined and the details of a new panel method have been presented. The new method is based on the use of continuous circular arc panels to model a two dimensional surface. A surface singularity represented as a higher order sine series expansion is then distributed on the panels. This distribution is given a specified degree of continuity, appropriate velocity boundary conditions are applied, and the problem is reduced to a system of linear algebraic equations in which the unknowns are constants in the assumed singularity distribution.

There are several parameters in this formulation which affect its results, including type of singularity, number of terms in the series, the continuity class, number of panels, curvature of the panels, and control point location on the



panels. In the next two chapters the method will be applied to the problems of flow over a circular cylinder, and flow over several different airfoils. The effects of the parameters noted above will be evaluated, and the results will be compared with those of other two dimensional methods.

#### IV. Application to the Circular Cylinder

The purpose of this chapter is to apply the present method to the problem of flow over a circular cylinder, which has been chosen as a test case for a number of reasons. First, the circle is a simple shape for which the exact solution in terms of both singularity distribution and surface velocity is easily computed. Additionally, the surface is free of slope discontinuities which will remove the ambiguities noted earlier which are associated with a surface singularity distribution at a corner and with the application of the Kutta Condition. It is realized, of course, that the circle would seem to be ideally suited for a method which uses circular arcs for panels.

An extensive study will also be conducted to determine the effect of a number of parameters on the accuracy of the solution. These include the singularity type, the number of terms in the singularity distribution, the number of panels, continuity, and control point location. The following sections will discuss the exact solution with which the computed solution will be compared, the panel method formulation of the problem, and the results of the parameter sensitivity studies.

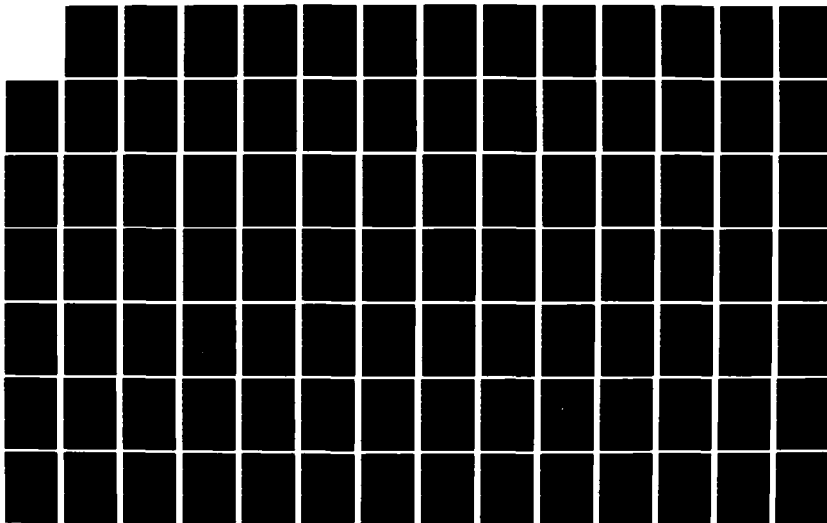
AO-A124 896

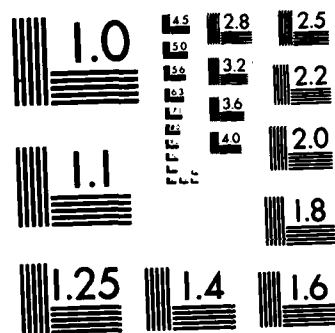
COMPUTATION OF INCOMPRESSIBLE POTENTIAL FLOW OVER AN  
AIRFOIL USING A HIGH. (U) AIR FORCE INST OF TECH  
WRIGHT-PATTERSON AFB OH SCHOOL OF ENGI. J DEJONGH  
AUG 82 AFIT/DS/AR/82-1 F/G 12/1

2/3

UNCLASSIFIED

NL





MICROCOPY RESOLUTION TEST CHART  
NATIONAL BUREAU OF STANDARDS-1963-A

### Exact Solution

Consider the classic problem of uniform flow over a circular cylinder as shown in Figure 15. Although this problem can be solved in several ways, the exact solution will be developed in terms of source and vorticity surface singularity distributions. This will provide an introduction to the use of this method to obtain approximate solutions to more complicated problems.

Source Distribution. Assume there exists a surface source distribution,  $\sigma(\theta)$ , on the cylinder shown in Figure 15, and apply a zero normal velocity condition to this problem. Let P go to p on the surface  $r=1$  to obtain from Eq 28, the normal velocity component induced by the source sheet as

$$v_r(1, \theta) = \frac{\sigma(\theta)}{2} + \frac{1}{4\pi} \int_0^{2\pi} \sigma(\theta_0) d\theta_0 \quad (52)$$

The boundary condition is

$$v_r(1, \theta) + V_{\infty} \cos \theta = 0$$

so that Eq 52 becomes

$$\sigma(\theta) + \frac{1}{2\pi} \int_0^{2\pi} \sigma(\theta_0) d\theta_0 = -2 \cos \theta \quad (53)$$

This is a Fredholm Equation of the Second Kind with parameter  $\lambda = \frac{-1}{2\pi}$ . Since  $\lambda$  is not an eigenvalue Eq 53 has

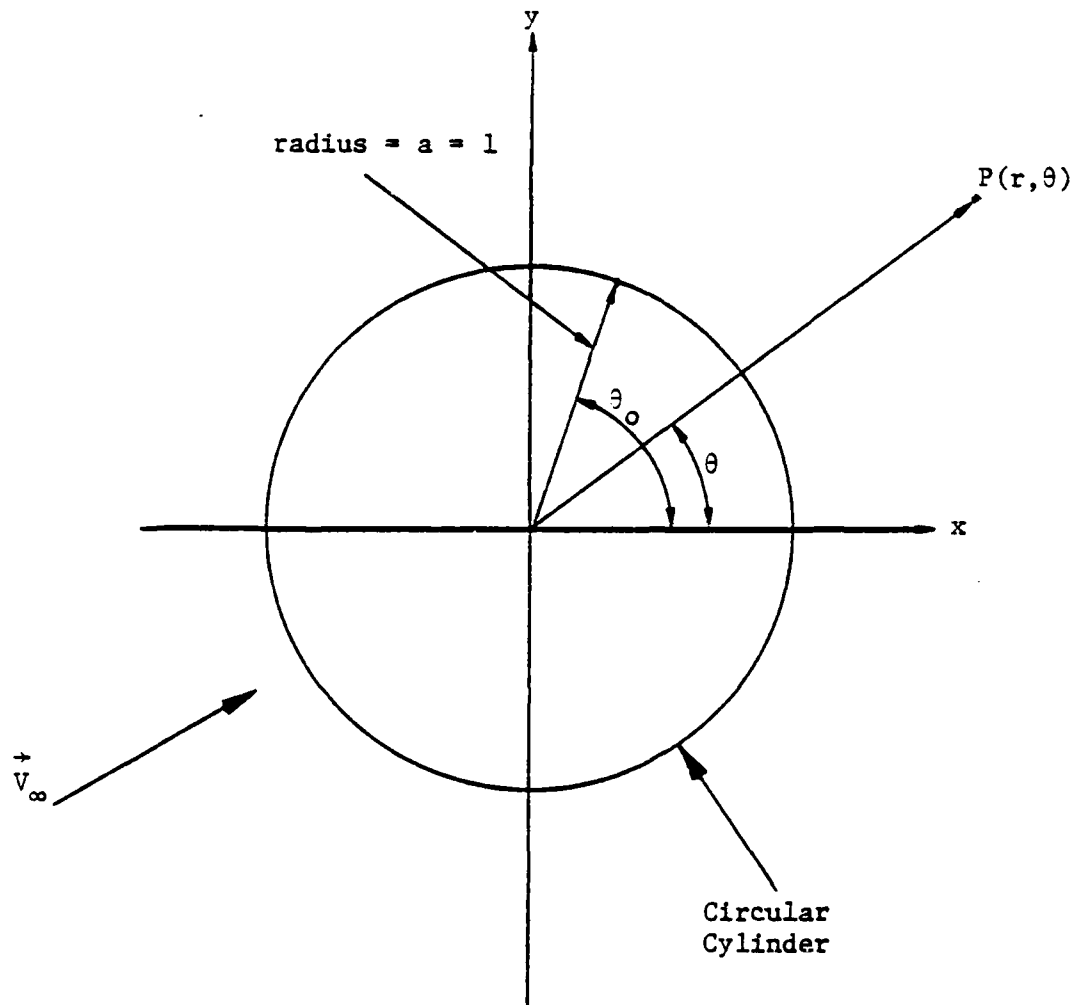


Figure 15 - Flow Over a Circular Cylinder

a unique nontrivial solution. It can be obtained by integrating Eq 53 to get

$$\int_0^{2\pi} \sigma(\theta) d\theta + \int_0^{2\pi} \left[ \frac{1}{2\pi} \int_0^{2\pi} \sigma(\theta_0) d\theta_0 \right] d\theta = \int_0^{2\pi} -2 \cos \theta d\theta \quad (54)$$

Letting

$$Q_S = \frac{1}{2\pi} \int_0^{2\pi} \sigma(\theta_0) d\theta_0$$

where  $Q_S$  is the total source strength  
Eq 54 becomes

$$2\pi Q_S + Q_S = 0$$

Therefore

$$Q_S = 0$$

and

$$\sigma(\theta) = -2 \cos \theta$$

The induced normal and tangential velocities on the surface are

$$v_r(1, \theta) = -\cos \theta$$

and

$$v_t(1, \theta) = -\sin \theta$$

and the total tangential surface velocity is

$$V_t = v_t + V_{\infty t} = -2 \sin \theta \quad (56)$$

The natural result of this formulation is that the total source strength is zero, as should be expected both in this exact solution and in the subsequent approximate solutions. The deviation from zero of the total source strength can be used as a measure of the accuracy of the approximate solution.

As was discussed in Chapter II, the flow in the interior region of a closed body is independent of that in the exterior region. For the choice of a source distribution on the cylinder with a zero normal velocity boundary condition, the flow pattern in the interior of the cylinder is shown in Figure 16a.

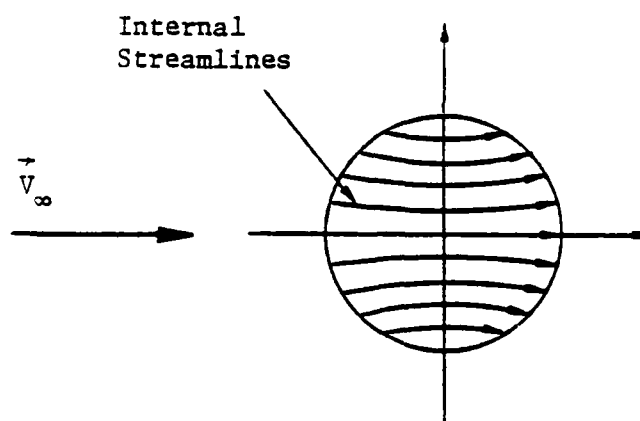
Vorticity Distribution. This problem can also be solved using a surface vorticity distribution and a zero internal tangential velocity boundary condition. In this case the perturbation tangential velocity on the interior surface of the cylinder due to a vorticity distribution,  $\gamma(\theta)$  is

$$v_t(1, \theta) = \frac{-\gamma(\theta)}{2} + \frac{1}{4\pi} \int_0^{2\pi} \gamma(\theta_0) d\theta_0 \quad (57)$$

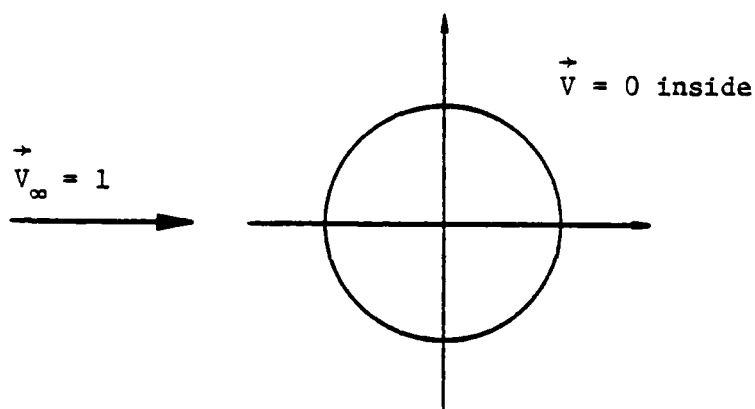
Applying the boundary condition

$$v_t + V_{t_\infty} = v_t - \sin \theta = 0$$

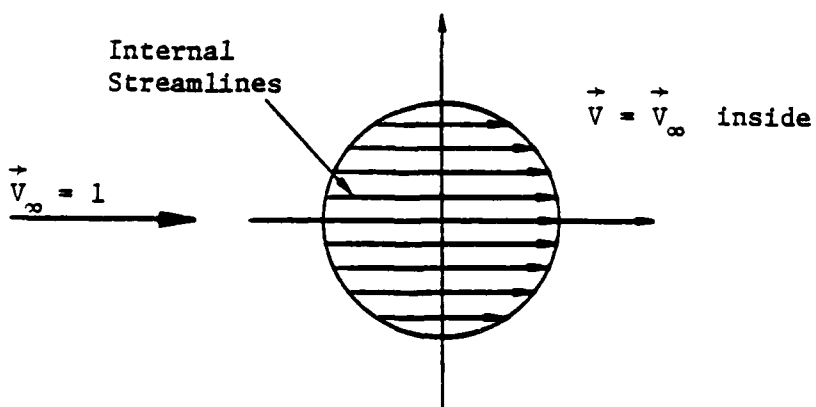




a. Source Distribution,  $V_{n_e} = 0$



b. Vortex Distribution,  $V_{t_i} = 0$



c. Source/Vortex Distribution,  $V_{n_e} = 0$

Figure 16 - Internal Flow Patterns

Eq 57 becomes

$$\gamma(\theta) - \frac{1}{2\pi} \int_0^{2\pi} \gamma(\theta_0) d\theta_0 = -2 \sin \theta \quad (58)$$

Recall that this is a Fredholm Integral Equation of the Second Kind with parameter  $\lambda = \frac{1}{2\pi}$ . Since  $\lambda$  is an eigenvalue, a solution to Eq 58 exists only if

$$\int_0^{2\pi} u(\theta_0) f(\theta_0) d\theta_0 = 0 \quad (59)$$

when  $f(\theta_0) = -2 \sin \theta_0$

and where  $u(\theta_0)$  is a solution to

$$u(\theta) - \frac{1}{2\pi} \int_0^{2\pi} u(\theta_0) d\theta_0 = 0 \quad (60)$$

Clearly  $u(\theta_0) = c_j$  (where  $c_j$  is any constant is a solution to Eq 60, and thus is an eigenfunction of Eq 58. Given any  $c_j$  Eq 59 holds; therefore, the general solution to Eq 58 is

$$\gamma(\theta) = \gamma_p(\theta) + \sum_j c_j$$

where  $\gamma_p(\theta)$  is a particular solution and  $\sum_j c_j$  is a sum over all linearly independent eigenfunctions. But since each  $c_j$  is a constant only one will be linearly independent; therefore  $\sum_j c_j = D$  where  $D$  is any constant. By inspection,  $\gamma_p(\theta) = -2 \sin \theta$ , so that

inside the cylinder (see Figure 16b) compared with the non zero flow produced by the source distribution.

Combined Source/Vorticity Distribution. The preceeding two approaches can be combined by assuming source and vorticity distributions of the form

$$\sigma(\theta) = -A \cos \theta \quad (64c)$$

$$\gamma(\theta) = -B \sin \theta + \frac{\Gamma}{2\pi} \quad (64b)$$

where A and B are constants to be determined. The total external normal velocity is then

$$V_n(1, \theta) = (1 - \frac{A+B}{2}) \cos \theta \quad (65)$$

and a zero normal velocity boundary condition requires that

$$A + B = 2 \quad (66)$$

The total tangential velocity is then, using Eq 66,

$$V_t(1, \theta) = -\sin \theta - \frac{A+B}{2} \sin \theta + \frac{\Gamma}{2\pi} = -2\sin\theta + \frac{\Gamma}{2\pi} \quad (67)$$

The velocity given by Eq 67 is the same for any values of A and B as long as Eq 66 is satisfied.

For example, choosing  $A = B = 1$  is equivalent to setting the source strength equal to the normal component

### Panel Method Solution

The method developed in Chapter III will now be applied to the circular cylinder problem. The circle will be divided into  $N$  panels of equal arc length with panel number 1 centered on the trailing edge stagnation point, as shown in Figure 17. While Eq 48, termed the element centered formulation, is the preferred singularity distribution for the case of a general body, when it is used for the case of a circle with equally spaced panels with control points at panel centers (the points about which the distribution is expanded) some elements of the velocity influence coefficients become zero, producing a singular matrix. For this reason Eq 47, termed the element non-centered formulation, will be used to represent the singularity distribution for flow over a circle.

An advantage of using this series is that the continuity matrices become diagonal. A disadvantage is that the results are not completely symmetric. The degree of symmetry increases as the overall accuracy of the solution is increased by varying other parameters. The results do exhibit a polar symmetry about the origin. That is, the results on a ray connecting two points on the circle and passing through the origin are identical. Note that a solution which assumes symmetry has not been developed so that the method may be applied to asymmetric airfoils.

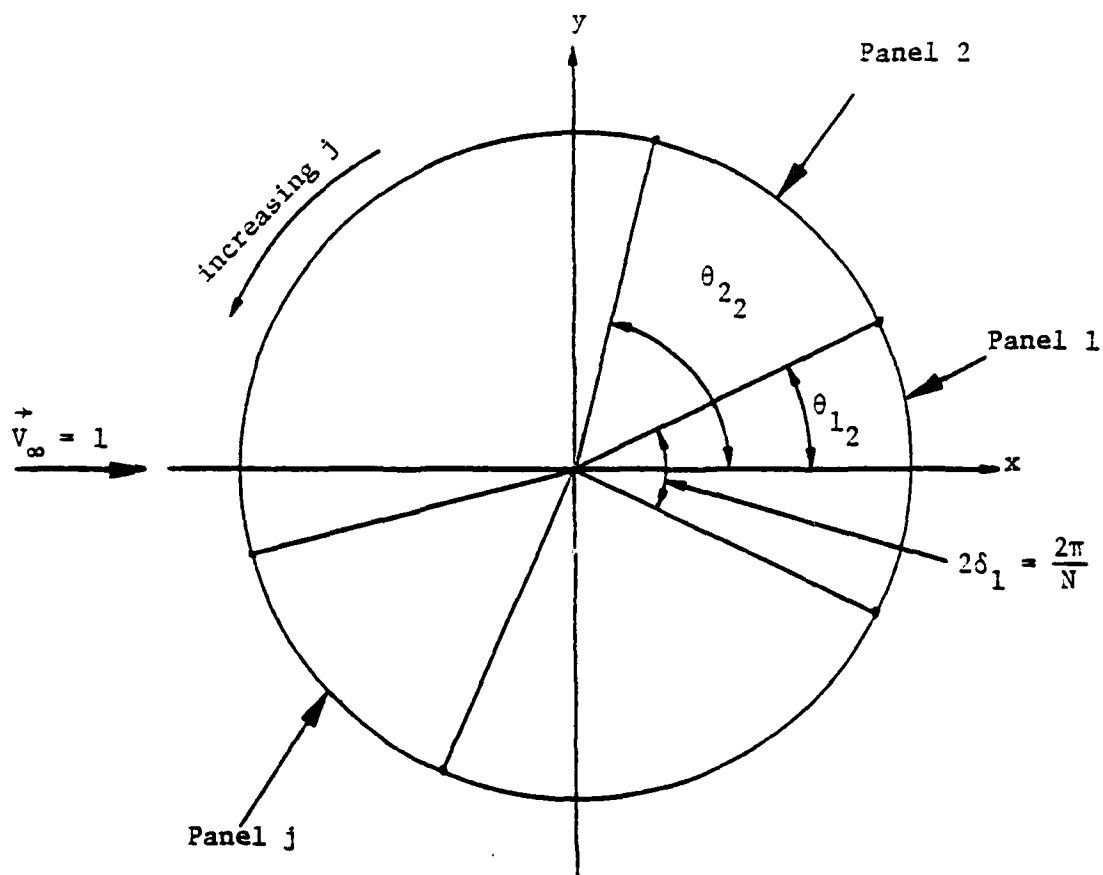


Figure 17 - Circular Cylinder Paneling

## Results

The results of the application of the method to the circular cylinder problem will be presented in terms of velocity error plots since the exact velocity on the cylinder can be computed. First, the effects of the various parameters will be compared using a series of maximum absolute velocity error plots. This will be followed by a consideration of the local error distribution on the surface, and finally a discussion of the sensitivity of the solutions to control point location will be presented. Although no special attention was given to the question of computational efficiency, a limited assessment of the effect of the higher order method on efficiency will be made. In general, each solution presented required no more than several seconds of computer time on a CDC 6600/CYBER 74 computer.

Global Error. Figures 18 to 21 show the effects on accuracy due to panel size, or number of elements ( $N$ ), continuity ( $C$ ), and number of terms ( $Q$ ) in the singularity distributions for various choices of singularity and boundary condition. Figure 18 also shows lines of constant computer time which will be discussed later. These charts show the maximum absolute value error in surface normal or tangential velocity versus  $N$  for various combinations of  $Q$

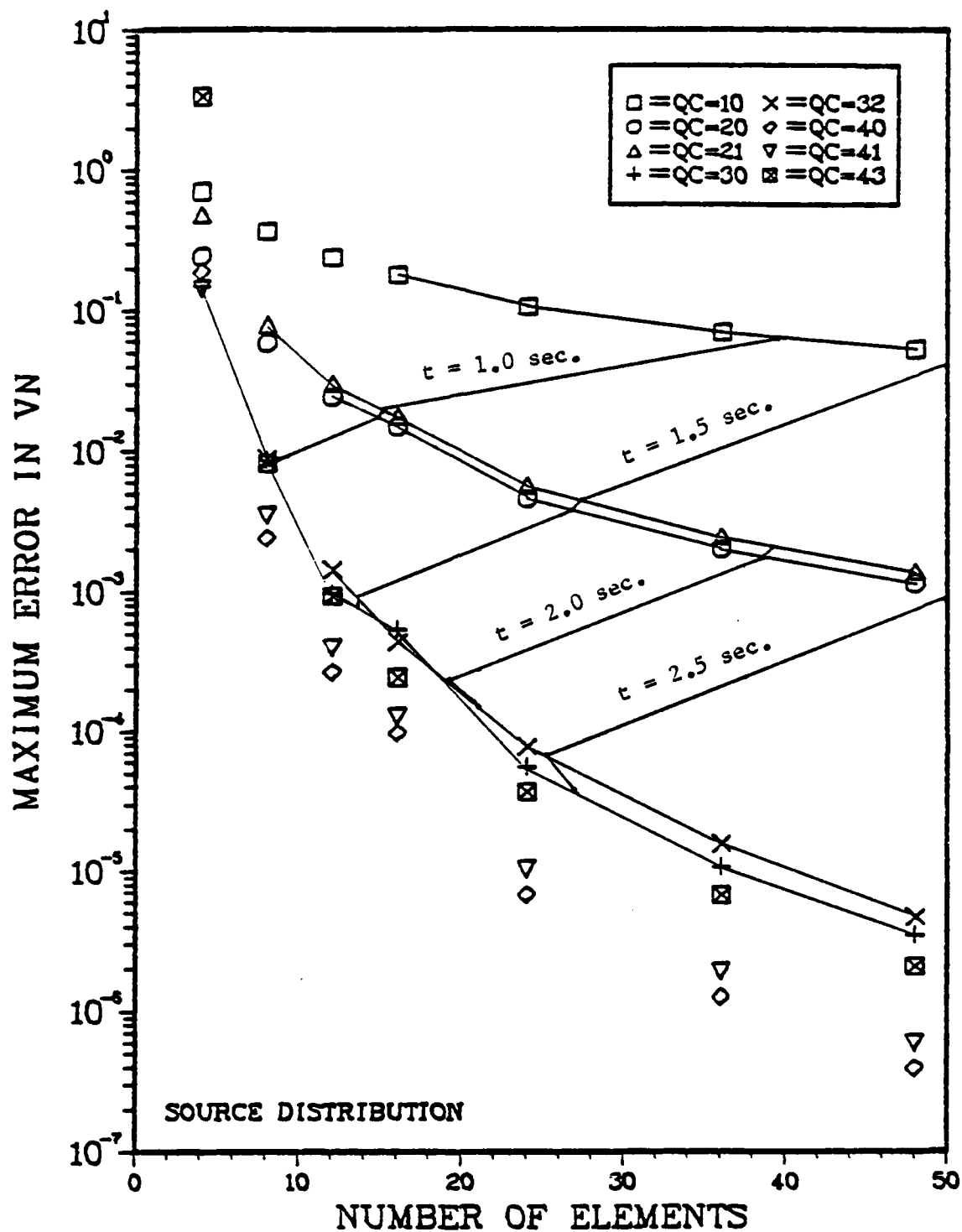


Figure 18. Maximum Absolute Normal Velocity Error on a Circle, Source Distribution, Normal Velocity Boundary Condition.

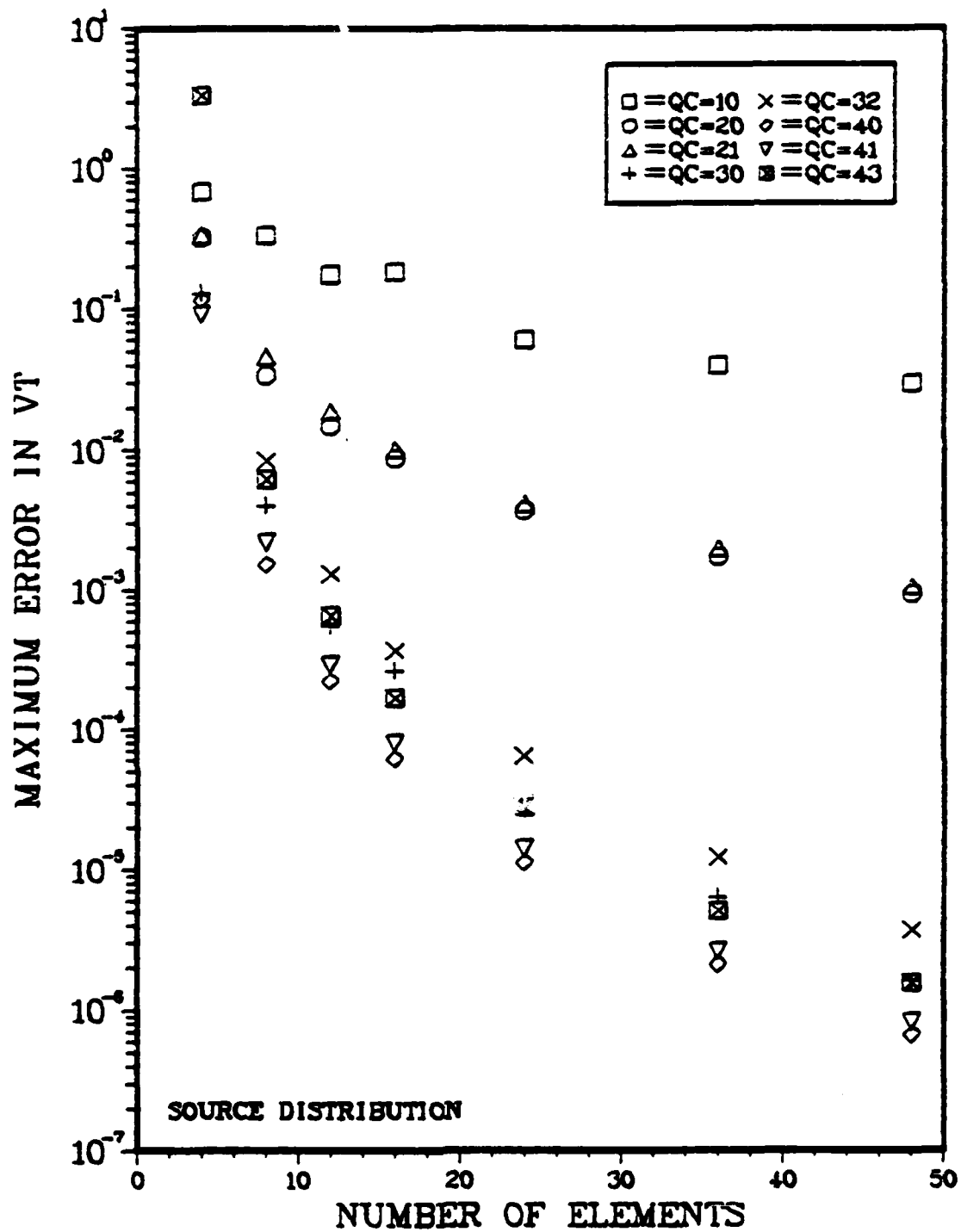


Figure 19. Maximum Absolute Tangential Velocity Error on a Circle, Source Distribution, Normal Velocity, Boundary Condition.



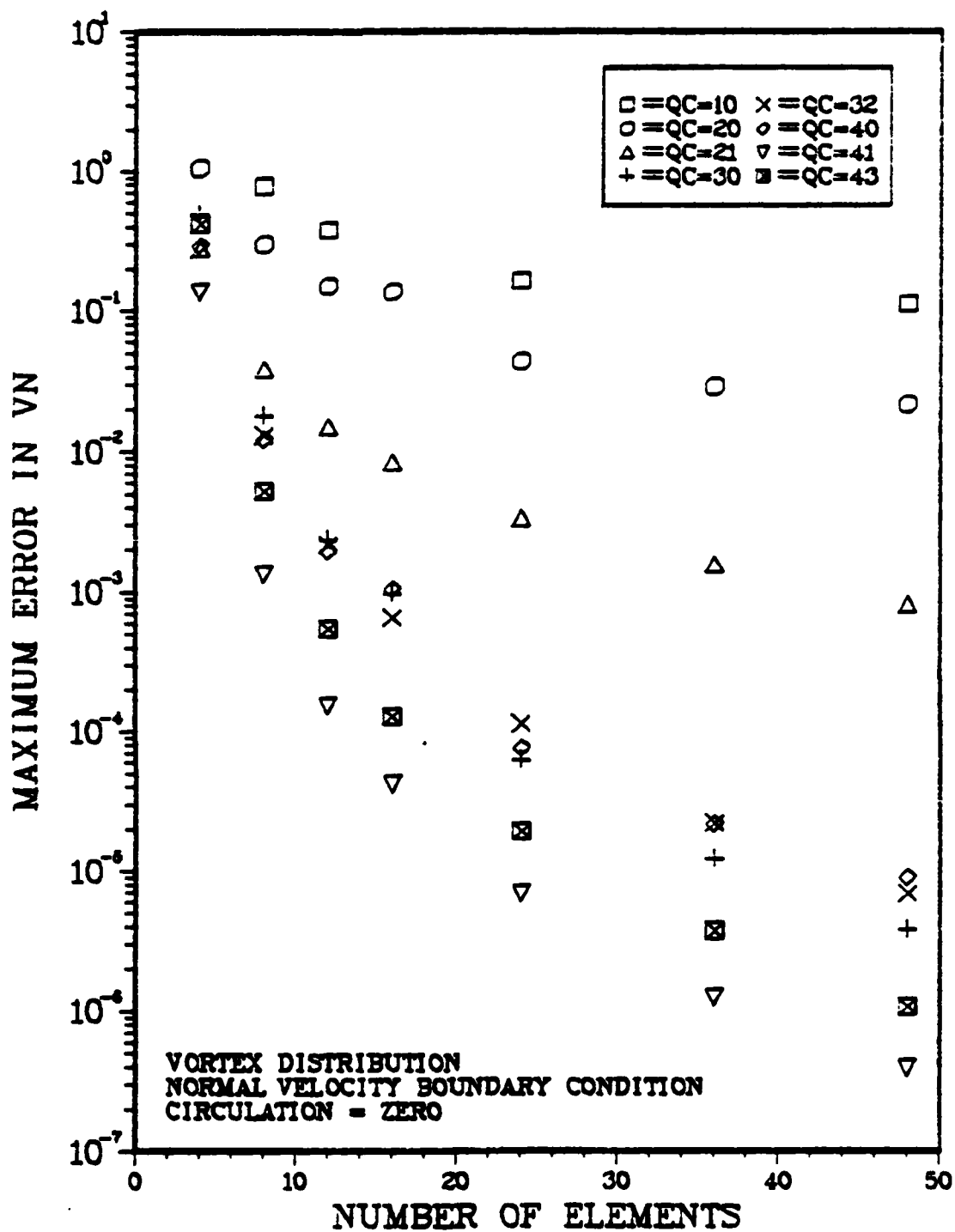


Figure 20. Maximum Absolute Normal Velocity Error on a Circle, Vortex Distribution, Normal Velocity Boundary Condition.

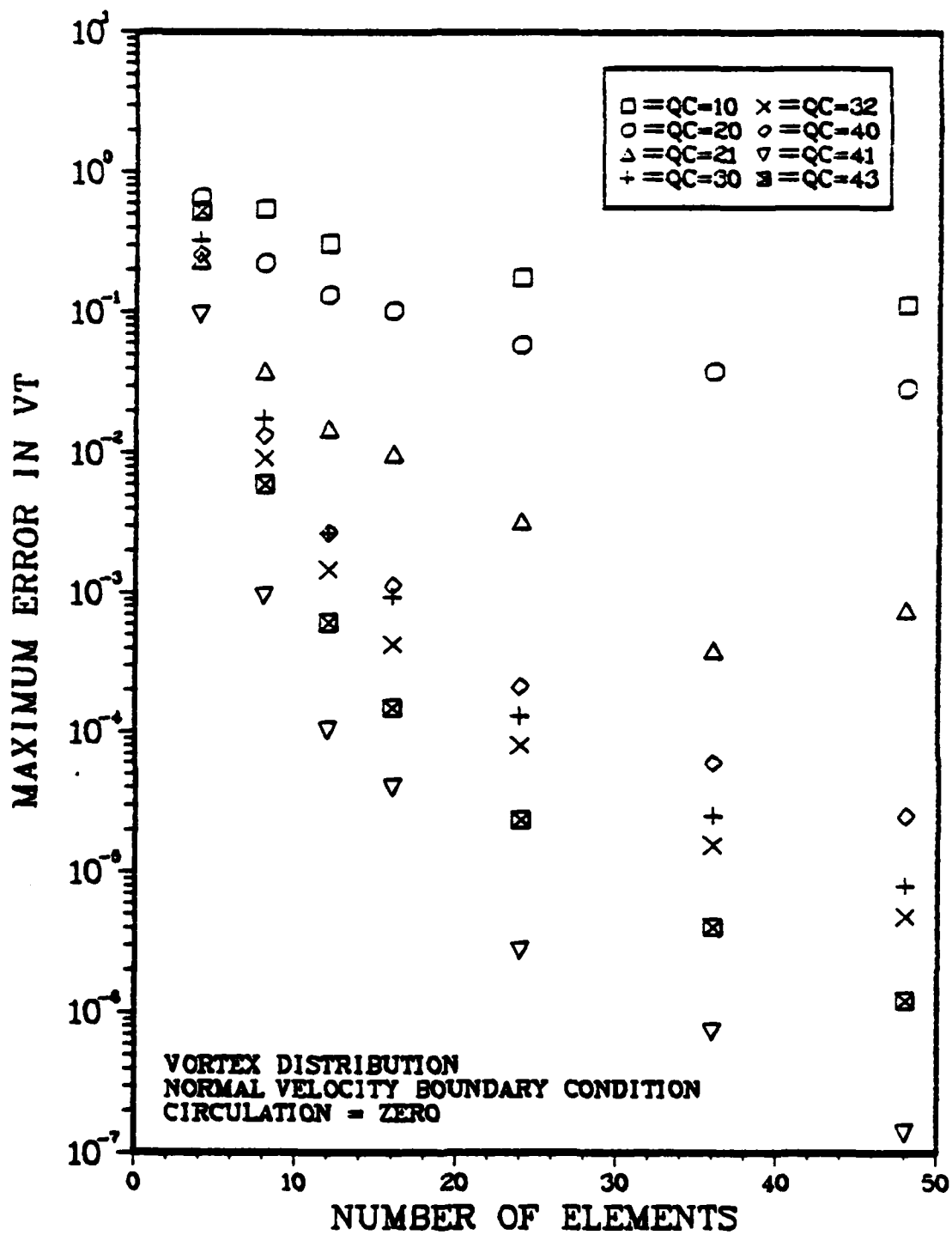


Figure 21. Maximum Absolute Tangential Velocity Error on a Circle, Vortex Distribution, Normal Velocity Boundary Condition.

and C. The ranges on these parameters are

$$4 \leq N \leq 48$$

$$1 \leq Q \leq 4$$

$$0 \leq C \leq 3$$

$$L + Q - C = \begin{array}{l} \text{Control Points} \\ \text{Per Panel} \end{array}$$

From the solution obtained for each case, velocities on the circle were computed at 120 equally spaced points around the circle, and from these the largest absolute value errors were determined according to Eq 69.

$$E_{QC} = \text{MAX} \left[ \frac{V_{\text{comp}}(\theta_i) - V_{\text{ex}}(\theta_i)}{V_{\infty}} \right] \quad (69)$$

$$\theta_i = \frac{i}{120} \quad i = 1, 2, \dots, 120$$

This approach is a simple way of comparing the effect of the above parameters on the relative accuracy of the computed solutions for various choices of the parameters, and it allows the effects of these parameters on the solution to be studied. The values for maximum error are not to be interpreted, however, as the largest error anywhere on the surface for a particular solution. Since the velocities are singular at panel endpoints the error there can be made arbitrarily large by computing velocities at points closer and closer to the panel endpoints (at least for the discontinuous cases). Another fact to note concerning the

above figures is that points are missing for certain parameter combinations because the influence coefficient matrices were singular. Examination of the matrices in question revealed that this phenomena is a numerical result of the symmetry of the circle problem.

Figures 18 and 19 show the maximum absolute errors in normal and tangential velocity respectively for a source distribution on the circle using a normal velocity boundary condition. Figures 20 and 21 show the same maximum absolute errors for a vorticity distribution for which the total circulation was specified as zero. Results for the case of non zero circulation were nearly identical.

The symmetry of the problem resulted in three interesting effects. First, the total source strength is identically zero for all cases as it should be for an exact solution. Second, total circulation in the vorticity case can be specified without adding an additional equation to the system. The reason for this is that the expression for net circulation is embedded in the left hand side of the problem, and can be conveniently extracted and fixed. Although this would not in general be an acceptable method of specifying circulation, the symmetry of the problem ensures that this technique will be successful for the circular cylinder case. Third, while the case of a vortex only distribution with normal velocity boundary conditions

difference, and the rate of accuracy improvement both increase up to the  $Q=3$  cases. However as  $Q$  goes from  $Q=3$  to  $Q=4$  the effects of continuity seem to play a more important role than in the source case. For the  $Q=2$  case the continuous solution is much better than the discontinuous solution, in contrast to the source case where the two were very close, with the discontinuous case being slightly better. Considering the  $Q=3$  cases, it is found that both the  $C=0$  and  $C=2$  cases are actually better than the  $Q=4$ ,  $C=0$  case. In fact, if  $E_{QC}$  denotes the error for the case  $Q$  and  $C$ , the relative level of error for the normal velocity is seen to be

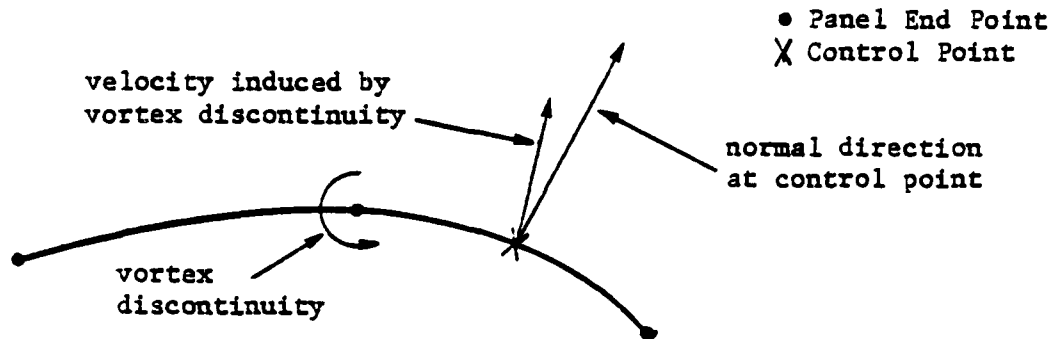
$$E_{41} < E_{43} < E_{30} < E_{32} < E_{40}$$

while that for the tangential velocity is seen to be

$$E_{41} < E_{43} < E_{32} < E_{30} < E_{40}$$

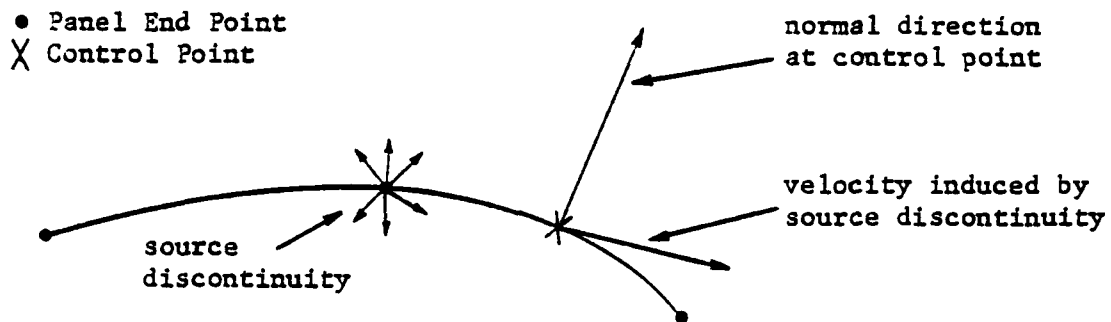
For a given value of  $Q$ , continuity is important for the tangential velocity error, but additional degrees of continuity beyond  $C=1$  are not required. Also, the effect of increasing  $Q$  from 3 to 4 is not clear in that, contrary to what might be expected, the benefit of the additional term seems to depend on the particular continuity requirement that is imposed.

It has been noted that a discontinuous distribution of



sources gives better results than does a continuous distribution, while the opposite is true for the vortex case. A possible explanation for this lies in the characteristics of the singularities themselves coupled with the normal velocity type boundary condition which was used in the above cases.

For the case of a vortex distribution, a discontinuity in strength at a panel juncture will act like a line vortex, the effect of which will be felt mainly by control points near the panel juncture, as opposed to control points which are far away from it. The velocity induced by this line vortex at these nearby control points will usually have a significant component normal to the panel because most panels are not highly curved. This can be seen qualitatively in the sketch above. This normal component of



velocity which would not be there if the singularity distribution were continuous, is very effectively cancelled by the normal velocity boundary condition which was used, but the vortex strength solution thus obtained is not what it would be if the vortex distribution was continuous. Thus it seems reasonable that the vortex case would be sensitive to whether or not a continuous distribution was used.

It is also reasonable to expect that the source distribution might be less sensitive to imposition of continuity for similar reasons. In the source case the velocity component induced by a discontinuity at a panel juncture at a nearby control point would be small if the panel was not highly curved (See the sketch above). Thus this normal component of velocity would not have a large

effect on the source strength solution obtained by applying a normal velocity boundary condition.

Hess (Ref 12) has developed a criterion for mathematical consistency of a panel method. This criterion is that the singularity distribution should be of an order one degree lower than the order of the surface element. He notes, however that others (Ref 25) have violated this rule and have obtained good results. The present results for the cylinder given above are also in violation of this rule, because, although the circular arc is a quadratic element, accuracy improvements were obtained for the  $Q=2,3$  and 4 cases. It is felt that the errors introduced during the numerical implementation of the present method, or other methods, probably overshadow the mathematical argument for consistency.

Figure 22 shows the maximum error in normal velocity for a source versus a vortex solution for several combinations of  $Q$  and  $C$ . The element number ranges from 4 to 12. The vortex results were obtained using a tangential velocity boundary condition. The maximum error in the vortex solution is seen to be consistently less than that for the source solution for the same number of elements.

### Efficiency

Superimposed on Figure 18 are lines of constant computer time for a CDC 6600/CYBER 74 computer. These times



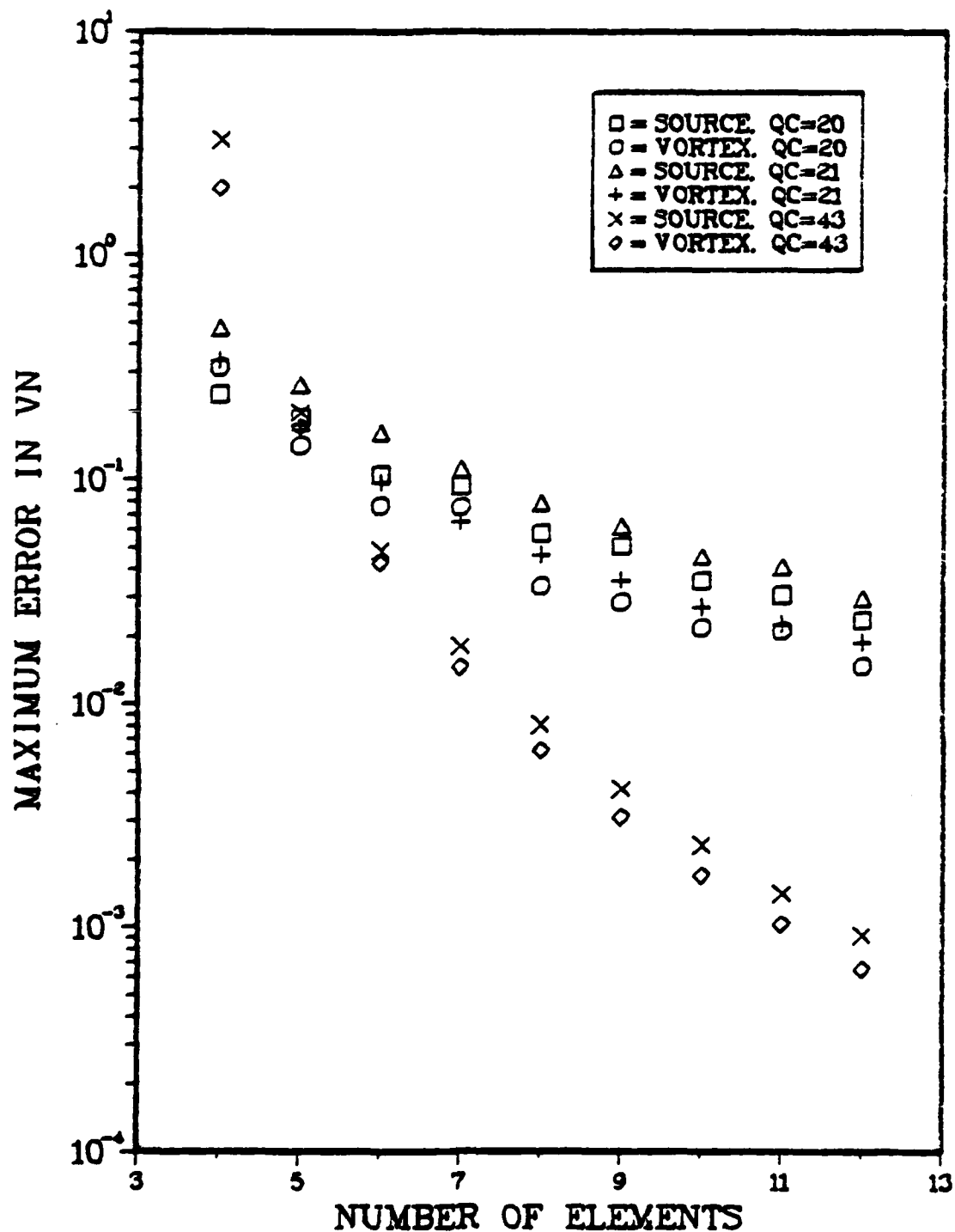


Figure 22. Maximum Absolute Normal Velocity Error on a Circle, Source and Vortex Distributions for Different QC Combinations.

are useful only for comparing the effects of the parameters shown on computational efficiency for the present method. It can be seen that to obtain a given level of accuracy, for example an error of  $10E-3$ , one needs roughly 1.5 seconds of computer time for a 3 term series, roughly 2.5 seconds for a 2 term series, and some much larger amount of time for a 1 term series. This means that, although for a given number of elements computer time increases with  $Q$ , the level of error is decreasing at a faster rate than  $Q$  is increasing. Thus, for the present method with the ranges of  $Q$  and  $N$  shown, the higher order singularity distribution is more efficient than a lower order distribution.

Local Error. The previous discussion dealt with a measure of what might be called global error. Now consider a local error by looking at the actual error distribution on the circle surface. Figures 23 through 28 show the normal and tangential velocity errors on the surface, computed at 120 equally spaced points, as a function of angle measured counterclockwise from the trailing edge stagnation point. Results for the zero circulation case are given only for the upper half circle because of flow symmetry. The errors have the form

$$E_{QC} = \frac{V_{comp} - V_{ex}}{V_{\infty}}$$

The error in normal velocity is a measure of the leakage through the surface. Since  $V_{n_{ex}} = 0$ ,  $V_{n_{er}}$  equals

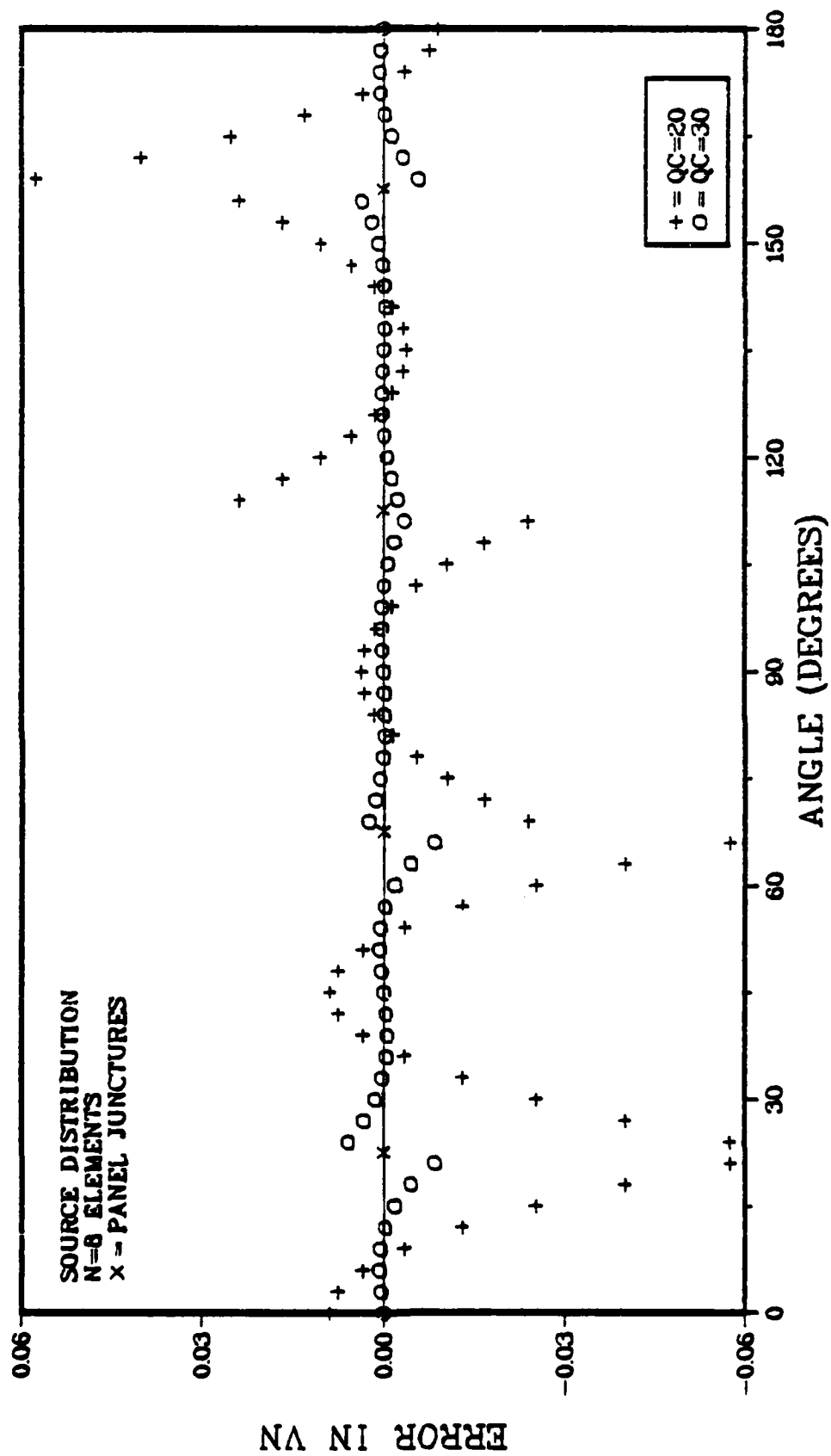


Figure 23b. Effect of Q on Normal Velocity Error for a Circle, QC = 20 and QC = 30.

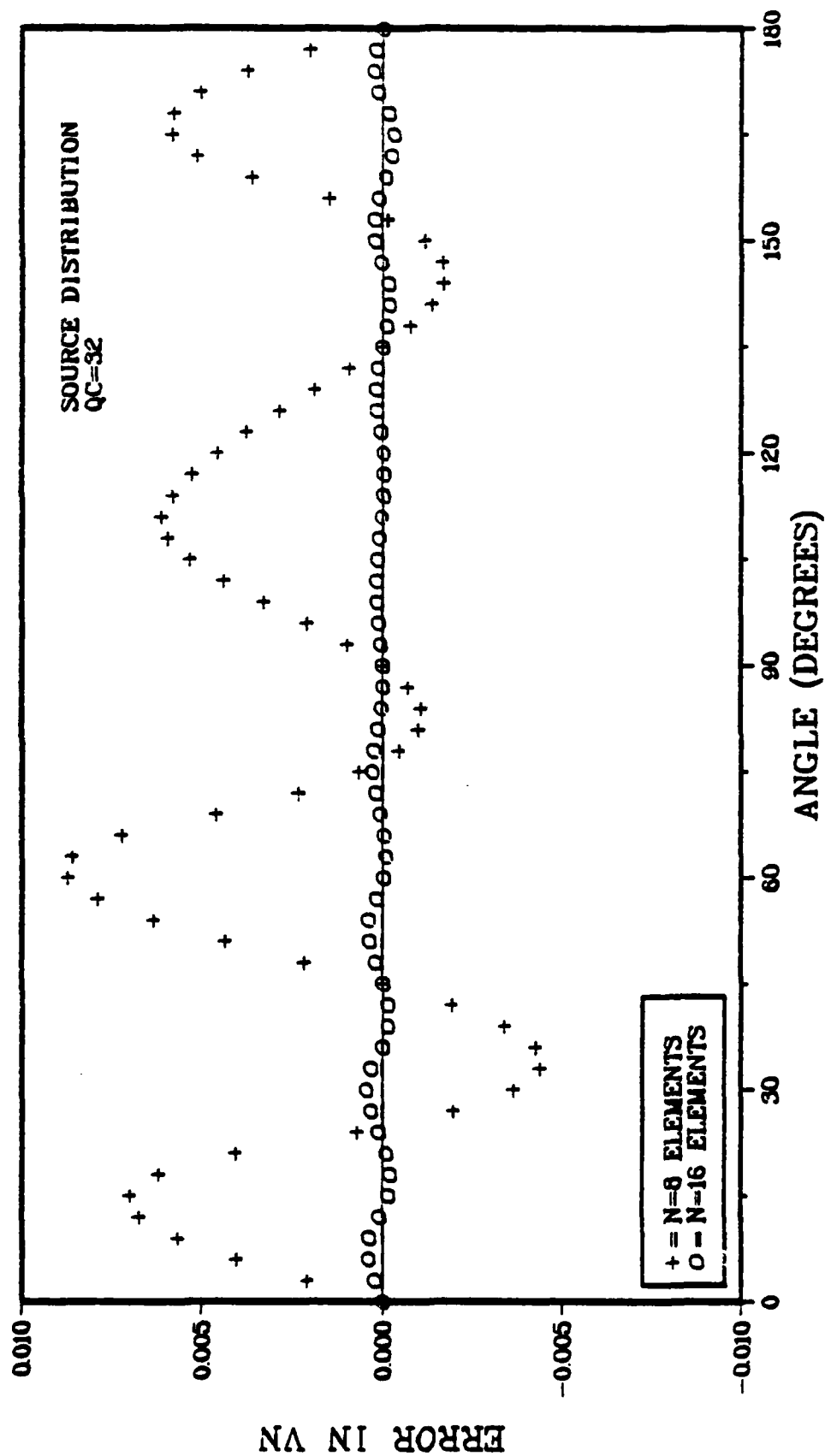


Figure 24. Effect of N on Normal Velocity Error for a Circle.

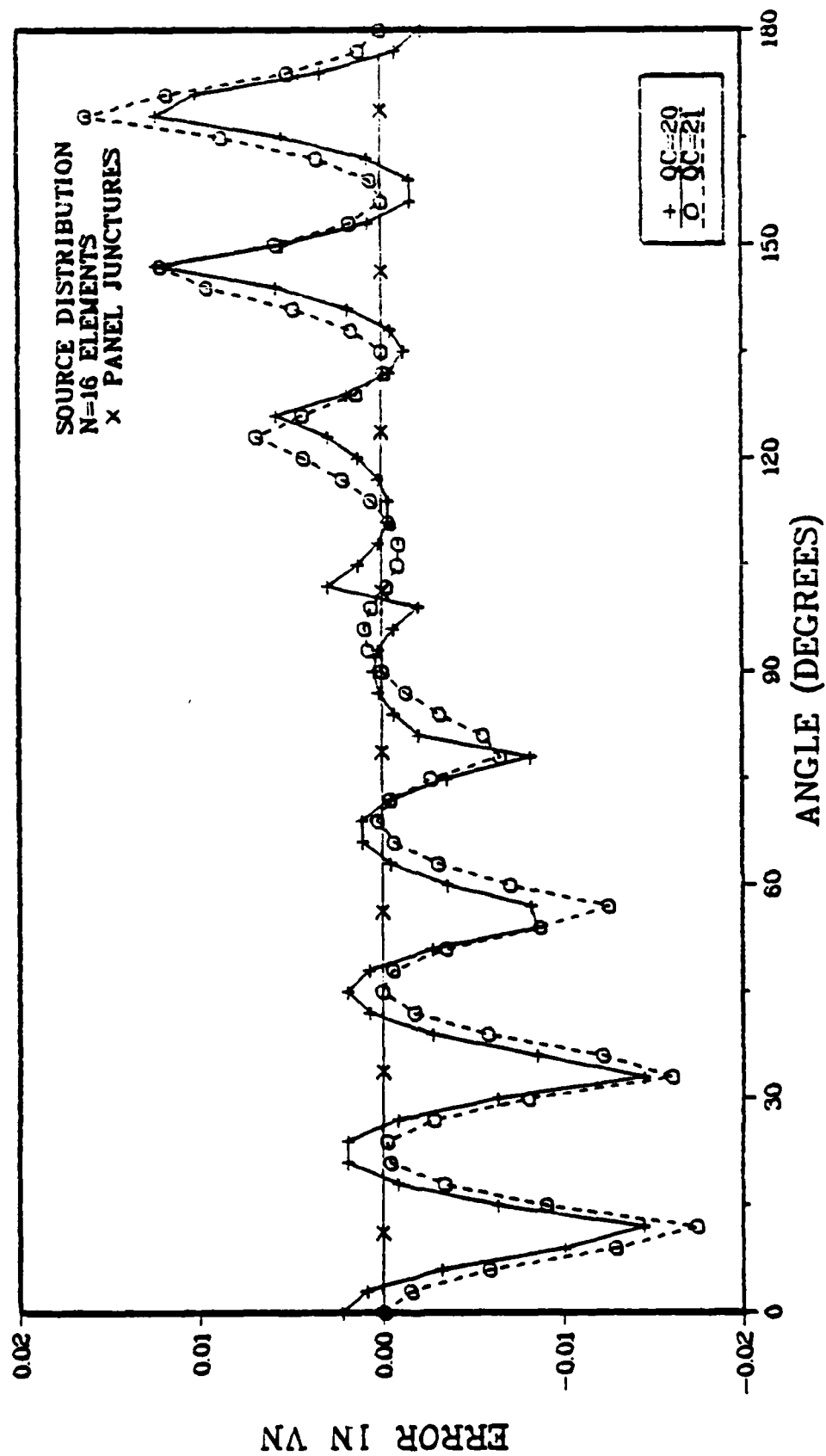


Figure 25a. Effect of C on Normal Velocity Error for a Circle, QC=20 and QC=21.

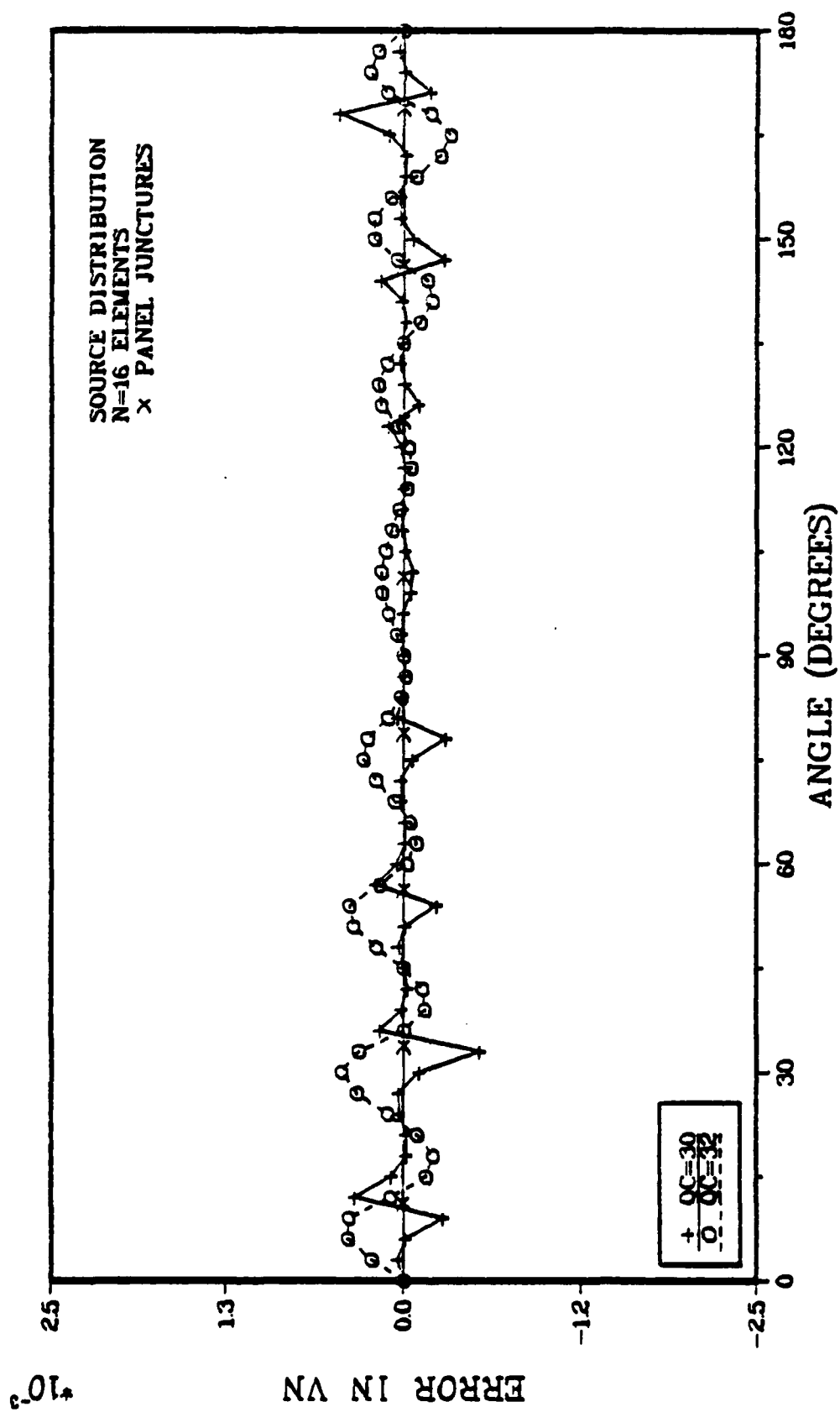


Figure 25b. Effect of C on Normal Velocity Error for a Circle, QC=30 and QC=32.

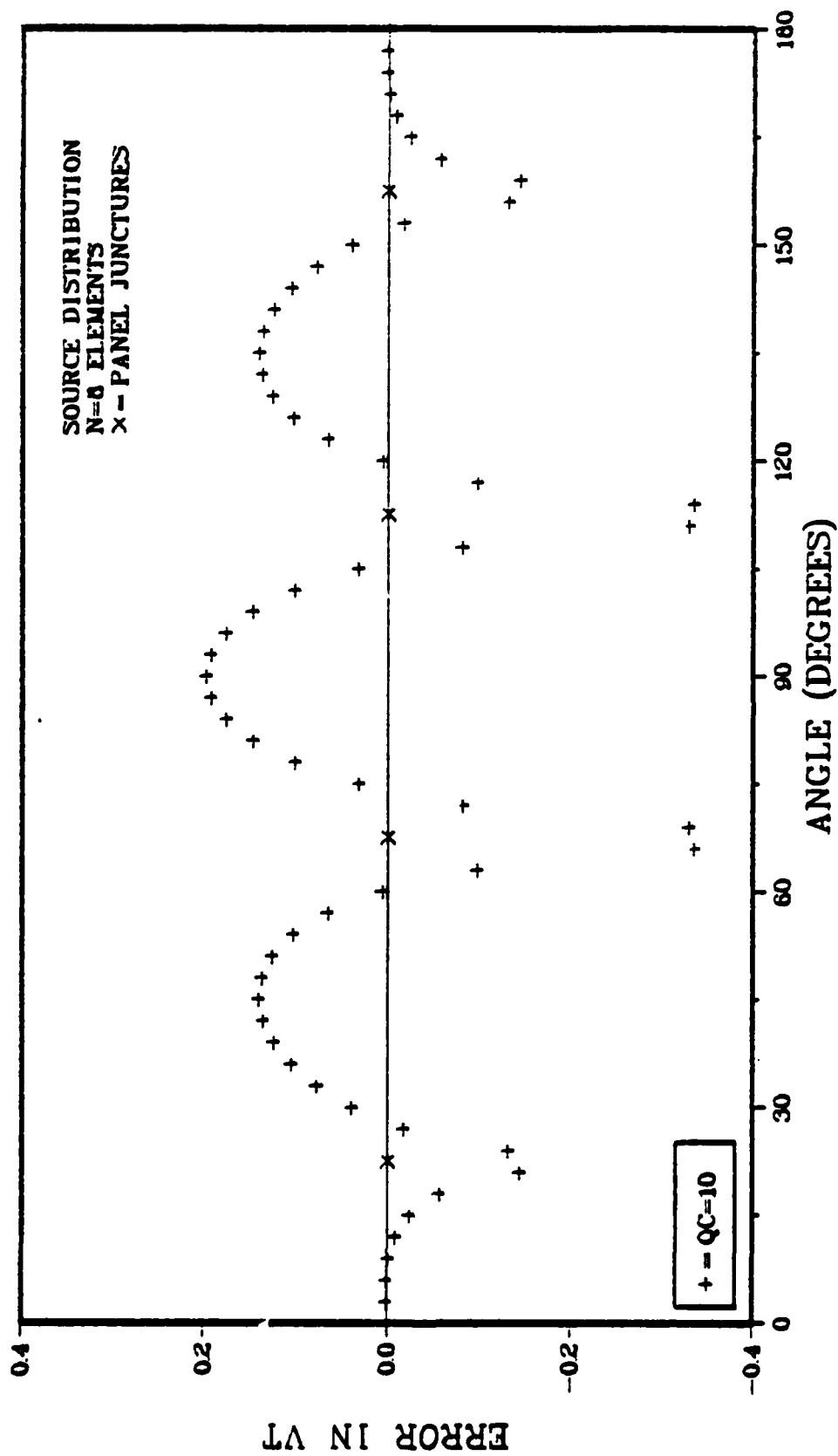


Figure 20a. Effect of Q on Tangential Velocity Error for a Circle, QC = 10.

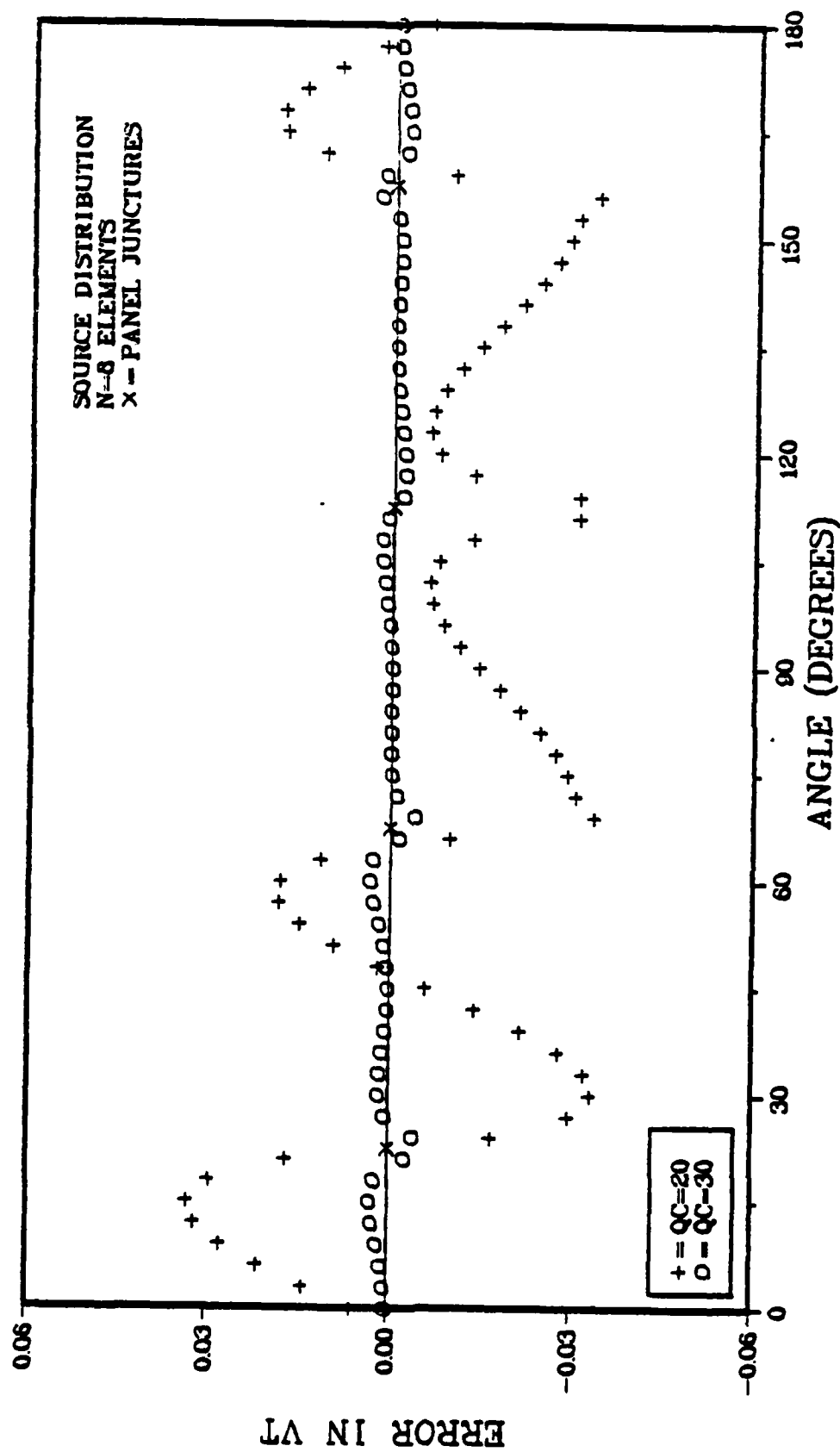


Figure 26b. Effect of Q on Tangential Velocity Error for a Circle, QC=20, and QC=30.



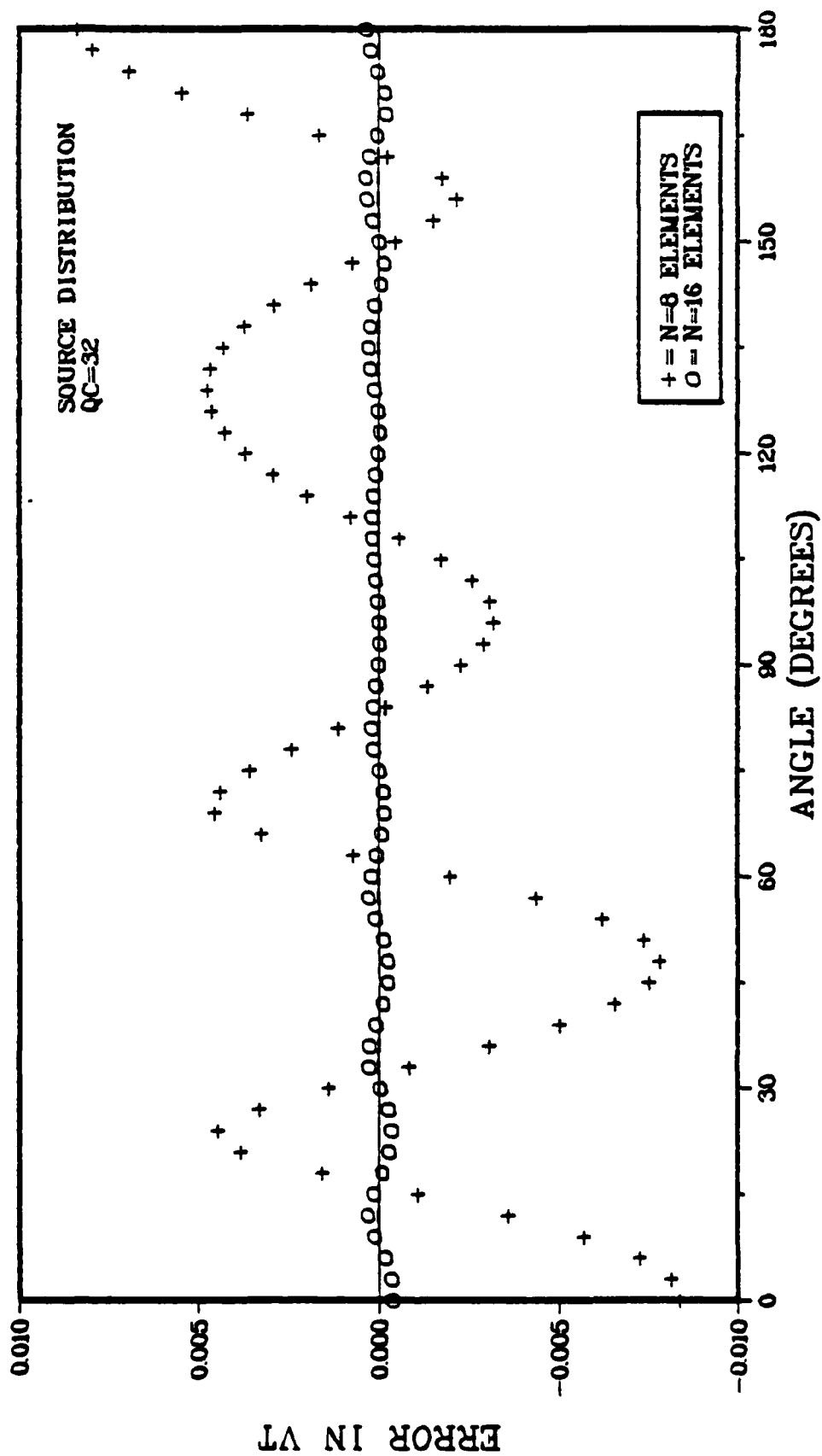


Figure 27. Effect of N on Tangential Velocity Error for a Circle.

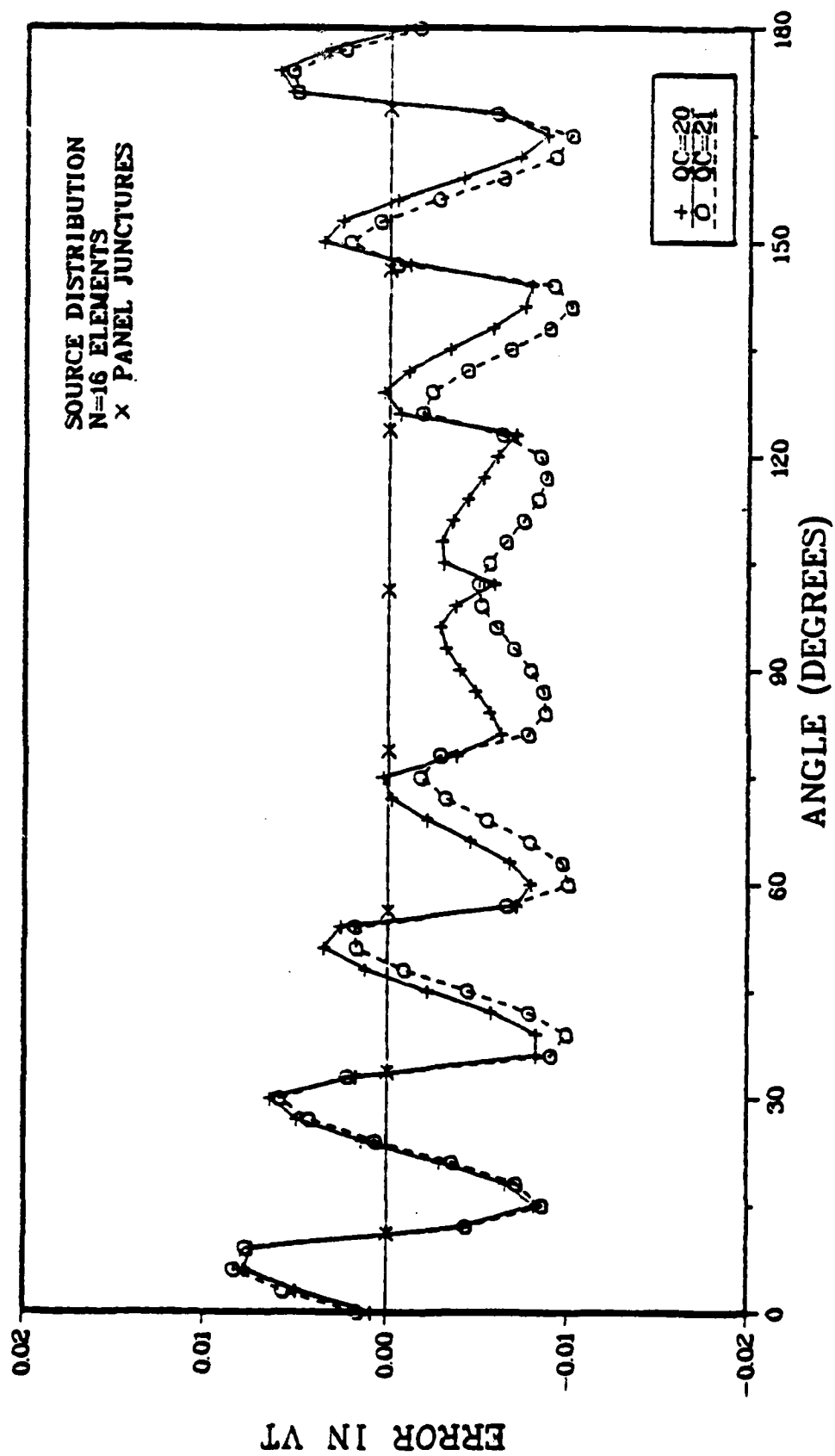


Figure 28a. Effect of C on Tangential Velocity Error for a Circle, QC=20 and QC=21.

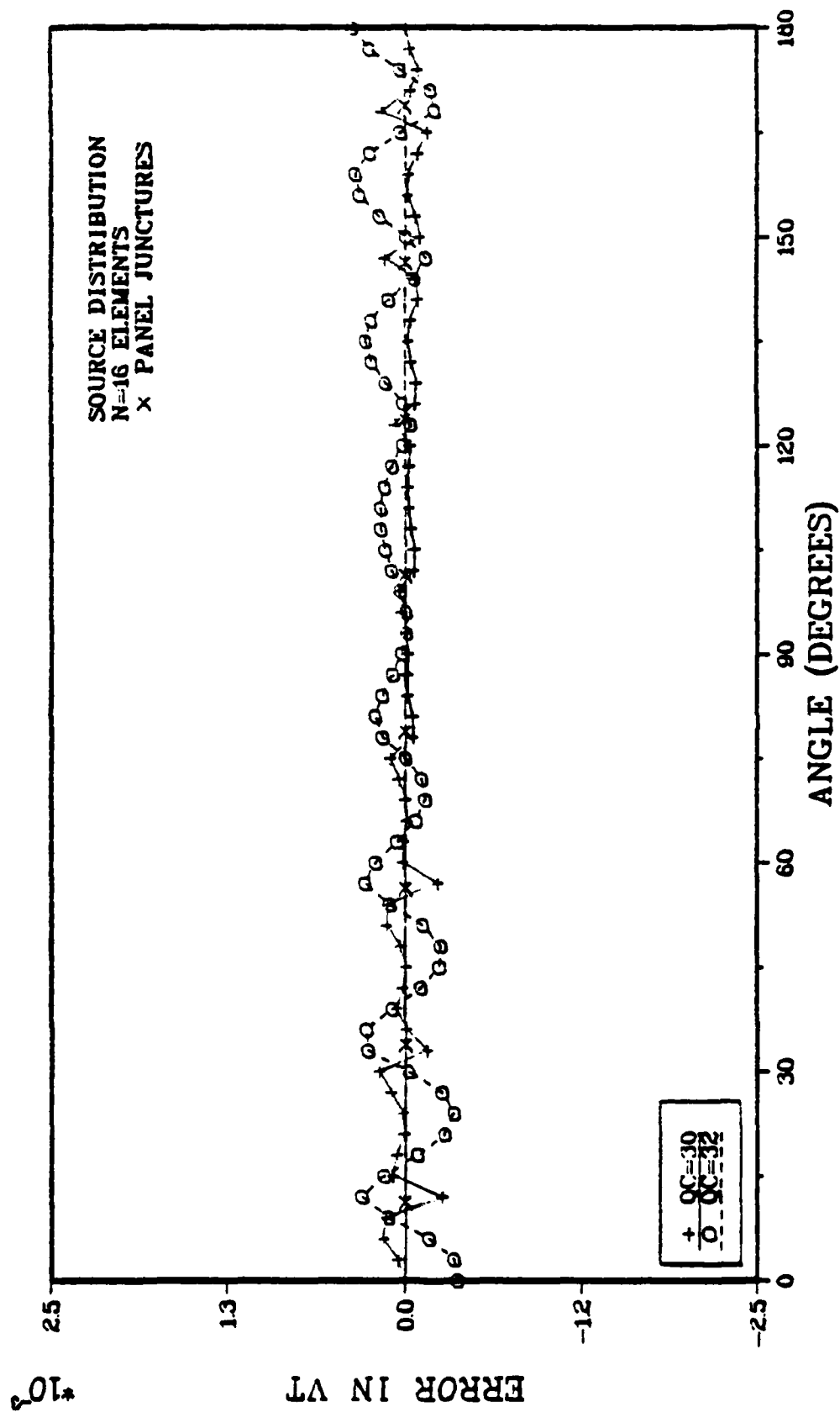


Figure 28b. Effect of C on Tangential Velocity Error for a Circle, QC=30 and QC=32.

the computed value  $V_{n\_comp}$ , and it can be shown that  $2V_n = \sigma_{comp} - \sigma_{ex}$  where  $\sigma_{comp}$  is the computed source strength and  $\sigma_{ex}$  is the exact source strength. Thus the error in normal velocity is also a direct measure of the error of the computed source distribution. All of these results are for source distributions.

Figures 23a and 23b show the effect of  $Q$  on the normal velocity error distribution for several 8 element cases. These are all  $C=0$  cases, and this is reflected in the discontinuous nature of the error distributions. Note the difference in scale between the  $Q=1$  case, and the  $Q=2$  and  $Q=3$  cases. Also note the reduction in magnitude and the general flattening of the curves on a panel as  $Q$  increases. This is a result of the fact that more control points on a panel provide better control of the normal flow through the panel.

Figure 24 shows the effect of  $N$  on the normal velocity error distribution for the  $QC=32$  case. Although the overall level of error for either case is small, the effect of doubling the number of elements is dramatic. Although these curves seem to exhibit an oscillatory nature, this is to be expected since the boundary conditions are satisfied only at discrete points. In between these discrete points the solution effectively over- and under-shoots the correct solution. The magnitude of the apparent oscillations decreases as  $N$  and  $Q$  increase.

Figures 25a and 25b show the effect of continuity on the normal velocity error distribution on a 16 element circle for the  $Q=2$  and  $Q=3$  cases. Although the continuity of the singularity distributions is reflected in the smoothness of the error curves (in these and previous figures) the level of error does not seem to be significantly affected by the degree of continuity. This is consistent with previous results for the maximum absolute velocity errors.

Figures 26 through 28 present similar figures for the distribution of tangential velocity error. The general improvement in accuracy as  $N$  and  $Q$  increase is apparent, as is the general flattening of the error distributions as  $Q$  increases.

Parameter Study. An extensive study using a source distribution with  $N=16$  was made to determine the sensitivity of the solution to control point location on a panel. All the results to this point have been for control points which were equally spaced on a panel. For cases which require one control point per panel the location of the control point was varied between 20% and 80% of a panel's arc length. For cases which require more than one control point per panel all but one were equally spaced and fixed on a panel, while one was allowed to vary between the aforementioned limits. In one case which required two control points per panel both

TABLE V  
Fixed Control Point Location  
(fraction of panel arc length)

| Control Point No. | 40  | 41  | 30  | 20  |
|-------------------|-----|-----|-----|-----|
| 1                 | .25 | .33 | .33 | .50 |
| 2                 | .50 | .67 | .67 |     |
| 3                 | .75 |     |     |     |

were allowed to vary.

Figures 29a and 29b show the effect of control point location on maximum absolute normal and tangential velocity error. The format of these figures is the same as in Figures 18 through 21. Table V shows the locations of the fixed control points for the multiple control point cases. In general these figures show a relatively small effect of control point location on the overall level of error in an absolute sense, with similar results for both normal and tangential velocity errors. A general observation that can be made is that the  $C=0$  curves are all concave upward, while the continuous cases are all concave downward, except for the  $QC=32$  case. This would indicate that for  $C=0$  cases

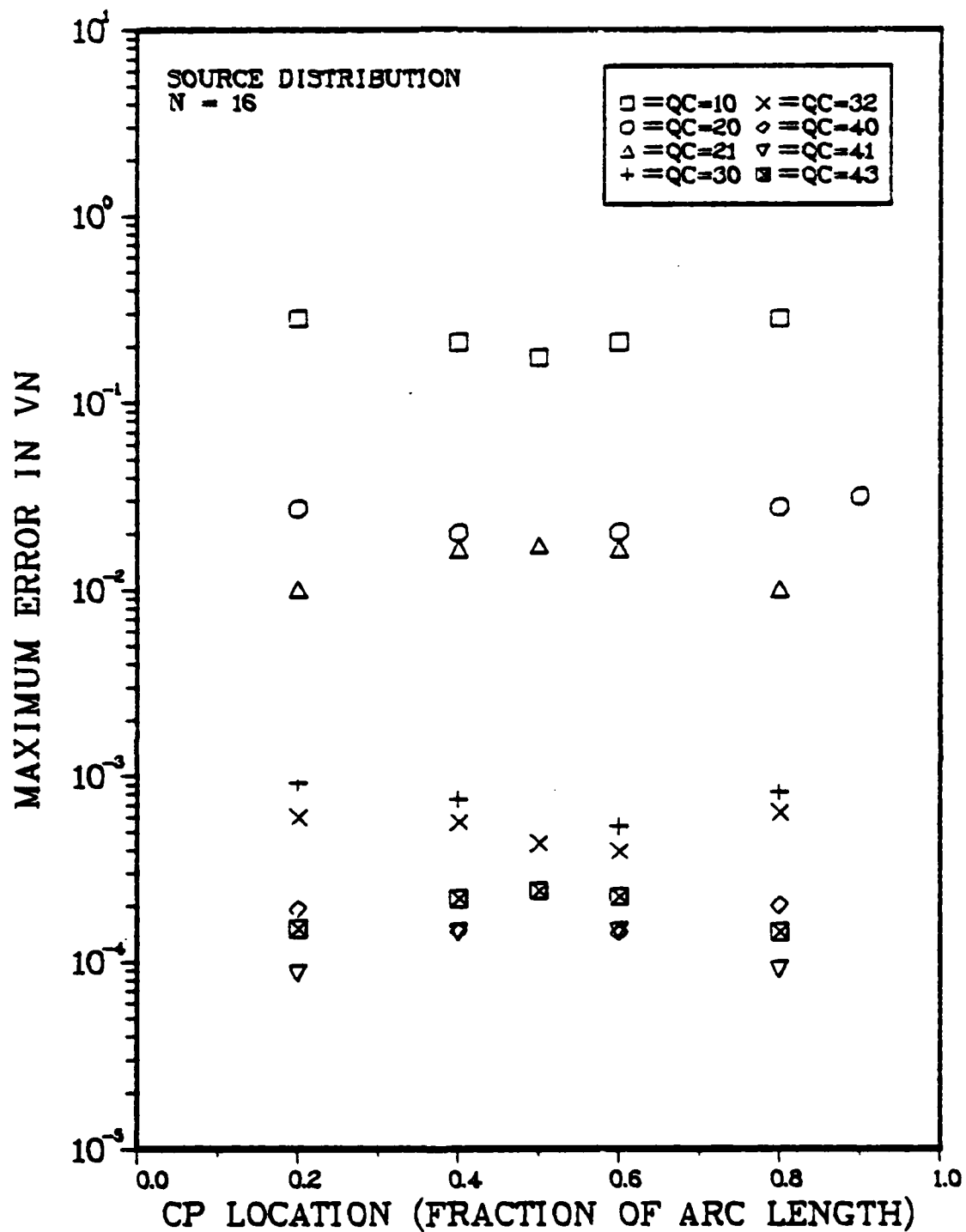


Figure 29a. Effect of Control Point Location on Maximum Absolute Velocity Error for Circle, Source Distribution with Different QC Combinations, and with N=16, Normal Velocity Error.

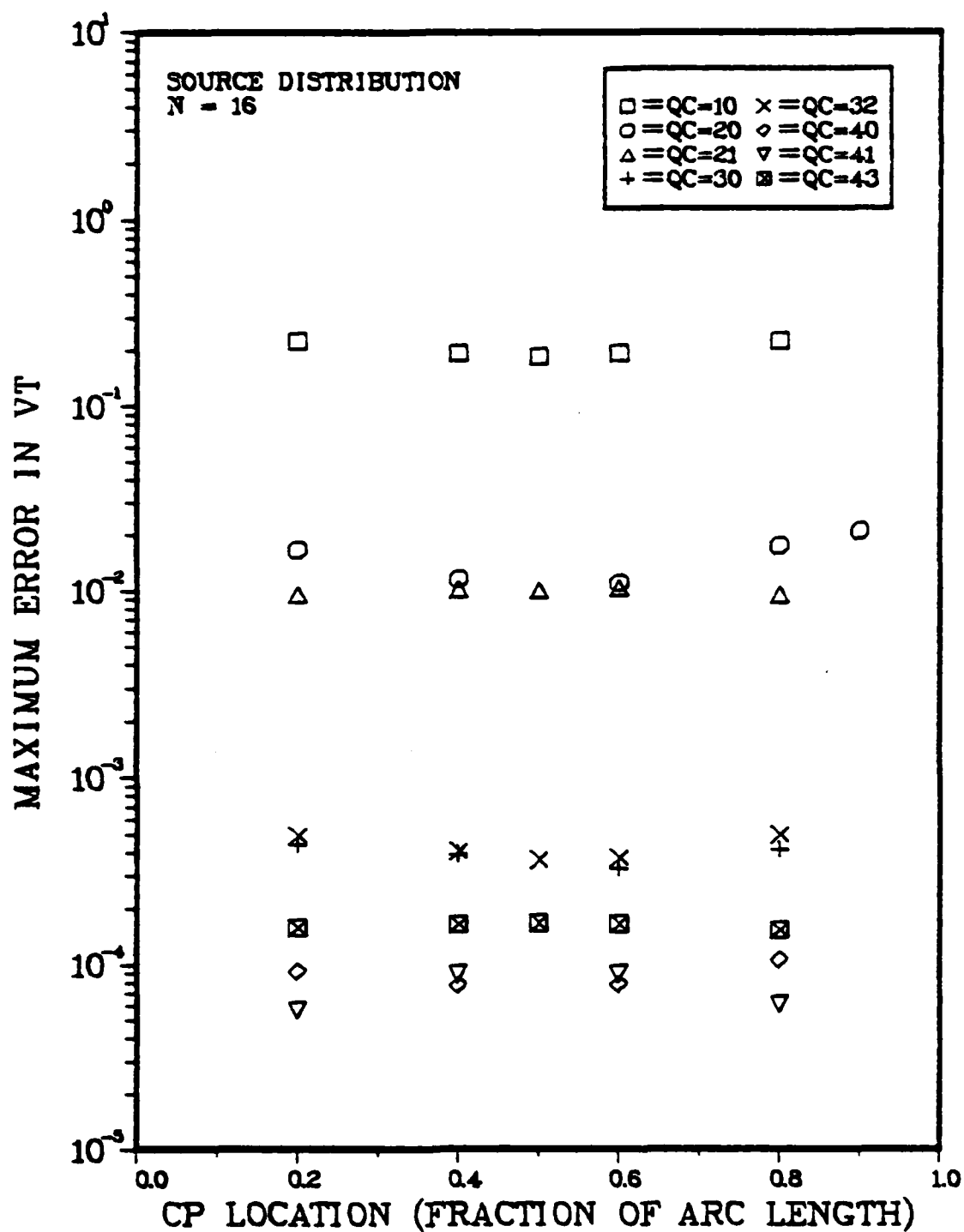


Figure 29b. Effect of Control Point Location on Maximum Absolute Velocity Error for Circle, Source Distribution with Different QC Combinations, and with N=16, Tangential Velocity Error.



control points nearer the panel center would be more effective, while the reverse would be true for the  $C$  not equal to zero cases.

Figure 30 shows more detailed comparisons for the  $N=16$ ,  $QC=20$  case. Since this case requires two control points per panel, one was fixed, successively, at 10%, 25%, and 50% of panel arc length, while the other was varied between 20% and 90% of the panel arc length. When the fixed control points are at 10% and 25% of the panel arc length, the smallest errors occur when the free control point is near 80%, and the minimum for the case of the fixed control point at 50% is when the free control point is also near 50%. This indicates that a symmetric placement of control points on a panel gives the smallest level of maximum error.

Figure 31 shows results for the only case in which more than one control point was moved. In this case, where  $QC=20$ , the control points were initially placed at 20% and 80% of the panel arc length, and then they were moved closer together at the same rate. The abscissa,  $S$ , represents a fraction of panel arc length with one control point at  $S$  and the second one at  $1-S$ . These curves have minimums in roughly the 20% to 30% range.

The results shown in Figures 29a and 29b are absolute velocity errors. Figures 32a and 32b (1 control point case) and 32c, and 32d (more than 1 control point case) reformat this data by normalizing each curve by its own maximum value

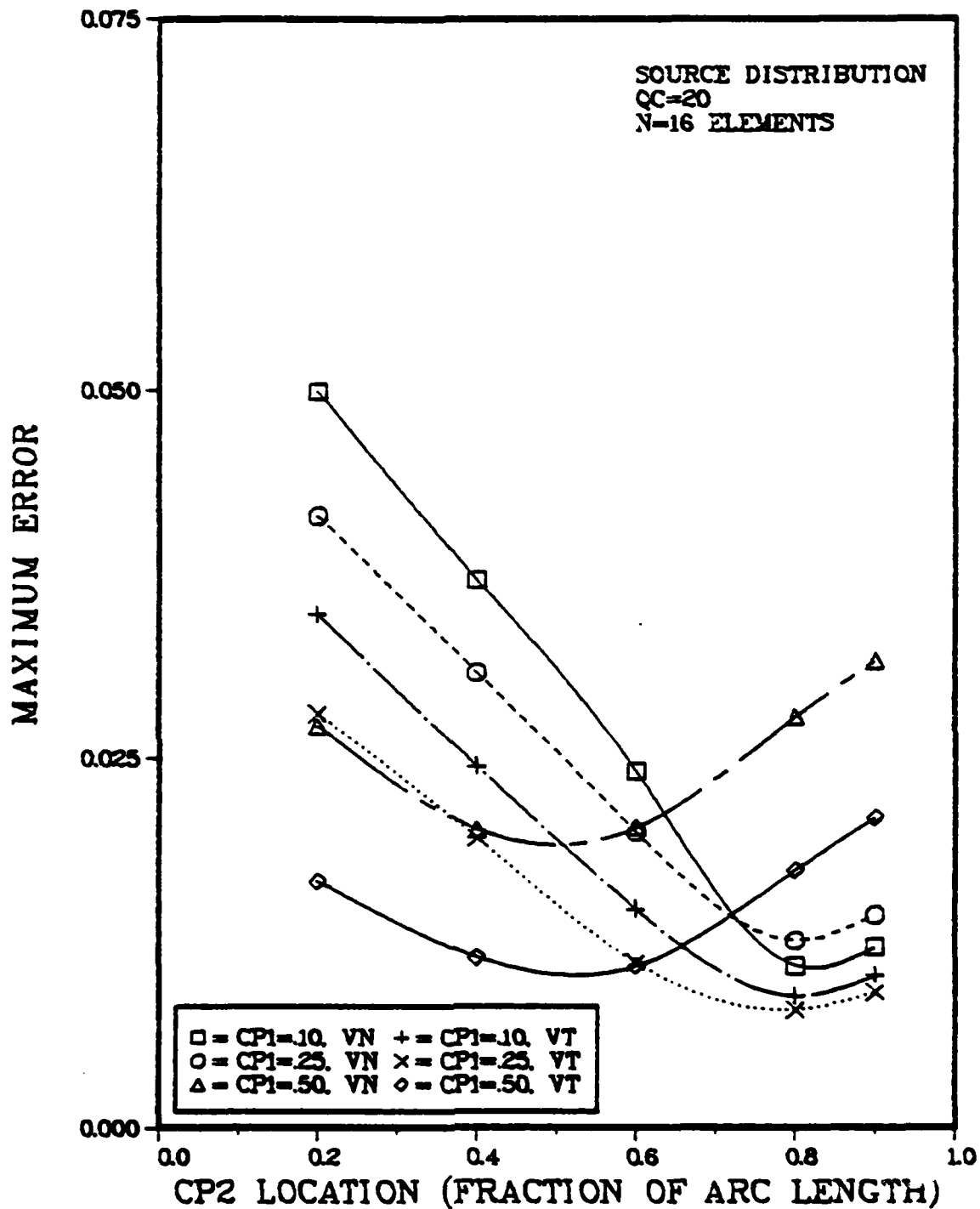


Figure 30. Comparison of Effect of Control Point Location on Maximum Absolute Normal and Tangential Velocity Error for a Circle.

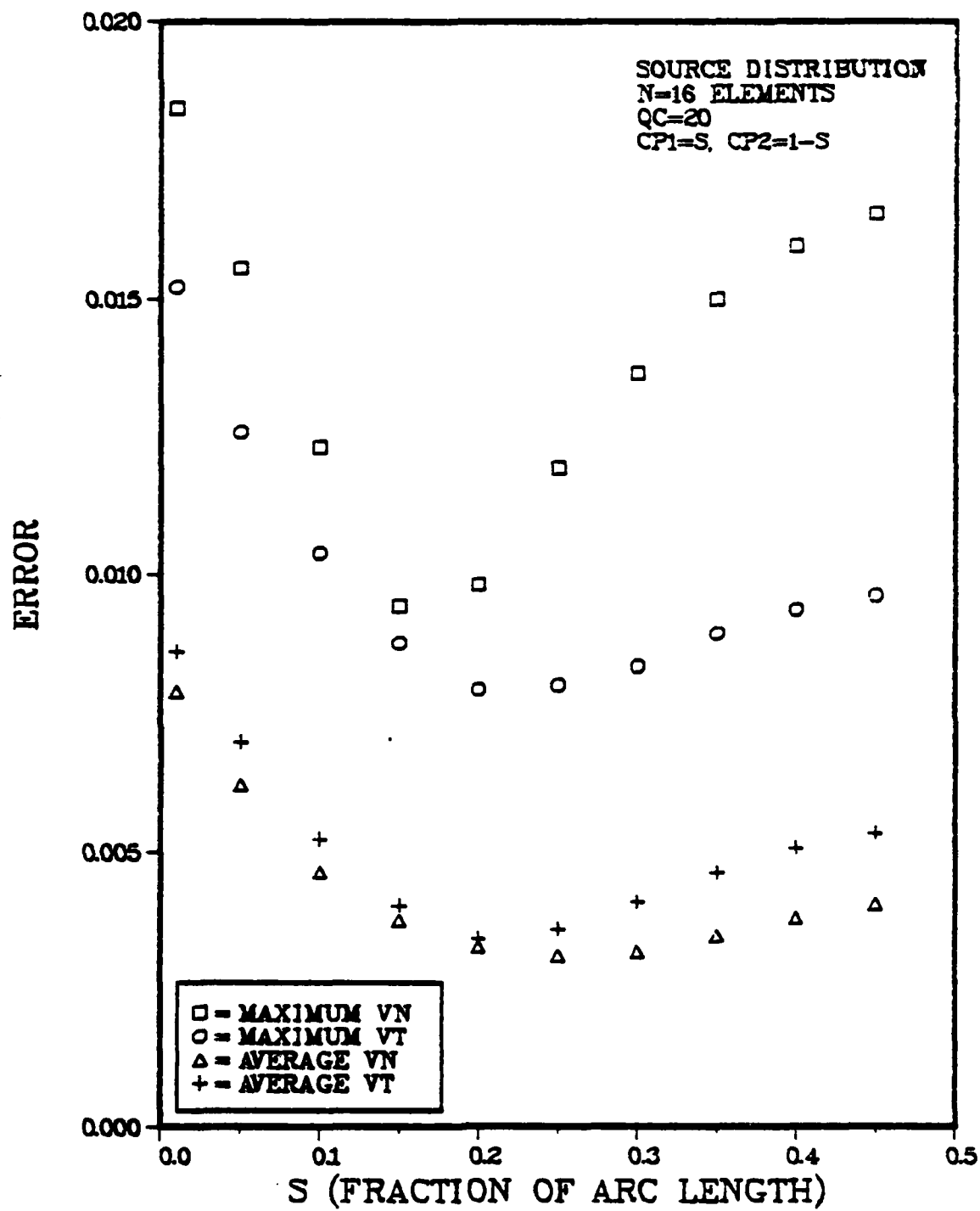


Figure 31. Effect of Varying Two Control Points on Absolute Velocity Error for a Circle.

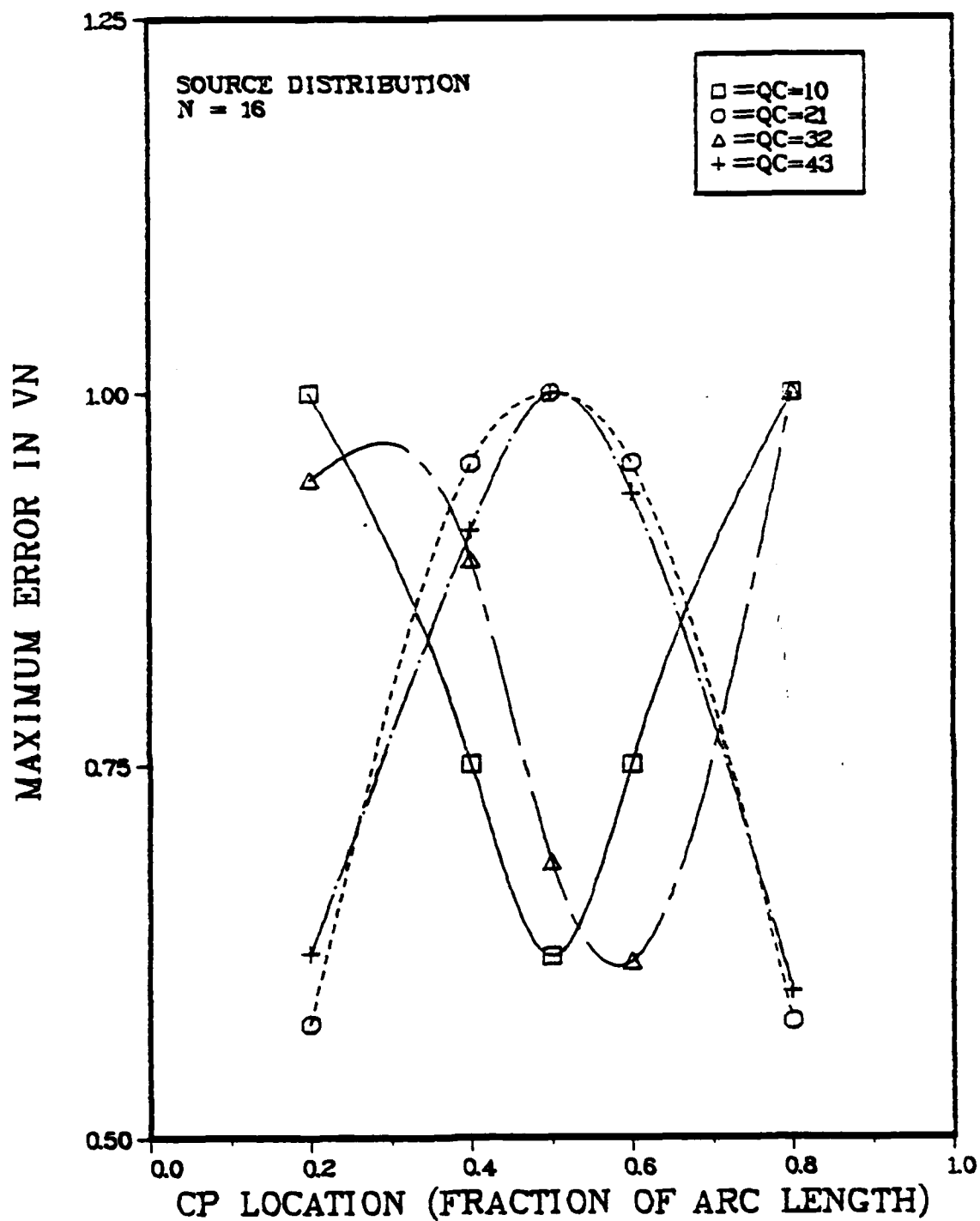


Figure 32a. Effect of Control Point Location on Normalized Maximum Velocity Error for a Circle, Source Distribution, N=16, Normal Velocity, 1 Control Point Cases.

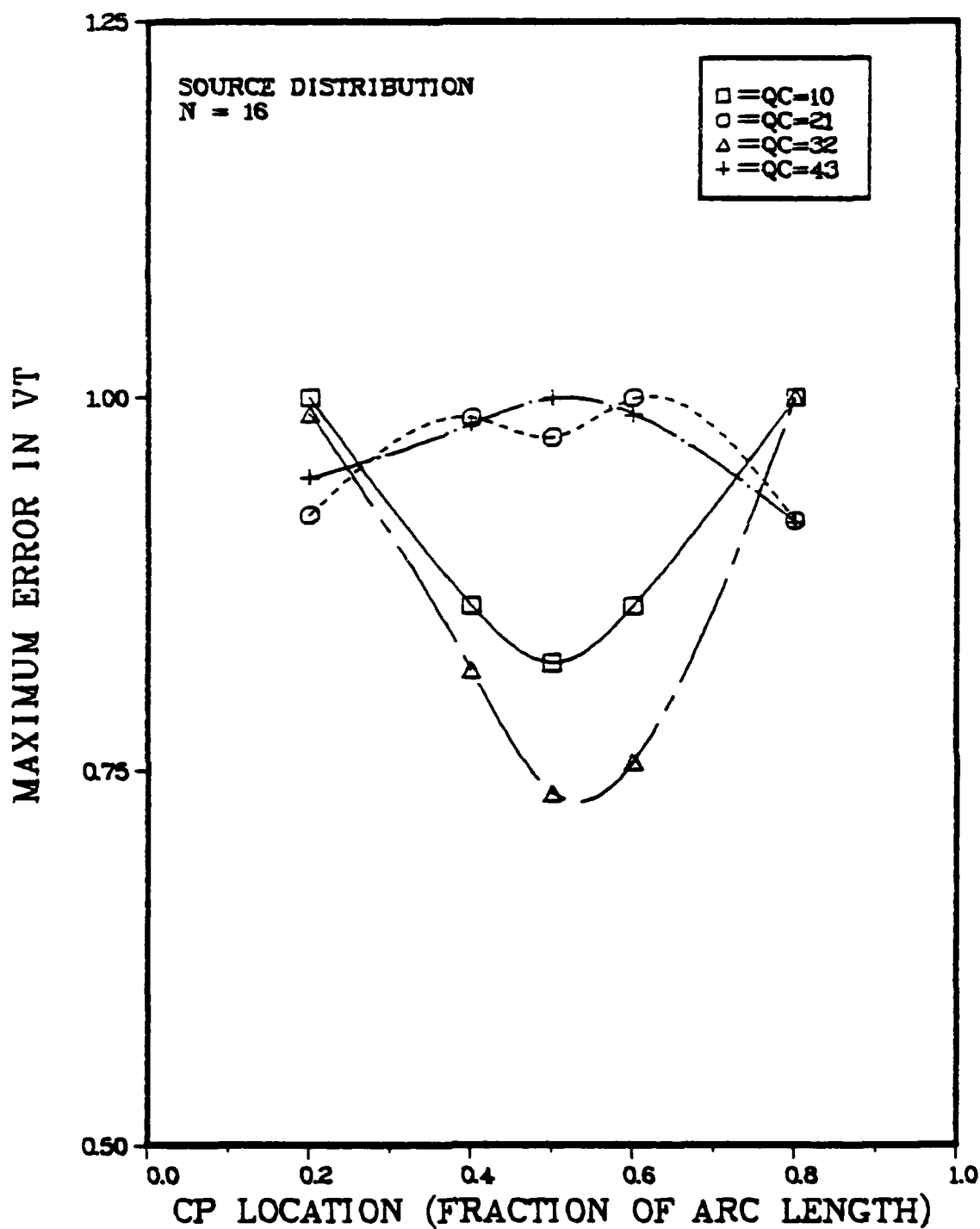


Figure 32b. Effect of Control Point Location on Normalized Maximum Velocity Error for a Circle, Source Distribution, N=16, Tangential Velocity, 1 Control Point Cases.

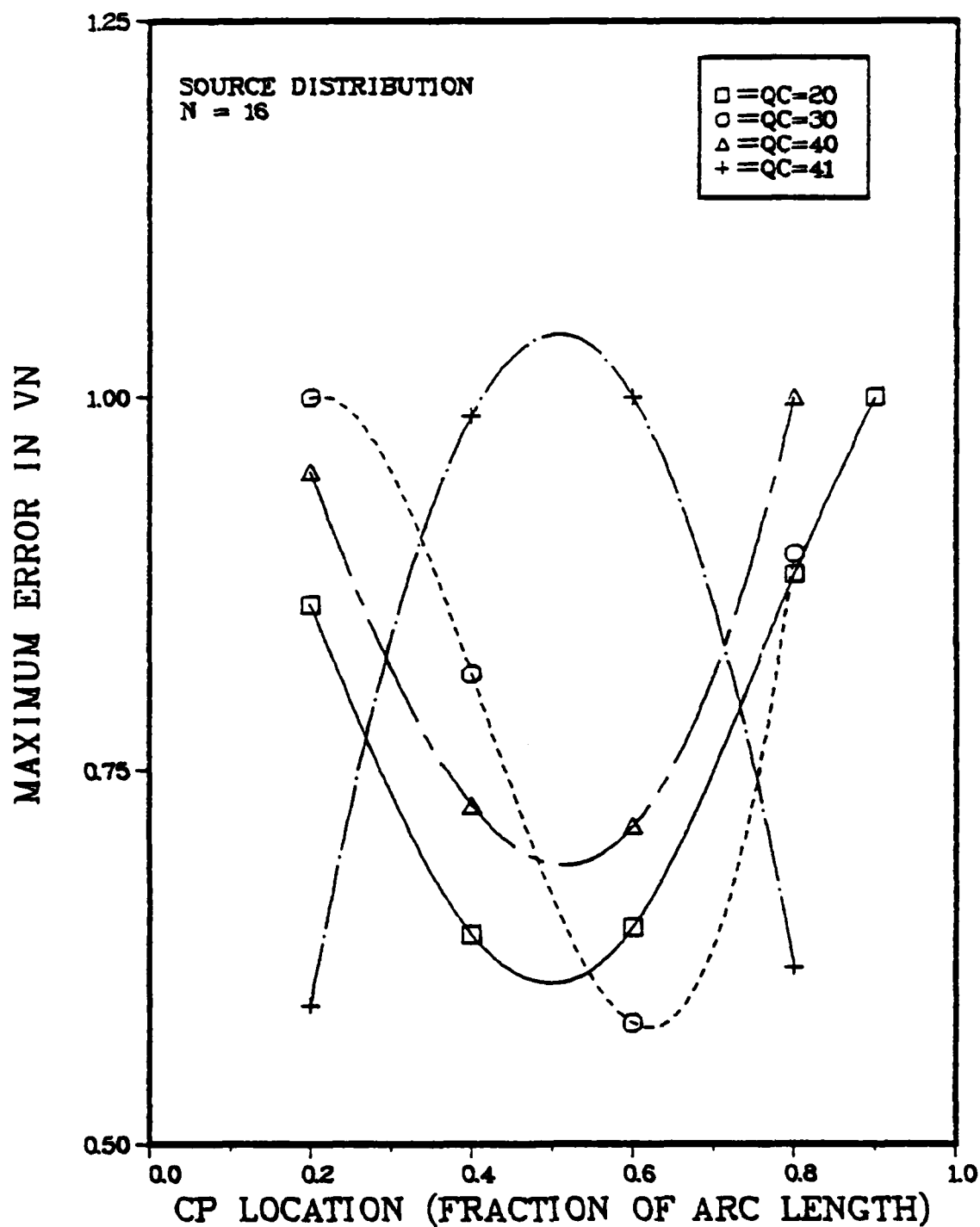


Figure 32c. Effect of Control Point Location on Normalized Maximum Velocity Error for a Circle, Source Distribution, N=16, Normal Velocity, Remaining Cases.

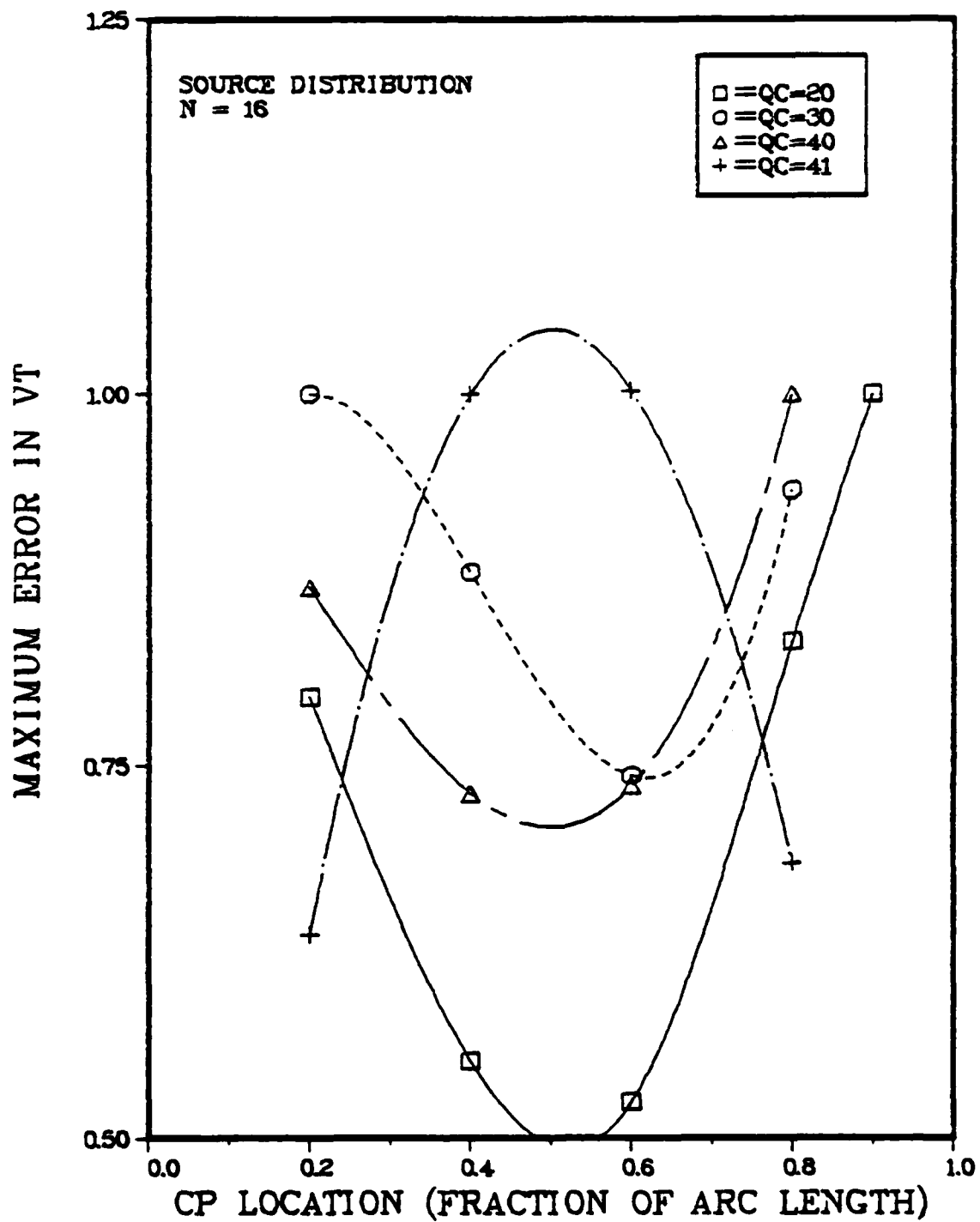


Figure 32d. Effect of Control Point Location on Normalized Maximum Velocity Error for a Circle, Source Distribution, N=16, Tangential Velocity, Remaining Cases.

TABLE VI  
Maximum Absolute Normal and Tangential Velocities

| QC | VN MAX    | VT MAX    |
|----|-----------|-----------|
| 10 | 280.70955 | 225.44110 |
| 20 | 31.58174  | 21.06721  |
| 21 | 17.45405  | 10.39468  |
| 30 | .91676    | .44371    |
| 32 | .63308    | .49764    |
| 40 | .20180    | .10712    |
| 41 | .14625    | .08988    |
| 43 | .24076    | .16825    |

so that the maximum value on each curve is 1. The values used to normalize each curve are given in Table VI. Although this presentation accentuates the effects of control point location, previous comments remain valid.

In general, the variation in tangential velocity error due to control point location was under 40%, and was often under 25%. The method was judged to be not critically sensitive to control point location since shifting this location did not make order of magnitude changes in accuracy. The study does not, however, indicate overwhelming evidence which would support one control point location over another as a general rule. Thus the choice of equally spaced control point locations is a rational and



acceptable choice, and will be used in the airfoil applications which will follow.

Combined Distribution. Results presented up to this point have been for source distributions or for vortex distributions. Intuitively one might expect some advantage to be gained by a combined source-vortex or source-doublet solution method. That this approach seems fundamentally sound can be argued as follows: source singularities are more effective near stagnation points. In the forward stagnation region the free stream must be countered by a strong efflux and near the rear stagnation point the flow must be drawn in by a strong influx. On the other hand, vorticity or doublet singularities are more effective in generating and controlling surface tangential velocities, and thus should dominate on those parts of the body where tangential velocities are large. This precise behavior is demonstrated by the source only and vorticity only exact solutions.

Bristow (Ref 29) has found that a hybrid method based on Green's third identity and employing higher order curved panels is both accurate and numerically stable. In this formulation, Green's identity specifies that the source strength density,  $\sigma$ , be equated to the surface normal perturbation velocity component  $\frac{\partial \phi}{\partial n}$ . Then

$$\sigma(\theta) = \frac{\partial \phi}{\partial n} = -V_{\infty} \cos \theta$$

A similar hybrid version of the present method was developed by superimposing the source only and vorticity only panel methods. This approach is tantamount to splitting the free stream velocity into two equal parts, one each for solving source only and vortex only problems. This approach is identical to the  $A=B=1$  version of the superimposed exact solution discussed earlier.

Solutions obtained in this way were substantially the same as the vorticity panel results and offered no apparent advantage since numerical instabilities were absent in both methods. Figures 33 and 34 show the effects of  $N$ ,  $Q$ , and  $C$  on maximum absolute velocity errors for a source/vortex combined distribution. An attempt to deviate from the Green's identity specification of  $\sigma$  was made by first solving for  $\phi$  by the source panel method using the full free stream velocity and then solving for  $\gamma$  under the influence of the source distribution. For both cyclic and acyclic problems this led to  $\gamma = \text{constant}$  for  $Q=1$ , and numerical difficulties for  $Q=2$ .

Based on these results for the use of circular arc panels to model flow past a circular cylinder, with and without circulation, the computational evidence indicated no advantage of the hybrid method, at least when satisfying Neumann type boundary conditions. Also, from the standpoint

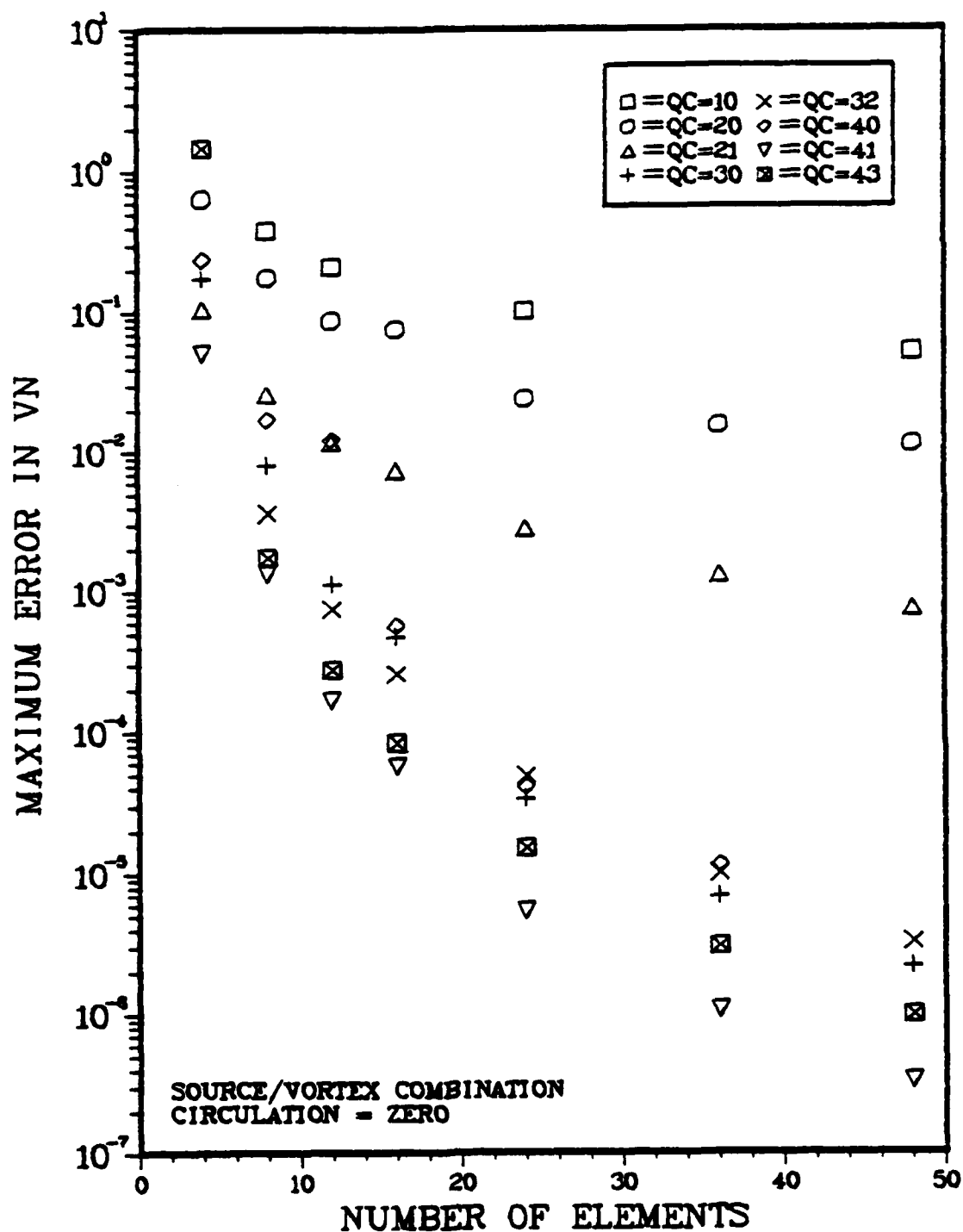


Figure 33. Maximum Absolute Error in Normal Velocity for a Circle, Source/Vortex Combination with  $\Gamma=0$ .

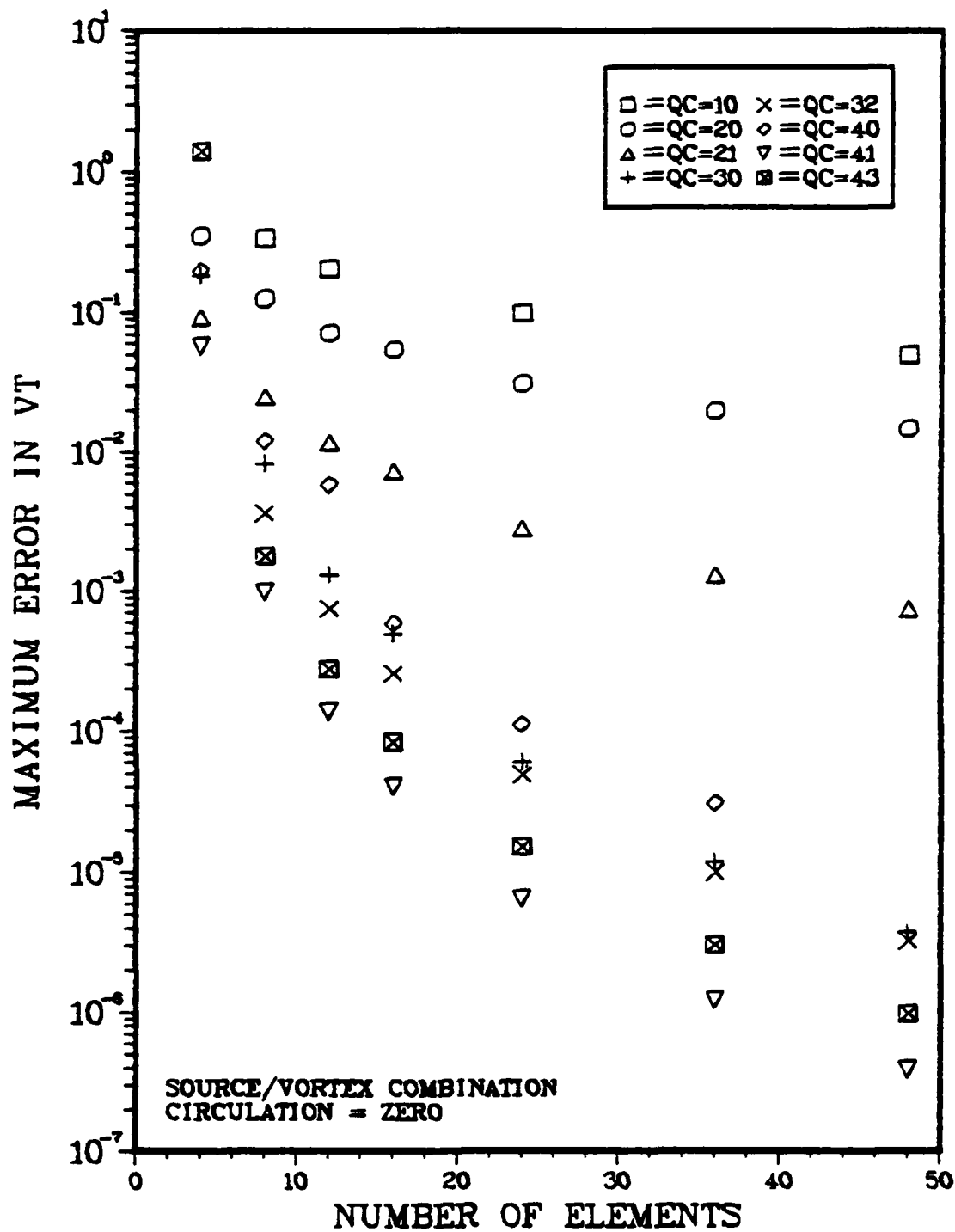


Figure 34. Maximum Absolute Error in Tangential Velocity for a Circle, Source/Vortex Combination with  $\Gamma=0$ .

of comparing and the physical vorticity distribution, the hybrid method is inferior to a vorticity only solution.

Summary. Several conclusions can be drawn from this study of the circular cylinder problem:

1. The accuracies obtainable from source only, vorticity only, and combined source/vortex methods are roughly equivalent. The vorticity method appears to be superior for three reasons: its applicability to flows with lift, its more accurate results for tangential velocity and thus surface pressure, and its more accurate modeling of physical vorticity.

2. Dramatic reductions in velocity errors are achieved by increasing  $Q$ , the number of terms in the series representation of singularity strength, through  $Q=3$ . A linear distribution ( $Q=2$ ) may, however, represent the best compromise between simplicity and accuracy.

3. Accuracy improvements were achieved by increasing  $N$  (decreasing panel size), panel junctures, the surface velocity distributions were smooth with continuity and discontinuous without it.

5. The method is not critically sensitive to control point location provided control points are not located too near panel edges.

## V. Application to Airfoils

The purpose of this chapter is to apply the method developed previously to several types of airfoils in order to assess its performance in these cases. The airfoils which have been studied are a symmetric Joukowski airfoil, an NACA 0024 airfoil, a thin symmetrical airfoil, and two types of Karman-Trefftz airfoil. Initially a source distribution was used to compute the potential flow over the Joukowski airfoil to indicate whether or not the kind of results obtained in Chapter IV for the circle could also be obtained for an airfoil. Since these preliminary efforts were promising, a source distribution was then used to compute the flow over an NACA 0024 airfoil. This was used because it is more representative of a real airfoil section (i.e. it has a non zero trailing edge angle compared to the Joukowski airfoil's cusped trailing edge), and other computational and experimental results were available for comparison. A vortex distribution was then used to compute the thin symmetrical airfoil.

These studies led to the application of the method using source and vortex distributions to both a symmetric and a cambered Karman-Trefftz airfoil. The bulk of the effort was concentrated on these airfoils because they have

a non zero trailing edge angle, and because exact solutions are readily available for comparison. The unsuccessful results using certain parameter combinations in computing these airfoil cases led to the selection of a baseline method which was then used in an extensive parameter study and error analysis. This study was made for both types of Karman-Trefftz airfoils at various angles of attack. It included the effects of panel size, number of terms in the singularity distribution, panel distribution characteristics, and point source location. An analysis of the error introduced into the solution by the error in surface slope and position at control points was also accomplished.

In the succeeding sections of this chapter results of the application of the method to a Joukowski airfoil will be presented, followed by results for the NACA 0024 airfoil, and for a thin symmetrical airfoil. Results for Karman-Trefftz airfoils, including detailed parameter studies, will then be presented. Finally, conclusions regarding the value of the method for airfoil applications will be discussed.

#### Joukowski Airfoil

As an initial test of the method when applied to an airfoil, a 13% thick, symmetric Joukowski airfoil was modeled using a source distribution. Cases were computed for several combinations of  $N$  and  $Q$ , and the effect of panel curvature was also investigated.

TABLE VII

## Paneling Nomenclature

| P = NN.SYY |  |
|------------|--|
| NN         | Number of Panels   |
| S          | Paneling Symmetry Indicator<br>S=1 - Symmetric Panel Arrangement about X Axis<br>S=2 - Unsymmetric Panel Arrangement about X Axis  |
| YY         | Unique Identifier (Number) for Panel Arrangement<br>YY=00 - Paneling Generated from Equal Angular Increments in Complex Circle Plane<br>YY=01,02 etc - Different Panelings Generated from Unequal Angular Increments in Complex Circle Plane |

arrangement as paneling  $P=NN.SYY$  where this nomenclature is defined in Table VII. For example, paneling  $P=45.100$  represents an airfoil with 45 panels which are symmetrically arranged about the x axis and which were generated by equal angle increments in the complex circle plane.

Most of the results will be presented as plots of surface tangential velocity error at control points. This procedure implicitly assumes that the paneling is a good model of the actual surface. Referring to Figure 43, the exact and computed tangential velocities are determined at the points  $P_S$  and  $P_M$  respectively. The point  $P_S$  is



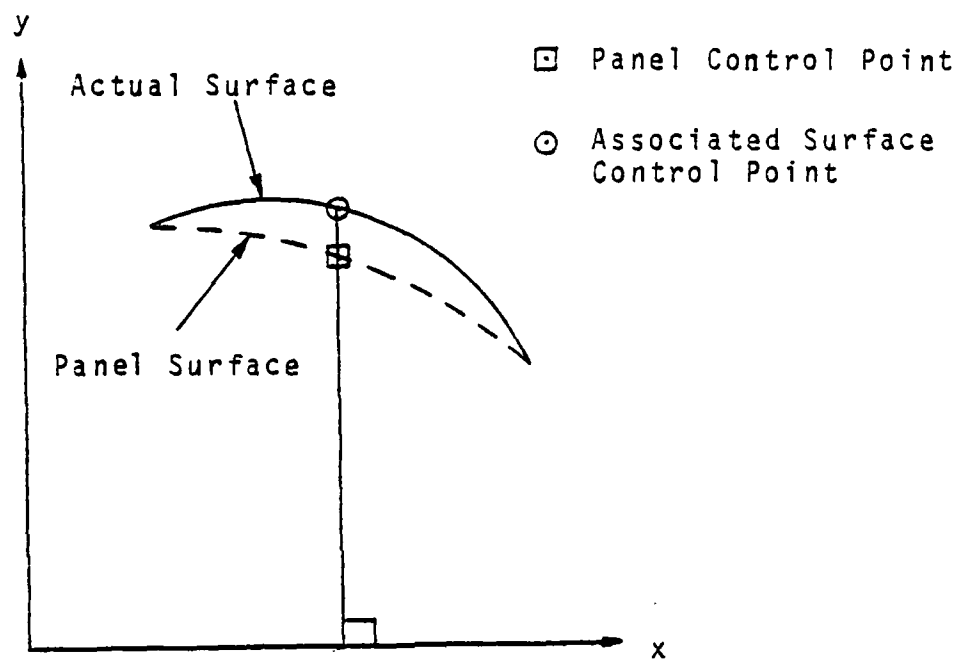


Figure 43. Surface Points for Velocity Error Comparison.

TABLE VIII

## Preliminary Results for the Karman-Trefftz Airfoil

| Method            | QC |    |    |    |    |    |
|-------------------|----|----|----|----|----|----|
|                   | 10 | 20 | 21 | 30 | 31 | 32 |
| Source, $V_n = 0$ | S  | S  | U  | S  | U  | S  |
| Vortex, $V_t = 0$ | S  | S  | U  | S  | U  | U* |
| Vortex, $V_n = 0$ | U  | U  | S  | U  | S  | U  |

S = Successful

U = Unsuccessful

\* = Non Oscillatory Solution,  
But Incorrect Lift

determined by requiring that it have the same  $x$  coordinate as  $P_M$ .

Preliminary Results. The method was initially applied to a 19 panel model of the chosen Karman-Trefftz airfoil. Both source and vortex singularities were used with the singularity distributions expanded about the panel center point, for various combinations of  $Q$  and  $C$ . Table VIII indicates which of these initial efforts were successful. Successful cases are those cases for which at least a reasonable solution was obtained. Unsuccessful cases are those cases for which the aerodynamic influence matrices

were either algorithmically singular, or for which the solution exhibited an oscillatory behavior. The asterisked case was one for which the solution seemed reasonable, except that the lift was considerably in error. Figures 44 and 45 show typical tangential velocity error results for successful source and vortex calculations. For the vortex case the Kutta condition was satisfied by placing an internal point source at  $X_S = .5$ , and specifying zero vorticity at the trailing edge.

Several approaches were tried to obtain successful solutions for all cases. For the vortex cases a number of alternate Kutta conditions were used. These were a specification of zero vorticity at the trailing edge with an internal point source, a specification of net circulation in an error parameter approach, and a specification of zero velocity normal to a trailing edge bisector at a point slightly downstream of the trailing edge using both an internal source, and an error parameter approach. The results of these attempts were essentially identical to those shown in Table VIII. The error parameter approach is equivalent to the internal point source approach, based on results to date. The unsuccessful cases were also attempted using the non centered form of the series expansion with no change in the results.

For the source case, Fig 46 shows an unsuccessful

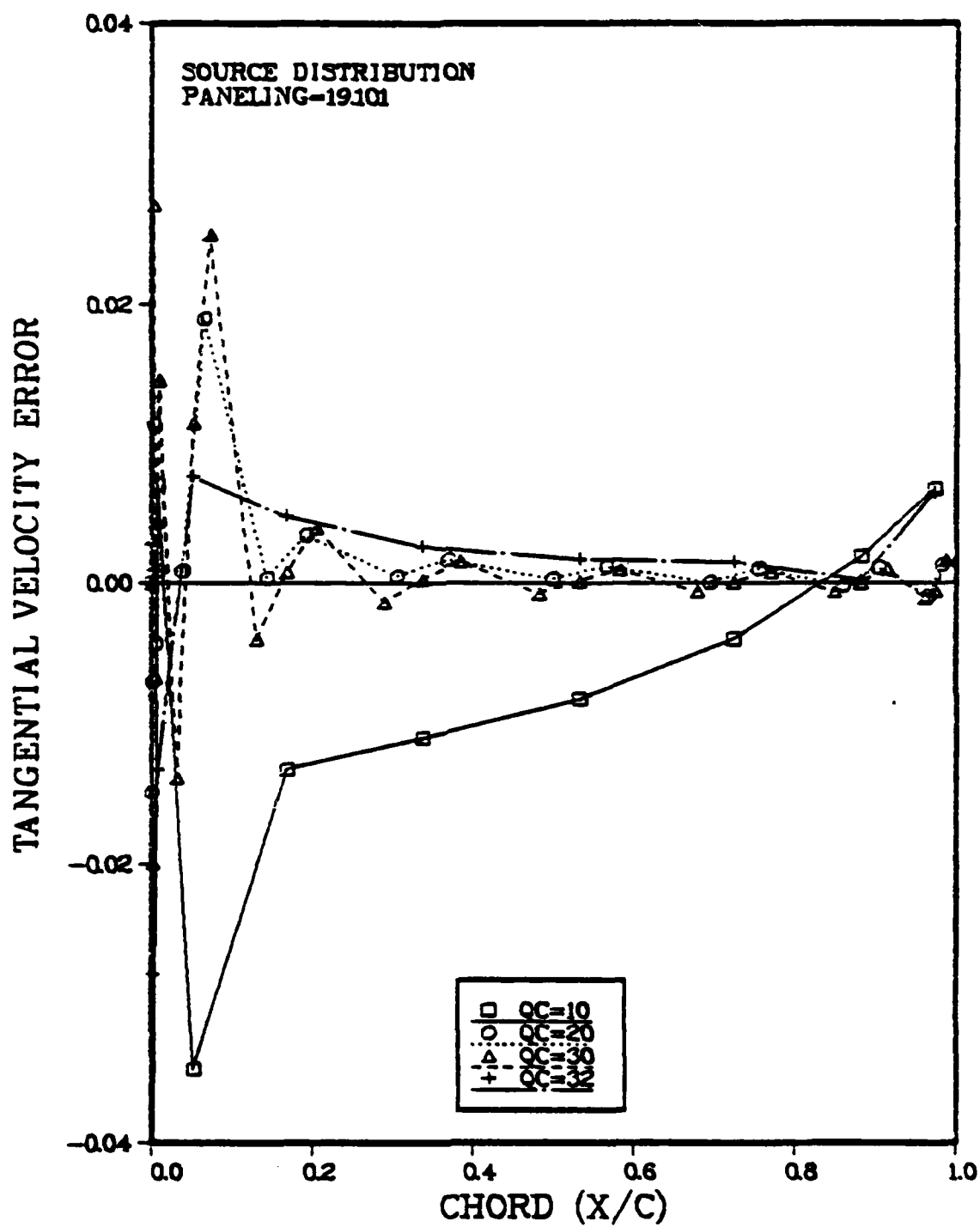


Figure 44. Karman-Trefftz Airfoil, Successful Cases, Source Distribution.

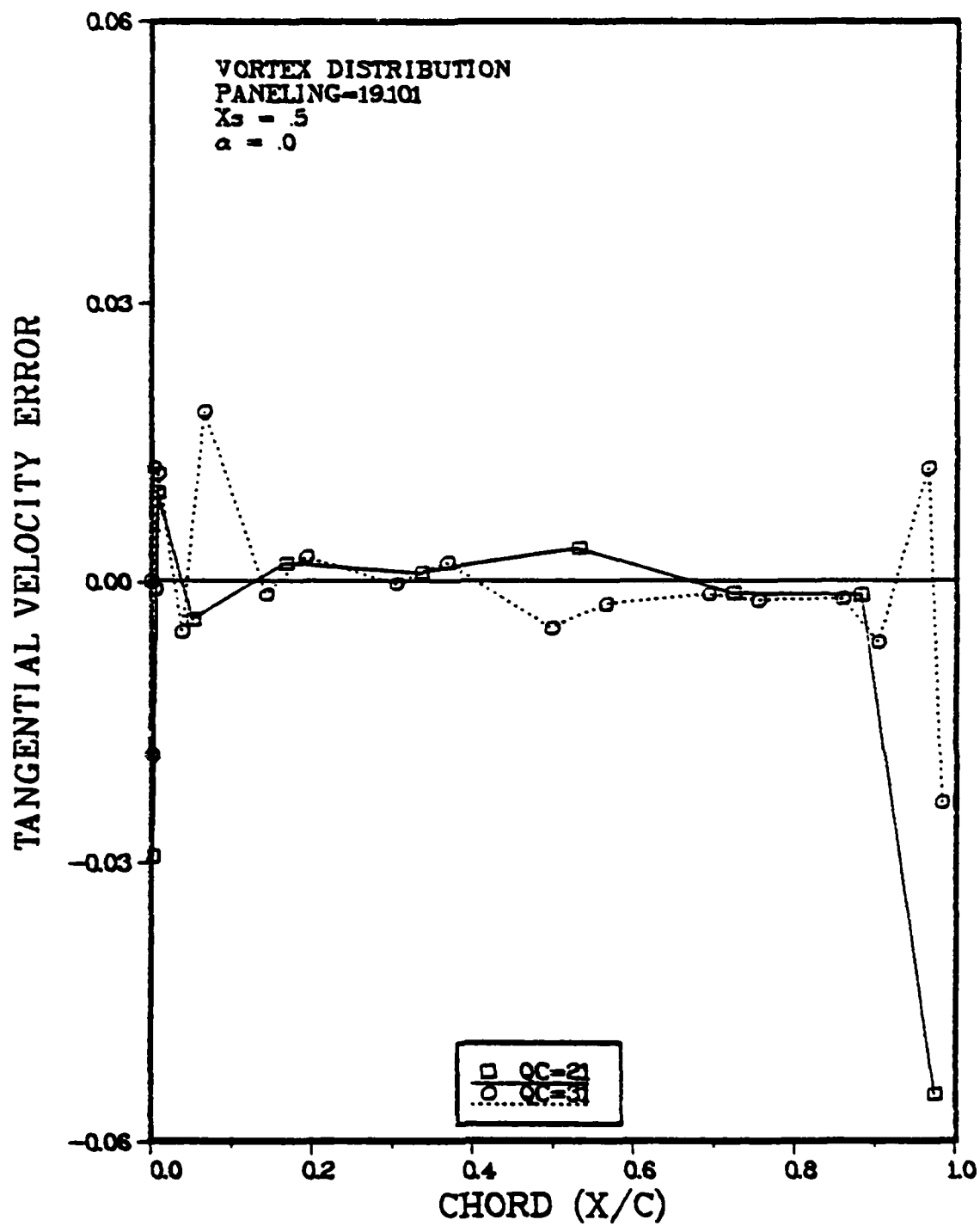


Figure 45. Karman-Trefftz Airfoil, Successful Cases, Vortex Distribution.

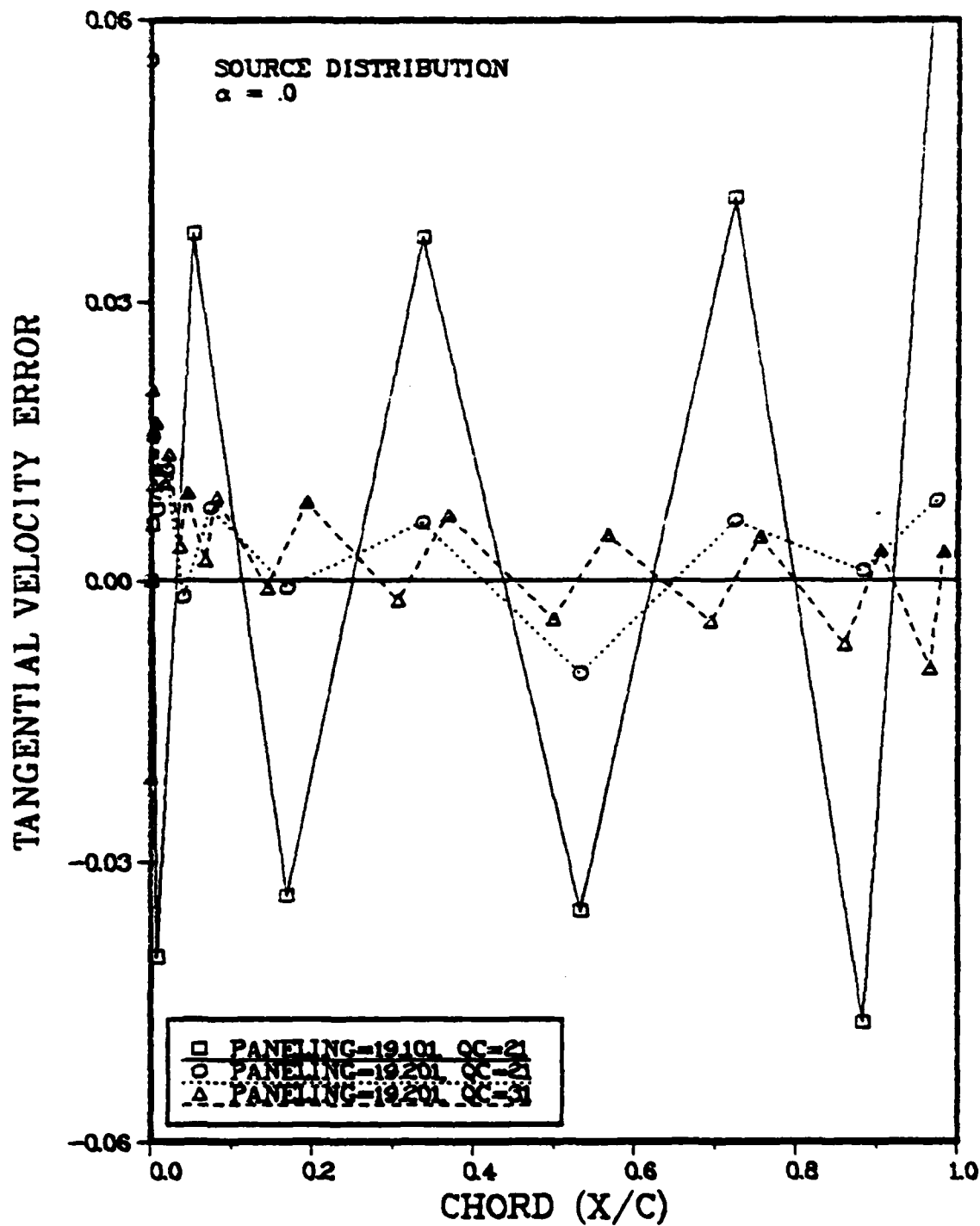


Figure 46. Karman-Trefftz Airfoil, Unsuccessful Cases, Source Distribution.

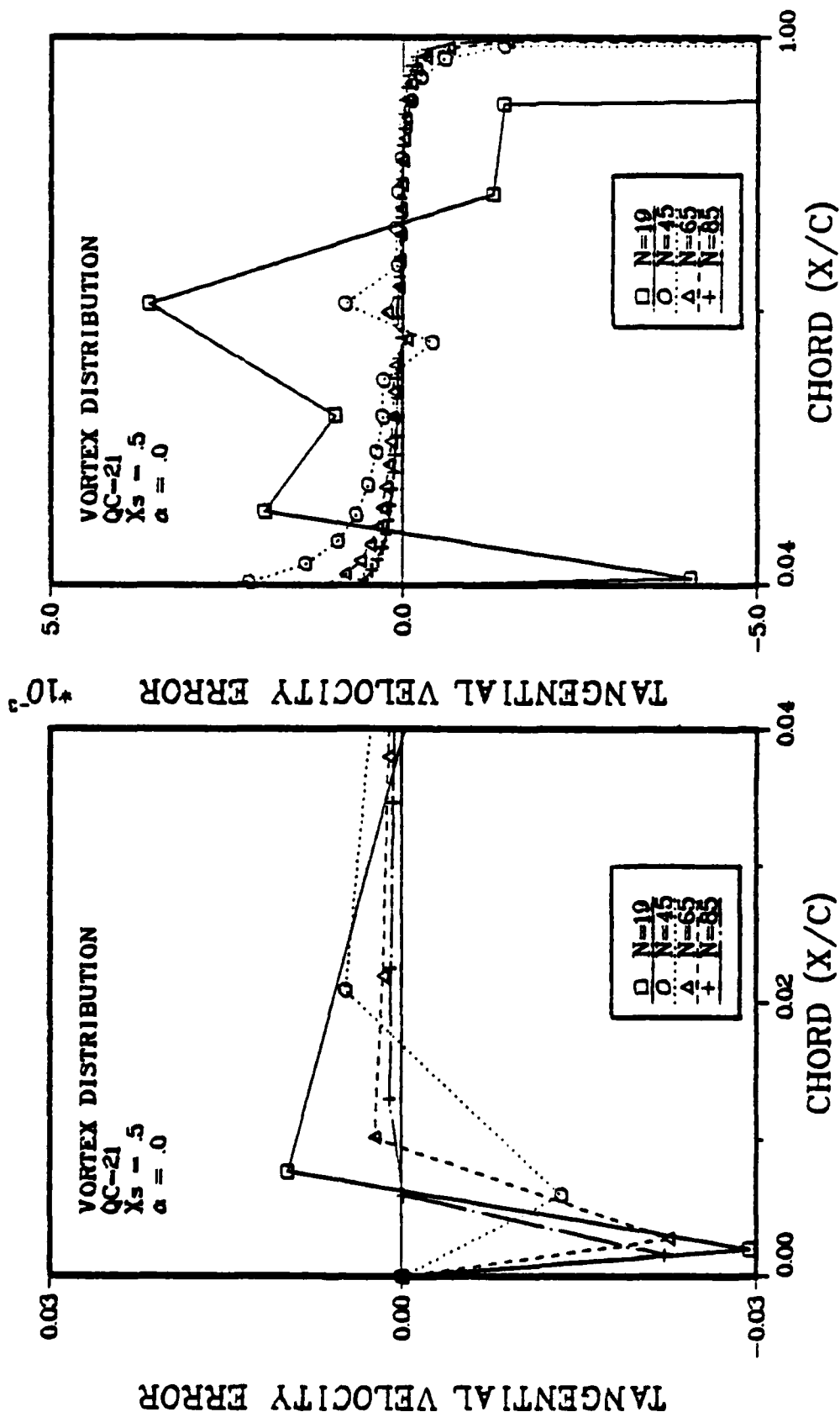


Figure 47a. Effect of N on Tangential Velocity Error, QC=21, for a Karman-Trefftz Airfoil,  $\alpha=.0$ .

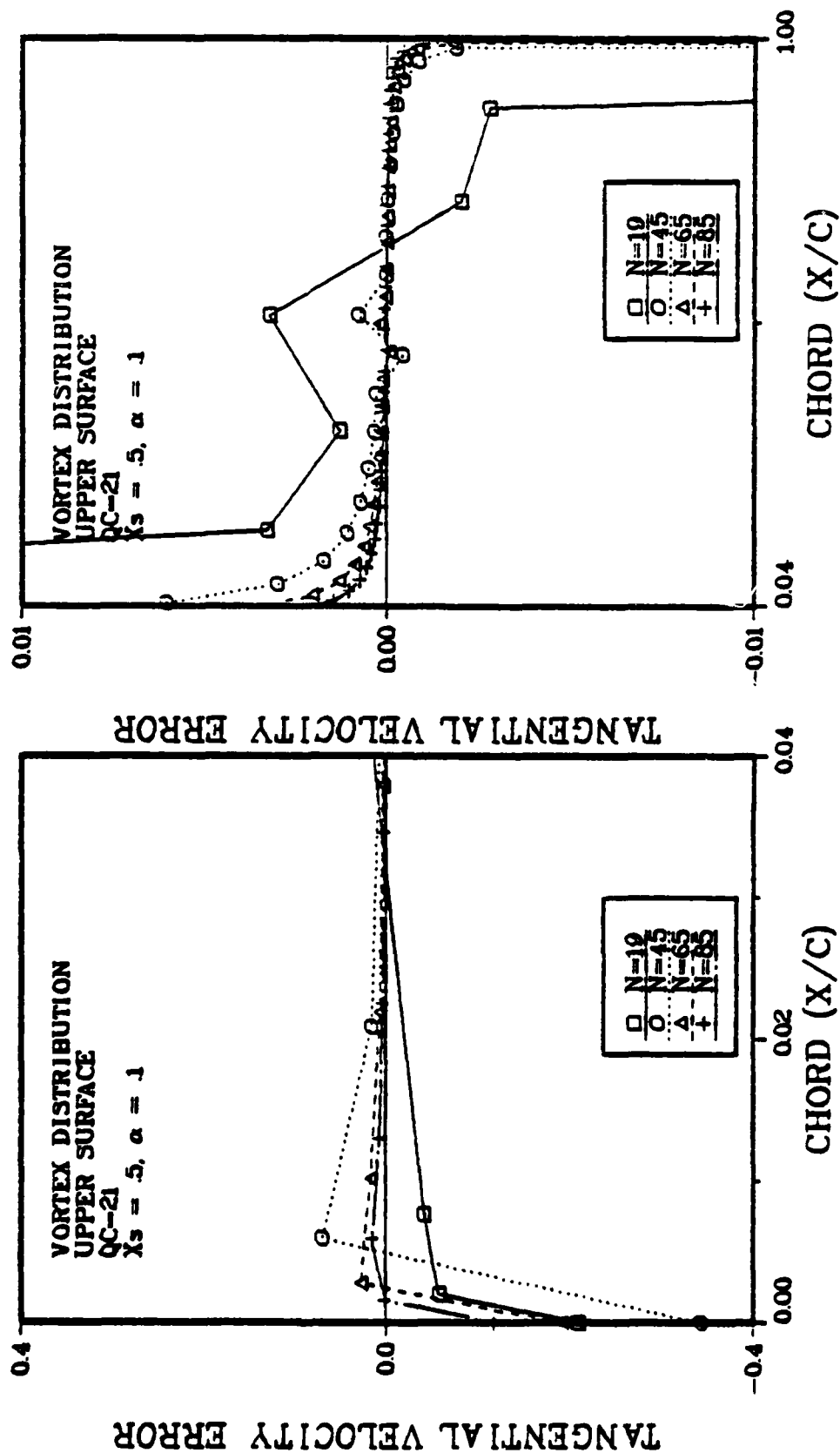


Figure 47b. Effect of N on Tangential Velocity Error, QC=21, for  $\alpha=1$  radians, Upper Surface.



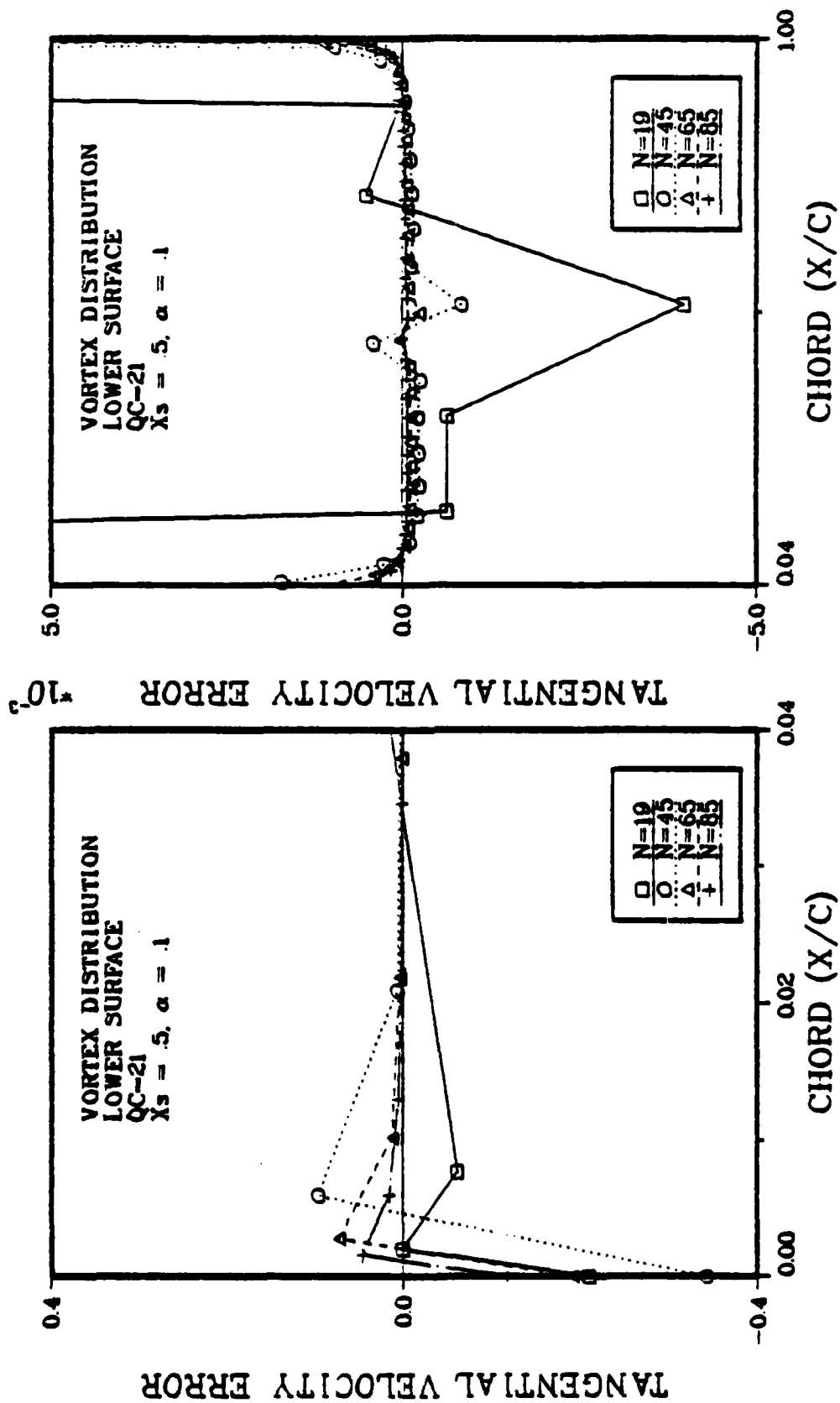


Figure 47c. Effect of  $N$  on Tangential Velocity Error, QC=21, for  $\alpha=.1$  radians, Lower Surface.

of increasing  $N$  is to decrease the magnitude of the point source strength and thus the velocities induced by the source are correspondingly reduced. Figure 48 shows the effect of changing  $Q$  for a 45 element case. This effect is not large, but it is interesting to note that the  $Q=3$  cases do not exhibit the source induced error apparent in the  $Q=2$  cases, although the magnitude of the source strengths are of the same order. The  $Q=3$  case, however, has two control points on a panel, and with this additional control point the normal flow on the panel is more effectively controlled.

Figure 49 shows the effect of additional panels (and control points) near the source location. The airfoil used in this figure is the 65 element airfoil of Figure 47, with the addition of 10 panels on each of the upper and lower surfaces between 40% and 60% chord for a total paneling of 85 elements. The point source location remained at  $X_S=.5$ . The result is that the additional control points in the vicinity of the source control the source strength quite well.

Effect of Point Source Location. A study was conducted to determine more precisely the effect of the point source location on the solution. Figures 50a and 50b show the tangential velocity error for a 45 element airfoil for the  $Q=2$  and 3 cases at  $\alpha = .0$  where the internal point was placed at one of four locations,  $X_S$ . There are two interesting points to note in these figures. The first is

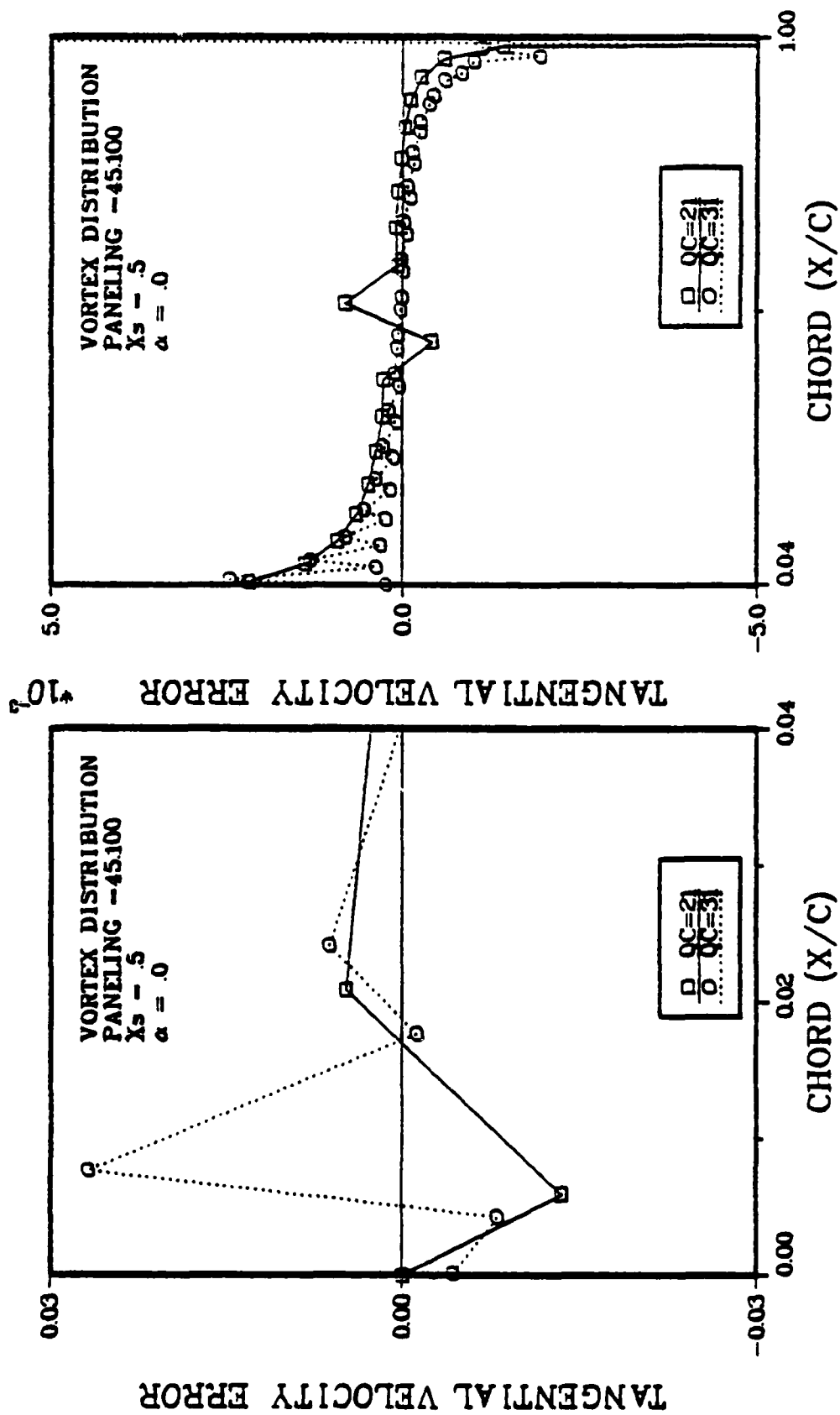


Figure 48. Effect of  $Q$  on Tangential Velocity Error for a Karman-Trefftz Airfoil.

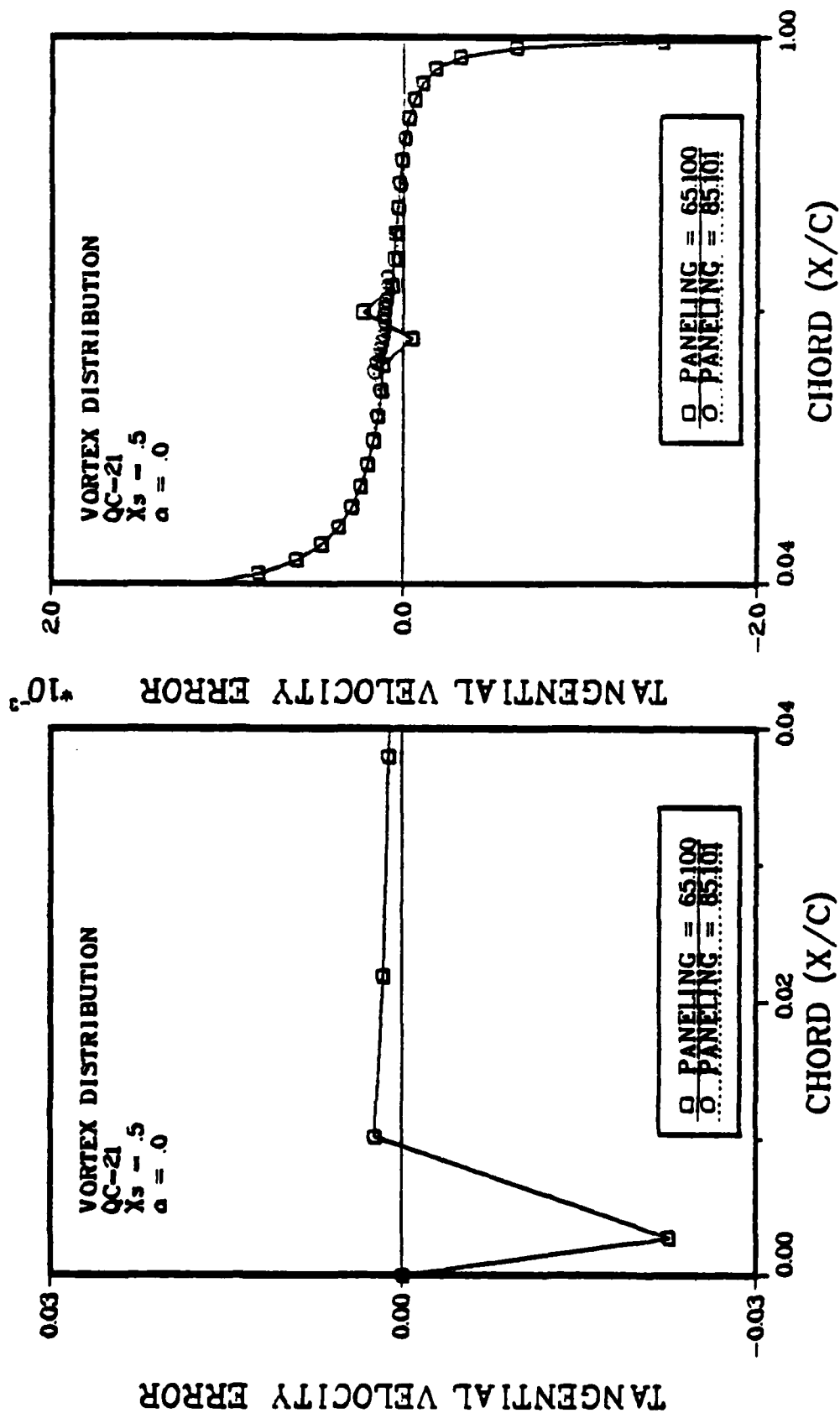


Figure 49. Effect of  $N$  on Source Induced Tangential Velocity Error for a Karman-Trefftz Airfoil.

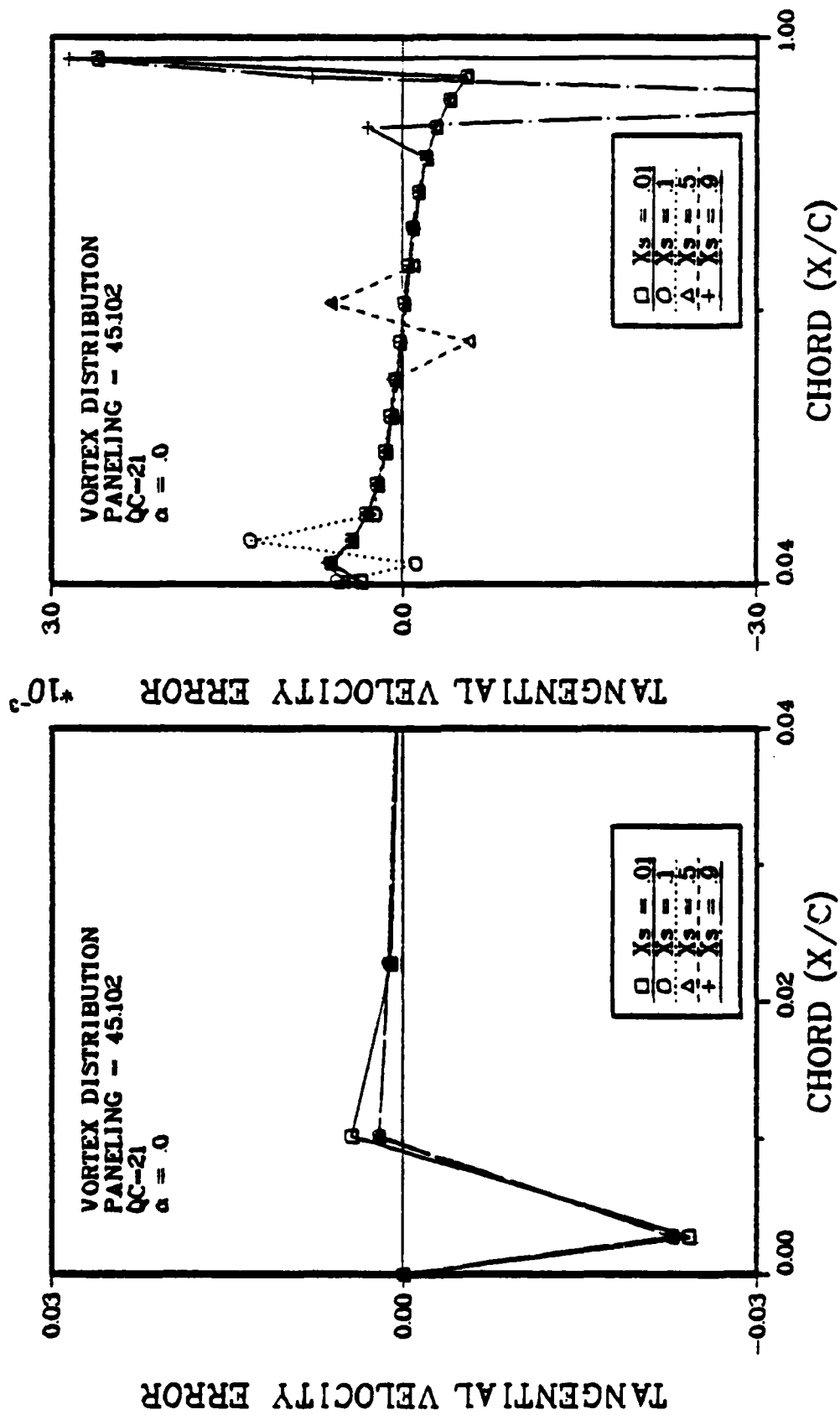


Figure 50a. Effect of Point Source Location on Tangential Velocity Error for a Karman-Trefftz Airfoil, QC=21.

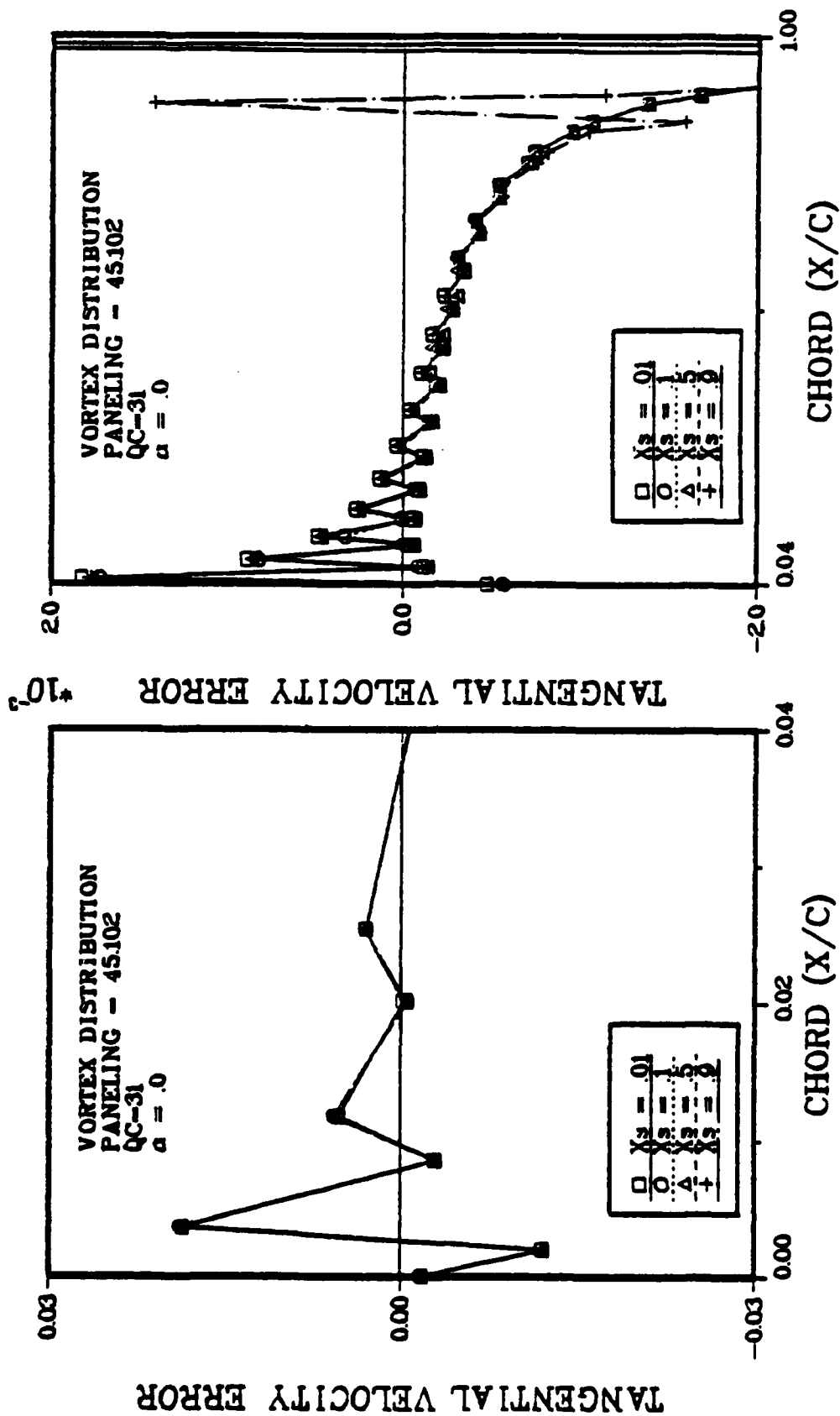


Figure 50b. Effect of Point Source Location on Tangential Velocity Error for a Karman-Trefftz Airfoil, QC=31.

that the effect of changing from  $Q=2$  to  $Q=3$  removes the source induced error for reasons discussed above. The second is that the source induced error is indeed a very local effect. Whether the source is at  $X_s=.01$ ,  $.1$ , or  $.5$ , the solution at the trailing edge remains unaffected, and when the source is at  $X_s = .9$ , the solution over the leading 80% of the airfoil is unchanged.

The effects are local because the source strengths are small, and their effect on velocity falls off as the inverse square of the distance from the source. It should be mentioned that another way of diffusing the effect of the point source would be to use a distributed source on a line inside the airfoil.

If the accuracy of the solution over the whole airfoil is considered, these results indicate that the best location for the point source is very near the leading edge. For this case the solution is excellent over 99% of the airfoil, while the source induced error at the nose is masked somewhat by the, in general, larger error that occurs in this region. These errors are partly due to the fact that a panel method will have difficulty accounting for the rapid changes that occur in velocity as one moves away from the stagnation point. On physical grounds it might also be argued that for an airfoil with a blunt nose, a point source near the nose would be able to more effectively control the

oncoming free stream than would the surface vorticity in the nose region.

Effect of Panel Geometry Characteristics. A study was also conducted to determine the effects of panel geometric characteristics on the solution. A number of these geometric parameters are involved in the present method, including the angle subtended by each panel, the arc length of each panel, and the curvature of each panel. One would intuitively expect these geometric parameters to vary in a smooth manner around the airfoil, making a reasonable approximation to the actual airfoil characteristics. The panel approximation is of course, only a piecewise continuous representation of the surface, and will exhibit discontinuities of curvature. The curvature of a panel in a flat panel method is constant and equal to zero over a panel, while in the present method the curvature is constant but not zero over a panel, with variations from panel to panel. One would also expect the panel arc length to vary somewhat smoothly around the airfoil. One would not expect good results with a very small panel between two large panels since the small panel's control point would be overpowered by the nearby larger panels. Several investigators (Henshaw, Ref 25, Hess, Ref 12) have suggested as a rule of thumb that the ratio of arc lengths of adjacent panels be less than 1.5, but this is merely a suggestion



which is probably somewhat dependent on the method being used.

Figures 51a - 51c show paneling characteristics for five different panel arrangements for the Karman-Trefftz airfoil being considered. The angle subtended by each panel, the panel radius, and a normalized panel arc length are plotted against panel number where panel one is the first panel at the trailing edge. Since the airfoil and all these panelings are symmetric only upper surface quantities have been plotted. The panel models compared to the actual surface have been plotted with an expanded vertical scale in Figures 52a-52d. As was the case in Figure 42 almost no difference between the two can be seen, except in the paneling = 45.101 case which will be discussed below. The tangential velocity errors for these panelings are shown in Figures 53a and 53b for  $QC=21$  and  $QC=31$  respectively, with  $\alpha = 0$  radians. Similar results for  $\alpha = .1$  radians are shown in Figures 53c-53f. In these cases results are shown for both upper and lower surfaces since they are not the same at non-zero angle of attack.

The first panel arrangement which was computed was the  $p=45.100$  scheme, and while the geometric characteristics as well as the velocity error results appear reasonable, it was felt that some improvements could be obtained, particularly in the leading edge region. This paneling was then modified slightly by shifting panels toward the nose and the tail to

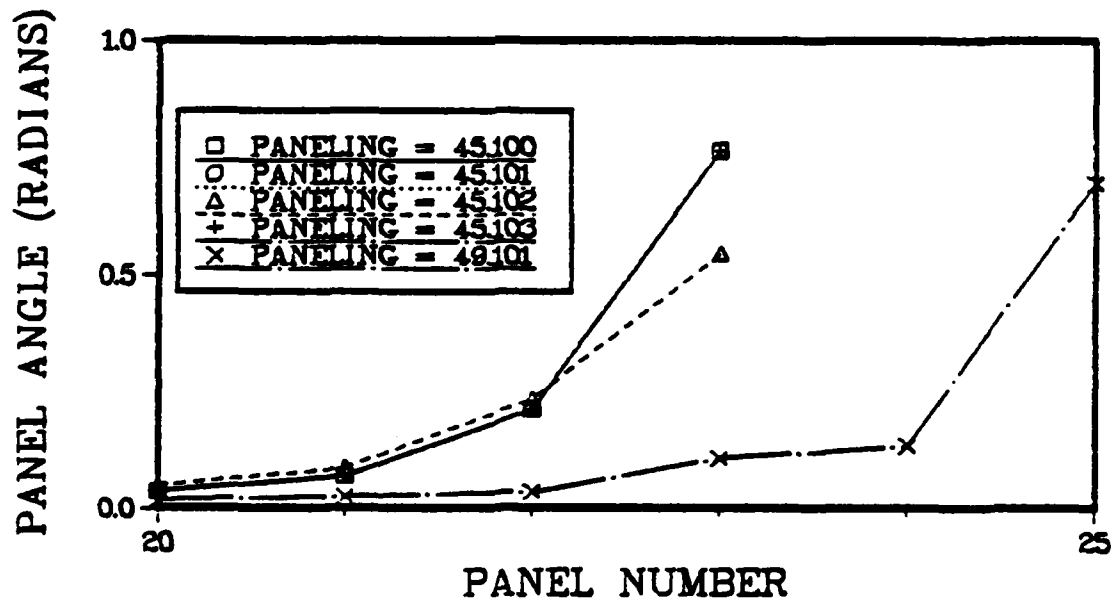
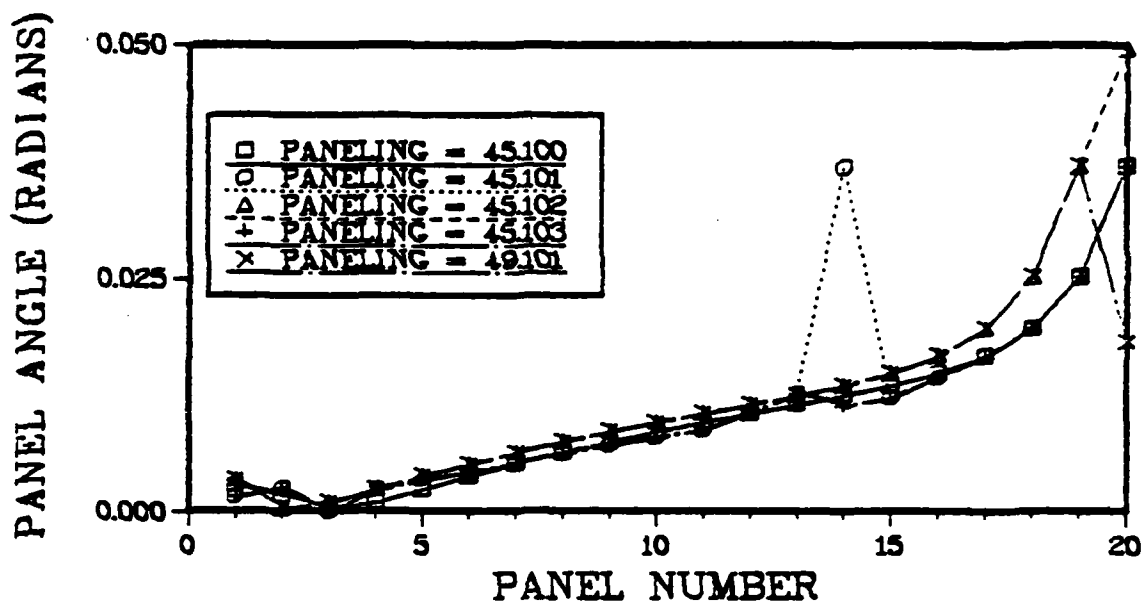


Figure 51a. Paneling Geometric Characteristics for a Karman-Trefftz Airfoil, Panel Subtended Angle.

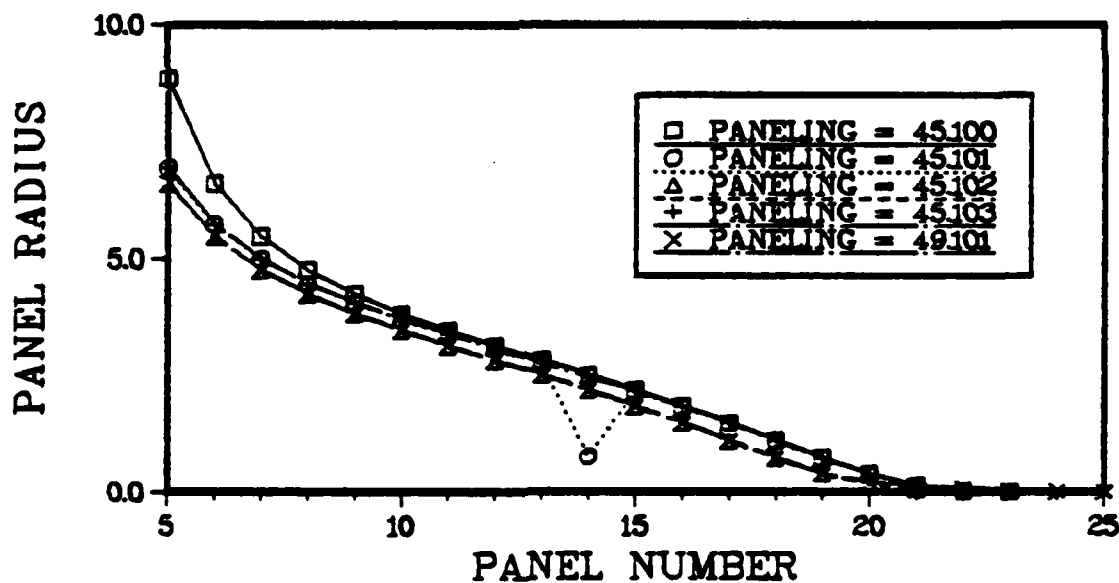
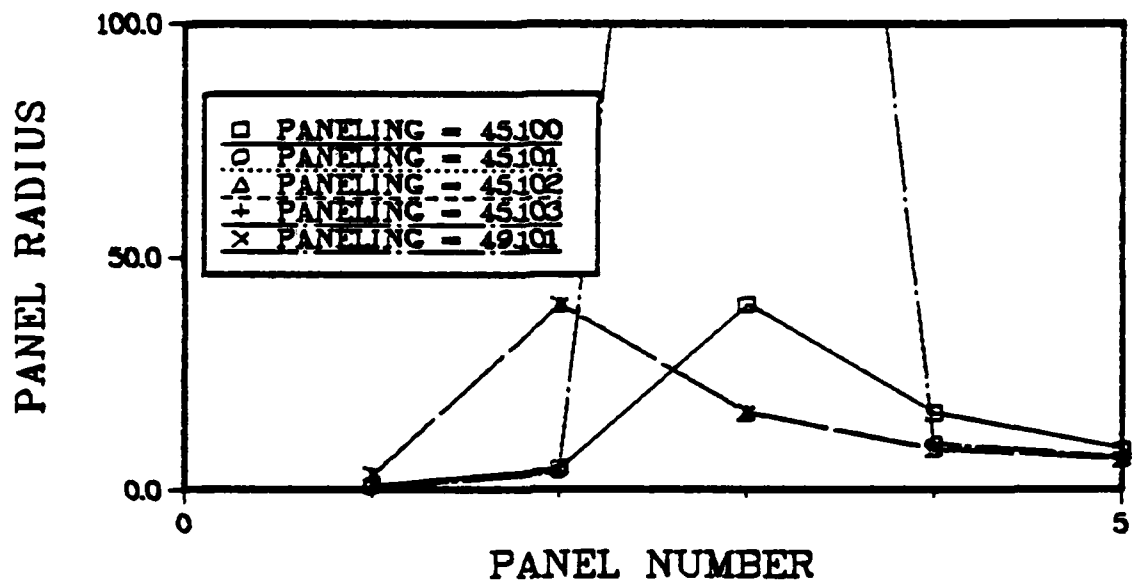


Figure 51b. Paneling Geometric Characteristics for a Karman-Trefftz Airfoil, Panel Radius.

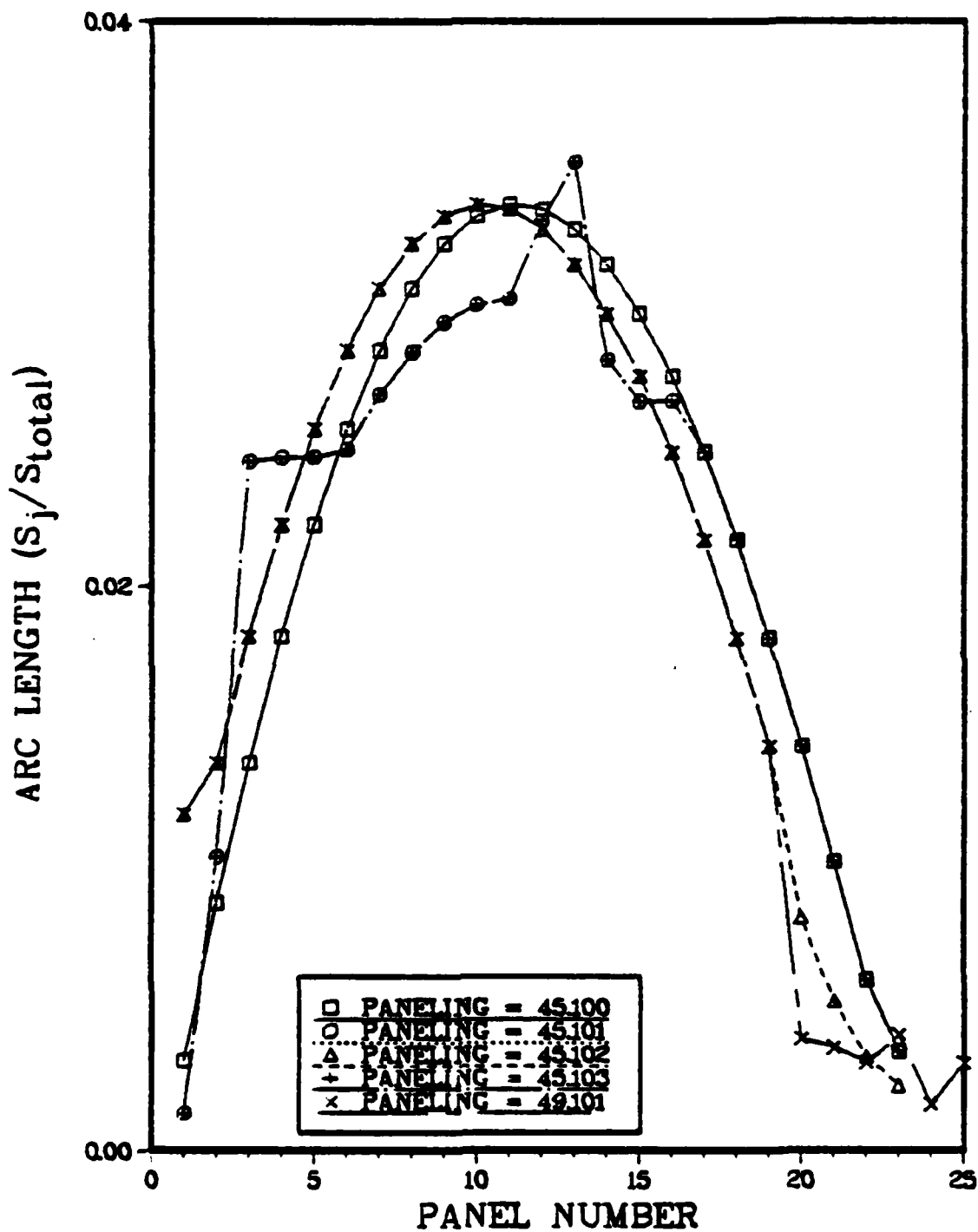


Figure 51c. Paneling Geometric Characteristics for a Karman-Trefftz Airfoil, Panel Arc Length.

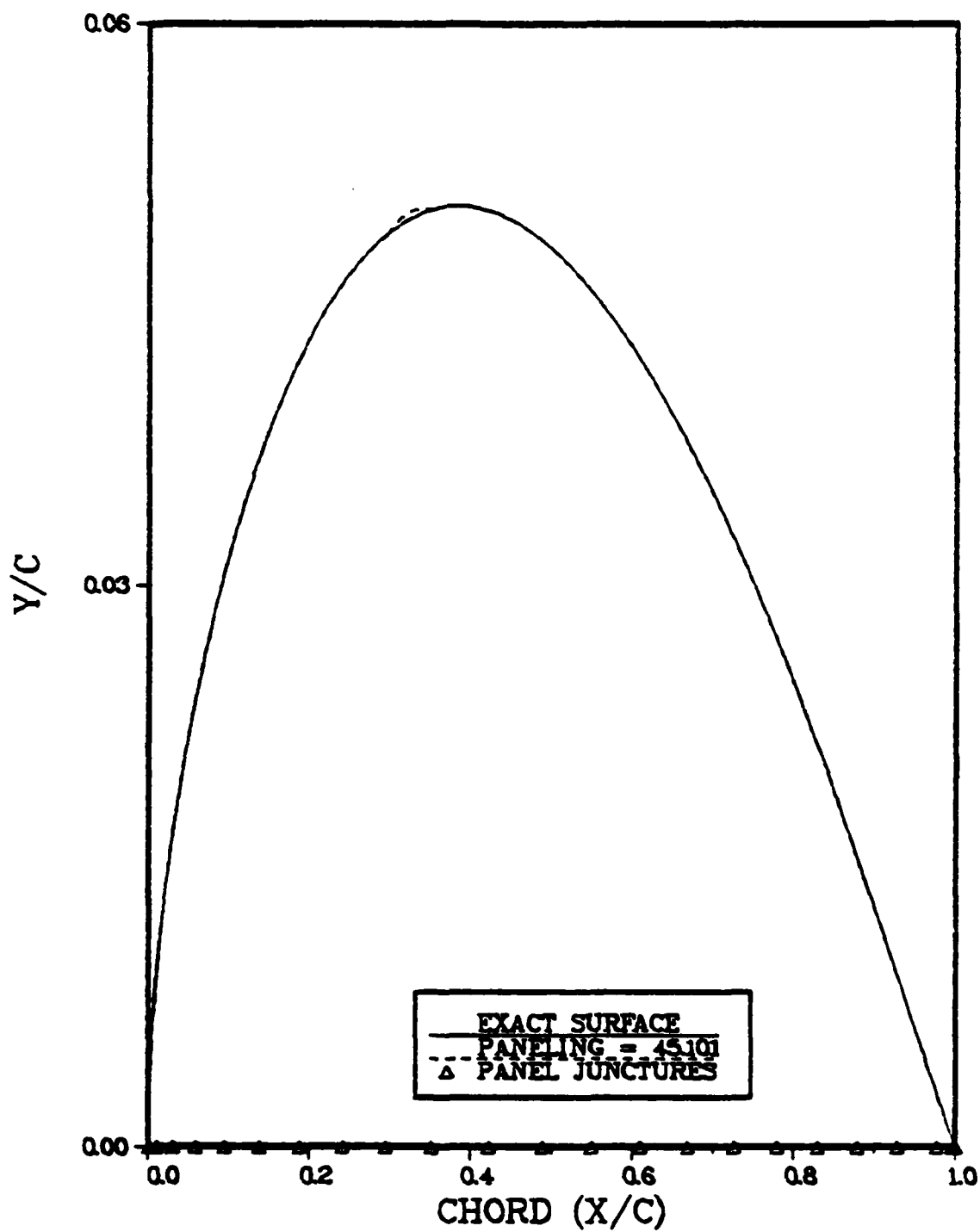


Figure 32a. Comparison of Panel Model with Actual Surface for a Karman-Trefftz Airfoil, Paneling=45.101.

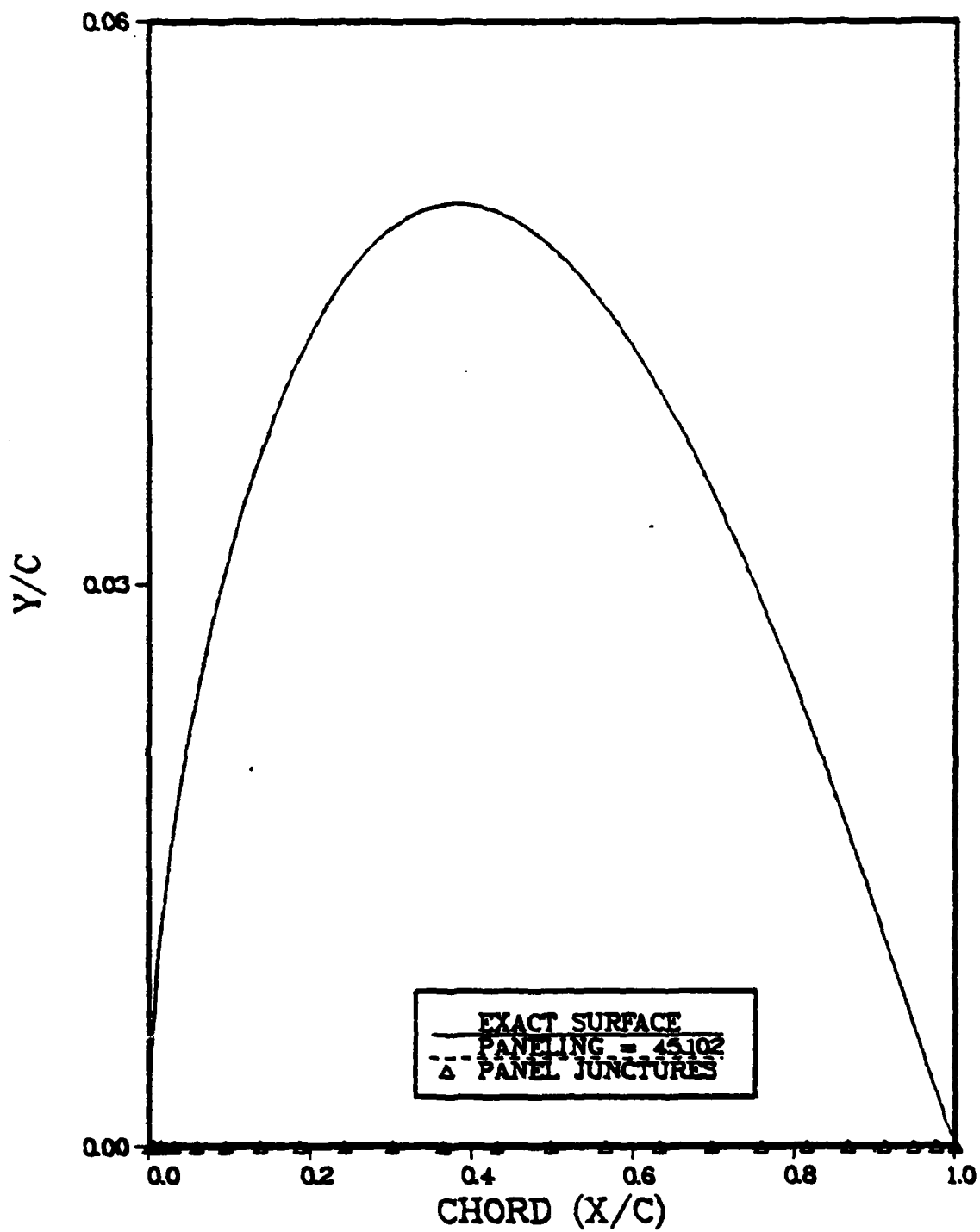


Figure 52b. Comparison of Panel Model with Actual Surface for a Karman-Trefftz Airfoil, Paneling=45.102.

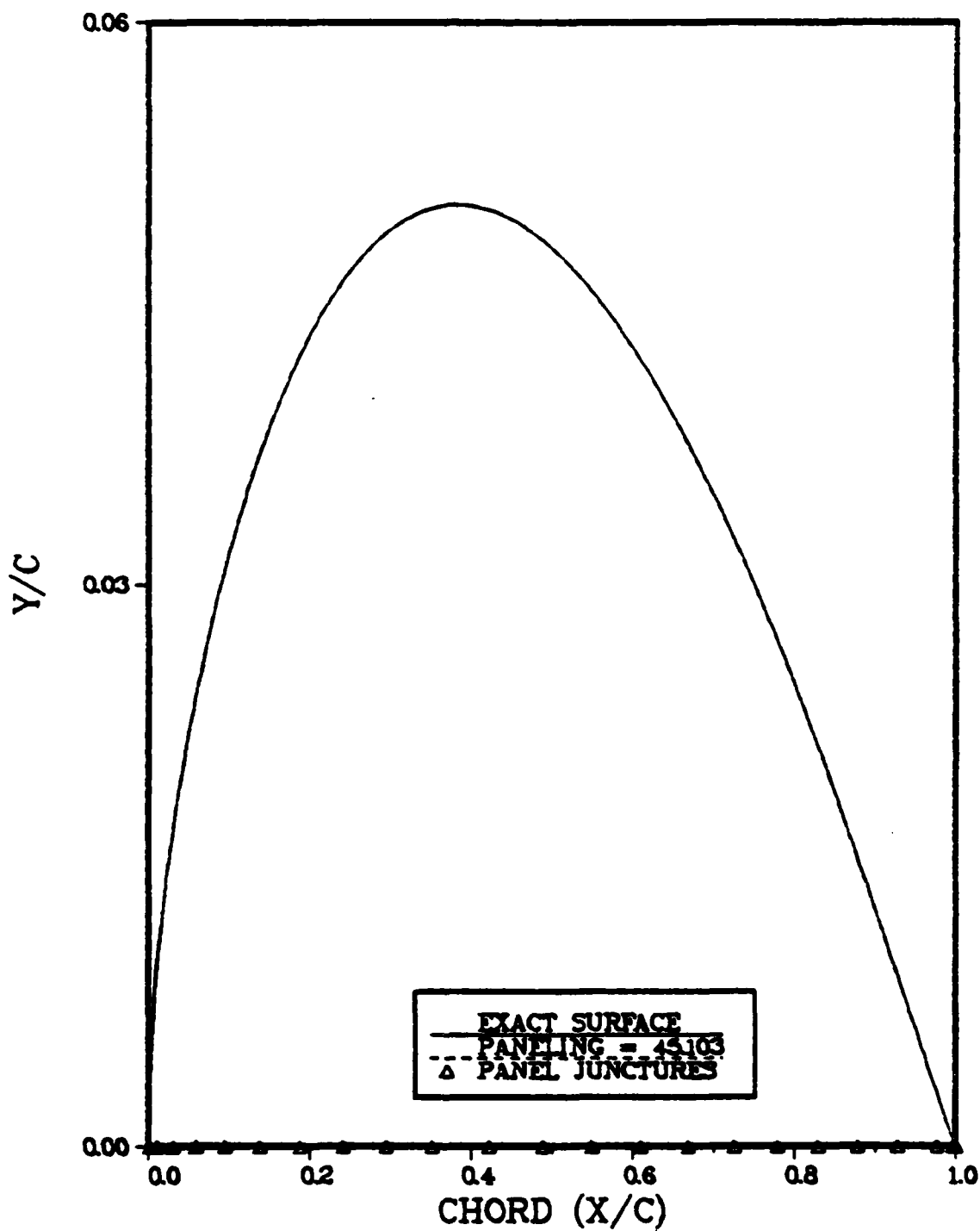


Figure 52c. Comparison of Panel Model with Actual Surface for a Karman-Trefftz Airfoil, Paneling=45.103.

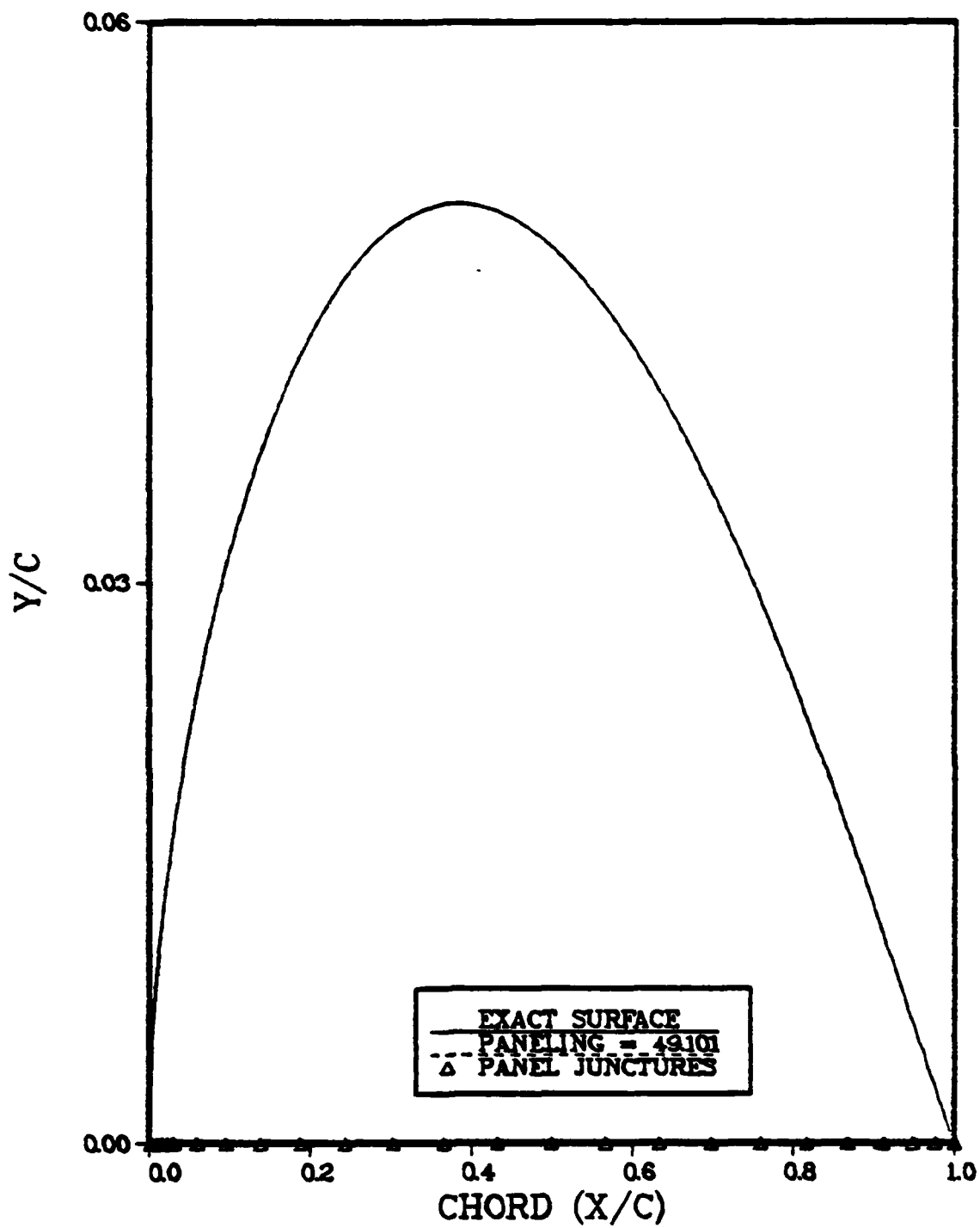


Figure 52d. Comparison of Panel Model with Actual Surface for a Karman-Trefftz Airfoil, Paneling=49.101.



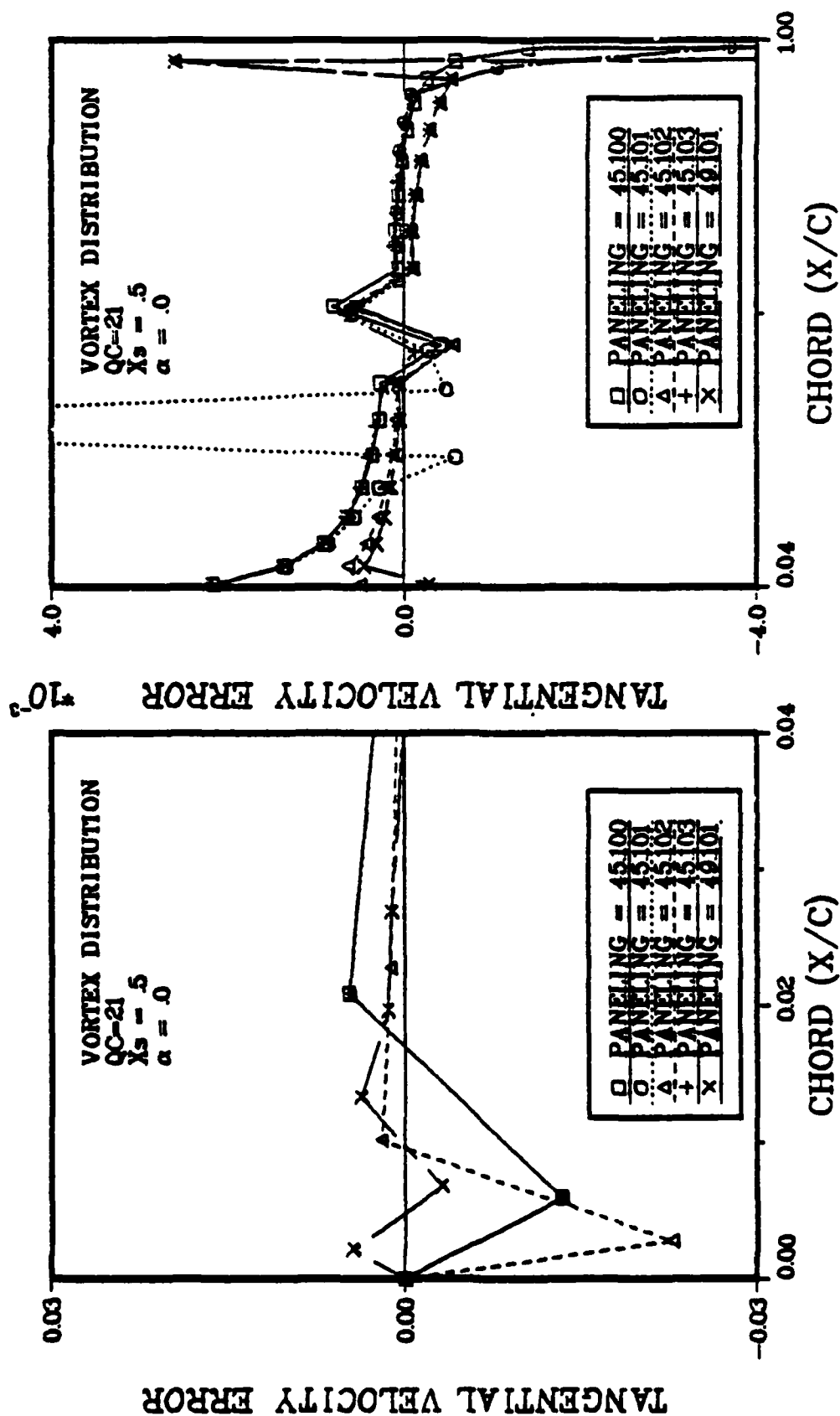


Figure 53a. Effect of Paneling Characteristics on Tangential Velocity Error for a Karman-Trefftz Airfoil, QC=21,  $\alpha=.0$  radians.

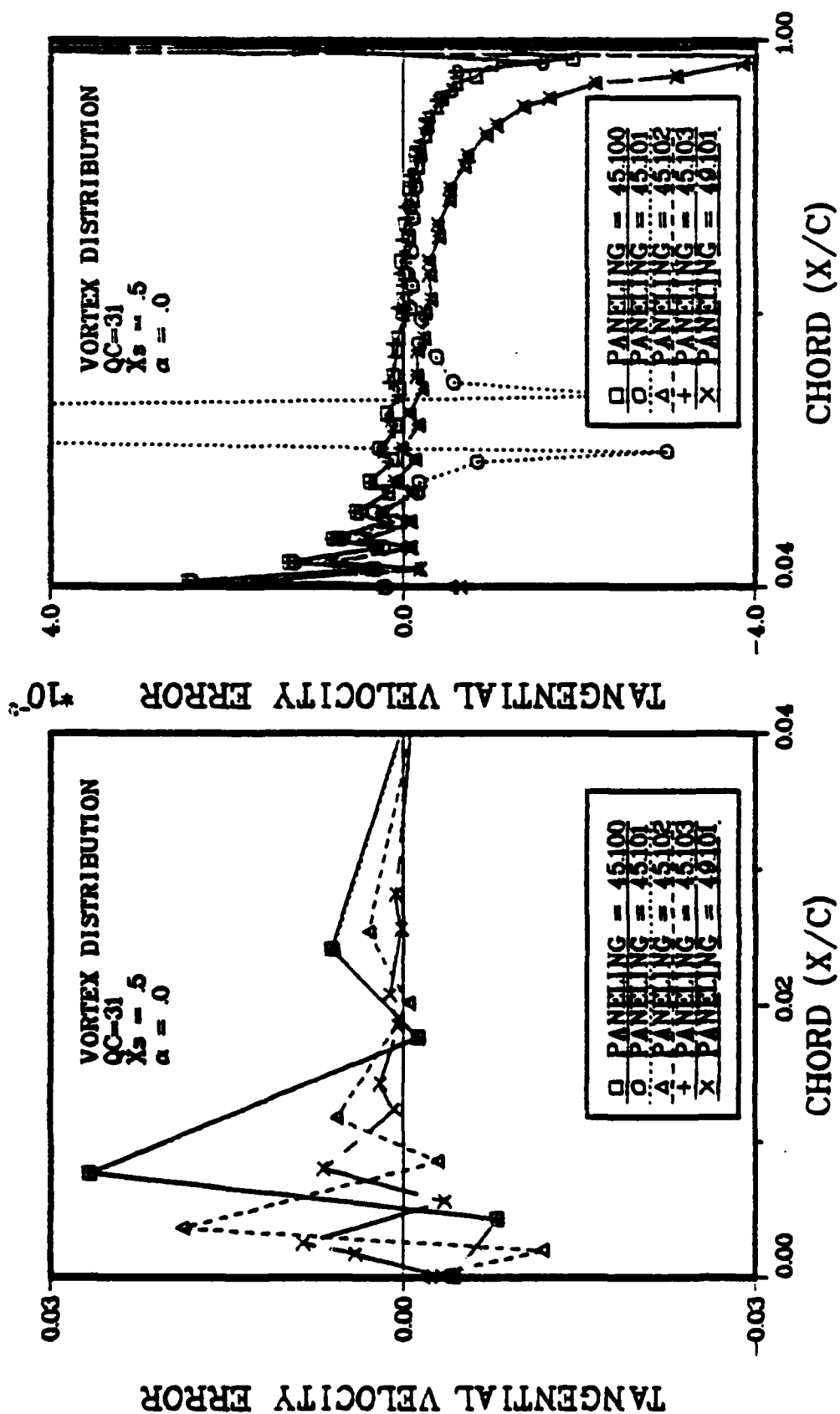


Figure 53b. Effect of Paneling Characteristics on Tangential Velocity Error for a Karman-Trefftz Airfoil, QC=31,  $\alpha=.0$  radians.

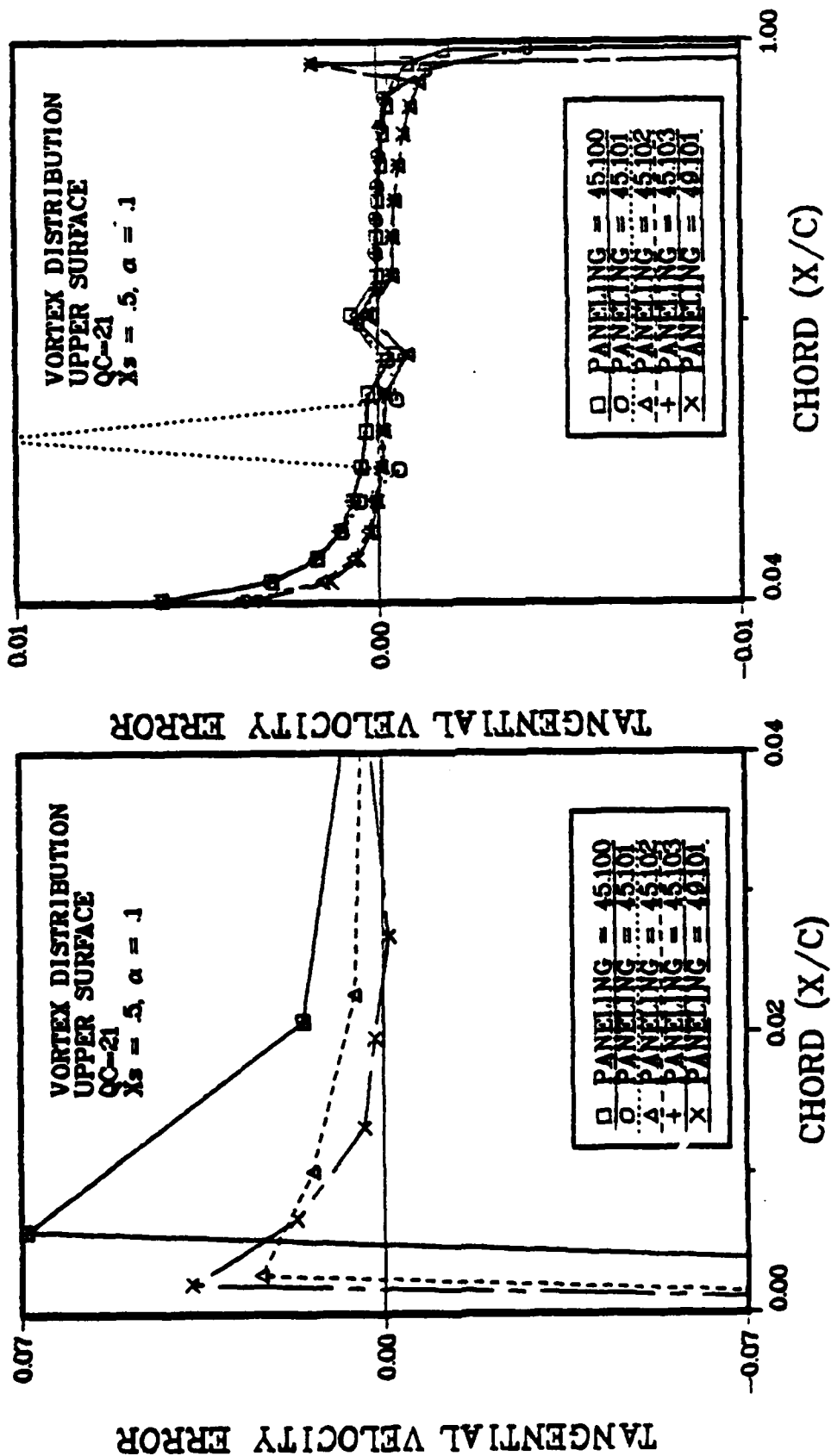


Figure 53c. Effect of Paneling Characteristics on Tangential Velocity Error for a Karman-Trefftz Airfoil, QC=21,  $\alpha=.1$  radians, Upper Surface.

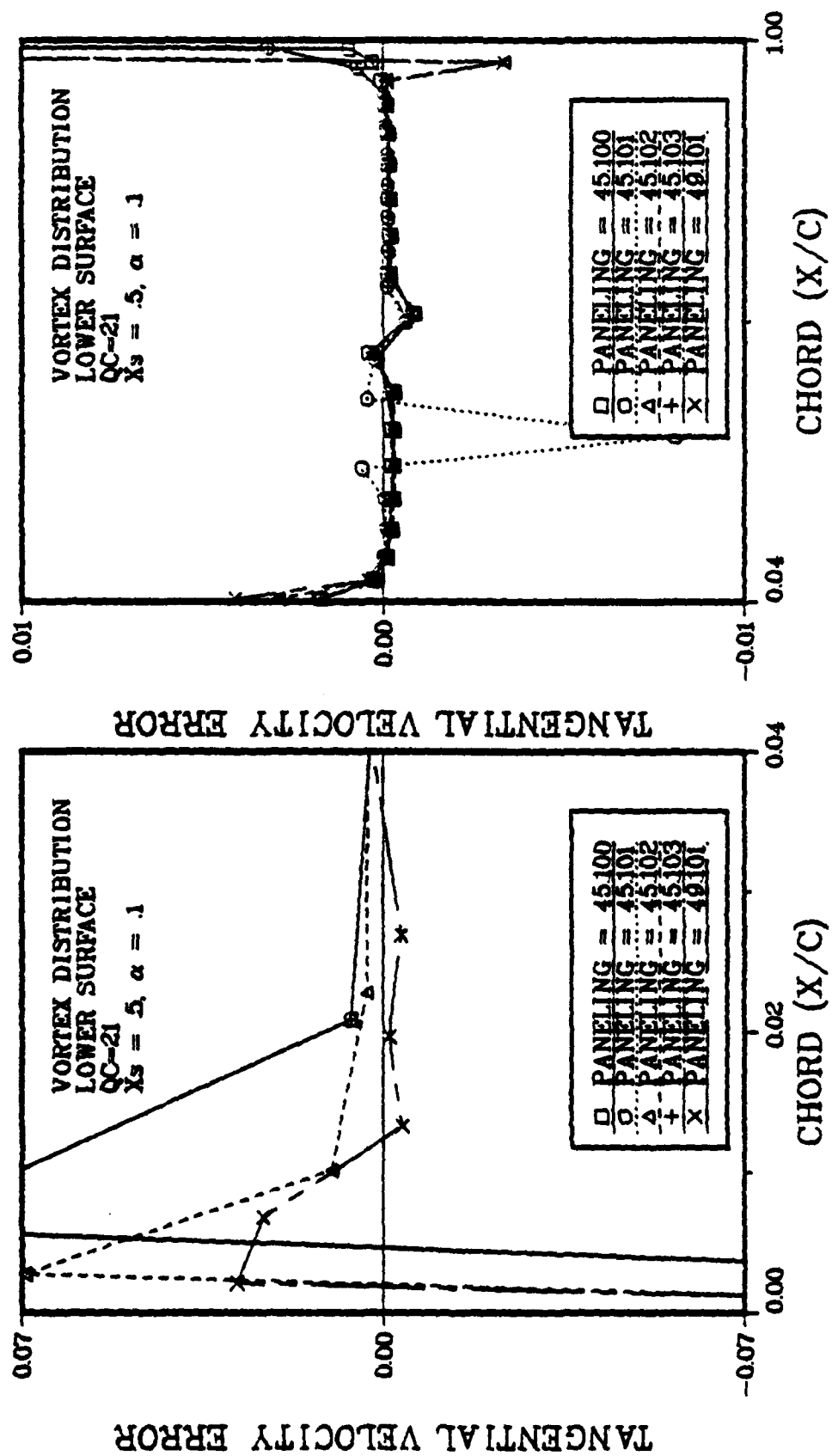


Figure 53d. Effect of Paneling Characteristics on Tangential Velocity Error for a Karman-Trefftz Airfoil, QC=21,  $\alpha=.1$  radians, Lower Surface.

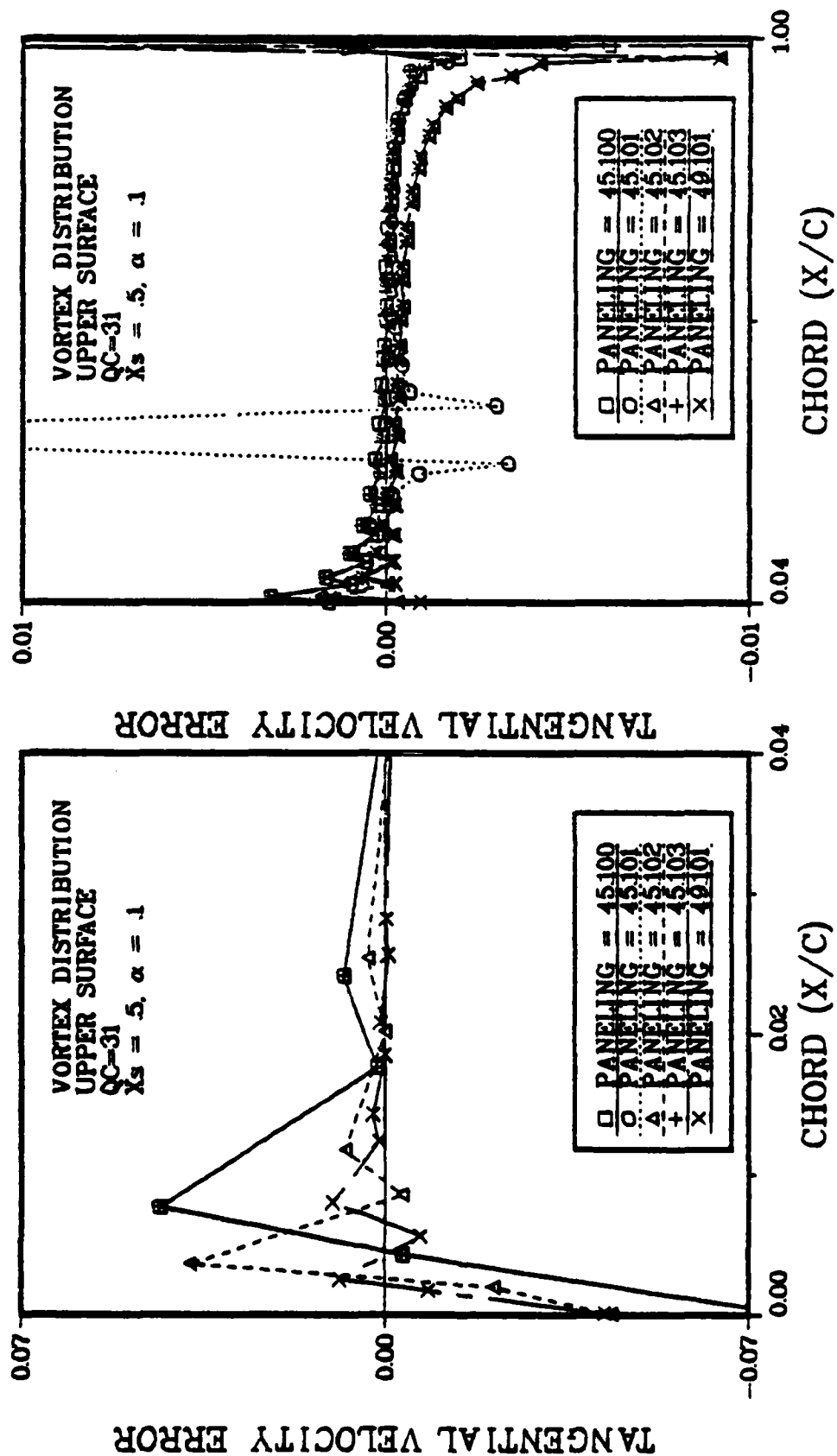


Figure 53e. Effect of Paneling Characteristics on Tangential Velocity Error for a Karman-Trefftz Airfoil, QC-31,  $\alpha = .1$  radians, Upper Surface.

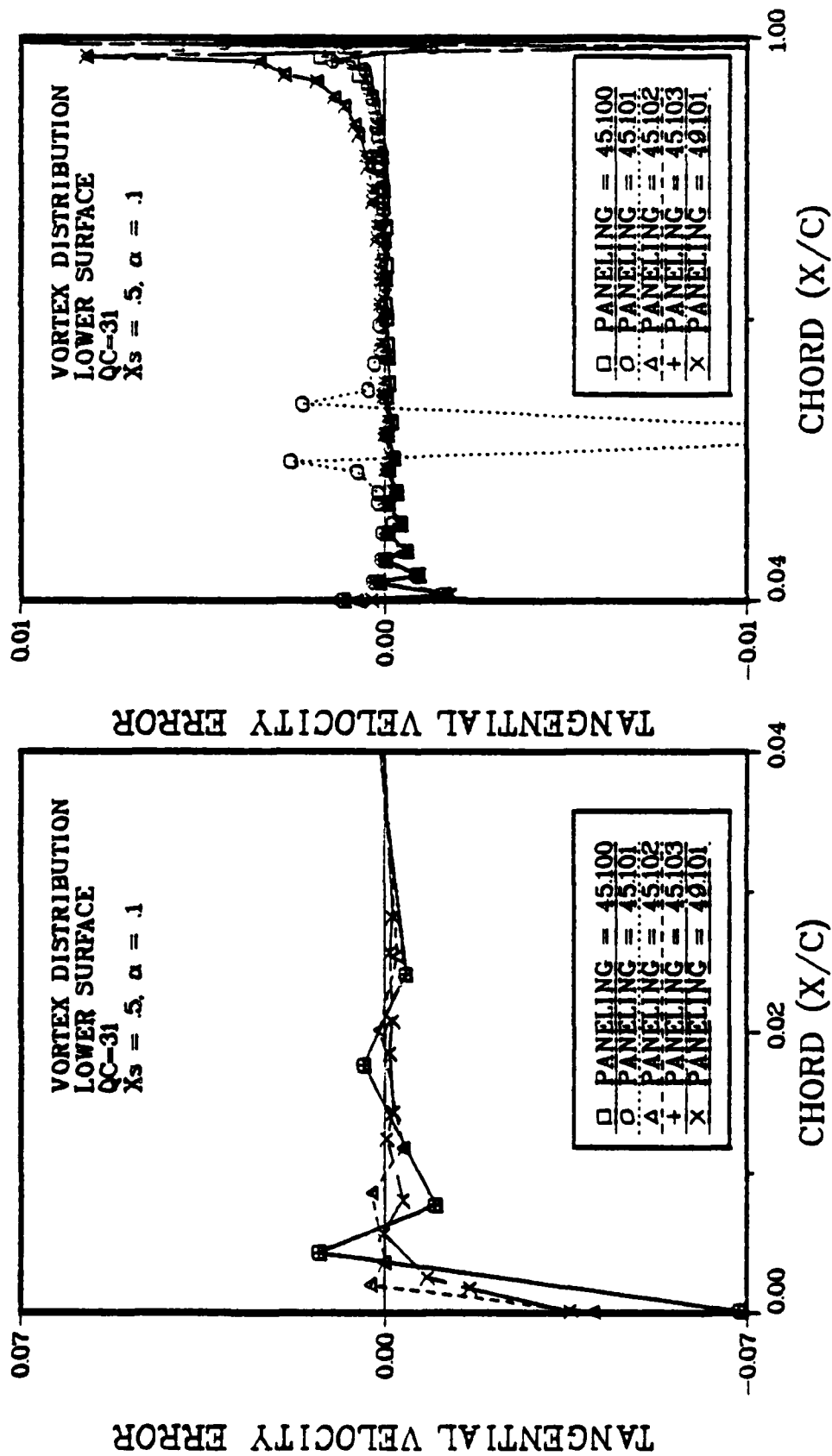


Figure 53f. Effect of Paneling Characteristics on Tangential Velocity Error for a Karman-Trefftz Airfoil. QC = 31,  $\alpha = .1$  radians, Lower Surface.

produce the  $P = 45.101$  paneling, but in so doing, a rather large jump in all of the panel geometric characteristics is introduced near the 30% chord point at panel No.14. The effect on the surface modeling of this modification can be seen in Figure 52a. Figures 53a-53f show the dramatic effect of this discontinuity on the velocity error, but note that the effect is quite localized near the discontinuity.

The  $P=45.101$  paneling was then modified by slightly moving slightly one of the panel defining points for the panel on which the curvature jump takes place. The resultant  $P=45.103$  paneling is only slightly different than the  $P=45.101$  case, yet the curvature jump is gone and the resultant error plots are much improved as shown in Figures 53a-53f.

The original  $P=45.100$  paneling was modified in a different way by removing panels at the nose and tail while requiring that the 1.5 rule hold in these regions, and adding panels over the mid section of the airfoil. This arrangement is the  $P = 45.102$  paneling and the velocity error plots for this case indeed show a reduction in error at the leading and trailing edges compared to the  $P = 45.100$  case, indicating the validity of the 1.5 rule. This paneling was then further modified by adding panels at the leading and trailing edge to obtain the  $P=49.101$  paneling. The errors for this case are similar to those for the

P=45.102 arrangement with perhaps slight improvement near the leading edge which may be attributable to the slightly increased panel density.

These studies have shown that the present method is rather insensitive to changes in geometric paneling characteristics provided that these characteristics conform generally to what might be expected of a good model of the airfoil; that is, the characteristics vary smoothly over the airfoil. The method is sensitive to these characteristics only when large changes occur over a small part of the airfoil, but in these cases the sensitivity effects are localized. The effects are localized for the same reason that the effect of the point source was a local one, i.e. the effect of a panel decreases with distance from the panel. The reason that the method is sensitive, locally, to geometric characteristics is that the method is capable of modeling geometry very well, particularly as  $N$  is increased. This capability for faithful geometric representation is one of the attractive features of panel methods in general.

Effect of Panel Curvature A study was also conducted to determine the effects of panel curvature on the computed solution. The parameter controls the curvature of each panel by moving the third point, through which the circle is drawn, in from the originally specified point on the airfoil surface toward the straight line connecting the panel end points. Thus  $\beta = 0$  would be, in the limit, a flat panel,



and  $\beta = 1$  is the normal case where the circle is drawn through the three input points on the airfoil surface.

Figures 54a-54f show results for the P=45.102 airfoil with a point source at  $X_S = .01$  for a range of  $\beta$ 's from 1 to 0.2, and for two angles of attack. Note that the errors increase as the panel becomes flatter. Also note that as the panel becomes flatter the error is larger for the three term series than for the two term series in all cases. It seems that as the panel becomes flatter, or approaches a lower order representation of the surface, a lower order representation of the singularity (i.e. a 2 term rather than a 3 term series) is sufficient to produce a certain level of error. Of course these errors are larger than are obtained by using the full circular arc panel. The reason that better results are obtained using the more highly curved panels is that they provide a better representation of the surface in terms of location of the singularity, and location of the control point.

Effect of Angle of Attack. The results presented to this point have included angles of attack  $\alpha = .0$ , and .1 radians, and have exhibited no strong sensitivity to the angle of attack. To study more carefully the effects of angle of attack, an N=19 element symmetrically paneled airfoil was computed at various  $\alpha$ 's between 0., and .55 radians for both the two and the three term singularity

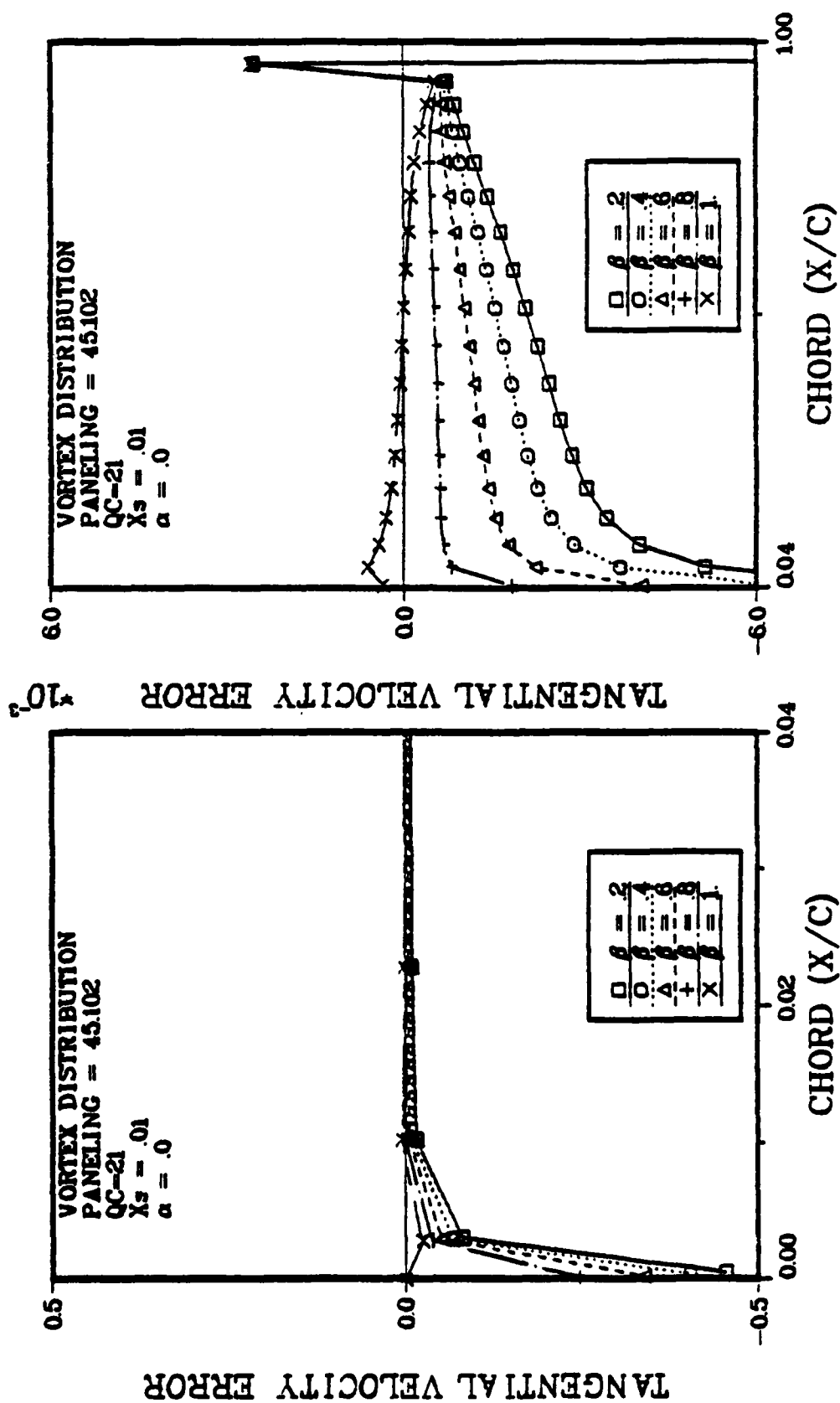


Figure 54a. Effect of Panel Curvature on Tangential Velocity Error for a Karman-Trefftz Airfoil, QC=21,  $\alpha=0$  radians.

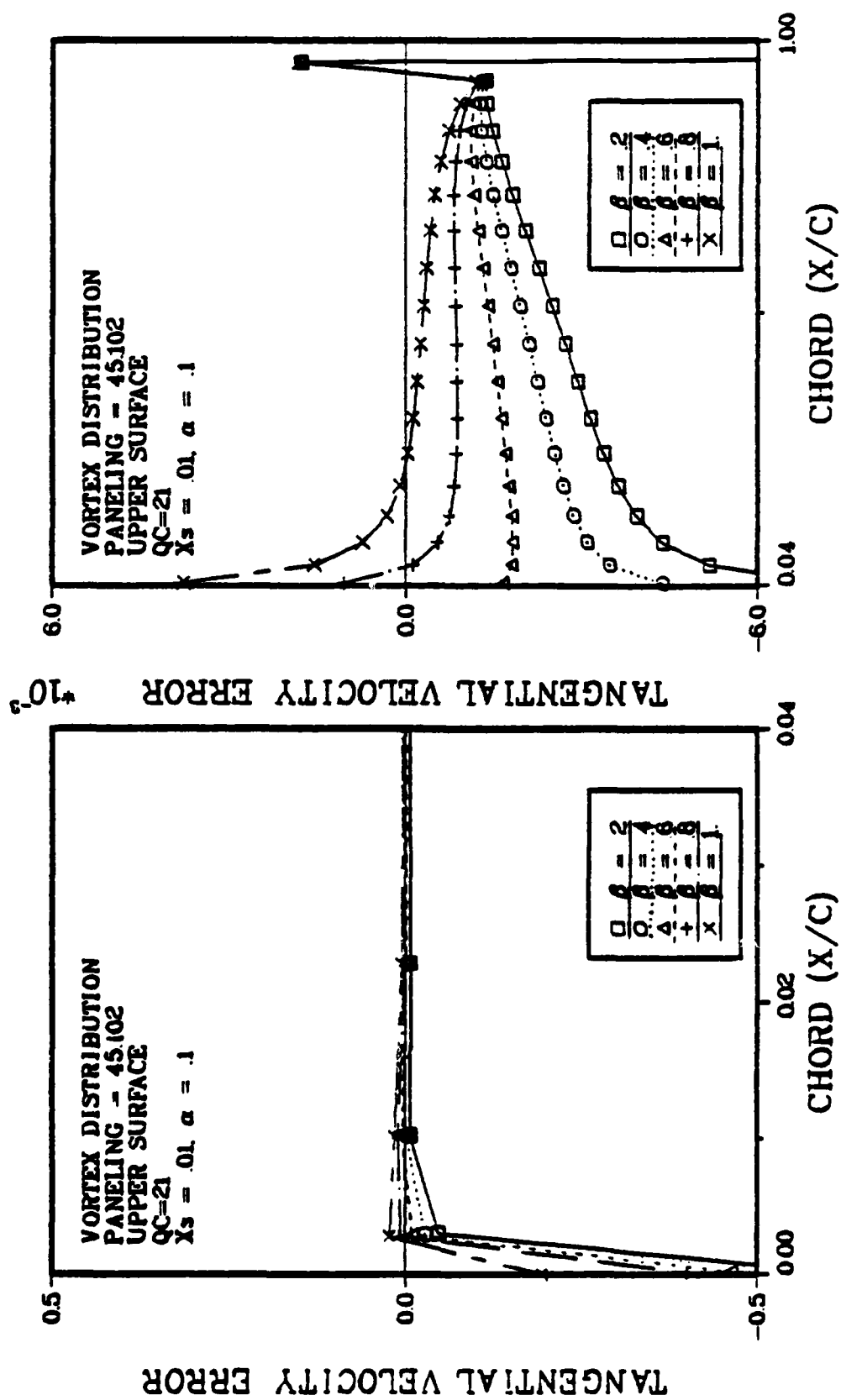


Figure 54b. Effect of Panel Curvature on Tangential Velocity Error for a Karman-Trefftz Airfoil,  $QC=21$ ,  $\alpha=.1$  radians, Upper Surface.

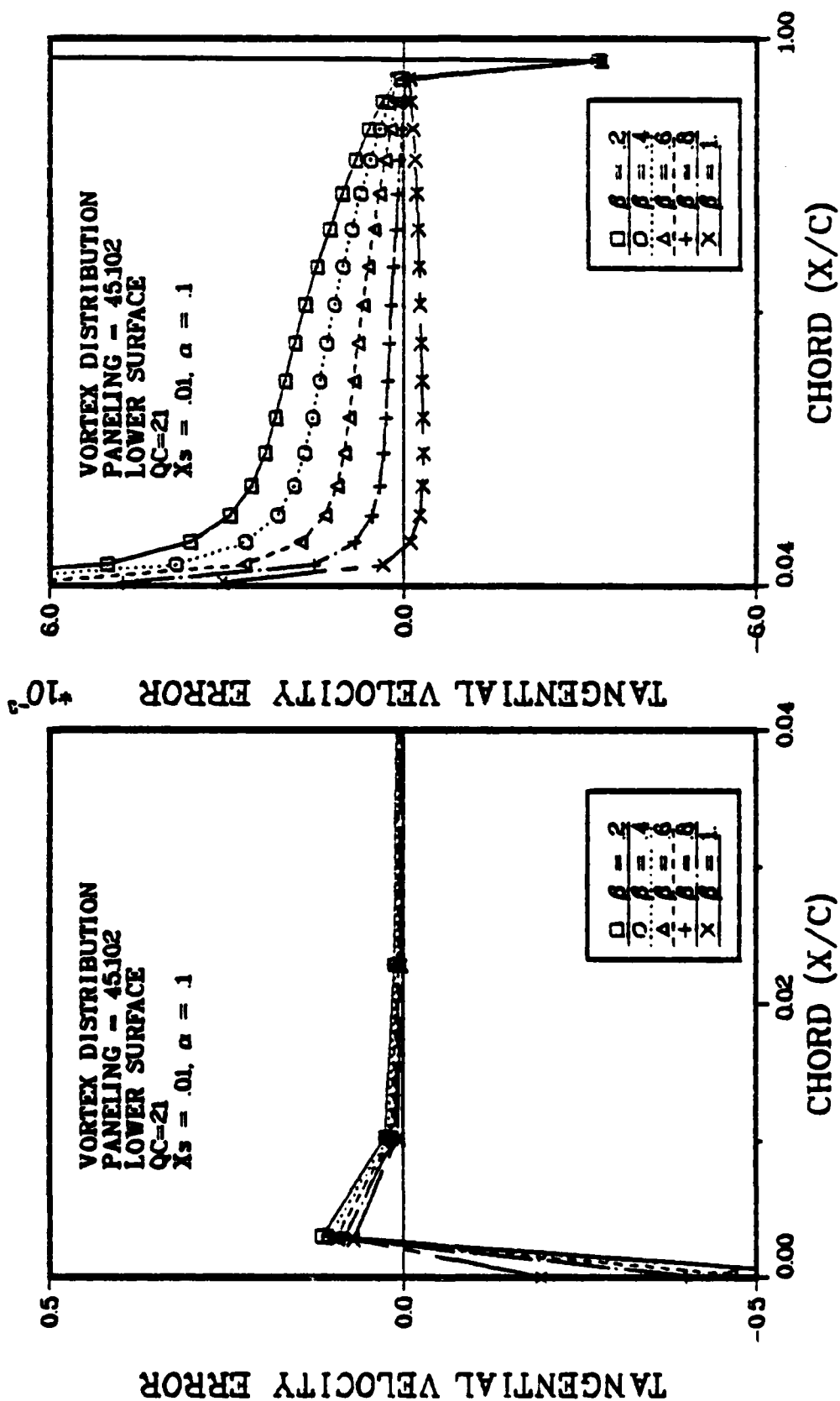


Figure 54c. Effect of Panel Curvature on Tangential Velocity Error for a Karman-Trefftz Airfoil, QC=21,  $\alpha=0.1$  radians, Lower Surface.

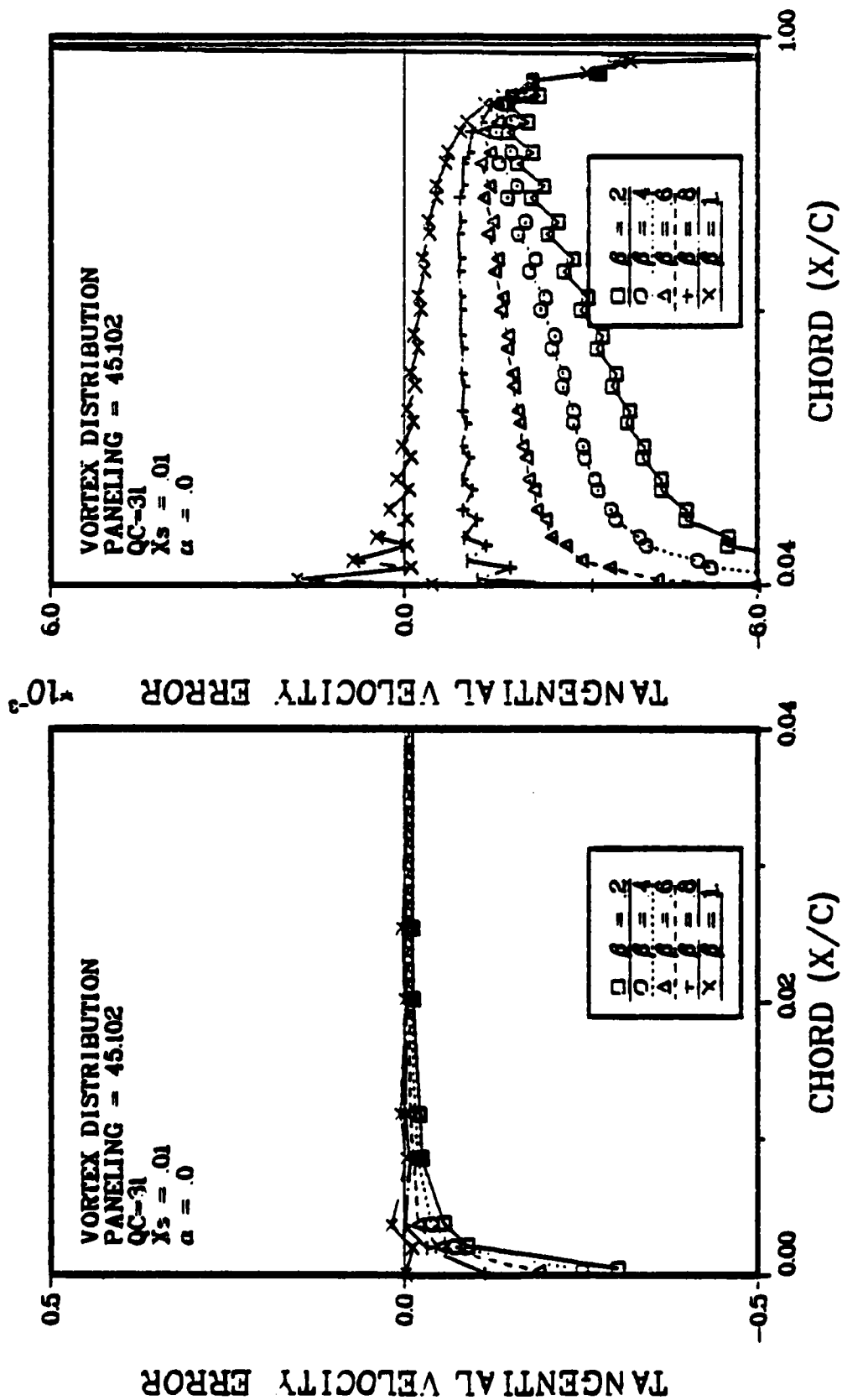


Figure 54d. Effect of Panel Curvature on Tangential Velocity Error for a Karman-Trefftz Airfoil, QC=31,  $\alpha=.0$  radians.



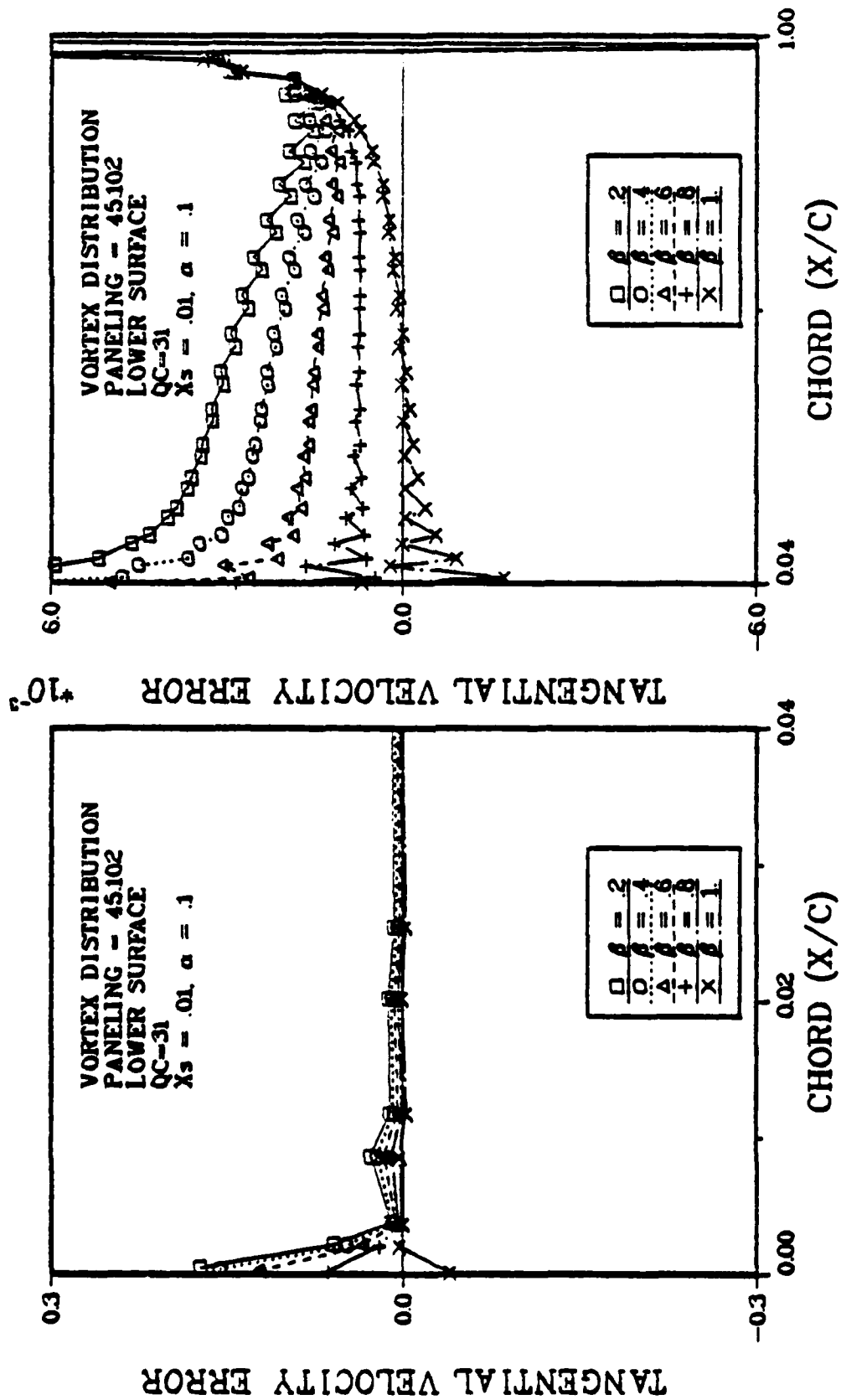


Figure 54f. Effect of Panel Curvature on Tangential Velocity Error for a Karman-Trefftz Airfoil,  $QC=31$ ,  $\alpha=.1$  radians, Lower Surface.

series. The results of these calculations are presented in Figure 55 which shows excellent agreement for the lift coefficient over the entire angle of attack range for both two and three term cases. Figure 56 shows the error in lift coefficient; that is  $C_{L_{er}} = C_{L_{ex}} - C_{L_{comp}}$ . Note that both the two and three term curves are linear with  $\alpha$ , and that the error is quite small. Also, the error for the three term case is less than for the two term case, and the slope of the three term curve is less than that for the two term case so that the difference increases with  $\alpha$ . A consequence of the linearity of these curves is that the figure relative error, defined as  $C_{L_{rel}} = 1 - \frac{C_{L_{comp}}}{C_{L_{ex}}}$ , is essentially a constant. For  $Q=2$ ,  $C_{L_{rel}} = .00697$ , and for  $Q=3$ ,  $C_{L_{rel}} = .00578$ .

Effect of Control Point Location. An important question which arises in the discussion of any panel method is the sensitivity of the solution to control point placement. In the present method, the control point location is assumed to be on the circular arc which represents the surface, and similarly, the normal to the surface is represented by the normal to the circular arc. Thus there is an error in both the control point location, and the surface slope. Since surface location and slope can be computed exactly for a Karman-Trefftz airfoil, a study was done to determine the sensitivity of the current method to these errors. Since these two parameters are independent



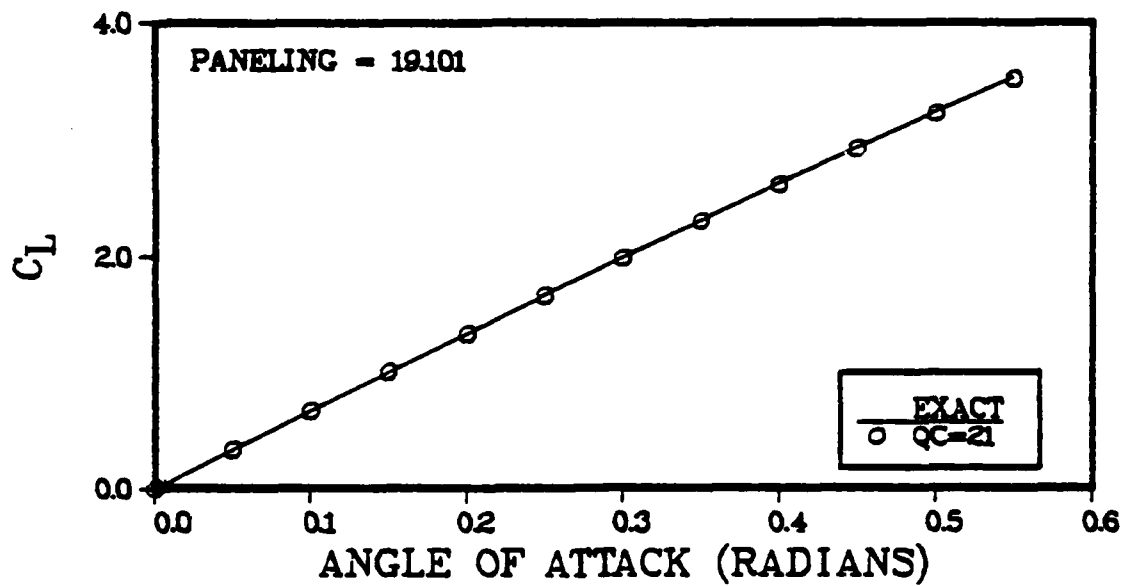
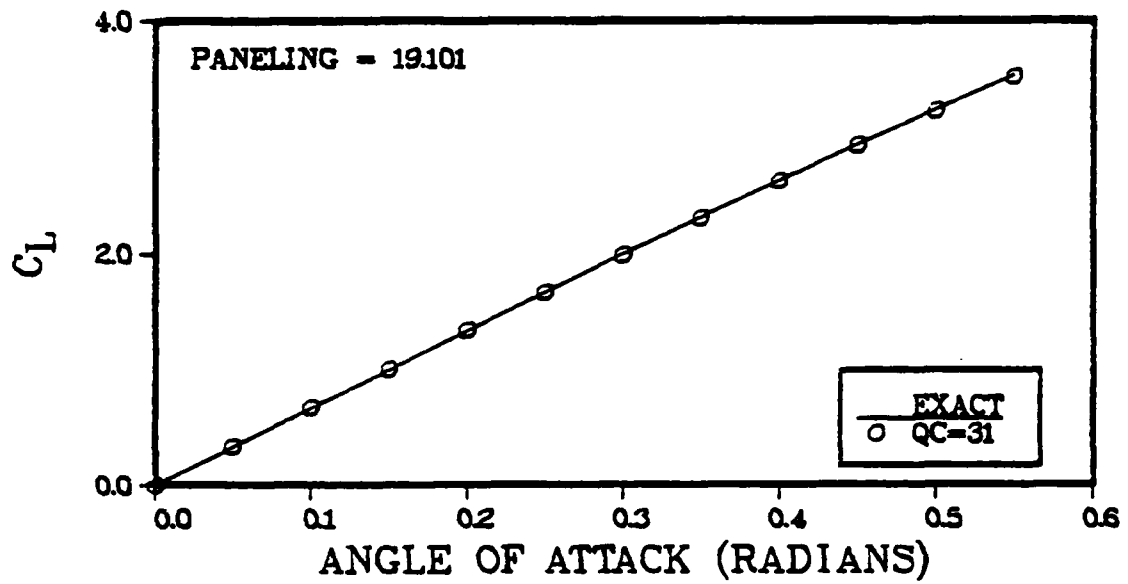


Figure 55. Effect of Angle of Attack on Lift Coefficient for a Karman-Trefftz Airfoil.

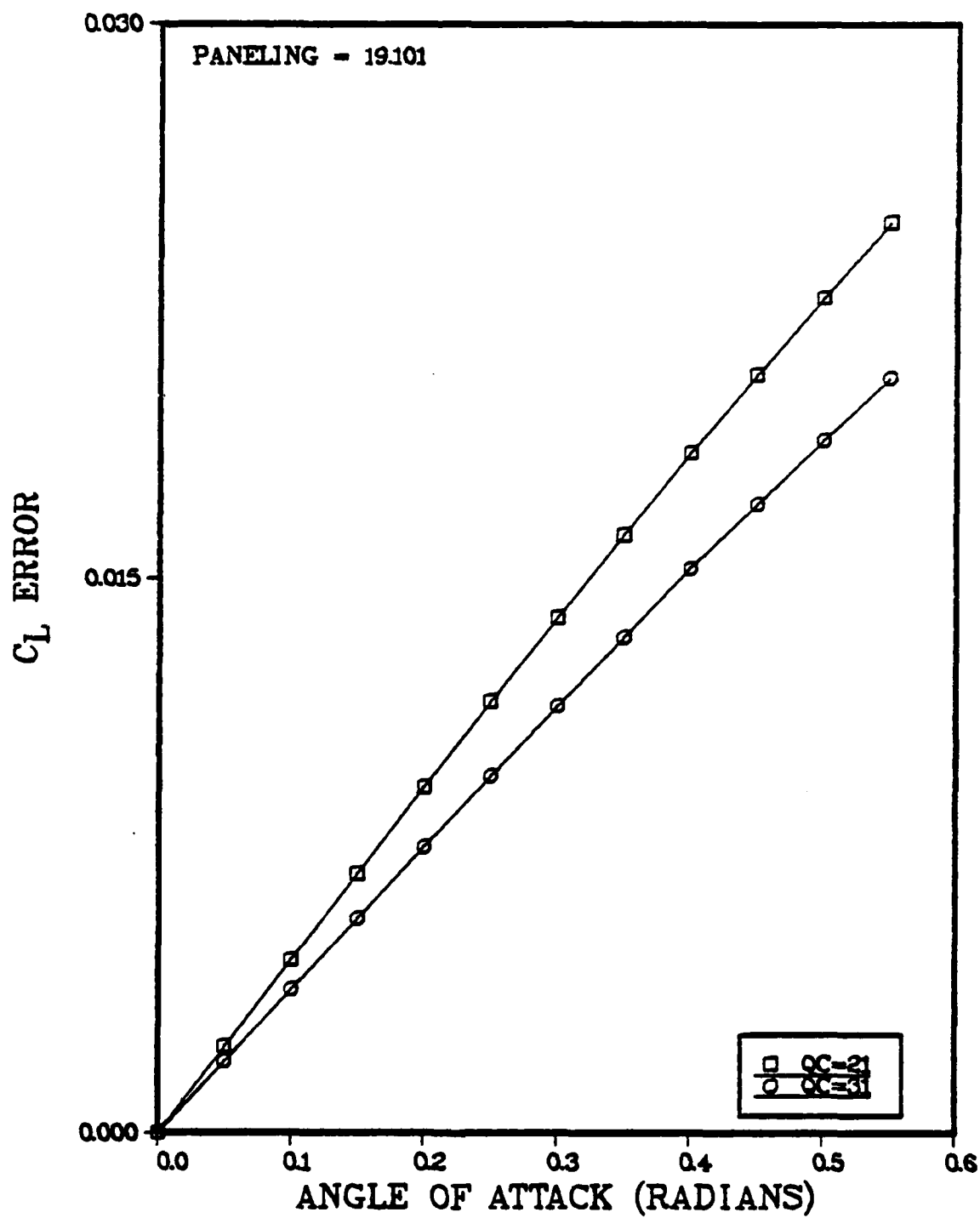


Figure 56. Effect of Angle of Attack on Lift Coefficient Error for a Karman-Trefftz Airfoil.

four cases can be considered:

1. the location and slope are computed, as in the basic method, using circular arc panels.
2. the location is exact but the slope is computed from the circular arc.
3. the location is computed from the circular arc panels but the slope is exact, and
4. both the location and the slope are exact.

For the two term model, in which there is one control point per panel, the third panel defining point is used as the control point in cases two and four. For the three term model, where two control points are required on a panel instead of one, this approach cannot be used; so for the three term model only cases one and three have been studied.

Figures 57a-e and 58a-e show tangential velocity error results for the four cases as a function of several parameters. Figures 57a and 57b are results for a nine element airfoil at  $\alpha = 0$  for  $QC=21$  and  $QC=31$ . While these figures do not give a clear indication of which combinations of slope and control point parameters are superior, they do show that contrary to what might be expected, the use of the exact slope and control point location is clearly not the best. Results for  $\alpha = .1$  radians shown in Figures 57c-e are similar. However, results for a ten element airfoil, given in Figs 58a-e, show that

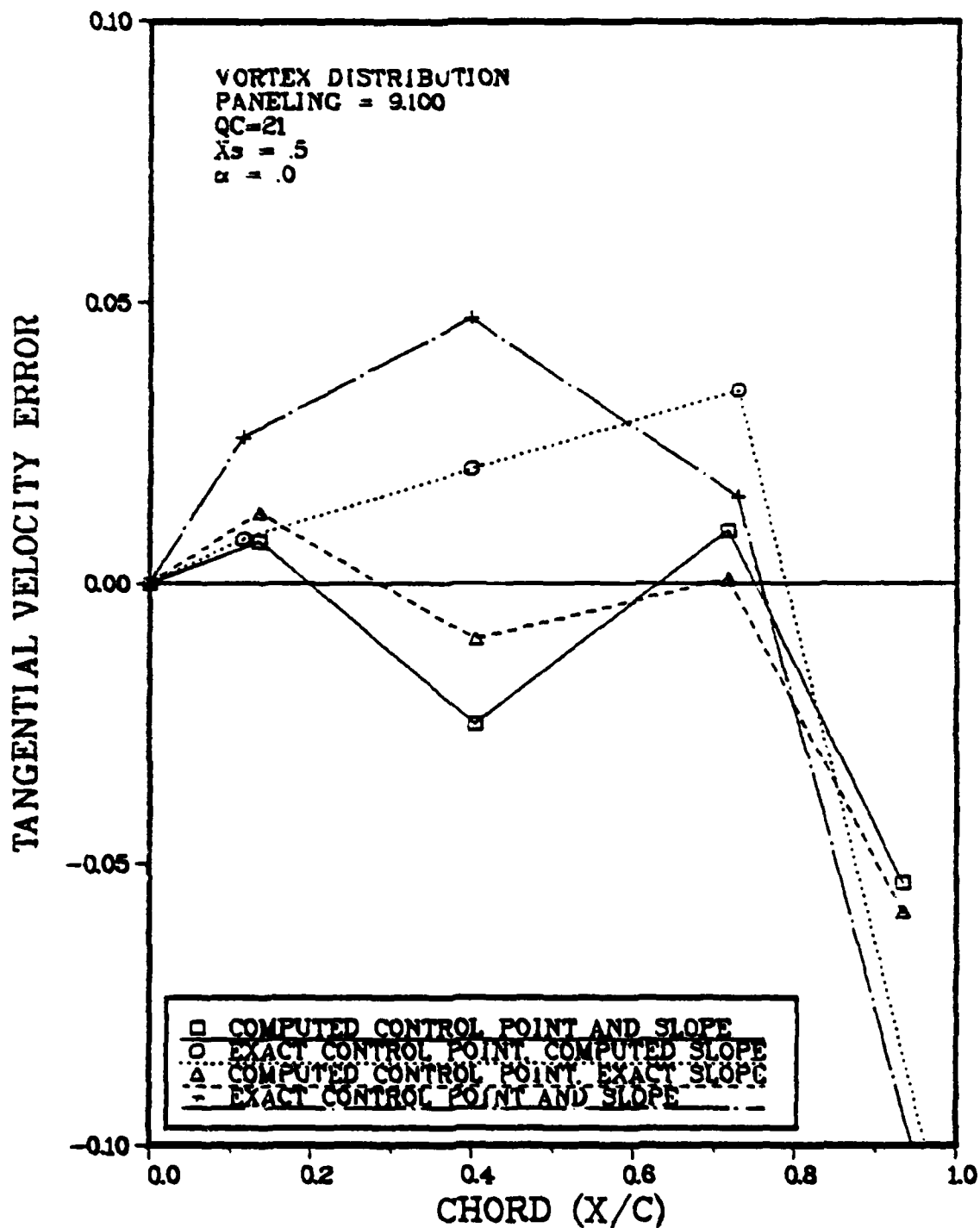


Figure 57a. Effect of Control Point Location and Slope on Tangential Velocity Error for a Karman-Trefftz Airfoil,  $N=9$ ,  $QC=21$ ,  $\alpha=.0$  radians.

AD-A124 896

COMPUTATION OF INCOMPRESSIBLE POTENTIAL FLOW OVER AN  
AIRFOIL USING A HIGH- (U) AIR FORCE INST OF TECH  
WRIGHT-PATTERSON AFB OH SCHOOL OF ENGI. J DEJONGH  
AUG 82 AFIT/DS/AA/82-1 F/G 12/1

3/3

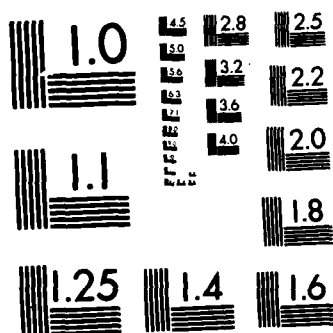
UNCLASSIFIED

NL

|  |  |  |  |  |  |  |  |  |  |  |  |  |  |
|--|--|--|--|--|--|--|--|--|--|--|--|--|--|
|  |  |  |  |  |  |  |  |  |  |  |  |  |  |
|  |  |  |  |  |  |  |  |  |  |  |  |  |  |
|  |  |  |  |  |  |  |  |  |  |  |  |  |  |
|  |  |  |  |  |  |  |  |  |  |  |  |  |  |
|  |  |  |  |  |  |  |  |  |  |  |  |  |  |

END

FILED  
11  
DTIC



MICROCOPY RESOLUTION TEST CHART  
NATIONAL BUREAU OF STANDARDS-1963-A

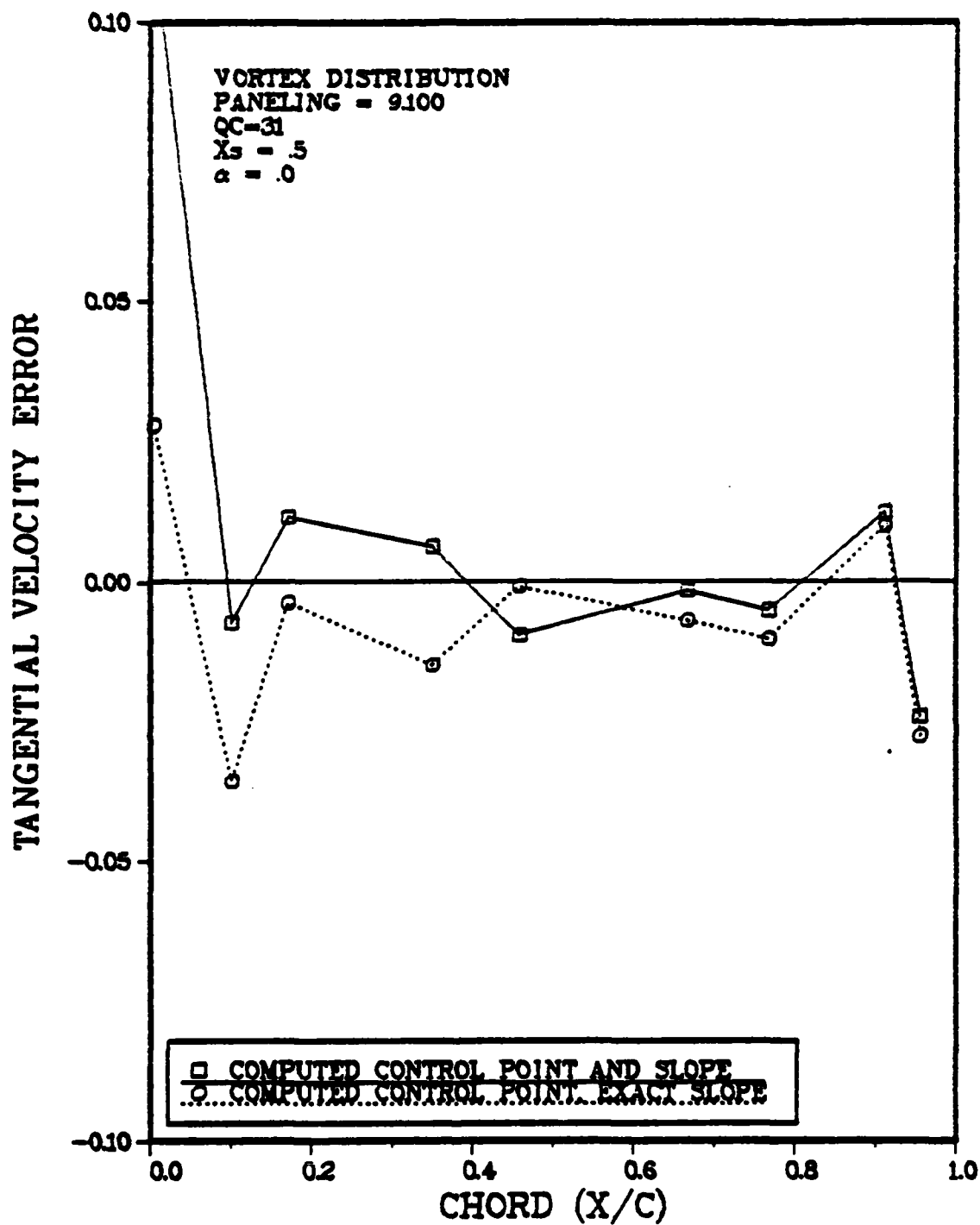


Figure 57b. Effect of Control Point Location and Slope on Tangential Velocity Error for a Karman-Trefftz Airfoil,  $N=9$ ,  $QC=31$ ,  $\alpha=.0$  radians.

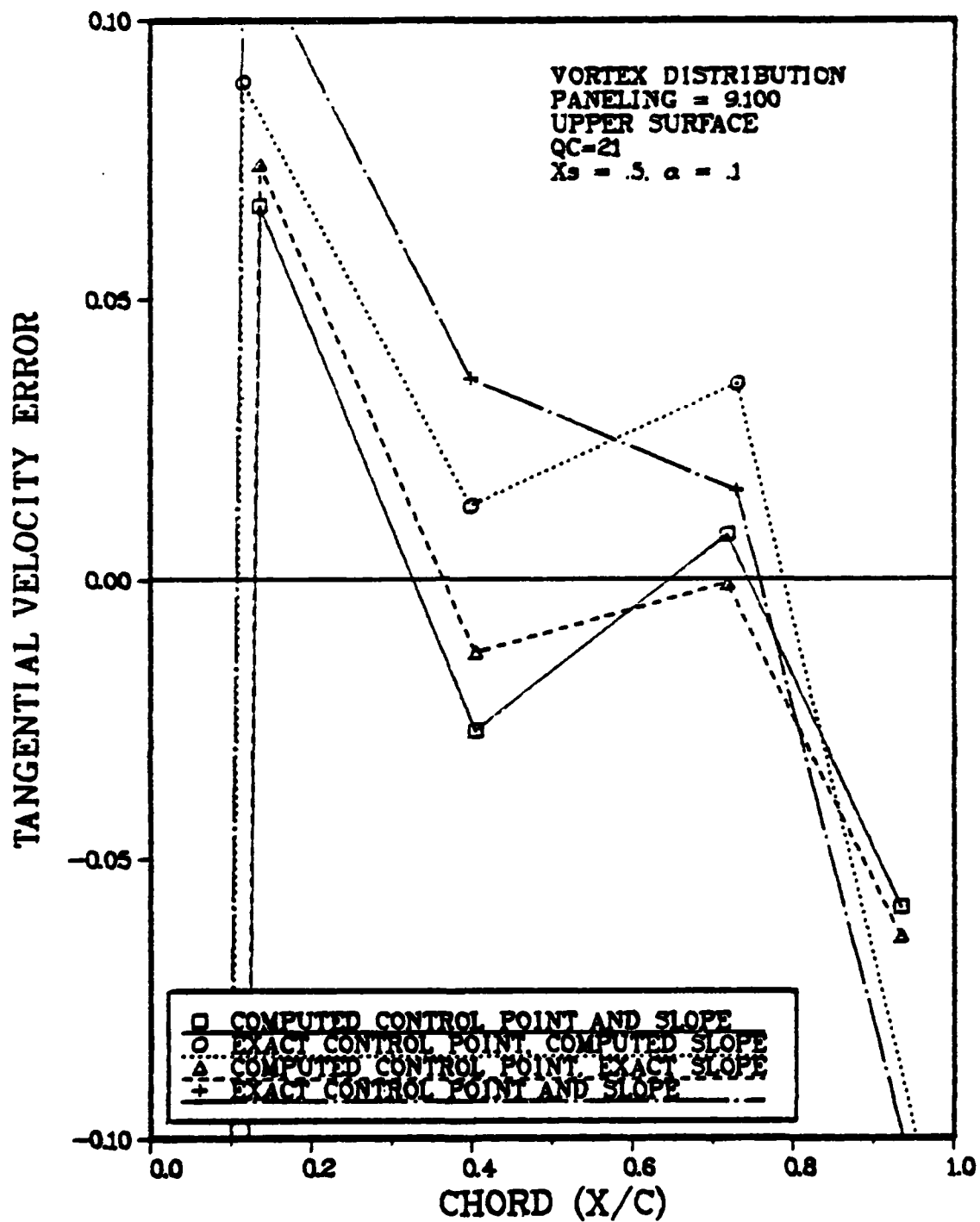


Figure 57c. Effect of Control Point Location and Slope on Tangential Velocity Error for a Karman-Trefftz Airfoil,  $N=9$ ,  $QC=21$ ,  $\alpha=.1$  radians, Upper Surface.



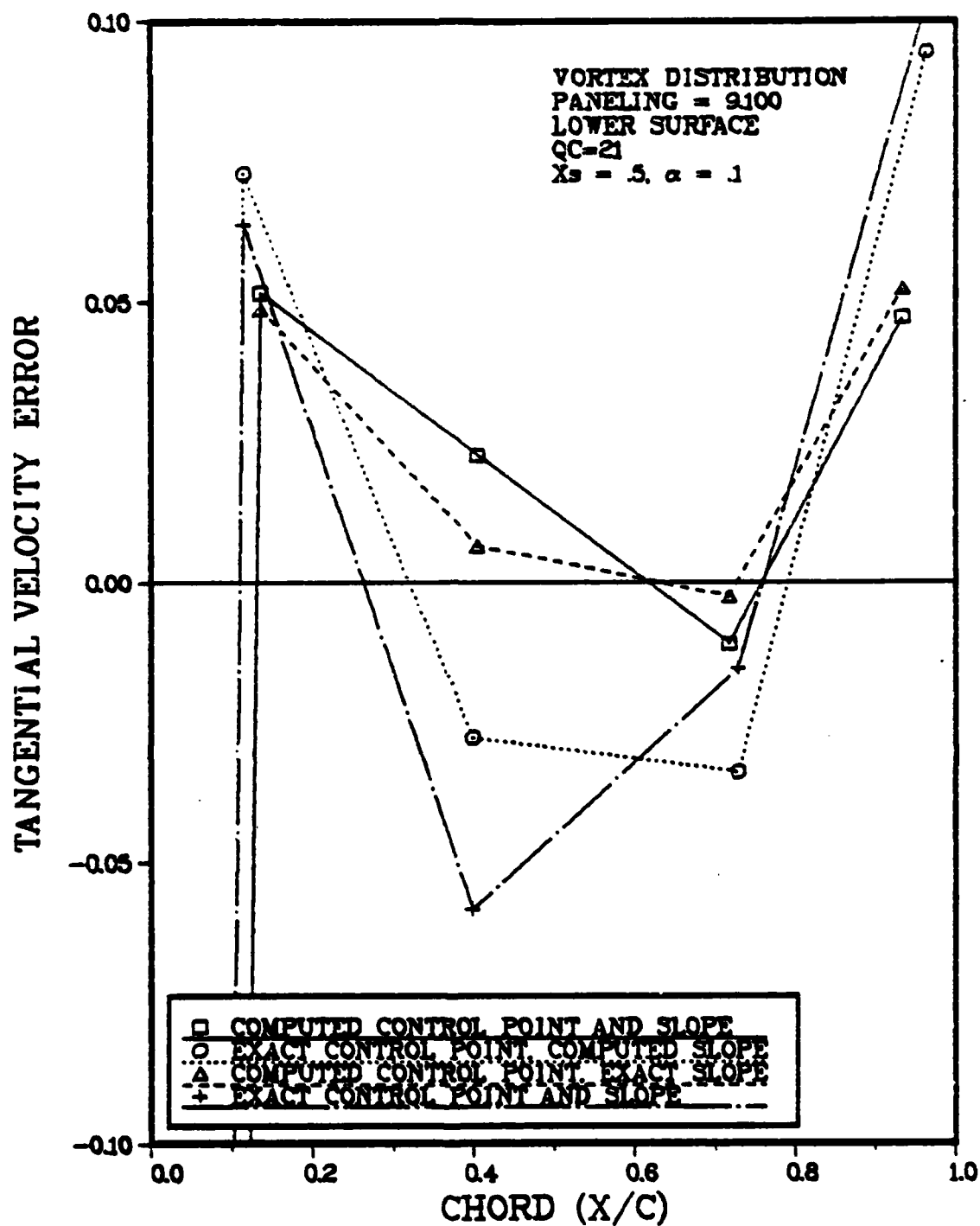


Figure 57d. Effect of Control Point Location and Slope on Tangential Velocity Error for a Karman-Trefftz Airfoil,  $N=9$ ,  $QC=21$ ,  $\alpha=.1$  radians, Lower Surface.

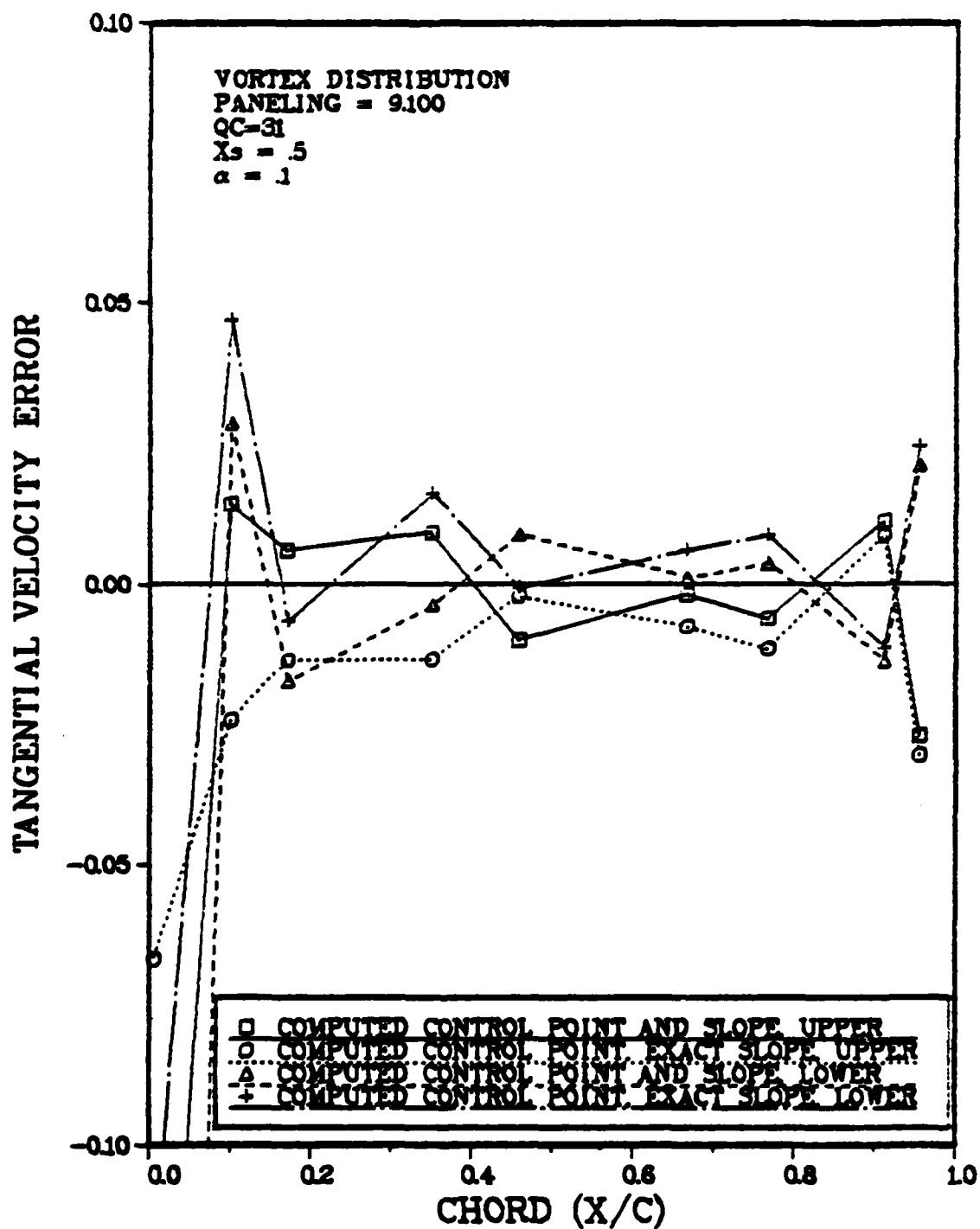


Figure 57e. Effect of Control Point Location and Slope on Tangential Velocity Error for a Karman-Trefftz Airfoil,  $N=9$ ,  $QC=31$ ,  $\alpha=.1$  radians.

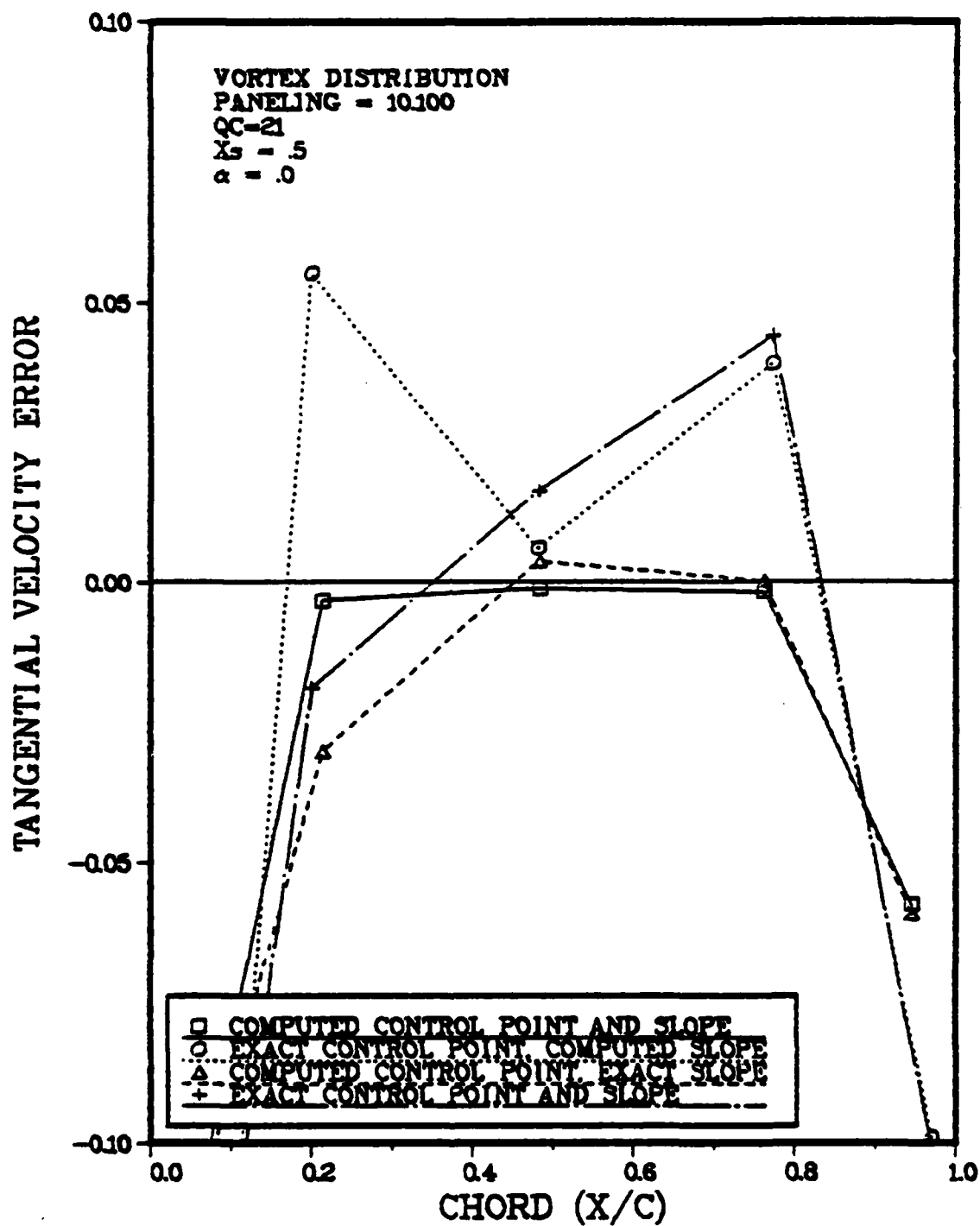


Figure 58a. Effect of Control Point Location and Slope on Tangential Velocity Error for a Karman-Trefftz Airfoil,  $N=10$ ,  $QC=21$ ,  $\alpha=.0$  radians.

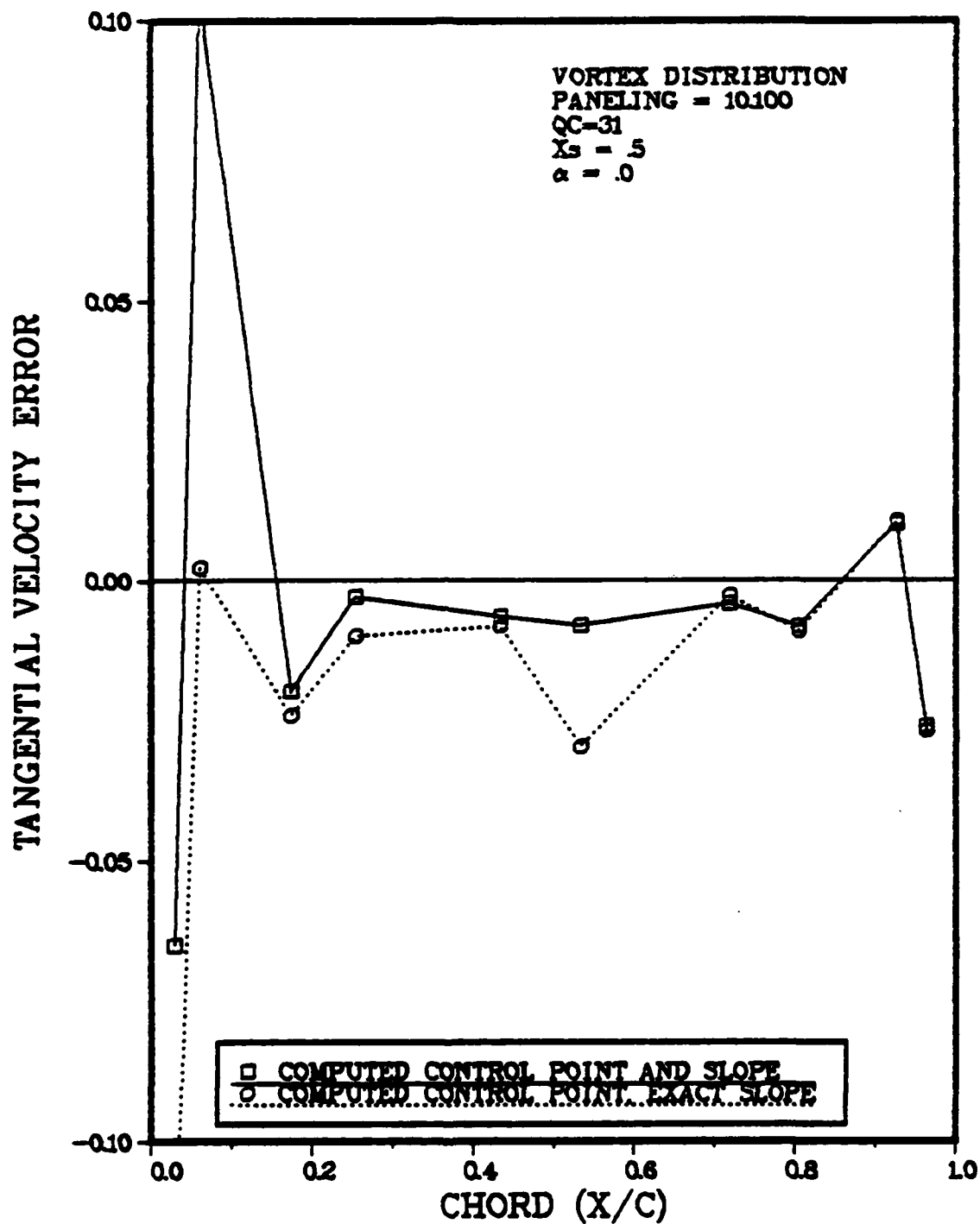


Figure 58b. Effect of Control Point Location and Slope on Tangential Velocity Error for a Karman-Trefftz Airfoil,  $N=10$ ,  $QC=31$ ,  $\alpha=.0$  radians.

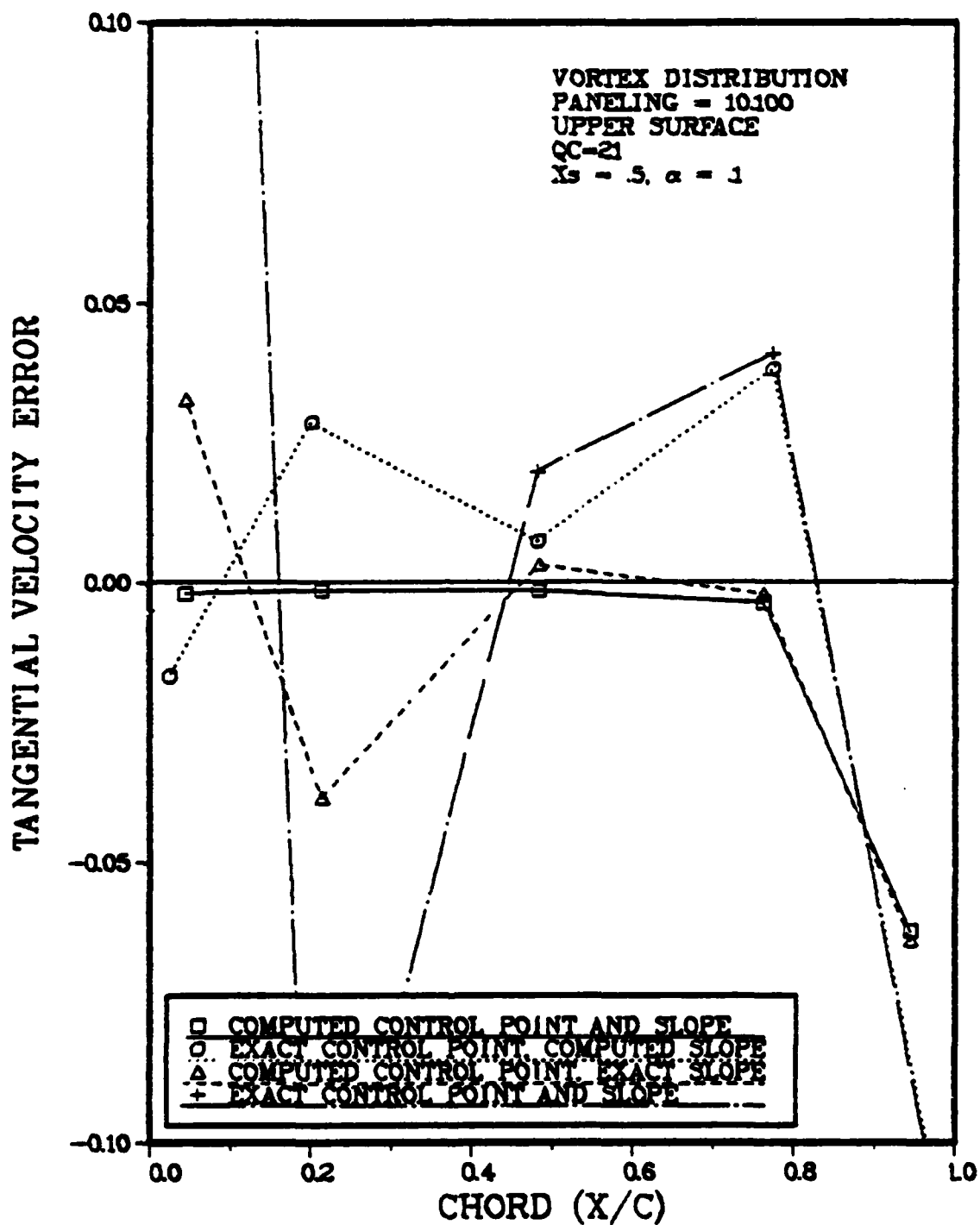


Figure 58c. Effect of Control Point Location and Slope on Tangential Velocity Error for a Karman-Trefftz Airfoil,  $N=10$ ,  $QC=21$ ,  $\alpha=.1$  radians, Upper Surface.

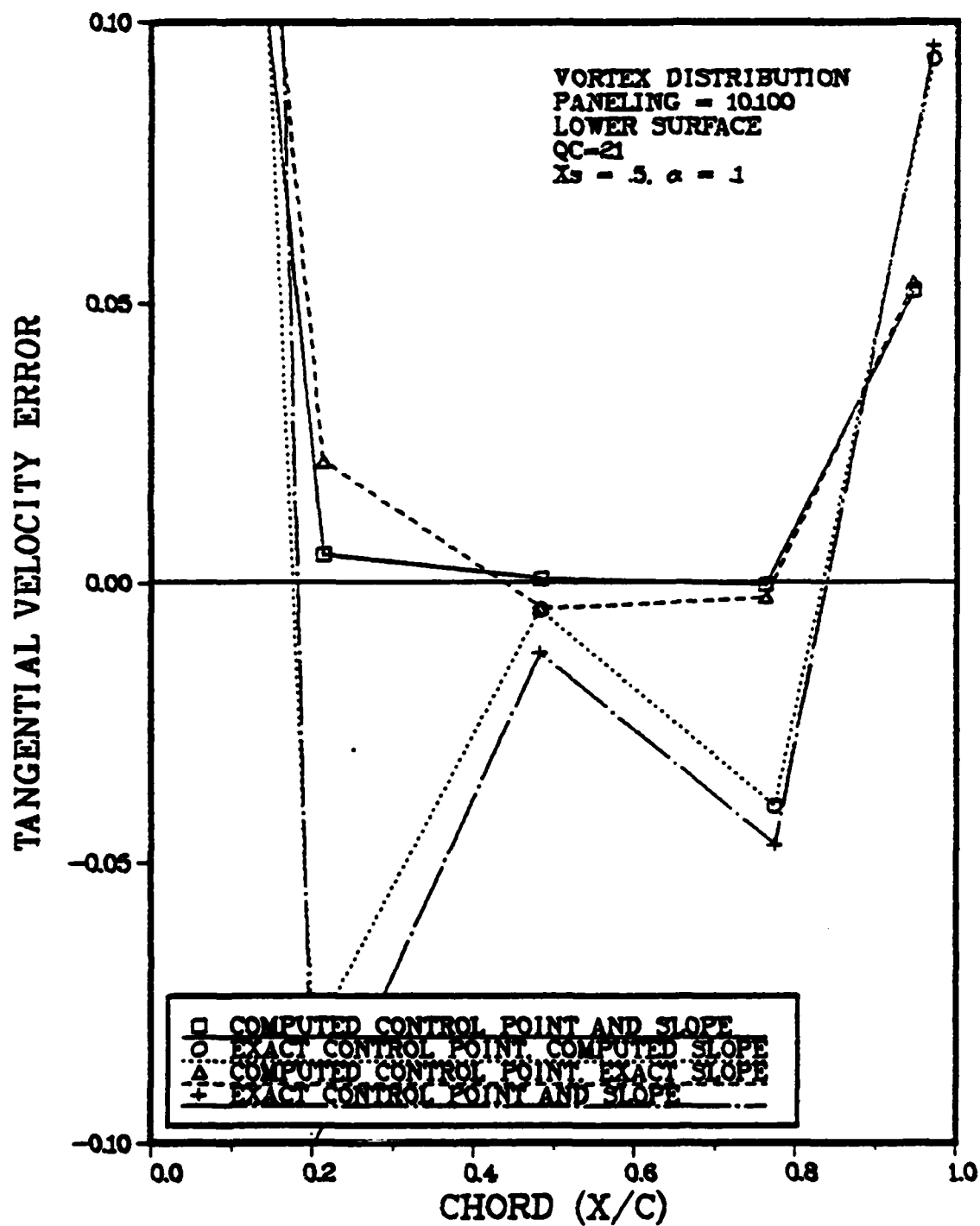


Figure 58d. Effect of Control Point Location and Slope on Tangential Velocity Error for a Karman-Trefftz Airfoil,  $N=10, QC=21, \alpha=.1$  radians, Lower Surface.

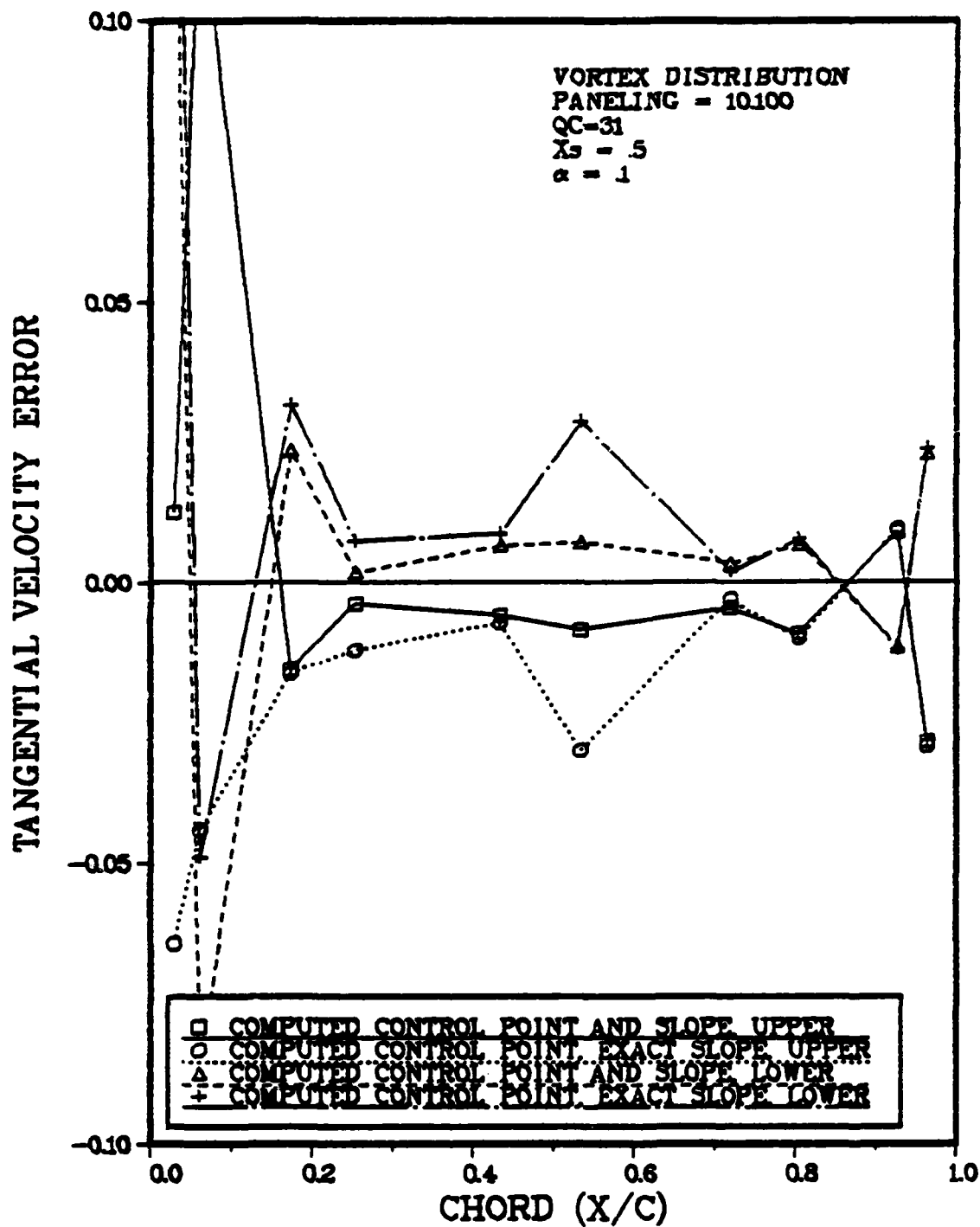


Figure 58e. Effect of Control Point Location and Slope on Tangential Velocity Error for a Karman-Trefftz Airfoil,  $N=10$ ,  $QC=31$ ,  $\alpha=.1$  radians.

the error using the basic method is generally small and relatively constant over the center part of the airfoil, while the other cases give somewhat larger errors which also tend to vary more dramatically. As before, the use of the exact slope and control point location clearly does not lead to the best solution.

It is instructive to look at the slope percentage error that results from using a computed control point. Figure 59 shows the slope error for a 19 element and a 45 element airfoil with  $QC=21$  and  $QC=31$ , using a computed control point (i.e. the basic method). Note that the slope error is constant and small over most of the airfoil for both element numbers and for both values of  $Q$ . It is also clear that increased panel density in the nose region significantly reduces the slope error there. Since the errors on one or two panels near the leading edge are relatively large compared to the rest of the airfoil, one might suppose that these errors account in part for the relatively larger errors in tangential velocity that have been noted in the nose region. This could not be the only cause of these errors, though, since larger errors are encountered in the trailing edge region as well, yet the slope errors in this region are very small.

This study has shown that, contrary to what might be expected, use of exact control point location and slope information in the present method does not lead to improved



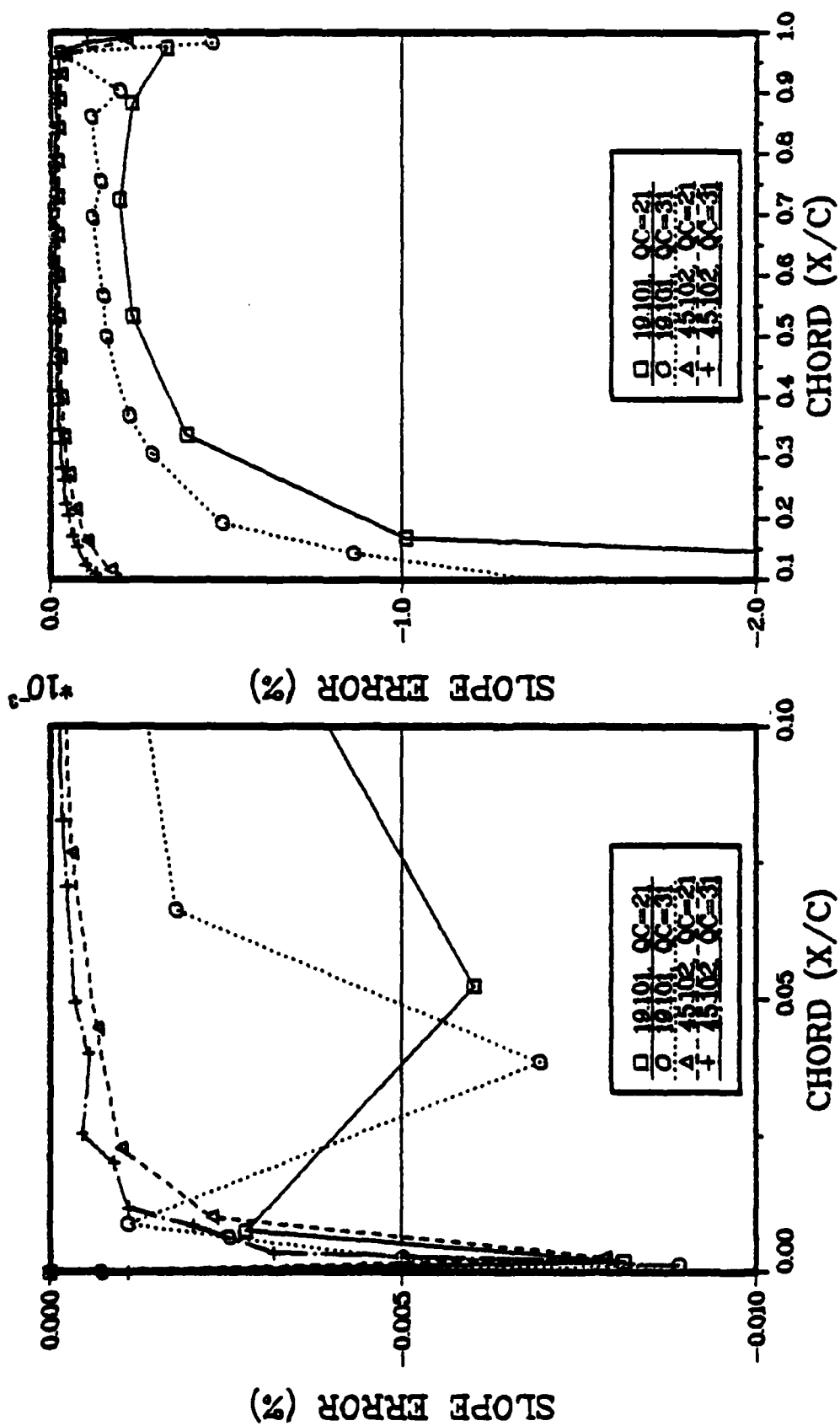


Figure 59 Error in Surface Slope at Computed Control Points for a Karman-Trefftz Airfoil.

accuracy in the solution. Since the representation of the surface geometry in terms of slope error was seen to be very good, other sources of error in the method probably drive the error in the solution. The most likely sources of error are the discrete application of the boundary conditions, and the series approximation to the singularity distribution. Thus the additional input data which would be required to use exact slope and control point location is not justified, and the use of computed slope and location information is completely adequate to represent the surface geometry, at least as far as the present method is concerned.

Effect of Camber. The airfoils which have been studied up to this point have been symmetric. Now, the present method will be applied to a slightly cambered Karman-Trefftz airfoil which has a camber parameter of  $3\pi/4$ , a trailing edge angle of 0.2356 radians, and a zero lift angle of attack of -.0275 radians. The airfoil was paneled with 45 elements equally spaced in the circle plane, which produces a slightly asymmetric paneling (designated as P=45.201) in the airfoil plane. The basic method was used with  $X_s=.01$  and  $\beta=1$ . Results for the QC=21 case at angles of attack 0.0 and 0.1 radians are shown in Figures 60a and 60b. Both upper and lower surfaces are plotted since the paneling is not symmetric. Figures 60c and 60d show similar results for the QC=31 cases. These curves exhibit characteristics similar to those noted earlier for

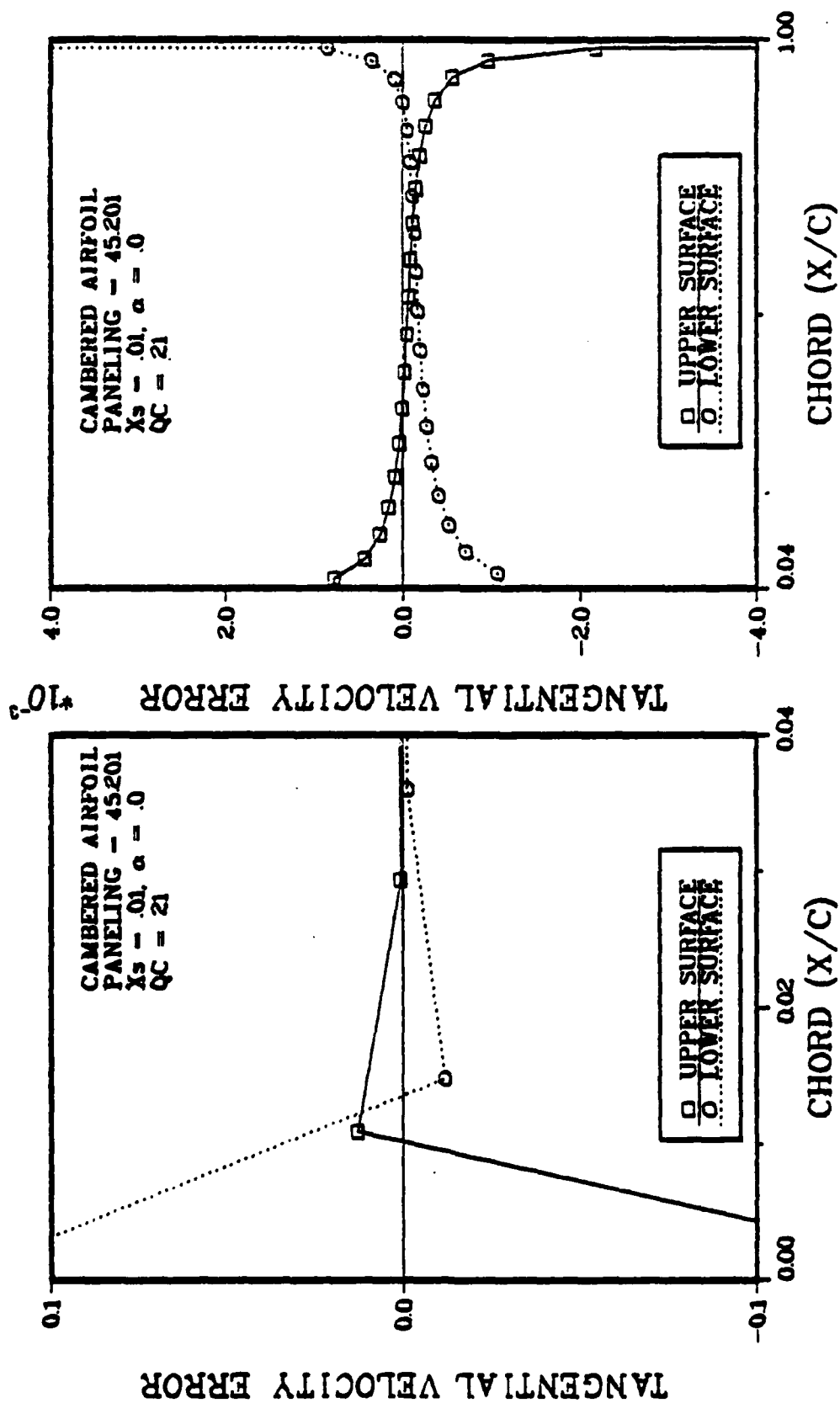


Figure 60a. Tangential Velocity Error for a Cambered Karman-Trefftz Airfoil,  $QC=21$ ,  $\alpha=.0$  radians.

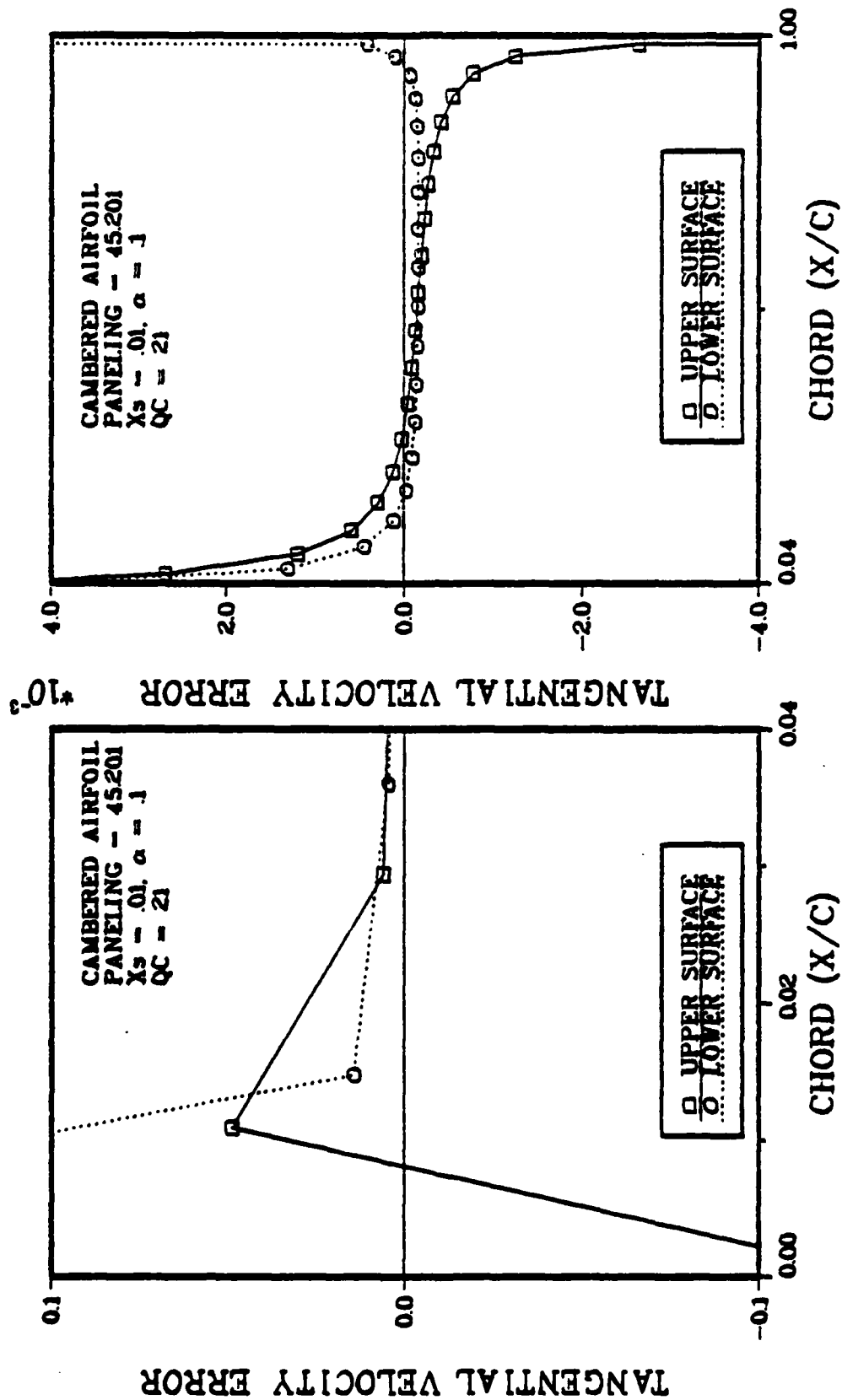


Figure 60b. Tangential Velocity Error for a Cambered Karman-Trefftz Airfoil,  $QC=21$ ,  $\alpha=.1$  radians.

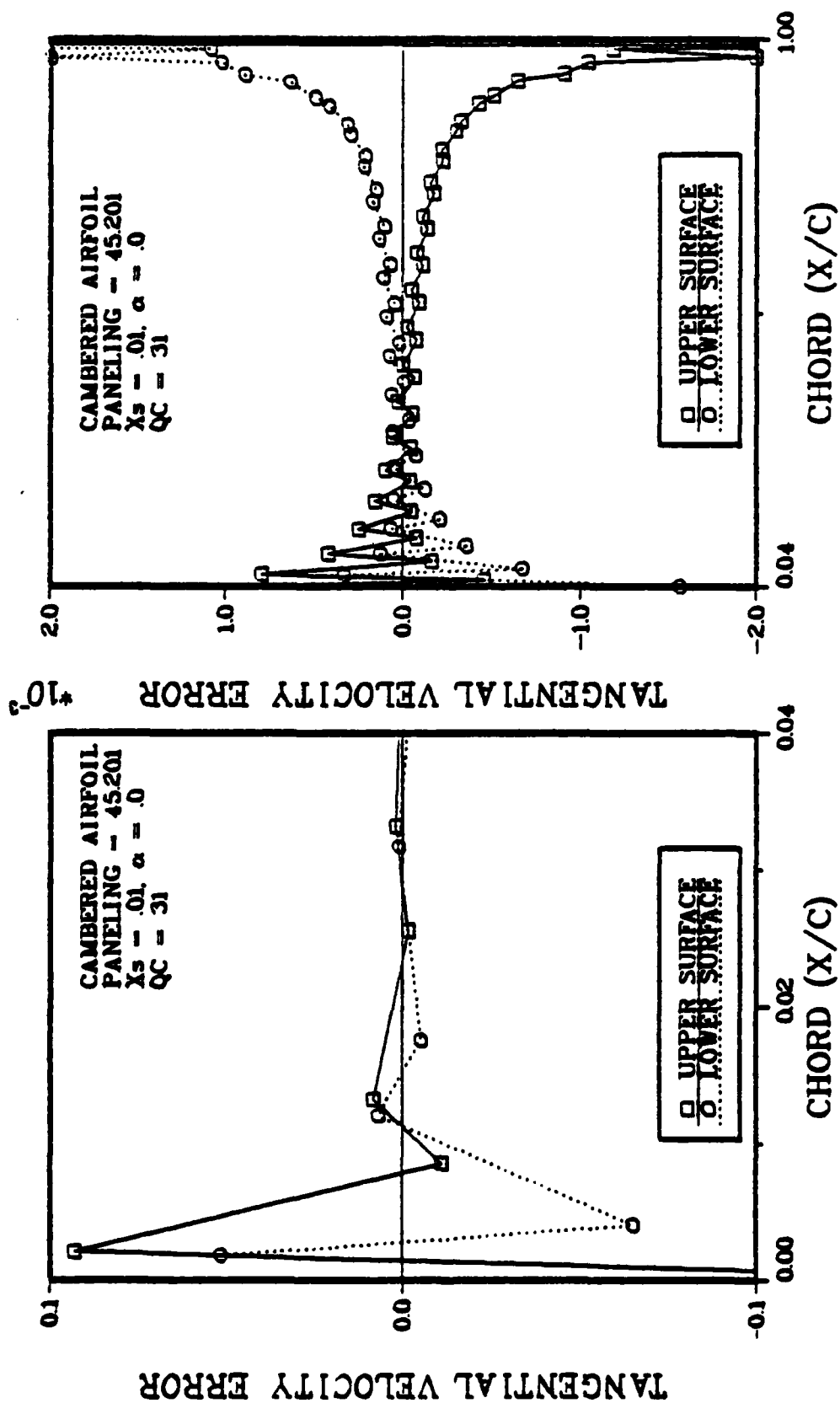


Figure 60c. Tangential Velocity Error for a Cambered Karman-Trefftz Airfoil,  $QC=31, \alpha=.0$  radians.

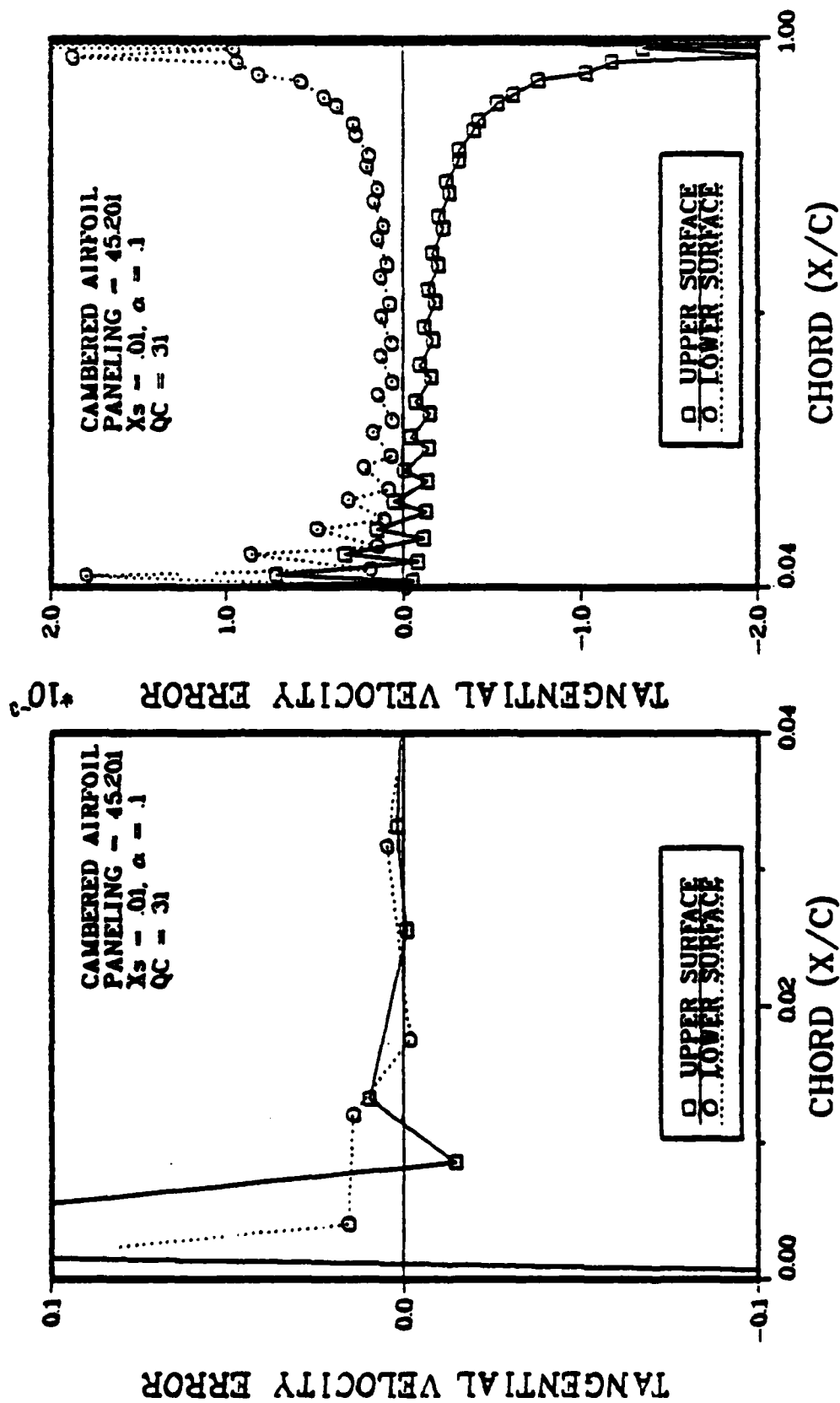


Figure 60d. Tangential Velocity Error for a Cambered Karman-Trefftz Airfoil,  $QC=31$ ,  $\alpha=.1$  radians.

the symmetric airfoil. These velocity errors near the nose do appear to be larger, but this may be due in part to the fact that the point source was placed very near the nose, and also to the fact that the stagnation point at the nose is not near the control point of the nose panel. For the symmetric airfoil cases with a similar paneling the nose panel control point was located at the stagnation point, so that the correct solution was obtained at that point.

### Summary

In this chapter the method of circular arc panels was applied to several different types of airfoils, and the characteristics which define the method were varied systematically to determine their effect on solution accuracy. The method was first applied to a Joukowski airfoil, an NACA 0024 airfoil, a thin symmetric airfoil, and a Karman-Trefftz airfoil using different combinations of singularity type and varying the number of terms in the series and the degree of continuity imposed. These preliminary studies showed that accurate results were consistently obtained for different types of airfoils and for lifting and non-lifting cases by using the following approach (which can be compared with the characteristics shown in Table I): a 2 or 3 term (linear or quadratic) vortex distribution is placed on each panel, and continuity of the distribution is enforced at panel junctures. The

panels are piecewise continuous circular arc elements generated from the surface geometry with no series expansion approximations. The boundary condition imposed at control point is zero external normal velocity. The Kutta condition is met by specifying zero vorticity at the trailing edge on both upper and lower surfaces, and an internal point source is added to close the formulation. All integrations are performed analytically for maximum computational efficiency. This basic method was then exercised on both symmetric and cambered Karman-Trefftz airfoils at different angles of attack to determine the effects of  $N$ ,  $Q$ , panel geometry, point source location, panel curvature, and control point characteristics on the accuracy of the method. The following conclusions can be drawn:

1. Increasing  $N$  and/or  $Q$  produces more accurate results.
2. The method is somewhat sensitive to paneling geometric characteristics (panel subtended angle, panel radius, and panel arc length), but the effect is local.
3. The effect of the internal point source can be relatively large, but it is very localized and can be controlled by using additional control points in the vicinity of the source.
4. The accuracy of the solution generally increases as the curvature of the panels is varied from nearly flat to the circular arc model.



5. The effect of exact representation of control point location and slope does not lead to more accurate solutions compared to results based on the computation of the location and slope from the circular arc model.

6. The method produces good results over a range of angles of attack, although the accuracy decreases linearly as angle of attack increases.

The next chapter will summarize the development of the present method, draw conclusions concerning the application of the method to the circular cylinder and to airfoils, and present suggestions for future work in this area.

## VI. Conclusions and Recommendations

### Conclusions

The purpose of this effort was to develop a better understanding of the effects of the several characteristics involved in a panel method solution, and to provide guidance and understanding for the further development of two and three dimensional panel methods. To reach this goal, a new panel method, based on the fundamental concepts of potential theory and on a simple approach to curve approximation, has been developed. This method used a new approximating element, the circular arc; and a new singularity representation, the sine series.

The method was initially applied to the problem of flow over a circular cylinder and the effects of varying several parameters were studied. This effort showed that the current method was capable of accurate results (which were noted earlier), and it allowed an assessment of the effects of the many characteristics which impact a solution. This assessment was used to develop the method further.

Based on these studies of the circular cylinder the method was applied to a Joukowski airfoil, an NACA 0024 airfoil, a thin symmetric airfoil and a Karman-Trefftz airfoil. Initial studies were performed to assess the

applicability of the method to airfoil shapes as a function of singularity type, number of terms in the series (Q), degree of continuity (C), type of boundary condition, and Kutta condition formulation. Source and vortex distributions were used, while values of Q varied from 1 to 3 and values of C varied from 0 to 2. For the vortex cases 3 types of Kutta condition were investigated: an error parameter approach with a trailing edge bisector condition, an internal point source with a trailing edge bisector condition, and an internal point source with a specification of zero vorticity at the trailing edge. These studies indicated that the method was not sensitive to the type of Kutta condition used. Also not all combinations of Q and C yielded acceptable solutions, depending on the type of singularity which was used.

As a result of these preliminary studies a basic method was chosen for further investigation. This method used a continuous 2 or 3 term vorticity distribution with a normal velocity boundary condition, and an internal point source with zero vorticity at the trailing edge to satisfy the Kutta condition. This basic method was then applied to a symmetric Karman-Trefftz airfoil and detailed studies were conducted to determine the effects of number of panels (N), number of terms, point source location, geometric paneling characteristics, panel curvature, angle of attack, control

point location and slope, and airfoil camber. Conclusions which can be drawn from this study are:

1. The method produces very accurate solutions over the major part of the airfoil, with the largest errors occurring at the leading and trailing edges (i.e. the stagnation point). These errors are, however, always small compared to the free stream and are small compared to the exact solution except at points next to the stagnation points.

2. Significant error reduction occurs as  $N$  is increased, and reasonable, though not as large a reduction, occurs as  $Q$  is increased from 2 to 3.

3. The effect of point source location is large but is very local. It was found that these source induced errors can be effectively controlled by either a 3 term series, or by placing additional control points near the source.

4. The method is generally insensitive to minor variations in paneling as long as the geometric parameters governing the paneling: That is, panel curvature and panel subtended angle, vary in a smooth manner around the airfoil. Additionally, the requirement that adjacent panels maintain a 3:2 or less ratio in arc length was found to be effective in reducing errors, particularly at the trailing edge.

5. The effect of panel curvature is that accuracy increases as the curvature increases from that of a nearly

flat panel to that of a circular arc panel with three points on the circular arc coincident with the airfoil surface for both the 2 and 3 term series expansions.

6. The accuracy of the solution decreases slightly as the angle of attack increases.

7. It was found that improved accuracy is not generally obtained when either exact control point location or slope information is used as opposed to when these quantities are computed from the circular arc panel. Since one might expect that the additional exact information would improve the solution, the fact that it does not indicates that other errors inherent in the formulation, such as the singularity formulation and the discretization process itself, may be the primary causes of error.

8. The method provides accurate results for a non-symmetric airfoil, although the accuracy is not quite as good as for the symmetric case.

#### Recommendations

Several areas for further work have become apparent during the course of this research. These include improving the method as a two dimensional tool and extending the method to the three dimensional case. In terms of improvement of the two dimensional method, further study to improve the solution at the leading and trailing edges could

be undertaken. A possible approach to doing this would be to modify the singularity distribution on one or several panels at the leading or trailing edges. The rationale for this approach is that the gradients in singularity strength are largest in these regions, and it is possible that the same series representation of the singularity can not adequately model these gradients. For example, one might use, at the trailing edges, a singularity strength which is proportional to the square root of the arc length measured from the trailing edge because this singularity will go to zero at the trailing edge more quickly than will a linear function. A disadvantage, however, to using more complicated representations of the singularity is that numerical integration might be required to obtain the influence coefficients for the panels involved.

Another approach to quickly improving solution accuracy is based on the observation that the tangential velocity errors near the leading and trailing edges do not vary smoothly. This is true over a larger portion of the airfoil for the 3 term series expansion cases as well. As a way of smoothing these curves and reducing the overall error in the solution a new velocity curve could be fitted to the calculated results using a least squares procedure, or some type of averaging procedure. A systematic study of a particular algorithm for doing this would be required to establish the validity of this approach for the case of a

general airfoil.

A third area for additional study is related to the initial results presented in Chapter V. Further investigation of the failure of certain parameter combinations to yield solutions is required to fully understand the proper way of to numerically solve the integral equations of potential flow using the panel method approach. This should include further study of the application of the Kutta condition, particularly in the case in which a solution was obtained using the internal velocity boundary condition.

The method could also be extended to three dimensions. For example, consider the case of a finite wing. Paneling in the spanwise direction would have to be developed. A scheme using flat panels spanwise, or one using curved panels whose radii varied in the spanwise direction could be investigated. Another alternative would be a complete numerical integration in the spanwise direction coupled with analytic intergration chordwise. If circular arc panels were developed spanwise, the resulting integrations to obtain the influence coefficients would probably have to be performed numerically since the resulting equations are elliptic. Another approach would be to use circular arc panels only at the leading edge or at the wing tips since these are the regions where wing surfaces typically exhibit

the largest curvatures.

An additional extension of the two dimensional method which would have application in three dimensional cases as well would be to develop a procedure for computing forces and moments on the airfoil or wing using computed velocities and the surface paneling. This is an area where the details of the surface model could play an important role, and an assessment of the effect of the circular arc panel model on these quantities would be a worthwhile result.



### Bibliography

1. Shapiro, A.H. The Dynamics and Thermodynamics of Compressible Fluid Flow, Vol I, John Wiley and Sons, New York, 1953.
2. Magnus, A.J., Epton, M.A., et al. "PAN AIR - A Computer Program for the Prediction of Subsonic or Supersonic Flow about Arbitrary Configurations, Volume 1-PAN AIR Theory", May, 1980.
3. Theodorsen, Theodore. Theory of Wing Sections of Arbitrary Shape, NACA Report No. 411, 1931.
4. Catherall, D., Foster D.N., and Sells, C.C.L. Two Dimensional Incompressible Flow Past a Lifting Airfoil, RAE-TR-69118, June 1969.
5. Murman, E.M. and Cole, J.D. "Calculation of Plane, Steady Transonic Flows", AIAA Journal, Vol.9, Jan 1971.
6. Bailey, F.R. and Ballhaus, W.F. "Comparison of Computed and Experimental Pressures for Transonic Flows About Isolated Wings and Wing-Fuselage Combination", Aerodynamic Analysis Requiring Advanced Computers Part II., NASA SP-347, 1975.
7. Caughey, D.A. and Jameson, A. "Numerical Calculation of Transonic Potential Flow About Wing-Body Combinations", AIAA Journal, Vol.17, No.2, Feb.1979.
8. Boppe, C.W. "Computational Transonic Flow About Realistic Aircraft Configurations", AIAA paper No.78-104, 1978.
9. Shen, S.F. "An Aerodynamicist Looks at the Finite Element Method", Finite Elements in Fluids Vol.2, John Wiley, N.Y., 1975.
10. Habashi, W.G. "A Study of the Finite Element Method for Aerodynamic Applications", PhD thesis Cornell University, 1975.

11. Marsh, J.E. "Prediction of Aerodynamic Forces on a Circular Cylinder and a Thin Airfoil in a Transonic Airstream by the Finite Element Method", Ph.D. thesis Air Force Institute of Technology, 1979.
12. Hess, J.L. "Review of Integral Equation Techniques for Solving Potential-Flow Problems with Emphasis on the Surface Source Method," Computer Methods in Applied Mechanics and Engineering Vol.5, 1975.
13. Lamb, H. Hydrodynamics, Dover Pub, N.Y., 1945.
14. Kellogg, O.D. Foundations of Potential Theory, Dover Pub., N.Y., 1953.
15. Hess, J.L. "Higher Order Numerical Solution of the Integral Equation for the Two-Dimensional Neumann Problem", Computer Methods in Applied Mechanics and Engineering Vol.2, 1973, p.1-15.
16. ----- "The Use of Higher-Order Surface Singularity Distributions to Obtain Improved Potential Flow Solutions for Two Dimensional Lifting Airfoils", Computer Methods in Applied Mechanics and Engineering Vol.5, 1975, p.11-35.
17. ----- Improved Solution for Potential Flow About Arbitrary Axisymmetric Bodies by the Use of a Higher-Order Surface Source Method", Computer Methods in Applied Mechanics and Engineering, Vol.5, 1975, p.297-308.
18. ----- and Smith, A.M.O. "Calculation of Potential Flow About Arbitrary Bodies", Progress in Aeronautical Sciences Vol.8, Pergammon Press, N.Y., 1966.
19. Henshaw, D.H. Two Dimensional Airfoil Analysis Using a Refined Finite Element Technique, LTR-LA-124, National Research Council Canada, May 1973.
20. ----- Application of Higher Order Surface Elements to the Solution of the Laplace Equation for the Example of a Conventional Airfoil, LTR-LA-127, National Research Council Canada, June 1973.
21. ----- Application of Higher Order Surface Elements to the Solution of the Laplace Equation for the Example of a Karman-Trefftz Venticular Airfoil, LTR-LA-129, National Research Council Canada, July 1973.

22. ----- A Testing of a Technique of Higher Order Boundary Elements for the Case of Two-Dimensional, Incompressible Potential Flow About a Thin Highly Cambered Body. LTR-LA-136, National Research Council Canada, Jan. 1974.
23. Henshaw, D.H. Consistent Formulations of the Integral Equations for the Two-Dimensional Neumann Problem, LTR-LA-141, National Research Council Canada, March 1974.
24. ----- A Singularly Consistent Higher Order Numerical Solution of the Laplace Equation for an 8:1 Ellipse, LTR-LA-143, National Research Council Canada, December 1973.
25. ----- Singularly Consistent, Higher Order, Vorticity Integral Equations for the Two Dimensional Neuman Problem, LTR-LA-146, National Research Council Canada, Jan. 1974.
26. ----- Singularly Consistent Higher Order Integral Equations for the Numerical Two-Dimensional Neuman Problem, LTR-LA-147, National Research Council Canada, Jan. 1974.
27. ----- Unified Boundary Conditions for the Numerical Solution of the Integral Equations for the Neumann Problem, LTR-LA-149, National Research Council Canada, Feb. 1974.
28. ----- Singularly Consistent Higher-Order Integral Equations for the Two-Dimensional Neumann Problem, LTR-LA-150, National Research Council Canada, Feb. 1974.
29. Bristow, D.R. "A New Surface Singularity Method for Multi-Element Airfoil Analysis and Design", AIAA paper 76-20, Jan. 1976.
30. ----- Incompressible Potential Flow: Numerical Characteristics of Three Classical Surface Singularity Representations, Report No. MDCA4407, McDonnell Douglas Corp., Sept 1976.
31. ----- Recent Improvements in Surface Singularity Methods for the Flow Field Analysis About Two Dimensional Airfoils, Report No. MCAIR 77-004, McDonnell Douglas Corp., June 1977.

32. Raj, P. "A Method of Computing the Potential Flow on Thick Wing Tips", Ph.D. thesis Georgia Institute of Technology, October 1976.
33. Keller, C.L. Integral Equation Methods for Two Dimensional Incompressible Flows For Multi-element Airfoils, AFFDL-TR-77-27, WPAFB, Ohio, April 1977.
34. Hess, J.L. "The Problem of Three-Dimensional Lifting Potential Flow and its Solution by Means of Surface Singularity Distributions", Computer Methods in Applied Mechanics and Engineering, Vol.4, 1975, 283-319.
35. ----- Calculation of Arbitrary Potential Flow About Arbitrary Three-Dimensional Lifting Bodies, Report No. MDC J5679-01, McDonnell Douglas Corp. Oct. 1972 (AD 755480).
36. ----- Status of a Higher-Order Panel Method for Nonlifting Three-Dimensional Potential Flow, Report No. NADC-76118-30, Naval Air Development Center, Warminster, Pa., Aug. 1977.
37. Woodward, F.A. "Analysis and Design of Wing-Body Combinations at Subsonic and Supersonic Speeds", Journal of Aircraft Vol.5 No.6, Nov.-Dec. 1968.
38. ----- An Improved Method for the Aerodynamic Analysis of Wing-Body-Tail Configurations in Subsonic and Supersonic Flow Part I, NASA CR-2228, May 1973.
39. ----- "The Supersonic Triplet - A New Aerodynamic Panel Singularity with Directional Properties", AIAA paper 79-0273, Jan. 1979.
40. Roberts, A. The Neumann Wing, Report MA 8, British Aircraft Corp., Aug. 1967.
41. ----- and Rundle, K. Computation of Incompressible Flow about Bodies and Thick Wings Using the Spline Mode System, Report Aero MA 19, British Aircraft Corp, April 1972.
42. ----- The Computation of First Order Compressible Flow About Wing-Body Configurations, Report Aero MA 20, British Aircraft Corp., Feb. 1973.

43. Morino, L. A General Theory of Unsteady Compressible Potential Aerodynamics, NASA CR-2464, Dec. 1974.
44. ----- and Kuo, C.C. "Subsonic Potential Aerodynamics for Complex Configurations: A General Theory", AIAA Journal Vol.12, No.2, Feb. 1974.
45. Morino, L. Chen, L.T., and Sucin, E.O. "Steady and Oscillatory Subsonic and Supersonic Aerodynamics around Complex Configurations", AIAA Journal, Vol.13, No.3, March 1975.
46. Rubbert, P.E., Saaris, G.R., et al, A General Method for Determining the Aerodynamic Characteristics of Fan in Wing Configurations, USAA VLABS Technical Report 67-61A, U.S. Army Aviation Material Labs, Fort Eustis, Va., Dec. 1967.
47. Rubbert, P.E. and Saaris, G.R. "Review and Evaluation of a Three-Dimensional Lifting Potential Flow Analysis Method for Arbitrary Configurations", AIAA paper 72-188, Jan. 1972.
48. Johnson, F.T. and Rubbert, P.E. "Advanced Panel-Type Influence Coefficient Method Applied to Subsonic Flows", AIAA paper 75-50, Jan. 1975.
49. Ehlers, F.E., Johnson, F.T., and Rubbert, P.E., "A Higher Order Panel Method for Linearized Supersonic Flow", AIAA paper 76-381, July 1976.
50. Ehlers, F.E., Epton, M.A., Johnson F.T., Magnus, A.E., and Rubbert, P.E. "An Improved Higher Order Panel Method for Linearized Supersonic Flow", AIAA paper 78-15, Jan. 1978.
51. Ehlers, F.E., Epton, M.A., et al. "Improved Higher-Order Panel Method for Linearized Supersonic Flow", AIAA Journal Vol.17, No.3, March 1979.
52. ----- A Higher Order Panel Method for Linearized Supersonic Flow, NASA CR-3062, May 1979.
53. Cenko, A., Tinoco, E.N., Dyer, R.D., and De Jongh, J.E., "PANAIR-Applications to Weapons Carriage and Separation", AIAA paper 80-0187, Jan. 1980.

54. Thomas, J.L. and Miller, D.S., "Numerical Comparisons of Panel Methods at Subsonic and Supersonic Speeds", AIAA paper 79-0404, Jan 1979.
55. Landrum, E.J. and Miller, D.S., "Assessment of Analytical Methods for the Prediction of Supersonic Flow over Bodies", AIAA paper 80-71, Jan. 1980.
56. Karamcheti, K. Principles of Ideal-Fluid Aerodynamics, John Wiley, N.Y. 1966.
57. Hess, J., Johnson, F.T., and Rubbert, P.E. "Panel Methods", AIAA Panel Methods Workshop Notebook, 1978.
58. Craggs, J.W. and Maugler, K.W. "Some Remarks on the Behaviour of Surface Source Distributions Near the Edge of a Body", RAE Technical Report 71085, April 1971.
59. Tricomi, F. Integral Equations, Interscience Publishers, N.Y., 1957.
60. Mikhlin, S.G. Integral Equations (translated by A.H. Armstrong), Pergamon Press, N.Y., 1957.
61. Lee, D.A., "Integral Equations-Lecture Notes", Air Force Institute of Technology, WPAFB, Ohio, 1977.
62. Sternberg, W.J. and Smith, T.L. The Theory of Potential and Spherical Harmonies, University of Toronto Press, Toronto, 1946.
63. Mikhlin, S.G. Linear Integral Equations, Hindustan Publishing Corp., Delhi, 1960.
64. Pogorzelski, W. Integral Equations and Their Applications Vol. I, Pergamon Press, N.Y., 1966.
65. Martensen, E. "Calculation of the Pressure Distribution on Thick Grid Airfoils by Means of Fredholm's Integral Equations of the Second Kind", translated by K Bennett Howe from Mitteilungen Aus Dem Max-Planck-Institute fur Stromungsforschung und der Aerodynamischen versuchsanstalt, No.23, Gottingen, 1959.
66. Johnson, C.D. "The Approximation of Plane Curves by Circular-Arc-Based Elements", Ph.D. thesis, University of California, Berkeley, Dec. 1977.

67. International Mathematical and Statistical Library (IMSL) Reference Manual, Vol. I, June, 1980.
68. Abbott, I.H. and Von Doenhoff, A.E. Theory of Wing Sections, Dover Publications, N.Y., 1959.
69. Gradsteyn, I.S., and Ryzhik, I.M. Table of Integrals, Series, and Products, Academic Press, New York, 1965.
70. Selby, S. ed. Standard Mathematical Tables, CRC Press, Cleveland, 1973.

## Appendix A

### Continuity Coefficient Matrices

The matrix equations governing singularity strength continuity across panel junctures are given by eq.51 as

$$\sum_{k=0}^{Q-1} [c_k^C] |q_k| = 0 \quad C = 0, 1, \dots, 3 \quad (51)$$

where the  $c_k^C$  are obtained from eqs.49 and 50. These matrices have the same form, shown in eq.70, for all values of C and k. Note that the elements of the matrices do depend on C and k but they have not been marked as such to reduce the complexity of the notation. For a given C and k these elements depend on panel geometric characteristics as defined in Fig 12. The elements themselves are defined in Tables IX and X for C=1,2 and 3. For the case C=0 all elements are zero. It should be noted also that the last row in each matrix, which destroys its bandedness, defines a relationship between the first and the last panel. In some cases, such as where a slope discontinuity exists across these panels, the conditions of continuity may be slightly modified.



$$C_k^C = \begin{bmatrix} e_1 & f_2 & 0 & . & . & . & . & 0 \\ 0 & e_2 & f_3 & & & & & . \\ . & & & & & & & . \\ . & & & & & & & . \\ . & & & & & & & . \\ . & & & & & & & 0 \\ 0 & & & & & 0 & e_{N-1} & f_N \\ f_1 & 0 & . & . & . & . & 0 & e_N \end{bmatrix} \quad (70)$$

TABLE IX

Form of  $e_i$ ,  $i = 1, \dots, N$ 

| C | k |                               |   |  |
|---|---|-------------------------------|---|--|
|   | 0 | 1                             | 2   | 3  |
| 1 | 1 | $\sin \delta_i$               | $\sin^2 \delta_i$                                     | $\sin^3 \delta_i$  |
| 2 | 0 | $\frac{\cos \delta_i}{a_i}$   | $\frac{\sin^2 \delta_i}{a_i}$                         | $\frac{3\sin^2 \delta_i \cos \delta_i}{a_i}$                         |
| 3 | 0 | $\frac{\sin \delta_i}{a_i^2}$ | $\frac{-2(\cos^2 \delta_i - \sin^2 \delta_i)}{a_i^2}$ | $\frac{-3\sin \delta_i (2\cos^2 \delta_i - \sin^2 \delta_i)}{a_i^2}$ |

TABLE X

Form of  $f_i$   $i=1,\dots,N$ 

| c | k      |        |        |        |
|---|--------|--------|--------|--------|
|   | 0      | 1      | 2      | 3      |
| 1 | $-e_i$ | $e_i$  | $-e_i$ | $e_i$  |
| 2 | 0      | $-e_i$ | $e_i$  | $-e_i$ |
| 3 | 0      | $e_i$  | $-e_i$ | $e_i$  |

## Appendix B

### Velocity Influence Coefficients

In this appendix the normal and tangential velocity influence coefficient matrices  $[R_k]$  and  $[T_k]$  will be computed. These matrices give the velocity at any point in the field that is induced by a source or vortex singularity distributed on a circular arc. Also the velocity influence coefficients for a reverse curvature panel, which are needed to model a general airfoil, will be developed.

### Source Distribution

Referring to Fig 12 and 61, the problem is to compute the velocity at a point  $P(r, \theta)$  due to a source distribution on a circular arc panel. The velocity is given by

$$\vec{V}(r, \theta) = \frac{1}{2\pi} \nabla \phi = \frac{1}{2\pi} \left[ \frac{\partial \phi}{\partial r} \hat{e}_r + \frac{1}{r} \frac{\partial \phi}{\partial \theta} \hat{e}_\theta \right] \quad (71)$$

where

$$\phi = \int_B \sigma \log R \, dl$$

$$R^2 = r^2 + a^2 - 2ar \cos(\theta - \theta_0)$$

Now

$$\frac{\partial \phi}{\partial r} = \int_B \sigma \frac{\partial R / \partial r}{R} \, dl$$

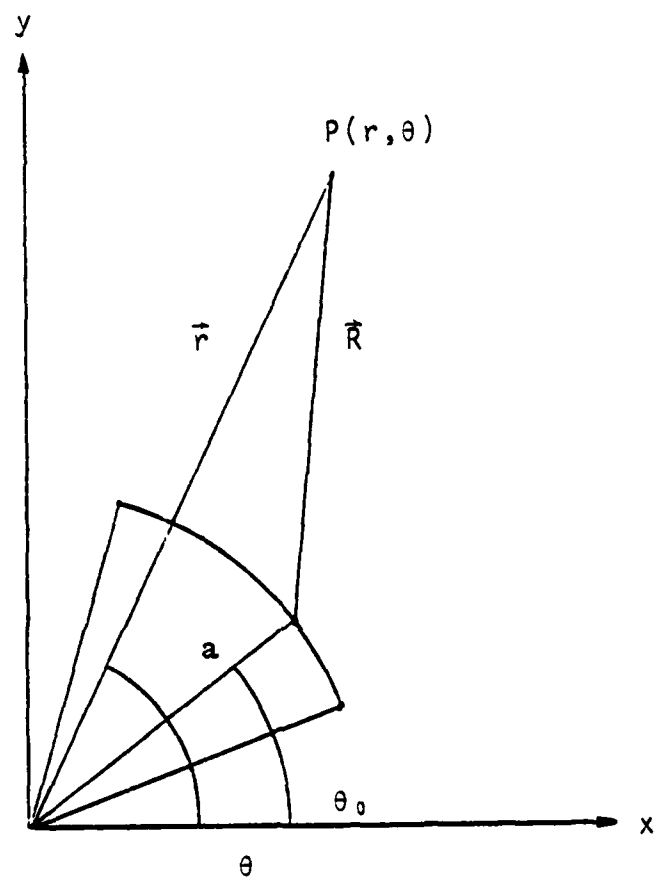


Figure 61. Panel Influence at a Point P.

where

$$dl = ad\theta_0, \quad \frac{\partial R}{\partial r} = r - a \cos(\theta - \theta_0)$$

Thus

$$\frac{\partial \phi}{\partial r} = \int_{\theta_{M-\delta}}^{\theta_{M+\delta}} \sigma(\theta_0) \frac{r - a \cos(\theta - \theta_0)}{r^2 + a^2 - 2ar \cos(\theta - \theta_0)} ad\theta_0$$

Now let

$$d = \frac{r}{a}, \quad D = \frac{r^2 + a^2}{2ar}$$

Then

$$\frac{\partial \phi}{\partial r} = a \int_{\theta_{M-\delta}}^{\theta_{M+\delta}} \frac{\sigma(\theta_0)[r - a \cos(\theta - \theta_0)]d\theta_0}{2ar[D - \cos(\theta - \theta_0)]}$$

or

$$\frac{\partial \phi}{\partial r} = \frac{a^2}{2ar} \int_{\theta_{M-\delta}}^{\theta_{M+\delta}} \frac{\sigma(\theta_0)[d - \cos(\theta - \theta_0)]d\theta_0}{D - \cos(\theta - \theta_0)}$$

and

$$V_r(r, \theta) = \frac{1}{4\pi d} \int_{\theta_{M-\delta}}^{\theta_{M+\delta}} \frac{\sigma(\theta_0)[d - \cos(\theta - \theta_0)]d\theta_0}{D - \cos(\theta - \theta_0)}$$

Similarly for  $\frac{\partial}{\partial \theta}$  :

$$\frac{\partial \phi}{\partial \theta} = \int_B \sigma \frac{\partial R}{\partial \theta} dl$$

where

$$\frac{\partial R}{\partial \theta} = \frac{\arcsin(\theta - \theta_0)}{R}$$

Therefore

$$v_{\theta}(r, \theta) = \frac{1}{4\pi d} \int_{\theta_M - \delta}^{\theta_M + \delta} \frac{\sigma(\theta_0) \sin(\theta - \theta_0) d\theta_0}{D - \cos(\theta - \theta_0)}$$

Now

$$\sigma(\theta_0) = \sum_{k=0}^{Q-1} q_k \sin^k(\theta_0 - \theta_M)$$

so that the general term is

$$v_r^k(r, \theta) = \frac{q_k}{4\pi d} \int_{\theta_M - \delta}^{\theta_M + \delta} \frac{\sin^k(\theta_0 - \theta_M) [d - \cos(\theta - \theta_0)] d\theta_0}{D - \cos(\theta - \theta_0)} \quad (72)$$

$$v_{\theta}^k(r, \theta) = \frac{q_k}{4\pi d} \int_{\theta_M - \delta}^{\theta_M + \delta} \frac{\sin^k(\theta_0 - \theta_M) \sin(\theta - \theta_0) d\theta_0}{D - \cos(\theta - \theta_0)} \quad (73)$$

Note that the integrands here are well behaved for  $r \neq a$ , since then  $D > 1$  and  $D - \cos(\theta - \theta_0) \neq 0$ , but at  $r = a$ ,  $D = 1$  so the point  $\theta_0 = \theta$  then requires special care. These expressions will be integrated assuming  $r \neq a$ , and then the limit as  $r \rightarrow a$  of the results will be taken.

Integration for  $r \neq a$  . To integrate these expressions the following transformation is made:

Let

$$X = \theta_0 - \theta$$

$$X_1 = \theta_M - \delta - \theta, \quad X_2 = \theta_M + \delta - \theta$$

$$\theta_0 - \theta_M = X + \theta - \theta_M$$

Therefore

$$V_r^k(r, \theta) = \frac{q_k}{4\pi d} \int_{X_1}^{X_2} \frac{\sin^k(X + \theta - \theta_M) [d - \cos X] dX}{D - \cos X} \quad (74)$$

$$V_\theta^k(r, \theta) = \frac{-q_k}{4\pi d} \int_{X_1}^{X_2} \frac{\sin^k(X + \theta - \theta_M) \sin X dX}{D - \cos X} \quad (75)$$

Now let

$$W = D - \cos X$$

and

$$y = 1 - \cos^2 X = 1 - (D - W)^2 = (1 - D^2) + 2DW - W^2$$

or

$$y = a + bw + cw^2$$

where

$$a = 1 - D^2$$

$$b = 2D$$

$$c = -1$$

Note that

$$dw = \sin X dX$$



and

$$\sin X = \sqrt{y}$$

The integrals in eqs. 74 and 75 can be obtained by reduction to the following standard forms (Refs 69 and 70):

$$\int \frac{dw}{\sqrt{y}} = -\sin^{-1}(\cos X) = -\sin^{-1}(D-W) \quad (76a)$$

$$\int \frac{dw}{\sqrt{y} w} = \frac{2}{\sqrt{D^2-1}} \tan^{-1} \left\{ \frac{\sqrt{D^2-1}}{D-1} \tan \frac{X}{2} \right\} \quad (76b)$$

$$\int \frac{\sqrt{y} dw}{w} = \sqrt{y} + D \int \frac{dw}{\sqrt{y}} + (1-D^2) \int \frac{dw}{\sqrt{y} w} \quad (76c)$$

$$\int \frac{wdw}{\sqrt{y}} = -\sqrt{y} + D \int \frac{dw}{\sqrt{y}} \quad (76d)$$

$$\int \frac{w^2 dw}{\sqrt{y}} = \frac{-w-3D}{2} \sqrt{y} + (D^2 + \frac{1}{2}) \int \frac{dw}{\sqrt{y} w} \quad (76e)$$

Note that eq. 76a evaluated at the integration limits gives

$$\int_{X_1}^{X_2} \frac{dw}{\sqrt{y}} = -[\sin^{-1}(\cos X_2) - \sin^{-1}(\cos X_1)] = X_2 - X_1$$

Using the above in eqs.74 and 75, and letting

$$F_1(r, \theta) = \frac{2(d-D)}{\sqrt{D^2-1}} \left[ \tan^{-1} \left\{ \frac{\sqrt{D^2-1}}{D-1} \tan \frac{\theta_M + \delta - \theta}{2} \right\} \right. \\ \left. - \tan^{-1} \left\{ \frac{\sqrt{D^2-1}}{D-1} \tan \frac{\theta_M - \delta - \theta}{2} \right\} \right] \quad (77)$$

$$F_2(r, \theta) = \ln \left\{ \frac{D - \cos(\delta - \theta + \theta_M)}{D - \cos(-\delta - \theta + \theta_M)} \right\} \quad (78)$$

$$X_2 = \delta - \theta + \theta_M \quad X_1 = -\delta - \theta + \theta_M \quad \omega = \delta + \theta - \theta_M$$

The following expressions for the velocities in the  $r$  and  $\theta$  directions due to a source distribution on a circular arc are obtained for  $k=0$  to  $k=3$ .

For  $k=0$

$$V_r^0(r, \theta) = \frac{q_0}{4\pi d} \{2\delta + (d-D)F_1(r, \theta)\} \quad (79a)$$

$$V_\theta^0(r, \theta) = \frac{-q_0}{4\pi d} F_2(r, \theta) \quad (79b)$$

For  $k=1$

$$V_r^1(r, \theta) = \frac{q_1}{4\pi d} \{ [(d-D)F_2(r, \theta) - \cos(X_2) + \cos(X_1)] \cos(\theta - \theta_M) \\ + [\sin(X_2) - \sin(X_1) - (d-D)2\delta + DF_1(r, \theta)] \sin(\theta - \theta_M) \} \quad (80a)$$

$$V_{\theta}^1(r, \theta) = \frac{-q_1}{4\pi d} \{ [2D\delta + \sin(X_2) - \sin(X_1) - (D^2 - 1)F_1(r, \theta)] \cos(\theta - \theta_M) \\ + [DF_2(r, \theta) + \cos(X_2) - \cos(X_1)] \sin(\theta - \theta_M) \} \quad (80b)$$

For  $k=2$

$$V_r^2(r, \theta) = \frac{q_2}{4\pi d} \left\{ \cos^2(\theta - \theta_M) \left[ (d-D) [\sin X_2 - \sin X_1] - \frac{\sin 2X_2 + \sin 2\omega}{4} \right. \right. \\ \left. \left. + 2\delta \left[ D(d-D) + \frac{1}{2} \right] - (D^2 - 1)(d-D)F_1(r, \theta) \right] \right. \\ \left. + \sin 2(\theta - \theta_M) \left[ D(d-D)F_2(r, \theta) + (d-D) [\cos X_2 - \cos X_1] \right. \right. \\ \left. \left. - \frac{\cos^2 X_2 - \cos^2 X_1}{2} \right] + \sin^2(\theta - \theta_M) \left[ (D(D-d) + \frac{1}{2}) 2\delta - (d-D) \right. \right. \\ \left. \left. \cdot \left[ \sin X_2 - \sin X_1 \right] + \frac{\sin 2X_2 + \sin 2\omega}{4} + D^2(d-D)F_1(r, \theta) \right] \right\} \quad (81a)$$

$$V_{\theta}^2(r, \theta) = \frac{-q_2}{4\pi d} \left\{ \cos^2(\theta - \theta_M) \left[ \frac{\cos^2 \omega - \cos^2 X_2}{2} - D(\cos X_2 - \cos \omega) \right. \right. \\ \left. \left. - (D^2 - 1)F_2(r, \theta) \right] + \sin 2(\theta - \theta_M) \left[ 2\delta(D^2 - \frac{1}{2}) + D(\sin X_2 + \sin \omega) \right. \right. \\ \left. \left. + \frac{\sin 2X_2 + \sin 2\omega}{4} - D(D^2 - 1)F_1(r, \theta) \right] + \sin^2(\theta - \theta_M) \right. \\ \left. \cdot \left[ D^2 F_2(r, \theta) + D(\cos X_2 - \cos \omega) + \frac{\cos^2 X_2 - \cos^2 \omega}{2} \right] \right\} \quad (81b)$$

and for  $k=3$

$$\begin{aligned}
 V_r^3(r, \theta) = \frac{q_3}{4\pi d} & \left\{ \cos^3(\theta - \theta_M) [(d-D)(1-D^2)F_2(r, \theta) \right. \\
 & + (d-D) \left[ 2D(\cos X_1 - \cos X_2) - \frac{1}{2}((D - \cos X_2)^2 - (D - \cos X_1)^2) \right] \\
 & + (1-D^2)[\cos X_1 - \cos X_2] + D[(D - \cos X_2)^2 - (D - \cos X_1)^2] \\
 & - \frac{1}{3}[(D - \cos X_2)^3 - (D - \cos X_1)^3] + 3\cos^2(\theta - \theta_M)\sin(\theta - \theta_M) \\
 & \cdot \left[ \frac{\sin^3 X_2 - \sin^3 X_1}{3} + D(1-D)(\sin X_2 - \sin X_1) \right. \\
 & + \frac{3D-d}{2} (\cos X_2 \sin X_2 - \cos X_1 \sin X_1) + (d-D)(D^2 - \frac{1}{2}) \\
 & \cdot (X_2 - X_1) + D(1-D^2)F_1(r, \theta) + 3\sin^2(\theta - \theta_M)\cos(\theta - \theta_M) \\
 & \cdot [D^2(d-D)F_2(r, \theta) + D(3D-2d)(\cos X_1 - \cos X_2) \\
 & + \frac{d-3D}{2}((D - \cos X_2)^2 - (D - \cos X_1)^2) \\
 & - \frac{1}{3}((D - \cos X_2)^3 - (D - \cos X_1)^3)] + \sin^3(\theta - \theta_M) \\
 & \cdot \left[ \left( \frac{-3Dd}{2} - \frac{11D^2-4}{6} \right) (\sin X_2 - \sin X_1) + \frac{3d-17D}{6} \right. \\
 & \cdot ((D - \cos X_2)\sin X_2 - (D - \cos X_1)\sin X_1)
 \end{aligned}$$

$$\begin{aligned}
& - \frac{1}{3}((D-\cos X_2)^3 \sin X_2 - (D-\cos X_1)^3 \sin X_1) \\
& + \delta D(3-2D^2) + [(d-D) \left( \frac{2D^2(D-1)+1}{2} \right) + \frac{3D}{2} \\
& \cdot (2D^2+1)] \frac{F_1(r, \theta)}{d-D} \Bigg] \Bigg\} \quad (83a)
\end{aligned}$$

$$\begin{aligned}
V_{\theta}^3(r, \theta) = & \frac{-q^3}{4\pi d} \{ \cos^3(\theta - \theta_M) \left[ \frac{\sin^3 X_2 - \sin^3 X_1}{3} - (D^2-1) \right. \\
& \cdot (\sin X_2 - \sin X_1) - \frac{D}{4}(\sin 2X_2 - \sin 2X_1) \\
& + \delta D(3-2D^2) + \frac{(1-D^2)^2}{d-D} F_1(r, \theta) \Bigg] + 3\sin(\theta - \theta_M) \cos^2(\theta - \theta_M) \\
& \cdot \left[ D(1-D^2)F_2(r, \theta) - (3D^2-1)(\cos X_1 - \cos X_2) \right. \\
& - \frac{3D}{2} [(D-\cos X_2)^2 - (D-\cos X_1)^2] + \frac{1}{3}[(D-\cos X_2)^3 \\
& - (D-\cos X_1)^3] \Bigg] + 3\sin^2(\theta - \theta_M) \cos(\theta - \theta_M) [D^2(\sin X_2 - \sin X_1) \\
& + 2\delta D(D^2 - \frac{1}{2}) + \frac{D}{2} [(D-\cos X_2)\sin X_2 - (D-\cos X_1)\sin X_1] \\
& - \frac{\sin^3 X_2 - \sin^3 X_1}{3} + \frac{D^2(1-D^2)}{d-D} F_1(r, \theta) + \sin^3(\theta - \theta_M) \\
& \cdot \left[ D^2 F_2(r, \theta) + 3D^2(\cos X_2 - \cos X_1) + \frac{3D}{2} [(D-\cos X_2)^2 \right. \\
& \left. - (D-\cos X_1)^2] - \frac{1}{3}[(D-\cos X_2)^3 - (D-\cos X_1)^3] \Bigg] \Bigg\} \quad (83b)
\end{aligned}$$

Limit as  $r \rightarrow a$  . The above formulas represent the effect of a source distribution on a circular arc at a point  $P(r, \theta)$  . They are clearly valid for  $r \neq a$  , but if  $P$  lies on the arc itself they exhibit special limiting behavior. In this case  $P(r, \theta) \rightarrow P(a, \theta)$  with  $\theta \in (\theta_M - \delta, \theta_M + \delta)$  and the unique limiting behavior is contained in terms with the factor  $F_1(r, \theta)$  . Now consider the factor  $\sqrt{D^2 - 1}/(D - 1)$  in Eq.77. As

$$r \rightarrow a, \quad \frac{\sqrt{D^2 - 1}}{(D - 1)} \rightarrow \infty,$$

But the tangent term multiplying this factor changes sign depending on the value of  $\theta$  relative to the panel. Referring to Fig. 62 consider a point  $P_1$  such that  $\theta_1 \notin (\theta_M - \delta, \theta_M + \delta)$ . Then both tangent terms in Eq.77 are negative; i.e.

$$\tan \frac{\theta_M + \delta - \theta_1}{2} < 0 \quad \text{and} \quad \tan \frac{\theta_M - \delta - \theta_1}{2} < 0$$

Thus as  $r \rightarrow a$  with  $r > a$  the inverse tangent difference term in Eq.77 becomes

$$\tan^{-1}(-\infty) - \tan^{-1}(-\infty) = 0$$

The same is true for the case of  $P_3$  , except that the tangents are positive. For the case of  $P_2$  , however,

$$\frac{\theta_M + \delta - \theta_2}{2} > 0$$

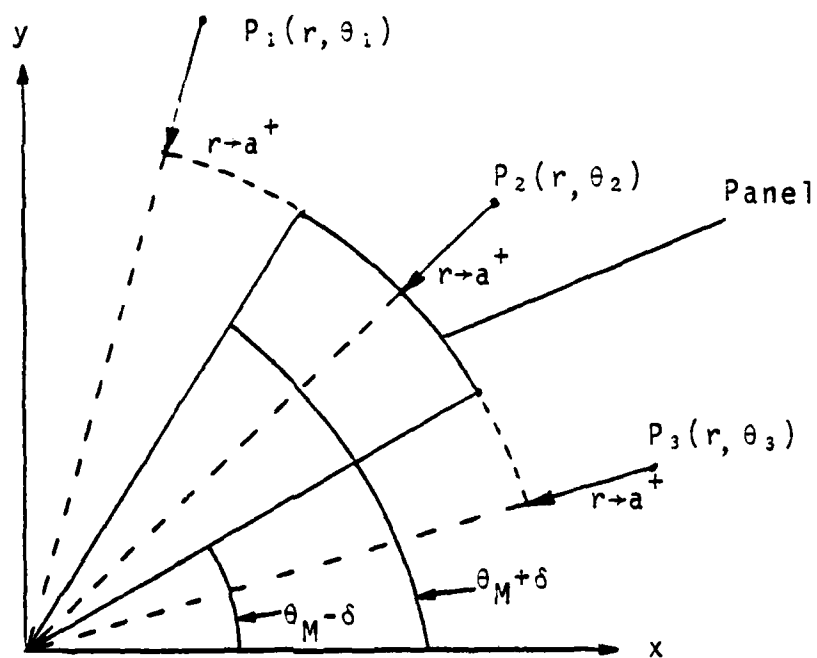


Figure 62. Limiting Behavior on a Panel as  $P(r, \theta)$  goes to  $P(a, \theta)$ .

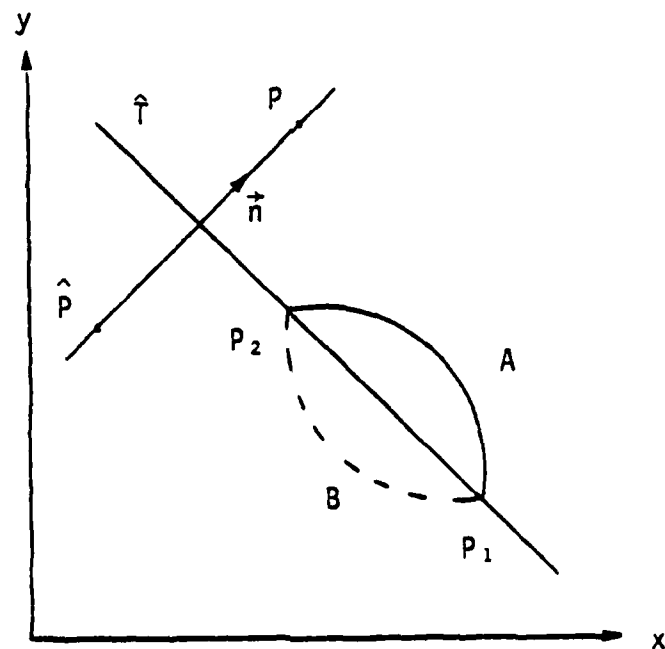


Figure 63. Reverse Curvature Formulation.

and

$$\frac{\theta_M - \delta - \theta_2}{2} < 0$$

Thus

$$\tan^{-1}(+\infty) - \tan^{-1}(-\infty) = \frac{\pi}{2} - (-\frac{\pi}{2}) = \pi$$

As an example, consider  $V_r(r, \theta)$  for the  $k=0$  case, and let  $r \rightarrow a^+$ . Note that

$$\lim_{r \rightarrow a} \frac{d-D}{\sqrt{D^2-1}} = \operatorname{sgn}(r-a)$$

Therefore

$$\text{as } r \rightarrow a^+ \quad \frac{d-D}{\sqrt{D^2-1}} \rightarrow 1$$

Thus for the case corresponding to  $P_2$  in Fig 61

$$V_r(a^+, \theta) = \frac{q_0}{4\pi} [2\delta + 2\pi]$$

While for the cases corresponding to  $P_1$  or  $P_3$ ,

$$V_r(a^+, \theta) = \frac{q_0}{4\pi} [2\delta]$$

An interesting feature of this expression is that for the



$k=0$  case the dependence of  $\theta$  is removed by the limiting process.

Transformation to Global Coordinates. Eqs 79-83 represent velocities at a point  $P$  in a polar coordinate system based on the circular arc panel. To obtain the global influence coefficient matrices  $[R_k]$  and  $[T_k]$  these equations must be transformed by a simple rotation into tangent and normal velocities defined at the point  $P$ .

#### Reverse Curvature Panels

The formulas that have been developed are written in a polar coordinate system in which the equation of the panel is  $r=a$ . In addition, the direction of increasing arc length along an element is assumed to be counterclockwise in such a coordinate system. This type of panel will be referred to as a standard panel. A general cambered airfoil, however, will have regions of curvature opposite to that of a standard panel. By applying a transformation the formulas for a standard panel can be used to compute the velocities due to a reverse curvature panel.

The problem is to compute the velocity at a point  $P$  due to a distribution on arc  $B$  (Fig 63). Let  $\hat{T}$  be a vector defined by connecting the panel endpoints  $P_1$  and  $P_2$ ; and let  $\hat{n}$  be the direction of the normal to  $\hat{T}$ . The point  $\hat{P}$  is then obtained by reflecting  $P$  about  $\hat{T}$ . Now it is clear that the velocity at  $\hat{P}$  in the  $\hat{T}$

direction due to arc A equals the velocity at P in the  $\hat{T}$  direction due to arc B. Similarly the velocity at P in the  $\hat{n}$  direction due to arc A can be related to the equivalent velocity at  $\hat{P}$  due to arc B. That is,

$$V_{\hat{T}_B}(P) = V_{\hat{T}_A}(\hat{P})$$

$$V_{\hat{n}_B}(P) = -V_{\hat{n}_A}(\hat{P})$$

Thus the velocity at a point P due to either a standard or a reverse curvature panel can be computed in terms of the local panel coordinate system. The components are then transformed into a global system in which the point is specified.

### Vorticity Distribution

In two dimensions the velocity components induced by a vortex distribution are directly related to those developed above for a source distribution. If the velocity due to a source is  $\vec{V}_s$  where

$$\vec{V}_s = V_{r_s} \hat{e}_r + V_{\theta_s} \hat{e}_\theta$$

Then the velocity due to a vortex  $\vec{V}_v$  is

$$\vec{V}_v = -V_{\theta_s} \hat{e}_r + V_{r_s} \hat{e}_\theta$$

Thus the potential flow problem can be immediately solved for a vorticity distribution using the equations already developed.

## VITA

Jay E. DeJongh was born on 13 June 1947 in Brooklyn, New York. He graduated first in his class from Groton High School, Groton, Massachusetts in 1965. He then attended Brown University from which he received a Sc. B. in Applied Mathematics (cum laude) in 1969. Upon graduating he was commissioned in the U.S. Air Force through the AFROTC program. He then attended Cornell University where he obtained a Master of Engineering degree in 1970. After spending two years in space defense operations, he was assigned to the Space Test Program Office at the Space and Missile Systems Organization as an aeronautical engineer. During this time he completed several graduate level aerospace engineering courses at the University of Southern California. In 1975 he entered the Air Force Institute of Technology to study for a doctorate in aerospace engineering. He is currently assigned to the Department of Aeronautics at the U.S. Air Force Academy.

Permanent Address

1115 Ortego Drive

Fairborn, Ohio 45324

END

FILMED

3-83

DTIC